



National Library  
of Canada

Acquisitions and  
Bibliographic Services Branch

395 Wellington Street  
Ottawa, Ontario  
K1A 0N4

Bibliothèque nationale  
du Canada

Direction des acquisitions et  
des services bibliographiques

395, rue Wellington  
Ottawa (Ontario)  
K1A 0N4

Acquisitions and Bibliographic Services

Direction des Services Bibliographiques

## NOTICE

The quality of this microform is heavily dependent upon the quality of the original thesis submitted for microfilming. Every effort has been made to ensure the highest quality of reproduction possible.

If pages are missing, contact the university which granted the degree.

Some pages may have indistinct print especially if the original pages were typed with a poor typewriter ribbon or if the university sent us an inferior photocopy.

Reproduction in full or in part of this microform is governed by the Canadian Copyright Act, R.S.C. 1970, c. C-30, and subsequent amendments.

## AVIS

La qualité de cette microforme dépend grandement de la qualité de la thèse soumise au microfilmage. Nous avons tout fait pour assurer une qualité supérieure de reproduction.

S'il manque des pages, veuillez communiquer avec l'université qui a conféré le grade.

La qualité d'impression de certaines pages peut laisser à désirer, surtout si les pages originales ont été dactylographiées à l'aide d'un ruban usé ou si l'université nous a fait parvenir une photocopie de qualité inférieure.

La reproduction, même partielle, de cette microforme est soumise à la Loi canadienne sur le droit d'auteur, SRC 1970, c. C-30, et ses amendements subséquents.

Canada

**UNIVERSITY OF ALBERTA**

**THE HYDROGEOLOGICAL CHARACTERIZATION OF OIL  
FIELDS IN NORTH-CENTRAL ALBERTA FOR  
EXPLORATION PURPOSES**

**BY**



**DANIEL BARSON**

**A THESIS  
SUBMITTED TO THE FACULTY OF GRADUATE  
STUDIES AND RESEARCH IN PARTIAL FULFILLMENT  
OF THE REQUIREMENTS FOR THE DEGREE OF  
DOCTOR OF PHILOSOPHY**

**DEPARTMENT OF GEOLOGY**

**EDMONTON, ALBERTA  
FALL, 1993**



National Library  
of Canada

Acquisitions and  
Bibliographic Services Branch

395 Wellington Street  
Ottawa, Ontario  
K1A 0N4

Bibliothèque nationale  
du Canada

Direction des acquisitions et  
des services bibliographiques

395, rue Wellington  
Ottawa (Ontario)  
K1A 0N4

*Your file - Votre référence*

*Our file - Notre référence*

**The author has granted an irrevocable non-exclusive licence allowing the National Library of Canada to reproduce, loan, distribute or sell copies of his/her thesis by any means and in any form or format, making this thesis available to interested persons.**

**L'auteur a accordé une licence irrévocable et non exclusive permettant à la Bibliothèque nationale du Canada de reproduire, prêter, distribuer ou vendre des copies de sa thèse de quelque manière et sous quelque forme que ce soit pour mettre des exemplaires de cette thèse à la disposition des personnes intéressées.**

**The author retains ownership of the copyright in his/her thesis. Neither the thesis nor substantial extracts from it may be printed or otherwise reproduced without his/her permission.**

**L'auteur conserve la propriété du droit d'auteur qui protège sa thèse. Ni la thèse ni des extraits substantiels de celle-ci ne doivent être imprimés ou autrement reproduits sans son autorisation.**

ISBN 0-315-88262-X

**Canada**

**UNIVERSITY OF ALBERTA  
RELEASE FORM**

**NAME OF AUTHOR: Dan Barson**

**TITLE OF THESIS: The Hydrogeological Characterization of  
Oil Fields in North-Central Alberta for Exploration Purposes.**

**DEGREE: Ph.D.**

**YEAR THIS DEGREE GRANTED: 1993**

Permission is hereby granted to the University of Alberta Library to reproduce single copies of this thesis and to lend or sell such copies for private, scholarly or scientific research purposes only.

The author reserves all other publication and other rights in association with the copyright in the thesis, and except as hereinbefore provided neither the thesis nor any substantial portion thereof may be printed or otherwise reproduced in any material form whatsoever without the authors prior written permission.

  
-----

**11212 70 Ave.  
Edmonton Alberta  
Canada T6H 2H1**

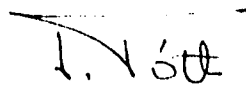
**DATE:** Friday 13 August 1993




UNIVERSITY OF ALBERTA

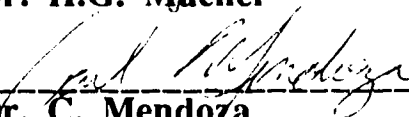
FACULTY OF GRADUATE STUDIES AND RESEARCH

The undersigned certify that they have read and recommend to the Faculty of Graduate Studies and Research for acceptance, a thesis entitled: **The Hydrogeological Characterization of Oil Fields in North-Central Alberta for Exploration Purposes**, submitted by Daniel Barson in partial fulfillment of the requirements for the degree of Ph.D.

  
-----  
Dr. J. Tóth (Supervisor)

  
-----  
Dr. F.W. Jones

  
-----  
Dr. H.G. Machel

  
-----  
Dr. C. Mendoza

  
-----  
Dr. K. Muehlenbachs

  
-----  
Dr. P.E. Gretener

5th. August, 1993

**Gods will! My liege, would you and I alone  
Without more help, might fight this battle out!**

**W.Shakespeare (Henry V, IV, iii, 27-80)**

## **Dedication**

For Louis and Lily

## **Abstract**

A petroleum hydrogeological study was conducted in the Panny-Senex region of north-central Alberta (Tps.89-102, Rs.23W4-14W5) focusing on the Granite Wash, Keg River and Slave Point Formations. The study proceeded in three phases. First structure contour maps, structural cross-sections and hydraulic conductivity maps were generated. Second water and oil flow fields were mapped, flow rates calculated and the distribution patterns of water chemistry, water temperature, and oil density of the reservoir formations were mapped. Finally the effect of water flow on oil migration and accumulation in the study area was considered. Techniques for culling water chemistry, temperature and pressure data and for dealing with the problem of production drawdown are presented.

In the southwest half of the study area, hydraulic heads in the Keg River, and possibly the Slave Point Aquifers, are controlled by the overlying water table topography. A vertically ascending discharge plume at Tp.94 Rs.6 and 7 W5, extends from the basement to the sub-Cretaceous unconformity. Discharge is focussed at the ground surface by the intersection of the Wabasca and Loon River channels. In the northeast, on the other hand, water flows laterally updip to low elevation outcrops beyond the study area. Down-dip, density-driven flow is locally significant.

At the regional scale of the present study, lithology is the dominant control on water chemistry, with flow producing local scale anomalies. Conduction dominates heat flow since water flow rates are too small for forced convection to be significant. The pattern of oil density variations is likewise unrelated to water flow.

Oil is often but not exclusively trapped in regions of hydraulic head minima. An oil head map of the Keg River Aquifer shows an elongate zone of high accumulation potential parallel to the Keg River reef edge between Tp.96 R.10 W5 and Tp.94 R.9 W5. Conventional migration theories cannot explain the presence of oil in the study area since the source rock is absent on the Peace River Arch, down dip from the study area. Northward water flow is promoted as the agent responsible for deflecting oil into the study area.

## **Acknowledgement**

This research was possible because of the enlightened practice of the Govt. of Alberta in allowing public access to subsurface data through the agency of the Energy and Resources Conservation Board (ERCB).

Acknowledgement is also given to NSERC for funding provided through a strategic research grant issued to my supervisor Dr. Tóth.

No progress is made in isolation. I have been very fortunate to have enjoyed the support and camaraderie of an exceptional group of colleagues at the University of Alberta. Thank you foremost to József Tóth, my steadfast advisor, for your integrity as a scientist, a teacher and a man. Your ideas have truly changed the way I see the world. To Mum and Dad for your unflagging support and confidence. To Leslie without whom I could never have started this work. To my Committee members for the considerable improvements you made to my First Draft. To Brian Chatterton, Yves Beaudoin and many other Geology Faculty and support staff. To Ben Rostron for your generosity with time and ideas and for your incisive approach to problem-solving. To Kriengsak for your companionship on the graveyard shifts. To Jacek, Irmi and Diana for 'colourful' life beyond campus. To Greg. To Lasko. To my friends and colleagues past and present at the U of A: Claus, Kevin, Duke, Kaush, Jamie, Diane, Lee, Steve, Joanne, Morris, Dave, Liane, John, Debashish and Kent. Lastly to Siegrid, for suffering through the dark times with me and for sharing the best of the light times. To the future!

## Table of Contents

<b>Introduction</b> .....	1
Objectives.....	3
<b>Chapter 1 Geology, Hydrogeology and Petroleum Geology of the Study Area</b> .....	4
1.1 Location.....	4
1.2 Geology.....	4
1.2.1 Regional Tectonics .....	4
1.2.2 Regional Stratigraphy and Geological History .....	5
1.2.3 Local Stratigraphy and Geological History.....	8
1.2.4 Surficial Geology .....	11
1.3 Hydrogeology.....	12
1.3.1 Topography and Climate.....	12
1.3.2 Hydrostratigraphy.....	13
1.3.3 Previous Hydrogeological Work.....	14
1.4 Petroleum Geology and Timing of Oil Migration.....	15
1.4.1 Regional Petroleum Geology .....	15
1.4.2 Local Petroleum Geology.....	15
<b>Chapter 2 The Hydrogeological Characterization of Oil Fields - Concepts and Principles</b> .....	18
2.1 Modes and Forces in Petroleum Migration and Accumulation.....	19
2.1.1 Petroleum Modes .....	19
2.1.2 Forces of Migration and Accumulation.....	20
2.2 Conventional Theories of Petroleum Migration.....	28
2.2.1 The Anticlinal Theory and the Structural Trap.....	28
2.2.2 The Stratigraphic Trap .....	28
2.2.3 Summary of Conventional Theories .....	29
2.3 Hydraulic Theories of Petroleum Migration.....	29
2.3.1 The Historical Evolution of Hydraulic Theories of Petroleum Migration.....	29
2.3.2 Hydraulically Favoured Petroleum Accumulation Sites.....	34
2.4 The Concept of Hydrogeological Indicators of Petroleum Accumulations.....	35
2.4.1 Hydrogeological Characteristics.....	35
2.4.2 Hydrogeological Indicators of Petroleum Accumulations.....	36

2.5 A Critical Evaluation of Pore Pressure, Temperature and Water Chemistry as Hydrogeological Characteristics.....	38
2.5.1 Pore pressure.....	39
2.5.2 Temperature.....	44
2.5.3 Water Chemistry.....	47
2.5.4 Summary.....	49
<b>Chapter 3 Data Processing for the Field Study - Data</b>	
<b>Sources and Culling Procedures.....</b>	<b>51</b>
3.1 Rock Framework Data.....	51
3.1.1 Formation Tops .....	51
3.1.2 Lithology .....	52
3.1.3 Porosity, Permeability and Hydraulic Conductivity.....	53
3.1.4 Storativity and Transmissivity .....	58
3.1.5 Thermal Conductivity.....	58
3.2 Pressure Data .....	59
3.2.1 Source of Pressure Data.....	60
3.2.2 Evaluation of CIFE DST Interpretation.....	60
3.2.3 Evaluation of Production Induced Drawdown (PID) and Injection Build-Up.....	62
3.2.4 Culling of Production Disturbed Pressure Data .....	76
3.2.5 Rationale for Using Non-Water Recoveries.....	77
3.2.6 Review of the Culled Data Set.....	78
3.3 Temperature Data.....	78
3.3.1 Thermal Disequilibrium and Correction Methods .....	79
3.3.2 Culling and Correcting BHT data.....	80
3.3.3 Temperature Data Quality Classes.....	83
3.3.4 Review of the Culled Data Set.....	83
3.4 Water Chemistry Data .....	83
3.4.1 Source and Type of Water Chemistry Data .....	83
3.4.2 Culling Criteria.....	84
3.4.3 Review of the Culled Data Set.....	87
3.5 Oil Density Data .....	87
3.5.1 ERCB Oil Analyses .....	87
3.5.2 Correcting Oil Densities to Reservoir Conditions.....	87
3.5.3 Review of the Data Set.....	88
3.6 Production Data.....	88

3.6.1 ERCB Production Records: PUBCO CD-Rom.....	88
3.6.2 Review of the Data Set.....	88
<b>Chapter 4 Presentation of the Culled Data - Representation of the Rock Framework and Indicator Patterns.....</b>	<b>89</b>
4.1 Representation of the Rock Framework.....	89
4.1.1 Computer Contouring.....	89
4.1.2 Structure Contour Maps.....	90
4.1.3 Isopach Maps.....	93
4.1.4 Hydraulic Conductivity Maps.....	93
4.1.5 Transmissivity in the Keg River Aquifer .....	95
4.2 Representation of Indicator Patterns.....	96
4.2.1 Pressure .....	96
4.2.2 Temperature.....	107
4.2.3 Water Chemistry.....	110
4.2.4 Oil Density .....	115
<b>Chapter 5 Interpretation of Results - Ramifications for Oil Migration on the Peace River Arch.....</b>	<b>117</b>
<b>Conclusions.....</b>	<b>119</b>
<b>Tables.....</b>	<b>124</b>
<b>Figures.....</b>	<b>148</b>
<b>References.....</b>	<b>220</b>
<b>Appendices.....</b>	<b>238</b>
Appendix 1 Laboratory Procedure for Core Analysis.....	238
Appendix 2 Quantitative DST Interpretation.....	242
Appendix 3 Instrument Error.....	257
Appendix 4 Culled Data Files.....	259
A4.1 Culled Pressure Data.....	260
A4.2 Culled Temperature Data .....	271
A4.3 Culled Major Ion Water Chemistry Data.....	289



## List of Tables

<b>Table 1.1</b> Stratigraphic Table with Hydrostratigraphy and Petroleum Geological Features.....	125
<b>Table 3.1</b> Average Hydraulic Properties of Hydrostratigraphic Units From Core Analyses.....	126
<b>Table 3.2</b> Permeability Determination: Drillstem Test Versus Core.....	127
<b>Table 3.3</b> Storativity and Transmissivity Calculation for the Keg River Aquifer. ....	128
<b>Table 3.4</b> Thermal Conductivity Values for Lithologies in the Alberta Basin.....	129
<b>Table 3.5</b> Thermal Conductivity Values for Hydrostratigraphic Units in the Study Area.....	130
<b>Table 3.6</b> Evaluation of CIFE DST Interpretation.....	131
<b>Table 3.7</b> Petroleum Production Statistics for the Study Area.....	132
<b>Table 3.8</b> Production Zones and Number of Production Wells.....	133
<b>Table 3.9</b> Summary of Production Induced Disturbance Calculations.....	134
<b>Table 3.10</b> Partial Drawdowns - Inter-well Distances, Pumping Intervals and Production Rates.....	135
<b>Table 3.11</b> Total Drawdown versus Closest Production Well, Number of Wells and Cumulative Interference Index.....	136
<b>Table 3.12</b> Static Oil “Overpressure” Evaluation.....	137
<b>Table 3.13</b> Summary of DSTs Undisturbed by Production.....	138
<b>Table 3.14</b> Culling Criteria for Major Ion Analyses (Keg River Fm.).....	139
<b>Table 3.15</b> Equivalent Weights Used in Calculation of Equivalentents per Litre.....	140
<b>Table 3.16</b> Average Formation Water Compositions for the Culled Database.....	141
<b>Table 3.17</b> Keg River-Granite Wash Fluid Densities at Reservoir Conditions.....	142
<b>Table 4.1</b> Data Used For Three-Point Determinations of Buoyancy-Modified Flux in Keg River Aquifer.....	143
<b>Table 4.2</b> Freshwater Head Gradient and Buoyancy-Modified Driving Force in Keg River Aquifer.....	144
<b>Table 4.3</b> Lateral Water Flow Rates in Keg River Aquifer.....	145

<b>Table 4.4</b>	Water Density Profile for Twps. 94-95, Rs. 6-7 W5.....	146
<b>Table 4.5</b>	Calculation of Vertical Flux in Keg River Fm. for Twps. 94-95, Rs. 6-7 W5.....	147
<b>Table A2.1</b>	DST Analysis Table for 10-34-91-24W4, DST#1. ....	249
<b>Table A2.2</b>	DST Analysis Table for 11-33-94-22W4, DST#1. ....	251
<b>Table A2.3</b>	DST Analysis Table for 6-31-98-22W4, DST#1.....	253
<b>Table A2.4</b>	DST Analysis Table for 3-31-100-22W4, DST#2. ....	255

## List of Figures

<b>Figure 1.1</b> Tectonic Elements of North America and Location of Western Canada Sedimentary Basin .....	149
<b>Figure 1.2</b> Western Canada Sedimentary Basin, Regional Dip Cross-Section Across Central Alberta .....	150
<b>Figure 1.3</b> Location Map of Present and Previous Study Areas in the Peace River Region .....	151
<b>Figure 1.4</b> Structural Cross-Section of Study Area Parallel To Basin Dip.....	152
<b>Figure 1.5</b> Structural Cross-Section of Study Area Parallel To Basin Strike .....	153
<b>Figure 1.6</b> Devonian Outcrop Adjacent to Study Area.....	154
<b>Figure 1.7</b> Structure Contours on Bedrock and Thickness of Drift .....	155
<b>Figure 1.8</b> Study Area Bedrock Geology .....	156
<b>Figure 1.9</b> Study Area Physiography.....	157
<b>Figure 1.10</b> Schematic Cross-Section Illustrating the Conventional (Buoyancy Driven) Oil Migration Model in the Peace River Arch Region.....	158
<b>Figure 1.11</b> Slave Point Fm. Facies Distribution and Inferred Oil Migration “Focusing” in Peace River Region.....	159
<b>Figure 1.12</b> Strike Section Across Peace River Arch .....	160
<b>Figure 2.1</b> Schematic Diagram of Darcy’s Fluid Flow Experiment.....	161
<b>Figure 2.2</b> Vector Diagram Illustrating the Twin Components of the Driving Force for Fluid Flow.....	162
<b>Figure 2.3.1</b> Water Flow in Response to the Freshwater Head Gradient .....	163
<b>Figure 2.3.2</b> Vector Diagrams Illustrating: a) Components of the Driving Force for Water Flow in Terms of Fluid Potential; b) Unique Direction and Magnitude of Driving Forces for Water, Oil and Gas Flow .....	164
<b>Figure 2.4</b> Conceptual Geologically Mature Basin Cross-Section Illustrating Potential Petroleum Accumulation Sites .....	165
<b>Figure 2.5</b> Conceptual Geologically Mature Basin Cross-Section Illustrating Hydrogeological Indicators of Various Regions of the Flow Field .....	166

<b>Figure 2.6 Pressure-Depth Relations: Hydrostatic, Hydrodynamic and Lithostatic.....</b>	<b>167</b>
<b>Figure 3.1 Characteristic Log Signatures for Palaeozoic Formations .....</b>	<b>168</b>
<b>Figure 3.2 Porosity Frequency Histogram .....</b>	<b>169</b>
<b>Figure 3.3 Representative Lateral Permeabilities at Various Scales.....</b>	<b>170</b>
<b>Figure 3.4 Permeability Frequency Histogram.....</b>	<b>171</b>
<b>Figure 3.5 Schematic Production History Graph.....</b>	<b>172</b>
<b>Figure 3.6 Graph of W(u) versus 1/u - the Theis Type Curve.....</b>	<b>173</b>
<b>Figure 3.7 The Influence on Drawdown of: a) Distance; b) Production Time; c) Production Rate .....</b>	<b>174</b>
<b>Figure 3.8 Partial Drawdown Versus Non-Cumulative Interference Index: a) All Data; b) Disturbed Wells at Enlarged Scale .....</b>	<b>175</b>
<b>Figure 3.9 Total Drawdown Versus Cumulative Interference Index: a) All Data; b) Disturbed Well Data at Enlarged Scale.....</b>	<b>176</b>
<b>Figure 3.10 Total Production Induced Drawdown Versus: a) Distance to Nearest Active Production Well; b) Number of Active Production Wells Within 10 km Radius.....</b>	<b>177</b>
<b>Figure 3.11.1 Production and Injection Wells Active Prior to Most Recent Drillstem Test.....</b>	<b>178</b>
<b>Figure 3.11.2 Calculated Production Drawdown in the Keg River Aquifer .....</b>	<b>179</b>
<b>Figure 3.12 Thermal Disequilibrium in a Borehole After Drilling.....</b>	<b>180</b>
<b>Figure 3.13 Procedure for Culling and Correcting BHT Data.....</b>	<b>181</b>
<b>Figure 3.14 Examples of Horner Plots of BHT Data - Used to Estimate Undisturbed Formation Temperature .....</b>	<b>182</b>
<b>Figure 3.15 Stiff Diagrams Showing Average Formation Water Compositions .....</b>	<b>183</b>
<b>Figure 3.16 Piper Diagram Showing Average Composition of Formation Waters in the Study Area.....</b>	<b>184</b>
<b>Figure 4.1 Well Locations, Oil Fields and Reef Margins .....</b>	<b>185</b>
<b>Figure 4.2 Structure Contours on Top of Pre-Cambrian Basement.....</b>	<b>186</b>
<b>Figure 4.3 Structure Contours on Top of Keg River Aquifer.....</b>	<b>187</b>
<b>Figure 4.4 Structure Contours on Top of Slave Point Aquifer .....</b>	<b>188</b>
<b>Figure 4.5 Structure Contours on Top of Upper Devonian-Basal Cretaceous Aquifer Showing Palaeozoic Formation Subcrops.....</b>	<b>189</b>

<b>Figure 4.6</b> Isopach of Muskeg Aquitard.....	190
<b>Figure 4.7</b> Muskeg Fm. Salt Distribution in Adjacent Wells - Probable Halite Dissolution.....	191
<b>Figure 4.8</b> Hydraulic Conductivity Distribution in Keg River Aquifer .....	192
<b>Figure 4.9</b> Hydraulic Conductivity Distribution in Slave Point Aquifer .....	193
<b>Figure 4.10</b> Hydraulic Conductivity Distribution in Upper Devonian-Basal Cretaceous Aquifer.....	194
<b>Figure 4.11</b> Transmissivity Distribution in Keg River Aquifer.....	195
<b>Figure 4.12</b> Hydraulic Head (Freshwater Equivalent) in Keg River Aquifer .....	196
<b>Figure 4.13.1</b> Buoyancy Modified Flow in Keg River Aquifer, Southwest Region .....	197
<b>Figure 4.13.2</b> Buoyancy Modified Flow in Keg River Aquifer, Northeast Region.....	198
<b>Figure 4.13.3</b> Buoyancy Modified Flow in Keg River Aquifer, North Region.....	199
<b>Figure 4.14</b> Ground Surface Topography.....	200
<b>Figure 4.15</b> Hydraulic Head (Freshwater Equivalent) in Slave Point Aquifer .....	201
<b>Figure 4.16</b> Hydraulic Head (Freshwater Equivalent) in Upper Devonian-Basal Cretaceous Aquifer.....	202
<b>Figure 4.17</b> Oil Head in Keg River Aquifer.....	203
<b>Figure 4.18</b> Pressure-Depth Plot for all Stable, Undisturbed Pressures, Grouped by Ground Surface Elevation Ranges.....	204
<b>Figure 4.19</b> Pressure-Depth Ratio versus Ground Surface Elevation for all Stable, Undisturbed Pressures.....	205
<b>Figure 4.19.1</b> Pressure Versus Depth Plot for Townships 94-95 Ranges 6-7W5: a) Ground Surface to Basement; b) Detail: Devonian Aquifers .....	206
<b>Figure 4.20</b> Temperature Distribution (BHT Data) at Top of Pre- Cambrian.....	207
<b>Figure 4.21</b> Average Geothermal Gradients (BHT Data) Between Ground Surface and Pre-Cambrian Basement.....	208

<b>Figure 4.21.1</b> BHT Data Analysis: a) Temperature Versus Depth, with Oilfield Wells; b) Wellhead Elevation Versus Temperature:Depth Ratio .....	209
<b>Figure 4.22</b> Maximum Halite Thickness in Muskeg Formation.....	210
<b>Figure 4.23</b> Isopach of Phanerozoic Strata (Total Sediment Thickness) .....	211
<b>Figure 4.24</b> Salinity (Total Dissolved Solids) in Keg River Aquifer .....	212
<b>Figure 4.25</b> Salinity (Total Dissolved Solids) in Slave Point Aquifer .....	213
<b>Figure 4.26</b> Oil Density (Corrected to Reservoir Conditions) in Keg River Aquifer.....	214
<b>Figure 4.27</b> Oil Density (Corrected to Reservoir Conditions) in Slave Point Aquifer .....	215
<b>Figure 5.1</b> Possible Hydrodynamic Oil Migration in Peace River Arch Region .....	216
<b>Figure 5.2</b> Regional Structural Cross-Section Along Axis of Peace River Arch, Parallel to Basin Dip.....	217
<b>Figure A2.1</b> Possible Causes of Characteristic Buildup Curves on an Idealized Horner Plot.....	218
<b>Figure A2.2</b> Characteristic Curves for Radial, Linear and Spherical Flow on Various Pressure Versus Time Plots .....	219
<b>Figure A2.3</b> Horner and Log-Log Plot for 10-34-91-24W4, DST#1.....	250
<b>Figure A2.4</b> Horner and Log-Log Plot for 11-33-94-22W4, DST#1.....	252
<b>Figure A2.5</b> Horner and Log-Log Plot for 6-31-98-22W4, DST#1.....	254
<b>Figure A2.6</b> Horner and Log-Log Plot for 3-31-100-22W4, DST#2.....	256

## List of Symbols

### Roman Symbols

$b$	vertical extent of continuous petroleum phase.
$d$	depth below ground surface.
$E_b$	bouyant driving force per unit volume of petroleum.
$E_c$	capillary driving force per unit volume of petroleum.
$E_h$	hydraulic driving force per unit volume of petroleum.
$E_p$	total driving force per unit volume of petroleum.
$E_w$	driving force per unit mass of water.
$E_p$	total driving force per unit volume of petroleum.
$g$	gravitational constant.
$g$	gravity force per unit mass.
$h$	hydraulic head at reference state (fresh water equivalent).
$I$	interference index
$k$	intrinsic permeability tensor.
$k_{Hmax}$	maximum horizontal permeability.
$k_v$	vertical permeability.
$K$	hydraulic conductivity tensor.
$ka$	thousand years before present.
$m$	molality.
$Ma$	million years before present.
$n$	porosity (fraction).
$P$	total fluid pressure.
$P_b$	buoyant pressure.
$P_c$	capillary pressure.
$P_w$	water pressure.
$Q$	total fluid discharge (volume per unit area).
$q$	specific discharge vector (Darcy velocity) of water.
$q_p$	specific discharge vector (Darcy velocity) of petroleum.
$r$	radial distance between observation and pumping well.
$s$	hydraulic head drawdown.
$S$	storativity.
$t$	time.
$T$	transmissivity.

$v_w$	average linear velocity of water.
$v_p$	average linear velocity of petroleum.
w	subscript denoting water phase component.
$W(u)$	the well function.
z	elevation above mean sea level.

### Greek Symbols

$\beta$	compressibility of water at constant temperature.
$\Delta T$	temperature correction added to bottom hole temperature.
$\Sigma$	arithmetic summation symbol.
$\lambda$	thermal conductivity of water saturated rock.
$\lambda_m$	thermal conductivity of rock matrix.
$\lambda_w$	thermal conductivity of water.
$\mu_o$	fluid dynamic viscosity at reference state (freshwater).
$\mu_p$	petroleum dynamic viscosity.
$\mu_w$	water dynamic viscosity.
v	volume
$\rho_o$	fluid density at reference state (freshwater).
$\rho_p$	petroleum density.
$\rho_w$	water density.
$\zeta$	valence of ion

### Mathematical Symbols

<b>grad</b>	gradient operator ( $\partial/\partial x, \partial/\partial y, \partial/\partial z$ ).
-------------	--



## **Introduction**

The role of moving water as the principal agent of petroleum transport has been the subject of fruitful research since Munn published the first hydraulic theory of oil migration in 1909. Today the determination of flow rates and directions is a straightforward well-defined technical matter. The hydraulic continuity of geologically mature sedimentary basins is generally accepted and the dominance of topography-driven flow systems in these basins is acknowledged. The Generalized Hydraulic Theory of Petroleum Migration (Tóth, 1980) provides a sound conceptual framework for understanding the migration and accumulation of petroleum in such environments. Despite the widespread acceptance of the theory by hydrogeologists, it is still not generally applied as an exploration tool within the oil industry. Two recent studies of oil migration in the western Canada sedimentary basin (WCSB) illustrate this: neither Allan and Creaney (1990) nor Piggot and Lines (1990) consider the possibility of water flow as a motive agent in their conceptualization of petroleum migration patterns. Buoyant forces are promoted as the sole drive for migration with accumulations forming in structural and stratigraphic traps due to vertical or lateral capillary barriers. A field-based study evaluating the influence of flowing water on the migration and accumulation of petroleum within the WCSB is therefore considered worthwhile and necessary. If water flow is found to be influential then the utility of the concepts, methods and techniques presented in the study will have been demonstrated. It is intended that this study will serve as a practical guide which will further the incorporation of hydrogeological ideas into conventional practice to improve exploration efficiency.

The Senex-Panny region in north-central Alberta was selected for study because the hydrogeology of the area has been investigated before, this work providing a foundation for the current research. In addition, the region is an active exploration play with good well control and a largely modern database. Two major hydrogeological studies have been conducted in the region. Tóth (1978, 1979, 1983) elucidated the evolution of flow systems over geological time. Hitchon et al (1990) studied the flow and its relation to the regional distribution of temperature and water salinity. Tóth argued that oil pools in the main Middle Devonian reservoir, the Keg

River-Granite Wash aquifer, coincide with fluid potential minima (i.e., regions of lateral water flow convergence) of a potentiometric surface that was generated by the ground surface during the Pliocene. Hitchon et al did not address the distribution of petroleum directly. They concluded that although flow is topography-driven, salinity patterns are controlled regionally by temperature (i.e., depth) and locally by lithology. Their analysis of the temperature distribution indicated that the geothermal regime is conductive. Thus the effect of flow on the physicochemical character of formation fluids was judged to be minimal.

The present study builds on the previous work by directly assessing the effect of topography-driven flow on petroleum migration and accumulation. The influence of flow on fluid chemistry and temperature is evaluated at a finer scale than in any prior study in the area. Furthermore, criteria are developed by which to recognize representative water chemistry data, and methods are presented for evaluating and culling production-disturbed oilwell pressure measurements.

This thesis is addressed to the petroleum geologist. Its structure reflects the steps required for any petroleum hydrogeological study. Chapter 1 outlines the tectonics, stratigraphy and petroleum geology of the study area and raises problems with conventional explanations of petroleum migration (assuming hydrostatic conditions). Chapter 2 investigates the forces which control migration, clarifying the distinction between conventional and hydraulic models. The concepts and principles underlying hydraulic theories are discussed and the historical development of these theories is described. Hydrogeological characteristics are defined and critically analyzed. Chapter 3 describes the raw data obtained for the study, and presents criteria for data culling. Quantitative methods for dealing with the problem of production induced drawdown in order to obtain useful pressures are proposed. This chapter also evaluates the confidence limits of the residual data. Chapter 4 shows how the raw data are manipulated in the framework of a hydraulic theory of migration and provides methods and techniques of mapping and graphical analysis and their interpretation. Chapter 5 synthesizes the results and evaluates the influence of topography-driven flow on petroleum migration and accumulation in the Peace River Arch region.

## **Objectives**

The thesis will constitute a self-contained methodological guide for petroleum geologists to show how hydrogeological principles and techniques can be incorporated into a 'conventional' exploration effort. The availability of such a guide and the establishment of standard procedures for data culling and interpretation should help considerably to broaden petroleum hydrogeology as an applied exploration discipline.

The following working hypotheses will be evaluated within the limits of the study area:

- 1 The pore water is in motion.
- 2 Gravity-driven flow generated by the topographic relief of the water table is the main force causing fluid motion.
- 3 Flow paths within and between aquifers can be determined using existing oilwell data.
- 4 The flow pattern will reflect aquifer heterogeneities.
- 5 The geothermal regime is convective: average vertical temperature gradients and subsurface temperatures are influenced by forced convective heat transport via topography-driven flow systems.
- 6 Distribution patterns of major ions are influenced by flow patterns: water salinity (total dissolved solids) increases downstream.
- 7 Average oil pool mass density increases downstream.
- 8 Oil pools are concentrated in regional discharge zones.
- 9 Petroleum migration paths are being/have been influenced by topography-driven flow systems.

## **Chapter 1 Geology, Hydrogeology and Petroleum Geology of the Study Area**

### **1.1 Location**

The study area is a part of the western Canada sedimentary basin (WCSB); an intracratonic basin that underlies a large area of the Interior Plains of North America (see Figure 1.1). The WCSB extends from Alberta across Saskatchewan and Manitoba into the Dakota's of the USA. Its structural limits are arches to the north and south and the disturbed belt of the Rocky Mountains to the west. The original extent of the basin to the east is uncertain (Williams, 1983) since the present eastern margin is erosional. The Canadian Shield outcrops to the east of this truncated edge. The Alberta part of the basin forms a wedge shape in profile approximately 700 km long from east to west. It attains a maximum depth of six kilometres under the Rocky Mountain Foothills (see Figure 1.2) and thins eastwards to its eroded margin against the Shield.

The study area comprises the northeastern part of the Peace River Region in northern Alberta (see Figure 1.3). It extends from Township 102 Range 12 W5 (approximately 58°N 116°W) in the northwest, to Township 89 Range 23 W4 (approximately 56°30'N 113°30'W) in the southeast. The study area measures 167 km by 141 km occupying an area of about 23,500 km<sup>2</sup>. The western, eastern and southern margins are water sheds of the local uplands. Wells are scarce north of the northern boundary.

This area was selected for study because the hydrogeology is known from previous work (see Section 1.3.4). Moreover the region is an active exploration play so there are abundant wells and modern data are available.

### **1.2 Geology**

#### **1.2.1 Regional Tectonics**

The WCSB is a composite basin containing sediments that accumulated within two fundamentally distinct tectonic settings. A long-lived passive plate margin phase started with the initial rifting of the North American craton around 650 Ma and continued until the Late Jurassic about 150 Ma (Monger, 1989). Marine platform sediments were deposited in shelf environments over subsiding portions of the craton during this

period. The passive margin phase was succeeded by a phase of destructive convergence between the North American craton and the Pacific oceanic plate which continues today.

At intervals, terrane accretion at the plate margin (i.e., the welding of microcontinents rafted by the Pacific plate, onto the western edge of the craton), compressed the platform rocks of the western part of the passive margin basin, and drove them progressively eastward over the craton to form mountain ranges of stacked thrust sheets (Monger, 1989).

In the Alberta region, the tectonic loading produced a foreland basin. Clastic sediment eroded from the mountains was deposited in an eastward migrating trough which buried the undeformed platform rocks of the eastern part of the old passive margin basin.

In summary, the deepest (Palaeozoic to Jurassic) strata of the WCSB comprise marine platform sediments deposited within the limits of a regional depression on a passive continental plate margin. These are unconformably overlain by mixed marine-continental Cretaceous and Tertiary strata of the foreland basin phase.

The plate tectonic control on the nature of the sedimentary fill during the Phanerozoic history of the basin was unravelled by Beaumont (1981) and Porter et al. (1982). Chamberlain et al. (1989) recently presented a more sophisticated understanding of the linkage, correlating accelerated sedimentation rates in the basin with specific collision events i.e., with the arrival of individual terranes at the craton margin.

### **1.2.2 Regional Stratigraphy and Geological History**

Table 1.1 is a stratigraphic table showing the age and lithology of the strata preserved in the study area. This table will serve as a framework for the following discussion of the stratigraphy and geological history of the basin. The local stratigraphy and geological history of the study area are described in the following section.

During the passive margin tectonic phase, pre-Devonian epiorogenic warping of the basement divided the WCSB into a number of sub-basins with intervening arches. The arches were deeply eroded during their formation and formed land masses limiting the extent of the early Devonian sea. The sea was connected to open ocean in the northwest and possibly in the northeast (Williams, 1983).

The Elk Point Group of Lower and Middle Devonian age comprises two transgressive cycles each of which is capped by evaporites (Table 1.1). The Lower Elk Point transgression was relatively minor extending only to central Alberta. The Upper Elk Point transgression inundated the craton as far as Manitoba and the Dakotas of the USA (Meijer-Drees, 1986). Reef-bearing carbonate platforms formed around basin arches during periods of open connection with the northern ocean. The evaporites attest to the arid, subtropical, climate and the equatorial location of the North American craton during early Devonian time.

Relative sea level rise continued during the Upper Devonian. The bathymetry of the sea floor was less uneven due to the levelling effect of the accumulated Lower and Middle Devonian sediments, and sedimentation patterns changed. Extensive carbonate platforms developed at the basin margins and also over prior depocentres in the basin interior. Major reef complexes developed on these platforms separated by relatively small shale basins (Bebout et al., 1973; Aprahamian, 1976). At the end of the Devonian Period the basement arches were fully subdued due to the combined effects of erosion, tectonic inversion and sea level rise (Williams, 1983).

By Mississippian time the North American plate had drifted beyond the equatorial realm, the climate was cooler and large scale evaporite deposition ceased. Shales were deposited along with carbonate platform rocks. Clastic sediments were derived from the east due to progressively increasing westerly tilting of the basin during the Permian to middle Jurassic. This tilting caused sediment condensation and the erosional truncation of strata in the east, these events being recorded in a series of eastward converging unconformities within the succession (Bally et al., 1966).

Destructive plate convergence started in Late Jurassic time completely changing the basin structure and transforming sedimentation patterns. Mountain ranges arose from the west in response to two separate orogenies caused by plate collisions (Taylor et al., 1964; Porter et al., 1982). Conglomerates, sandstones and shales were shed from these mountains into a foreland basin in the Alberta region forming the Cretaceous-Tertiary clastic wedge. The first collision produced the Columbian Orogeny that peaked during the Early Cretaceous depositing a blanket of coarse clastics across the basin. During a subsequent lull in

convergence in the early Late Cretaceous, a major Mesozoic aquitard, the Colorado shale, was deposited from an interior seaway that extended from the Boreal Sea to the Gulf of Mexico.

Plate convergence resumed in the Late Cretaceous and the first (minor) pulse of the Laramide Orogeny began. The platform rocks deformed during the Columbian Orogeny were detached from basement and tectonically prograded eastwards. A thick wedge of clastic sediment centered in the west Alberta Plains accumulated during the Palaeocene, remnants of which are preserved in the Foothills and in unglaciated uplands of southern Alberta and Saskatchewan.

The Rocky Mountains were thrust into place during the second (major) pulse of the Laramide Orogeny which started in the early Eocene and continued into the Oligocene (Klassen, 1989). The maximum topographic elevation of the land surface in the WCSB probably occurred during this period and Tóth (1978) considers that basin-wide topography driven flow systems started to replace compaction driven flow in the WCSB during the Eocene. The Eocene was also the period of maximum burial depth because since that time erosion has dominated.

Most of the Palaeocene clastic wedge, the molasse of early Laramide mountains, was removed by rivers draining the new Rocky Mountains. The soft Cretaceous sediments of the Alberta Plains were deeply incised by these rivers. It seems probable that erosion rates were greatest during the Eocene when the topographic gradient from the mountains to the Plains would have been steepest. Erosion continued through the late Tertiary possibly at an accelerated rate during the Pliocene (Taylor et al., 1964).

The total thickness of sediment eroded from the WCSB since the Eocene increases towards the Foothills. An estimated 2 km have been removed from central Alberta (Hacquebard, 1977; Nurkowski, 1984). Preserved Tertiary river channels in central and northern Alberta, now largely filled in with Quaternary deposits, are typically oriented northeast (Barton et al., 1964; Klassen, 1989) reflecting the topographic slope from the Rocky Mountains. The channels are deep with very wide (5 to 40 km) valleys.

Finally during the Pleistocene, the basin was glaciated. A firm date for the first glacial advance has not been established, largely because later advances tended to obliterate the traces of earlier glaciations (Fulton,

1989), but the oldest definitive glacial deposit in the region is represented by the Labuma Till in southern Alberta. At Medicine Hat, this till overlies a gravel deposit containing tephra that was dated by fission-track analysis as 435 ka (Westgate et al., 1978). The last (Late Wisconsinian) ice sheet retreated from extreme northeast Alberta just 10 ka (Klassen, 1989).

The Interior Plains experienced up to eight distinct glacial advances and retreats, related to climatic fluctuations that began about 2 Ma (Fulton, 1989). The Laurentide ice sheet originating on the Canadian Shield entered Alberta from the northeast to converge at times with the Cordilleran ice flowing out from the Rocky Mountains in western Alberta.

Most Pleistocene sedimentation took place during periods of glacial retreat as the waning ice sheet deposited a blanket of heterogeneous sediment across the Alberta Plains. Lakes filled ice-scoured and moraine-dammed hollows. Many river channels were carved as spillways from the latter. Glacial drainage channels are clearly distinguished from the more mature pre-glacial river valleys, by their east to west orientation and narrow (less than 2 km wide) steep sided form. The erosive force of Pleistocene rivers was enhanced by relatively low base levels (Rutter, 1993, pers comm).

### **1.2.3 Local Stratigraphy and Geological History**

Figures 1.4 and 1.5 are structural cross-sections of the study area oriented parallel to the dip and strike of the basin respectively (locations shown on Figure 1.3). A stratigraphic table is presented as Table 1.1. The section is greatly condensed compared to other parts of the WSCB due to episodes of erosion represented by the major (basin-wide) unconformities.

Each unconformity represents a major time gap. The hiatus between the crystalline basement in the study area (estimated to have formed during the Lower Proterozoic Hudsonian orogeny 1900 Ma) and the overlying Middle Devonian is 1500 m.y. The Devonian to Mississippian section is largely conformable, but Pennsylvanian to Lower Cretaceous strata are absent representing a time span of 230 m.y. Finally Upper Cretaceous and Tertiary strata are absent so that glacial drift lies on the lowermost Upper Cretaceous. This unconformity therefore represents a hiatus of about 90 m.y.



During Elk Point time, the present study area occupied a position on the northern margin of a peninsula of bare Pre-Cambrian rock extending northeast into the epicontinental Devonian sea. This land mass was the surface expression of the Peace River Arch (PRA). The Arch also extended to the southwest of the study area merging with the Western Alberta Ridge, another major Devonian upland which formed the western margin of the Elk Point basin in central Alberta. The PRA was stripped of sediment during its pre-Devonian uplift, and the oldest Phanerozoic sediments in the study area, deposited directly on Pre-Cambrian basement, are the Lower Devonian Ernestina Lake - Cold Lake evaporites. These rocks are present only in the extreme northwest of the study area and represent the depositional edge of the Lower Elk Point basin to the north of the PRA.

In the early Middle Devonian a major transgression started and an irregular blanket of arkosic sandstone comprising reworked Pre-Cambrian regolith was deposited as the sea moved into the study area. This sand comprises the diachronous Granite Wash Fm. (younger arkosic sands shed from the Arch are also called Granite Wash). Anhydrites and shales of the Chinchaga - Contact Rapids Formations were deposited over the Granite Wash. By Keg River time the coastline had shifted to the southwest corner of the study area, and as the basin continued to subside through Devonian time, the coastline migrated progressively further west moving beyond the study area, inland, up the PRA peninsula.

Carbonate platforms with reefs, fringed the peninsula throughout the Devonian. The reefs are arranged like the steps of a staircase mounting the PRA, each older reef lying to the west of its predecessor. Two of these reefs are present in the study area: the Keg River reef (Middle Devonian) and the Slave Point reef (Upper Devonian). The reefs strike northwest, the Keg River reef lies across the centre of the study area and the younger Slave Point reef, separated from the Keg River by the Muskeg - Prairie Evaporite Fm. lies in the southwest corner. The reef margins are shown in plan view on the oil field location map (Figure 4.1), and the vertical relationship of these units is shown on the dip cross-section (Figure 1.4). The Granite Wash, Keg River and Slave Point Formations constitute the major Middle and lower Upper Devonian aquifers and are the main carrier and reservoir beds for petroleum in the study area.

Moving up through the succession (Table 1.1), the next major carbonate unit encountered is the Grosmont Fm. overlying the Waterways Fm. shales and limestones. The Grosmont carbonate platform is time equivalent to the upper part of the Ireton Fm. (see Figure 1.4).

The PRA land mass was a local source of clastics and most carbonate formations develop sandy facies at their onlap edge. Most carbonates are also dolomitized on the Arch. (The high sand content and dolomitization of carbonates both tend to enhance the permeability of strata in the PRA region). At intervals the PRA shed thick aprons of arkosic sandstone and conglomerate such as the Granite Wash and Gilwood formations into the basin which Cant (1988) regards as indicators of tectonic activity on the PRA. Granite Wash clastics fill tensional fault structures (grabens and half-grabens) which were active periodically during the Devonian. The youngest Paleozoic sediments in the study area are Mississippian clastics which subcrop the Cretaceous in the extreme southwest.

In Mississippian time the PRA collapsed. Major block faults west of the present study area are dated to this period. The Devonian arch became a depocentre in the Cretaceous limiting the northward progression of regressive sands in the foreland basin and accumulating an unusually thick Cretaceous sequence (Cant, 1988).

Subsequent to the emplacement of the Rocky Mountains in the Eocene, the basin was uplifted and eroded. In the study area lowlands, erosion has removed all Tertiary and Cretaceous sediments almost to the base of the Colorado shale (the Shaftesbury Fm. shown on the stratigraphic table).

An important local event which probably occurred during the Pleistocene glaciation was the erosion of Cretaceous strata in northeast Alberta with the consequent subaerial exposure of permeable Devonian strata. This event may have drastically altered the boundary conditions for subsurface flow, and established a pattern of lateral flow, causing the basin to drain along the unconformity towards the north and east as postulated by Tóth (1978). Tóth considered the exposure a relatively recent event, favouring Pleistocene, i.e., glacial erosion as the probable agent.

Figure 1.6 shows the area of outcropping Devonian strata adjacent to the study area. To the east, the Ireton and Waterways Formations are exposed along the Athabasca River some 125 km from the eastern study

area boundary. To the northeast a wider outcrop exposes the entire base of the Devonian System from the Grosmont Fm. in the west to the Keg River Fm. in the east, abutting against the Pre-Cambrian. Surface elevations for all Devonian outcrops along the rivers range from 266 to 210 m. The closest outcrop is lower Grosmont equivalent strata (Mikkwa Fm.) exposed about 25 km north of the northeastern quadrant of the study area.

Quaternary geologic literature (Klassen, 1989) indicates that exposure of the Devonian outcrop region (see Figure 1.6) occurred, at least in part, just 10,000 years ago. The narrow Devonian outcrop, the west and north trending channel of the present day Clearwater - Athabasca Rivers was a spillway carved when a glacial lake at 480 m elevation, drained north into a glacial lake situated in the Peace River valley. Lake Peace was itself situated in front of an ice lobe pushing southwest from Lake Athabasca. The ice lobe as depicted by Klassen matches perfectly, the size and orientation of the broad Devonian outcrop to the north of the study area. Of course the lobe may have filled a pre-existing depression and the broad outcrop may be much older, but the Clearwater Spillway seems firmly established as a 10 ka feature.

#### **1.2.4 Surficial Geology**

##### **1.2.4.1 Drift**

The thickness of Laurentide drift varies from zero in the northwest on the Buffalo Head Hills upland to over 200 m in pre-glacial buried channels. These channels therefore form a significant proportion of the total thickness of the section (see Figures 1.4 and 1.5). Figure 1.7 is a map of the structure on the bedrock below the drift constructed for the present study using depth to bedrock data from Alberta Research Council test holes and hydrogeological maps, Alberta Environment water well drillers reports, and Canadian Stratigraphic Services lithologs.

There are two large pre-glacial bedrock channels in the study area. The Misaw Channel, identified by Ceroici (1979), in a region to the south of the study area, clearly does extend across the study area to drain into the Peace River ancestral channel to the north as postulated by Hitchon et al., (1990). This channel has the orientation and morphology typical of the Tertiary drainage system (Klassen, 1989). The bedrock channels form

relatively permeable bodies cutting deeply into local Cretaceous shale. Since the channels also occupy topographic lows of the modern land surface they may focus discharge from units lower in the section as suggested by Hitchon et al. (1990).

#### **1.2.4.2 Bedrock Geology**

Figure 1.8 shows the bedrock geology in the study area. Because Cretaceous strata dip very gently to the southwest (approximately 0.5 m per km), formation boundaries are virtually parallel to topographic contours. Devonian strata which are truncated at the unconformity dip more steeply (approximately 4 m per km) to the southwest so that progressively older formations subcrop the Cretaceous eastward.

### **1.3 Hydrogeology**

#### **1.3.1 Topography and Climate**

Figure 1.9 is a physiographic map of the study area which is located between the Peace and Athabasca River valleys in an area classified as the Interior Plains physiographic region of Canada (Ceroici, 1979). The area comprises a central lowland plain the Loon River - Mikkwa Plain Lowland surrounded by uplands on three sides: the Buffalo Head Hills to the west, Birch Mountain to the east, and Trout Mountain straddling the border in the southeast.

The area lies within the MacKenzie River drainage system. The Loon and Panny rivers drain into the Wabasca River, itself a tributary of the Peace River which lies 60 km to the north. The ground surface elevation ranges from over 880 m (above mean sea level) in the northwest Buffalo Head Hills, to 320 m in the Wabasca River valley at the northern boundary of the study area. The Buffalo Head Hills have the greatest relief exhibiting a 400 m high northeast and east facing escarpment with slopes exceeding 90 m/km. Birch Mountain has gentler slopes of less than 10 m/km. Regional slopes from uplands beyond the limits of the study area (Clear Hills to the west and Caribou Mountain to the north) are more subdued. The average slope from the west is about 1.5 m/km, and from the north about 2.1 m/km. The Rocky Mountain Front Ranges, 500 km to the southwest rise abruptly to over 2500 m but it is probable that the very high potentials of groundwater at these elevations are spent in local flow systems in the

disturbed belt that effectively isolate the mountains from the basin (Hitchon, 1984, p.735).

The climate is characterized by short cool summers, cold snowy winters and 360 to 500 mm (14 to 20 inches) of precipitation annually. Air temperatures in Alberta are on average 3.3°C below ground temperatures and at Fort Vermillion, 63 km north of the northern edge of the study area, the mean annual air temperature is 1.3°C (Judge, 1973). The average ground temperature in the study area is therefore about 4°C. The northern part of the area is within the zone of discontinuous permafrost (Ozoray, unpublished).

### **1.3.2 Hydrostratigraphy**

For a hydrogeological study, lithostratigraphic formations are re-arranged by combination or subdivision into hydrostratigraphic units which behave as effective water transmitting or water retarding entities (Tóth, 1978, p.807-808). This is an important step since each hydrostratigraphic unit (HSU) is subsequently treated for most purposes as a vertically homogeneous stratum for which average values of various hydraulic parameters are assumed to be representative (see Section 3.1). Table 1.1 summarizes the major lithologies of the formations and shows their primary designations as aquifers or aquitards based on available core and DST permeability data (see Chapter 3). Thirteen formations are categorized as aquifers and ten as aquitards in the study area which overlie the Pre-Cambrian aquiclude.

Formations were assigned to HSUs exactly as in Tóth (1978), and are referred to here by lithostratigraphic unit names appropriate to their scale. Thus the Keg River and Granite Wash Formations (Tóth's D1 aquifer) are referred to as the Keg River Aquifer. In like manner the Slave Point and Watt Mountain Formations together with the intervening Fort Vermillion anhydrite (Tóth's D2 aquifer) is called the Slave Point Aquifer. The Grosmont, Winterburn, Wabamun and Basal Mannville sands (Bluesky and Gething Formations) are combined as the Upper Devonian-Basal Cretaceous Aquifer.

Subaerial exposure, weathering and erosion will have affected all three of these surfaces which probably significantly enhanced their permeability.

### **1.3.3 Previous Hydrogeological Work**

Three previous studies encompassed the present study area (see Figure 1.3). Tóth (1978, 1979, 1983) focussed on the evolution of flow in the Red Earth Region. Hitchon (1984) studied the evolution of the geothermal regime in relation to flow in the same area. The Red Earth region was itself encompassed by the hydrogeological investigation of the entire Peace River Arch area by Hitchon et al (1990).

Tóth resolved flow in the Red Earth region to the level of the hydrodynamic zone, defined as “a set of hydrogeologic units, in each member of which the energy and flow are subject to similar factors” (1978, p.835). Tóth discerned three distinct flow zones. A basal zone (below the Ireton and Beaverhill Lake shales) governing flow in the Keg River and Slave Point aquifers was interpreted as the decaying relict of a flow pattern adjusted to a Pliocene topography. A middle zone channelled recharge from the uplands (and also from the deeper transient zone) along the highly transmissive sub-Cretaceous unconformity to discharge at low elevation outcrops of the unconformity east and north of the study area. This zone was formed by the exposure of the unconformity during the Pleistocene. Finally Tóth recognized an upper zone comprising local and intermediate scale flow systems in Pleistocene, Upper and Lower Cretaceous aquifers at shallow depths. These discharged in local topographic hollows and also fed water downwards through Cretaceous shales to the middle zone.

Hitchon (1984) reasoned that topography-driven flow in the WCSB probably originated in the Eocene with the emplacement of the Rocky Mountains.

Hitchon et al., (1990) studied the hydrogeology of the entire Peace River Arch region - an area approximately four times as large as the Red Earth region (see Figure 1.3). They investigated basinal flow patterns as well as the hydrochemistry and geothermics of the region. Hitchon et al conclude that flow throughout the Phanerozoic section is topography driven. They argue that highly transmissive portions of the basin in regions of low topographic elevation produce observable drawdown in the deepest aquifers (i.e., across the Muskeg aquitard). Despite this postulated drawdown affect, few other physicochemical features are attributed to flow. Salinity is considered to be temperature (i.e., depth) dependent, or

due to localized halite dissolution. The northward increase in geothermal gradient is attributed to a northward increase in basement heat flow or to variations in the thickness of sedimentary cover, and the geothermal regime, notwithstanding Hitchon's earlier perceptions (Hitchon, 1984), is judged to be conductive.

## **1.4 Petroleum Geology and Timing of Oil Migration**

### **1.4.1 Regional Petroleum Geology**

The Late Cretaceous was the time of maximum burial of source rocks in the basin and it is generally agreed that petroleum migration started at this time (e.g., Deroo et al., 1977, p.110). Allan and Creaney (1989) state that all source rocks in the basin reached peak maturity in a 20 m.y. period beginning about 60 Ma. The conventional view of migration is that the tilting of the basin during the Laramide Orogeny (during Late Cretaceous to Paleocene time) buried source rocks sufficiently deeply for them to gain maturity, and simultaneously supplied the northeasterly up-dip gradient for buoyancy driven migration (Podruski et al., 1987). Accumulations formed in structural closures and permeability pinch outs to the east. Where pathways of continuous permeability existed, oil migrated great distances laterally e.g., 400 km for the Viking Fm. oils in Saskatchewan (Allan et al., 1991). Although most sources agree oil generation started in the Late Cretaceous, the duration of migration is more contentious. Some authors believe migration was very rapid and that accumulations such as the Athabasca super giant bitumen deposit at the eastern basin edge formed during late Cretaceous or early Tertiary time (Mike Ranger pers. comm., 1992). Others believe long distance migration continued throughout the Tertiary over a period of some 50 m.y. (e.g., Jones, 1980; Garven, 1989).

### **1.4.2 Local Petroleum Geology**

Important conventional oil reservoirs within the study area are the Granite Wash, Keg River and Slave Point Formations. The Gilwood Member (age equivalent to the Watt Mountain Fm.) is the reservoir rock at the Nipisi and Utikuma fields just south of the study area. Free gas is produced from the Grosmont Fm. and contiguous Lower Mannville sands at the Liege field part of which extends into the southeast corner of the

study area. The oil field locations, distinguished by their respective reservoir rocks are shown in Figure 4.1.

Allan and Creaney (1989) present geochemical evidence that the oil in Middle Devonian reservoirs in the Peace River Arch (PRA) region was sourced from the Upper Devonian Duvernay shale which is mature on the south side of the PRA southwest of the study area. The Duvernay equivalent Muskwa Fm. may be an effective source rock north of the PRA. Allan and Creaney (1989) argue that the oil was expelled downwards (across the Beaverhill Lake Gp. shales and limestones) into the Slave Point Fm. and was thence driven by buoyancy updip to the northeast. Because of the regional basin dip, the Duvernay Fm. in the southwest is at a lower elevation than the older (Slave Point, Keg River and Granite Wash Fm.) reservoir rocks to the northeast. This structurally up, stratigraphically downward migration path is illustrated diagrammatically in Figure 1.10.

Piggot and Lines (1991) pointed out an anomaly in Allan and Creaney's conceptualization in that the Duvernay Fm., a relatively deep water facies, is absent over the PRA. If petroleum migration in this area were driven purely by buoyancy there would be a "shadow zone of no-charge" to the northeast (up-dip) along the axis of the Arch which is precisely where the oil fields in the present study area occur. Figure 1.11 taken from Piggot and Lines (1990, Figure 8) shows the location of the "shadow zone" updip from the region of non-deposition of source rock. Figure 1.12 is a structural cross-section across the PRA parallel to basin strike (Wright, 1984). The source rock clearly pinches out over the PRA which has little relief at the present day because the "arch" has been a negative structural feature since its collapse in the Mississippian (Cant, 1988).

Piggot and Lines suggest that oil migration was deflected to the north and oil was driven into the "shadow zone", by a postulated permeability barrier (a transition from dolomite to limestone) in the Slave Point Fm. Figure 1.11 illustrates the proposed migration path in the PRA region and shows the belt of Slave Point dolomite around the PRA.

Since Piggot and Lines suggest enhanced permeability of strata on and around the PRA as the cause of the migration pattern, they presumably invoke a capillary gradient (see Section 2.1.2.2) sufficient to overcome the buoyant forces which would have driven the oil updip to the northeast.



Such a gradient would require a *progressive* increase in pore diameters all the way along the proposed migration path. The dolomitization of carbonates fringing the PRA would be unlikely to produce this effect, and no evidence was presented to indicate that such a trend actually exists. Clearly hydrostatic migration models relying on either buoyant or capillary forces have serious difficulties in explaining the presence of petroleum in the present study area.

In order to evaluate the possible effect of fluid dynamics on petroleum migration in the PRA region it is necessary to consider in detail the concepts and principles on which petroleum migration models are based. These matters are dealt with in Chapter 2.

## **Chapter 2 The Hydrogeological Characterization of Oil Fields - Concepts and Principles**

The generation, migration and accumulation of petroleum are complex processes that occur in the deep subsurface on a geological time scale. The publication "Problems of Petroleum Migration" (Roberts and Cordell eds., 1980) provides examples of the diverse and often opposed ideas that exist concerning petroleum migration. Roberts notes in the introduction to this volume, that the processes dominating migration probably vary with space and time given the range of environments in which migration occurs and the changes which a sedimentary basin undergoes during its evolution. This point is exemplified by the contrast between the physical environments in geologically mature and immature sedimentary basins.

The soft sediments in a young submarine basin consolidate as they are buried. The porosity of these strata are thereby reduced, water being driven from the strata compacting at the highest rate (usually shales) and flowing out of the basin through the strata less prone to compaction (sandstones). When loading is rapid, compaction disequilibrium in poorly permeable mud rocks is common. Here the rate of pressure production (the stress imposed by the loading) exceeds its dissipation by flow and enormous fluid pressures are generated in 'geo-pressured' regions where the pore fluids temporarily assume the weight of the entire overburden. Such regions are inherently unstable. Over time the geo-pressured fluid moves out of the shales, transferring the weight of the solid overburden to the matrix. During the transitional period, the flow regime will be in a transient state controlled by the changing distribution of centres of compaction. Such a scenario contrasts strongly with the proceedings in a mature basin.

The basin is composed of rigid, fully compacted strata. Water saturates the interconnected pores of the basin sediments forming a hydraulic continuum from within a few metres below the ground surface to the crystalline basement. The basin has been uplifted above sea level and erosion has carved topographic relief on the land surface. The upper surface of the fluid saturated porous framework of the basin, the water table, follows the contours of the ground surface and where it is high in

upland recharge zones cool meteoric water enters the basin. This water and the connate water in the sediments, circulate slowly through and across the porous strata, the motion perpetually maintained by precipitation from the atmosphere, to emerge warm and salty in lowland discharge areas. Flow within the basin will tend to a steady pattern adjusted to the shape of the water table and modified locally by the geometry of juxtaposed resistant and conductive strata.

Petroleum may be generated in both mature and immature basins. It is unreasonable to suppose, given the contrasting fluid flow regimes, that a single approach to petroleum migration will suit both cases. The present research project is concerned with the role played by flowing water on petroleum migration and accumulation in a part of the WCSB, a geologically mature basin which developed the broad outline of its present geometry and structure, during the Eocene Period some 50 million years ago. This chapter begins by considering the forces which drive and arrest the movement of petroleum and proceeds to outline existing conventional and hydraulic migration theories. Finally the various observable physical and chemical parameters which may be used to evaluate conventional and hydraulic migration models are introduced and critically evaluated.

## **2.1 Modes and Forces in Petroleum Migration and Accumulation**

Excepting biogenic gas, generated only at very shallow depths, petroleum originates from the thermal degradation of kerogen in organic rich shales and fine grained carbonate source rocks. Time and temperature are the main variables that control kerogen maturation, whereas the type of petroleum generated (oil, wet or dry gas) depends on both the chemical composition of the source rock, and its maturation level (Tissot and Welte, 1978).

### **2.1.1 Petroleum Modes**

Oil migrates mainly as an immiscible phase. This fact is suggested by our understanding of the maturation of source rocks which generate hydrocarbons as petroleum-phase liquids. The clinching argument against aqueous phase oil migration is that crude oil as we find it in oil pools is deficient in water soluble hydrocarbons. In other words, an aqueous precipitate of those components of petroleum that are appreciably soluble

under the physical conditions which prevail in sedimentary basins, would be quite unlike any known crude oil (McAuliffe, 1980). In an aqueous transport scenario, some alternative agency would be required to transport the insoluble petroleum components and to deposit them at the precipitation site. Oil is generated, oil is found: it is reasonable to presume that oil migrates. Gas transport in aqueous solution may be more important, since low molecular weight hydrocarbons are relatively soluble in water and the chemistry of an aqueous precipitate of methane (for example) would match what we observe in gas pools.

Illing (1933) introduced the terms primary and secondary migration in recognition of the distinct processes that govern the expulsion of petroleum from fine grained source rocks (primary migration) and its subsequent long distance transport through coarse grained water-wet carrier beds to the site of accumulation (secondary migration). The problems associated with primary migration are outside the scope of this study. For secondary migration, petroleum in a permeable carrier bed (introduced by whatever means) is subject to a number of forces that drive it inexorably toward regions of energy minima from which it cannot escape and which constitute by definition petroleum traps.

### **2.1.2 Forces of Migration and Accumulation**

Three forces are recognized that affect the movement of petroleum in a water wet environment. The interplay between these forces governs petroleum migration and accumulation. The forces are:

- 1) a buoyant force proportional to the density contrast between the petroleum and the water and also to the vertical extent of the petroleum phase, that drives petroleum upwards;*
- 2) a capillary force proportional to the interfacial tension between water and petroleum that drives oil in a water wet medium into the largest interstices available and resists its movement through pore constrictions;*
- 3) a hydraulic force determined by the hydraulic head distribution which drives petroleum in the direction of the negative hydraulic gradient. This direction is often subparallel to aquifer bedding.*

### **2.1.2.1 The Buoyant Force**

A buoyant pressure  $P_b$  exists within a continuous petroleum column in excess of the fluid pressure in ambient water. This pressure is proportional to the density deficit between the immiscible fluids and to the vertical extent (i.e, height) of the continuous petroleum volume (Berg, 1975; Schowalter, 1979). Gas columns develop greater buoyant pressures than oil columns of the same height because gas is less dense than oil. Within a continuous petroleum column, buoyant pressure increases with height and is a maximum at the top of the column. Bethke et al., (1991), formulate the buoyant force relevant to migration ( $E_b$ ), as that component of the total buoyant force acting in a direction parallel to the aquifer dip which is expressed in units of kPa/m (or force per unit volume) as:

$$E_b = - \text{grad } z * g (\rho_w - \rho_p), \quad (2.1)$$

where  $\text{grad } z$  is the the slope of the top of the aquifer,  $g$  is the gravity constant in  $\text{m/s}^2$ ,  $\rho_w$  is the point density of water in  $10^3 \text{ kg/m}^3$  and  $\rho_p$  the point density of the petroleum phase in  $10^3 \text{ kg/m}^3$ . The force is oriented in the direction of the maximum decrease in elevation (i.e., updip).

### **2.1.2.2 The Capillary Force**

Capillary pressures exist when immiscible fluids with differing interfacial tensions coexist in a porous rock. Capillary pressure may be envisaged as a squeezing pressure exerted by the wetting phase (usually water) on the non-wetting oil or gas causing the pressure in the petroleum phase to exceed that in the ambient water. The squeezing pressure drives petroleum volumes into large pores and fractures and resists their movement through constrictions such as pore throats. Fine grained rocks have relatively high capillary pressures and this pressure difference works to prevent petroleum moving from coarser to finer grained strata. Hence capillary forces may cause petroleum entrapment. Capillary pressures are directly proportional to the difference in interfacial tension between the petroleum phase and water (Berg, 1975) which are higher for gas than for oil (North, 1985). The pressure  $P_p$  on a petroleum (oil or gas) volume in a porous rock generally exceeds the water pressure  $P$  by the capillary

pressure  $P_c$  so that  $P_p = P + P_c$ . The capillary force ( $E_c$ ) may be expressed, again in units of force per unit volume as (Bethke et al, 1991):

$$E_c = - \text{grad } P_c. \quad (2.2)$$

### 2.1.2.3 The Hydrodynamic Force

In a region of active flow, a third (hydrodynamic) force acting on petroleum must be considered. To understand this force, a brief excursion into the physics of groundwater flow is required.

#### *Hydraulic Head Defined*

At the outset, it is necessary to define hydraulic head since it is fundamental to the following discussion. The fresh water equivalent hydraulic head ( $h$ ) is simply the elevation (relative to a common datum such as mean sea level), at which a column of fresh water would stand, in an open pipe sunk from the ground surface, to a depth of interest in the subsurface. In physical terms, hydraulic head, is the mechanical energy per unit weight of fluid, defined by Hubbert (1940) as:

$$h = \frac{P}{\rho_o g} + z \quad (2.3)$$

where  $P$  is the fluid pressure in kPa,  $\rho_o g$ , the specific weight of fresh water in kPa/m and  $z$  the elevation in m of the point of interest. Use of these units yields hydraulic head in metres.

The significance of head for flow through porous media was established by a French engineer named Henri Darcy. Darcy (1856) packed a pipe with sand and connected the upper end of this vertical column to a tap and the lower end to a large measuring basin. Water was forced through the sand in the pipe at various steady flow rates. The hydraulic head of the flowing water was measured in U-tubes inserted into the column, one near the inflow end and the other near the outflow (see Figure 2.1). Darcy observed that as the steady flow rate through the column was increased there was a proportional increase in the difference between the water levels in the tubes (i.e., an increased hydraulic head gradient),

demonstrating that the hydraulic head gradient is a measure of the driving force for flow.

### *Darcy's Law*

The driving forces that determine the motion of water through a porous medium are expressed by Darcy's Law which indicates the volume of water passing across a unit area of rock per unit time, known as the flux or specific discharge. In its most general form (Bear, 1972; de Marsily, 1986) Darcy's Law, can be written as:

$$\mathbf{q} = -\frac{k}{\mu_w} (\mathbf{grad} P + \rho_w g \mathbf{grad} z). \quad (2.4)$$

The dimensions of flux are usually given as those of velocity i.e., length per unit time although the vector  $\mathbf{q}$  actually indicates the direction and the rate of flow in terms of volume discharge per unit area of porous medium. The average linear velocity is the flux divided by the porosity of the medium. In Equation 2.4, the bracketed terms indicate the driving force and the resulting flux is proportional to term  $k/\mu_w$ . A concise description of the relations embodied in this general formulation of Darcy's Law is given by Hanor (1987).

Mathematically, the driving force for flow in this formulation is the resultant of the vector sum:  $(-\mathbf{grad} P) + (-\rho_w g \mathbf{grad} z)$ . The orientation of the driving force therefore depends on the relative magnitudes of the component vectors, and the orientation of the pressure gradient. Figure 2.2 is a vector diagram illustrating these twin components of the driving force.

Resistance to the driving force depends on properties of both the rock and the fluid, which are expressed in the equation above by the term  $k/\mu_w$ . Flux is thus proportional to the intrinsic permeability ( $k$ ) of the rock (see Appendix 1) and is inversely proportional to the dynamic viscosity ( $\mu_w$ ) of the water.

Different rock types have characteristic ranges of permeability and most rocks are anisotropic with respect to permeability (the permeability is usually greatest parallel to bedding). For a given rock, the flux will be greatest if the driving force is oriented in the direction of the maximum permeability. Water viscosity increases with increasing salinity and

decreasing temperature. A given rock will transmit more fresh water than brine and more warm water than cold.

***Lateral and Vertical Fluid Flux***

Hubbert (1940) formulated Darcy's Law with the driving force expressed in terms of the freshwater equivalent hydraulic head gradient. From Equation 2.3:

$$\mathbf{grad} h = \frac{1}{\rho_o g} \mathbf{grad} P + \mathbf{grad} z, \quad (2.5.1)$$

where  $\rho_o$  is the density of freshwater. This equation can be rearranged as:

$$\frac{1}{\rho_o g} \mathbf{grad} P = \mathbf{grad} h - \mathbf{grad} z. \quad (2.5.2)$$

To express Darcy's Law in terms of the freshwater hydraulic head gradient, Equation 2.4 is treated thus:

$$\mathbf{q} = -\frac{k}{\mu_w} \left( \mathbf{grad} P + \rho_w g \mathbf{grad} z \right) * \frac{\rho_o g}{\rho_o g}, \quad (2.6.1)$$

giving:

$$\mathbf{q} = -\frac{k \rho_o g}{\mu_w} \left( \frac{1}{\rho_o g} \mathbf{grad} P + \frac{\rho_w}{\rho_o} \mathbf{grad} z \right). \quad (2.6.2)$$

Substituting Equation 2.5.2 into Equation 2.6.2, yields:

$$\mathbf{q} = -\frac{k \rho_o g}{\mu_w} \left( \mathbf{grad} h - \mathbf{grad} z + \frac{\rho_w}{\rho_o} \mathbf{grad} z \right). \quad (2.6.3)$$

which can be rearranged as:

$$\mathbf{q} = -\frac{k \rho_o g}{\mu_w} \left( \mathbf{grad} h + \mathbf{grad} z \left( \frac{\rho_w}{\rho_o} - 1 \right) \right). \quad (2.6.4)$$



Substituting the hydraulic conductivity (Equation 2.7) into Equation 2.6.4 yields the general form of Darcy's Law in terms of hydraulic head:

$$\mathbf{q} = - K \left( \text{grad } h + \text{grad } z \left( \frac{\rho_w}{\rho_o} - 1 \right) \right). \quad (2.6.5)$$

where the hydraulic conductivity tensor ( $K$ ) as defined by Hubbert (1940) is:

$$K = \frac{k \rho_o g}{\mu_w}. \quad (2.7)$$

An advantage of expressing the flux in terms of hydraulic head, the negative gradient of which now indicates the driving force, is that because head is a scalar quantity,  $h$  values calculated from pressures measured in a common aquifer, can be contoured to produce a map of the driving force distribution.

For confined, horizontal aquifers with horizontal flow, hydraulic head maps constitute potentiometric surfaces (Freeze and Cherry, 1979), which indicate the driving force for the lateral flow of water in an aquifer. When such aquifers are isotropic, flow will be orthogonal to hydraulic head contours, in the direction of decreasing head. Anisotropy in the plane of the potentiometric surface will refract flow towards the axis of maximum permeability. For inclined aquifers with heterogeneous (i.e., variable salinity) formation water, buoyant forces must be considered in addition to the hydraulic head distribution. Equation 2.6.5 is used in Chapter 4 to evaluate the effect of buoyant forces on water flow in the Keg River Aquifer.

Equation 2.6.2 can be used to calculate vertical flow rates when the vertical pressure gradient and vertical conductivity ( $K_v$ ) are known. Substituting Equation 2.7 into 2.6.2 gives:

$$\mathbf{q} = - K \left( \frac{1}{\rho_o g} \text{grad } P + \frac{\rho_w}{\rho_o} \text{grad } z \right). \quad (2.8)$$

Now, in the vertical plane:

$$K = K_z = K_v; \quad \text{grad } P = \frac{\partial P}{\partial z}; \quad \text{grad } z = \frac{\partial z}{\partial z} = 1. \quad (2.9)$$

Substituting these terms into Equation 2.8 yields the vertical flow component:

$$q_z = -K_z \left( \frac{1}{\rho_o g} \frac{\partial P}{\partial z} + \frac{\rho_w}{\rho_o} \right). \quad (2.10)$$

where  $\rho_w$  represents the density of the water at the point. This equation is used in Chapter 4 to estimate vertical flux in the study area. The relevant forms of Darcy's Law for inclined, horizontal and vertical flow are included in Figure 2.3.1. In each case the specific discharge 'q' (volume discharge per unit area of aquifer) can be converted to an average linear flow velocity 'v' through dividing by the porosity, i.e.

$$v = \left( \frac{q}{n} \right). \quad (2.11)$$

The driving force for water ( $E_w$ ) can be expressed in the same units (pressure per unit length) as the buoyant and capillary forces described earlier, by using the negative gradient of the hydraulic head distribution multiplied by the gravity constant (Hubbert, 1940):

$$E_w = -g \text{ grad } h = -\text{grad } \Phi = g - \frac{\text{grad } P}{\rho_o}, \quad (2.12)$$

A graphical representation of the fourth equality in Equation 2.12 is shown as Figure 2.3.2 (a).

### ***Hubbert's Hydrodynamic Driving Force for Oil***

Having established a formulation of the driving force for water, Hubbert then demonstrated that the motive force for petroleum migration (assuming small volumes of oil) can be expressed in the same terms. Thus the hydrodynamic force for oil migration ( $E_h$ ) is expressed in units of pressure per length as (Hubbert, 1953, Equation 41):

$$E_h = g + \frac{\rho_w}{\rho_p} (E_w - g), \quad (2.13)$$

where  $\rho_w$  is the water density and  $\rho_p$  the density of oil (or gas). A graphical representation of this equation for oil and for gas is shown in Figure 2.3.2 (b).

Hubbert's use of the gradient of hydraulic head as the driving force for flow is problematic for variable density brines (Hubbert, 1940; Bear, 1972; Davies, 1987; Hanor, 1987) such as are found in the Keg River aquifer in the present study area. The problem of inferring flow from the hydraulic head distribution when salinity related density variations exist is addressed in Section 4.2.1.1.

#### **2.1.2.4 Summary of Driving Forces For Oil Migration**

Combining Equations (2.1), (2.2) and (2.13), yields a total driving force for petroleum migration ( $E_p$ ) which accounts for the buoyant, capillary and hydrodynamic forces:

$$E_p = E_b + E_c + E_h, \quad (2.14)$$

Buoyancy impels oil (or gas) droplets, slugs or stringers upwards, displacing water from the rock pores. This upward drive is modified by capillary forces which assist petroleum migration into larger pores or fractures and resist its movement into smaller ones. Hydrodynamic forces, often directed parallel to bedding in aquifers due to flow refraction from subjacent aquitards (Hubbert, 1953), impel petroleum laterally in the direction of the water flow path. Petroleum migration stops and

entrapment occurs where buoyant, hydrodynamic and capillary forces are balanced.

Advances in geochemical techniques of source rock - reservoir oil correlation over the last decade provide unequivocal evidence of long-distance migration (e.g., Creaney et al., 1990). In cases where reservoir oils have been correlated with specific source rocks, such as in the present study area, possible migration paths are constrained which assists in the determination of the relative importance of the three forces discussed in this section. Conventional migration theories, as discussed in the following section, routinely ignore the hydrodynamic force, assuming hydrostatic conditions.

## **2.2 Conventional Theories of Petroleum Migration**

### **2.2.1 The Anticlinal Theory and the Structural Trap**

The first published account of the Anticlinal Theory was by a Geological Survey of Canada chemist (Hunt, 1861, 1862). Hunt observed that since petroleum liquids are usually lighter than water, buoyant segregation of oil and gas in water wet rocks should cause petroleum to accumulate in anticlinal apices where a reservoir rock is overlain by a fine grained cap rock. The modern concept of a structural trap has been broadened to include fault bounded reservoirs and oil pools associated with salt domes. The underlying rationale is unchanged: buoyancy causes petroleum to seek the highest structural elevation of the reservoir rock and capillary forces in small pore throats of the cap rock prevent continued upward migration thereby forming the trap. Howell (1934) gives a detailed review of the historical development of the concept of the structural trap.

### **2.2.2 The Stratigraphic Trap**

Levorsen (1936) recognized a stratigraphic component in many North American oil traps. Permeability reductions due to facies changes in carrier beds may create lateral capillary barriers forming oil or gas pools independent of antiform structure. Sandstone pinch-outs, carbonate reefs and unconformity truncations subsequently became common exploration targets and lithofacies analysis became a standard exploration tool.

### **2.2.3 Summary of Conventional Theories**

The structural and stratigraphic accumulation theories remain the foundation of modern petroleum exploration (Osadetz, 1989). Correspondingly exploration is in fact a search for reservoir rocks and geologic configurations that would trap oil in a hydrostatic environment. Explorationists have traditionally paid scant attention to the character and dynamics of the pore water within which petroleum migrates. Hubbert (1965) provides an interesting historical review of the history of petroleum exploration in North America, documenting with bewilderment and frustration the persistence with which hydrodynamics is ignored by North American petroleum geologists.

In the following section, the historical evolution of concepts concerning the movement of water in sedimentary basins is outlined. The application of these concepts to petroleum transport in hydraulic theories of petroleum migration, is then described.

## **2.3 Hydraulic Theories of Petroleum Migration**

### **2.3.1 The Historical Evolution of Hydraulic Theories of Petroleum Migration**

#### **2.3.1.1 Concepts of Topography-Driven Flow**

Two early field studies in the nineteenth century established the basis for categorizing groundwater flow under confined and unconfined conditions. Many years passed before these concepts were applied to petroleum migration. Domenico and Schwartz (1990, p.242-255) give a concise review of the historical development of concepts of topography-driven flow.

#### ***King (Unconfined Flow)***

King (1899) recognized that the water table is everywhere a subdued replica of the ground surface, and stated that shallow groundwater flows from upland areas to lowlands. Upland areas are drained and water is discharged in the lowlands. Flow is driven by elevation differences of the water table acting through a hydraulically continuous medium. Topographic irregularities influence flow directions in underlying aquifers and the maximum and minimum heads within a basin are fixed by the

maximum and minimum elevation of the water table. Without continuous replenishment by the infiltration of precipitation the water table would become flat and flow would cease.

***Chamberlin (Confined Flow)***

Chamberlin (1885) believed flow within dipping aquifers confined by poorly permeable beds was driven by the hydrostatic pressure generated by the weight of water up-dip. Water enters the aquifer at a high elevation outcrop and moves along the aquifer down the dip, to discharge either at a low elevation outcrop, or if the aquifer pinches out at depth, by cross-formational leakage through the confining beds. Perfectly confined aquifers exhibit unidirectional flow, parallel to the aquifer bedding, and overlying topographic irregularities cannot affect flow directions within the aquifer. The highest and lowest outcrop elevations determine the hydraulic head limits in the aquifer. As in King's conceptualization, the ultimate drive for flow is a sloping water table maintained by infiltrating precipitation.

***Hubbert (Fluid Potential)***

Hubbert - the "father of hydrodynamics" - quantified topography-driven flow recognizing hydraulic head as a measure of the fluid potential (Hubbert, 1940). He showed that fluids move from regions of high to regions of low potential. The field of force representable by the distribution of hydraulic head, was linked to the field of flow through Darcy's Law. Hubbert constructed flow nets as graphical representations of flow patterns, and gave a good explanation of the tangent law which governs flow line refraction at the boundaries of units of differing permeability. From the hydraulic viewpoint, he failed to appreciate the effect that local topographic relief exerts upon patterns of subsurface flow, and like Chamberlin (1885), Hubbert conceived of flow as essentially confined.

***Tóth (Regionally Unconfined Flow)***

Tóth recognized that the actuality of one or the other of the two contrasting views of subsurface flow depended on the degree of confinement. Ideal confinement (i.e., zero permeability), if it occurs at all, is exceedingly rare. Brace (1980) measured significant permeability in

crystalline and argillaceous rocks and concluded that average crustal permeability is around 10 millidarcies. Neuzil (1985) states that "...no properly tested geologic media have proved to be entirely impermeable", and notes that modern techniques and increasingly sophisticated instruments are allowing the determination of permeability in laboratory and field tests in progressively 'tighter' media. Tóth (1972) argues that since all sedimentary rocks exhibit finite permeability, sedimentary basins must function over geologic time as regions of hydraulic continuity. Tóth coined the phrase *regionally unconfined flow* to describe the nature of flow in a basin with hydraulic continuity.

Tóth's pioneering early work (1962, 1963) involved the mathematical formulation of the problem of groundwater flow in a small drainage basin. He modelled flow in a rectangular area representing a cross-section through a shallow sedimentary basin and determined that the topographic relief of the water table generates complex flow patterns that extend throughout a region of hydraulic continuity.

Tóth recognized that all flow patterns were composed of *flow systems*, each comprising an inflow region at high elevation where water recharges the basin, and a low elevation outflow region where water is discharged. Flow systems are of different scale: *local systems* that recharge and discharge at adjacent topographic highs and lows; *intermediate systems* with one or more topographic highs between their recharge and discharge sites; and *regional systems* that recharge at the topographically highest and discharge at the topographically lowest points on the ground surface. Fluids move vertically (cross-formationally) in recharge and discharge regions and laterally in the intervening hinge or mid line areas. Hydraulic gradients are steepest and flow rates highest in local flow systems which are restricted to shallow depths. Deeper regional scale systems are more sluggish since the potential energy derived from the slope of the water table is dissipated in transporting the water along its longer flow path, especially cross-formational flow across aquitards.

Tóth's results had important implications for flow in stratified basins even though his early work considered only homogeneous, isotropic media. Shallow aquifers within the depth range of local and intermediate scale flow systems would exhibit multiple complex flow directions and fluids should be transported between aquifers by cross-formational flow across

intervening aquitards. Deeper aquifers as the conduits for regional scale flow systems would exhibit more uniform flow rates and directions at more sluggish rates.

***Freeze and Witherspoon (Numerical Modeling)***

Topography driven flow patterns in stratified sequences were studied by Freeze and Witherspoon (1966, 1967) who investigated, through numerical modeling, the effects of flow line refraction at the boundaries of units of different permeability. This work confirmed the regionally unconfined nature of flow on a basinal scale.

**2.3.1.2 Hydraulic Theories of Petroleum Migration**

Progressively sophisticated hydraulic theories of petroleum migration were conceived as concepts of basin hydraulics developed.

***Munn***

Although apparently unaware of King and Chamberlin's ideas, Munn was an early proponent of moving subsurface water as the agent of petroleum migration. Munn's Hydraulic Theory (1909) recognized that all sedimentary rocks are permeable to water and advocated the cross-formational flow of water through shales. He conceived of water currents driven by capillarity, pushing petroleum ahead with accumulations forming where these currents converged. However, the debate was hopelessly bogged down with misconceptions about the hydrology of sedimentary basins - for example both Munn and his detractors believed that sedimentary basins were largely dry i.e., that many subsurface strata were unsaturated with fluid. Munn's theory also lacked a distributed driving force for water movement, and without this was of no practical value in the search for oil or the elucidation of real water flow patterns. It did however gain a number of adherents and stimulated a novel line of research in petroleum geology.

***Rich***

Rich's Hydraulic Theory (1921) had considerable predictive capabilities. Assuming confined flow conditions, Rich envisaged oil migration driven by the unidirectional movement of water along permeable aquifers on a basinal scale, establishing the concept of the long distance



carrier bed. Rich gave accurate qualitative descriptions of many of the effects that flowing water must exert upon petroleum accumulation which were at variance with the predictions of the Anticlinal Theory. In regions of strong lateral water flow he predicted tilted oil-water contacts and pools offset along structural culminations in the downstream direction.

The notion of stable petroleum accumulations in dynamic equilibrium with moving water greatly increased the range of potentially favourable geologic structures. Under the right flow conditions, unclosed structural flexures such as terraces on monoclines were as likely to contain oil as arches or domes. Moreover, fully closed structures would not contain petroleum at all if hydraulic currents were sufficiently strong to ‘flush’ them out. Rich also noted the potential of flowing water to improve or reduce trap capacity in the manner developed by Schowalter (1979) fifty years later. Considering the effect of the vertical sense of water flow on a stratigraphic trap Rich reasoned as follows: upward flow in a dipping aquifer acting in concert with the buoyant force of accumulating oil or gas would cause a given capillary barrier (e.g. a lateral grain size reduction) to leak petroleum when the pool was relatively small; downward water flow at the same location, would oppose the upward buoyant force allowing a much larger pool to be trapped.

### ***Hubbert***

Hubbert’s classic 1953 paper “Entrapment of Petroleum Under Hydrodynamic Conditions” describes the combined effect of hydraulic, buoyant and a capillary forces on the migration and accumulation of small volumes of oil and gas within a geologic framework. Hubbert showed that since fluids of different density (water, oil and gas) have distinct fluid potentials they are driven in different directions in a non-uniform potential energy field to distinct accumulation sites, contrary to the predictions of the Anticlinal Theory.

Hubbert devised a method (the so-called “UVZ method”, fully described in Section 4.2.1.2) for the quantitative determination of theoretical accumulation sites for petroleum in a dynamic flow field. Hubbert conceived of petroleum migrating as discrete bubble-like volumes and failed to evaluate the buoyant force that develops at the top of a

vertically extensive petroleum column which is now recognized as a potent force for migration (e.g. Berg, 1975; Tissot and Welte, 1978, p.349).

### ***Tóth - the Generalized Hydraulic Theory***

In 1980 after some 20 years of research in basin hydraulics Tóth published the Generalized Hydraulic Theory (GHT). The GHT is based on three successive conceptual steps:

- 1. Geologically mature sedimentary basins function as regions of hydraulic continuity.*
- 2. Groundwater flow systems develop, driven by elevation differences of the water table and modified by the permeability distribution, which may be of local, intermediate or regional extent.*
- 3. Hydrocarbons are mobilized, transported and deposited by groundwater as it moves along well-constrained flow paths.*

The GHT recognizes buoyancy as a driving force for petroleum phase migration and the high capillary pressures associated with the pore constrictions in fine grained strata as a retarding force which may cause accumulations to form. Fluid flow as explained below may act as an agent of petroleum transport and under certain conditions as an agent of concentration, confinement and accumulation. As for all useful scientific theories, postulates can be made on the basis of the GHT which can be tested against observed natural conditions.

### **2.3.2 Hydraulically Favoured Petroleum Accumulation Sites**

The GHT, adopting the concept of regionally unconfined flow differs from earlier hydraulic theories. Three favourable potential petroleum accumulation settings are postulated.

Firstly hydrodynamic traps in regions of lateral flow identical to those envisaged in the confined flow models of Rich and Hubbert. Hubbert's UVZ method (Section 4.2.1.2) outlines potential hydrodynamic trap locations for petroleum of a specified density within the limits of confidence in the geological structure and the fluid potential distribution. Secondly, a concept unique to the GHT is the hydraulic trap. Hydraulic traps form in stagnant and quasi-stagnant regions where flow paths are converging or abruptly changing direction, and flow rates are sluggish. Oil or gas pools in hydraulic traps can be identified only through flow analysis

since they may have no geological expression. Hydraulic traps may be identified on potentiometric surface maps and hydraulic cross-sections. Thirdly, *discharge zones* are generally favourable. Fluids converge within discharge zones after draining large volumes of rock so they may serve as natural focal mechanisms for concentrating petroleum. Hydrocarbons will be separated from the ascending water as it is driven cross-formationally through fine grained strata which function as capillary barriers. The variety of hydraulically favoured potential accumulation sites are shown in Figure 2.4.

## **2.4 The Concept of Hydrogeological Indicators of Petroleum Accumulations**

Within a geologically mature basin under a stable water table configuration, a steady state flow field will develop, constraining basin fluids to move along fixed flow paths. As water moves through the basin, its character changes. When such changes are caused primarily by flow, different regions of a flow field may develop distinctive physical and chemical fluid properties. Favourable sites for hydrocarbon accumulation are restricted as described in Section 2.3.2 (stagnant or quasi-stagnant regions and discharge zones). If the properties of water in these areas should differ from those of other parts of the flow field, such properties may be used as evidence of petroleum deposits. In the present study (Section 4.2) water pressure, water temperature and water chemistry are considered as potential indicators of petroleum accumulation sites.

### **2.4.1 Hydrogeological Characteristics**

The interpretive term “hydrogeological characteristics” is used to describe the physicochemical properties displayed by water that are caused by evolutionary trends along flow paths which override the particulars of stratigraphy and lithology. If, for instance, waters from two recharge areas of contrasting lithology are demonstrated to have features in common which distinguish them from waters in discharge areas, then the features which distinguish the recharge waters from the discharge waters may be described as hydrogeological characteristics.

### **2.4.2 Hydrogeological Indicators of Petroleum Accumulations**

Two general types of hydrogeological indicators of petroleum deposits are recognized, direct and indirect (Tóth, 1984, 1988).

#### ***2.4.2.1 Direct indicators***

Direct indicators are physical, chemical or biological phenomena which attest directly to the presence of petroleum. Geochemical exploration involves the detection of direct indicators at the ground surface. Examples include oil and gas seeps and hydrocarbon enriched soil gas anomalies (Horvitz, 1980). Biological phenomena include anomalous concentrations of oleophilic bacteria and stunted petroleum-sensitive flora. Oil and gas seeps are the most obvious and have been interpreted as evidence of subsurface accumulations for years by explorationists who had no conception of fluid flow. The key to their interpretation in terms of the GHT lies in the subsurface flow pattern which links the signature at the ground surface to its source in the reservoir.

Direct indicators occur downstream of an accumulation site having been transported beyond the oil or gas pool by flowing water which generally moves freely through the petroleum trap. The moderate success of surface geochemical exploration methods to date may be due to the simplistic notion of 'vertical migration' (MacElvain, 1963) whereby the accumulation is sought vertically below an anomaly detected at the ground surface, and no consideration is given to the flow pattern which could produce significant lateral offset. A recent study in the Wainwright area of eastern Alberta (Holysh, 1989) demonstrated the significance of fluid flow patterns by showing that recharge areas are poorly suited to surficial geochemical exploration programs since the downward movement of water retards the transmission of direct indicators from petroleum reservoirs to the ground surface.

Direct indicators can also be mapped in the subsurface. Impelling force fractionation will cause lighter petroleum to accumulate in relatively minor structural irregularities along a lateral flow route, while heavier hydrocarbon fluids will be transported further downstream. This is because the buoyant force vector which is always directed vertically upwards is greater for relatively light (i.e., low density) petroleum. Thus gas, for example, will be impelled upwards with only a slight deflection in the

direction of water flow. Relatively heavy oils whose density approaches that of water have negligible buoyancy and will be impelled directly along the water flow path. For this reason petroleum pools in an aquifer exhibiting lateral flow may exhibit an increase in density (mass per unit volume) in the flow direction. Non-horizontal oil-water contacts, tilted in the direction of flow (the negative hydraulic gradient) are indicators of active fluid flow. Using Hubbert's tilt amplification factor (Hubbert, 1953, p.1993) we can predict for a given hydraulic gradient and specified oil and water densities the magnitude of structural dip required to form a hydrodynamic trap. Anomalously high concentrations of oleophilic bacteria are direct biological indicators. Selected direct indicators are illustrated on a conceptualized cross-section in Figure 2.4.

#### **2.4.2.2 Indirect indicators**

Indirect indicators are physical, chemical and biological phenomena which indicate hydrogeological conditions suitable for petroleum accumulation. Such indicators are of limited significance individually because they are not uniquely attributable to fluid flow. A suite of parameters however can provide convincing evidence of flow conditions. Because quasi-stagnant zones and discharge areas are considered the most favourable flow sites for hydrocarbon accumulation, indirect indicators are those phenomena indicative of such areas. Relevant fluid dynamic parameters include: upward vertical flow at the accumulation site (indicated by hydraulic heads increasing downwards, and superhydrostatic vertical pressure gradients in and above the aquifer); lateral flow convergence within the aquifer toward the accumulation site (hydraulic head minima and flow line convergence in plan view) and sluggish flow rates. Hydraulic head maps and cross-sections, and pressure-depth plus pressure-elevation plots are useful tools for the determination of flow rates and directions. Figure 2.5 shows some postulated trends in water chemistry temperature and pressure in relation to the flow field on a conceptual basin cross-section. Note that the aquifers within the regional discharge zone exhibit anomalously high temperatures and temperature gradients; pressures and pressure gradients; as well as abnormal water chemistry.

Water is an efficient heat transporter because it has very high heat capacity (Gretener, 1981). Flowing water can therefore modify the

conductive heat flow from the basement to the ground surface and discharge zones should exhibit elevated geothermal gradients. Temperature contour maps for a hydrostratigraphic unit may reveal 'hot spots' caused by upwelling warm water which are interpreted as favourable exploration indicators.

Since water salinity (total dissolved solids) generally increases with residence time and distance travelled (increased rock-water interaction) discharge zones may be characterized by anomalously saline water. Concentrations of total dissolved solids plotted on plan view contour maps in relation to the hydraulic head distribution may show a correspondence between hydraulic head minima and TDS maxima. Discharge zones and quasi-stagnant zones occur where flow systems converge, so they may also exhibit anomalous chemical composition due to the mixing of waters with distinct provenance. The Chebotarev sequence predicts a progressive change in the composition of major anions along the flow path. Reduced (versus oxidizing) chemical conditions may also signify water discharging from depth and moreover may be caused by the presence of petroleum. Indirect biological indicators include land vegetation tolerant to excess moisture and salt in the soil both of which may be related to the discharge of saline groundwater.

### **2.5 A Critical Evaluation of Pore Pressure, Temperature and Water Chemistry as Hydrogeological Characteristics**

The purpose of this section is to critically evaluate the genetic relation between the topography driven flow of water and the subsurface distribution of temperature, pressure and water chemistry. Physicochemical phenomena can be generated by many processes. Some are entirely flow-dependant others require absolute hydraulic discontinuity in order to be effective. In this section forces other than topography-driven flow that may influence fluid movement are evaluated, and mechanisms and processes unrelated to fluid flow that may affect the evolution of "hydrogeological" phenomena are considered. The discussion will be limited to processes likely to be effective in the study area i.e., in a geologically mature sedimentary basin with a sub-aerially exposed upper surface, at depths not exceeding 2 km, pressures under 20 MPa and temperatures below 100°C.

### 2.5.1 Pore pressure

In a stationary body of uniform density water, pressure increases with depth at a hydrostatic rate. The fluid pressure ( $P$ ) depends only on the fluid density ( $\rho_w$ ) gravitational acceleration ( $g$ ) and the water depth ( $d$ ) and is given by:

$$P = \rho_w g d \quad (2.15)$$

where  $g$  is the gravitational constant. As expected on the basis of this equation, pore pressures in sedimentary basins increase with depth and are higher for saline than for fresh waters. Differentiating Equation 2.15 with respect to depth yields:

$$\partial P / \partial d = \rho_w g \quad (2.16)$$

which states that the vertical rate of pore pressure increase with depth in a hydrostatic hydraulically continuous environment is equal to the specific weight of the fluid ( $\rho_w g$ ). The fact that near hydrostatic pressures predominate in sedimentary basins (excepting the geo-pressured zones of young, compacting, marine basins) is reflected in the terminology of petroleum geology. Nonhydrostatic pressures are termed “anomalous”. Superhydrostatic pressures are called “abnormal” and subhydrostatic pressures “subnormal”. The widespread existence of near hydrostatic pressure in sedimentary basins provides strong support for the general hydraulic continuity of sediments.

Deviations from hydrostatic pressure do occur however and a number of mechanisms may be responsible some of which are discussed below.

#### 2.5.1.1 The Dynamic Pressure Increment

Tóth (1978) has shown that nonhydrostatic vertical pore pressure gradients are a natural consequence of fluid flux. In a region of upward flow the extra energy at depth (which drives the upward flow) over that available in a hydrostatic environment is reflected in a superhydrostatic gradient and

$$\partial P / \partial d > \rho_w g. \quad (2.17)$$

In a region of downward flow the energy content decreases with depth faster than it would in a hydrostatic case resulting in

$$\partial P / \partial d < \rho_w g. \quad (2.18)$$

Tóth's dynamic pressure increment ( $\Delta P$ ) is defined as the difference at a given location between the nominal hydrostatic pressure calculated by Equation 2.15 and the observed pressure. In a basin where fluid flow is topography-driven, superhydrostatic pressures (positive dynamic pressure increments) and pressure gradients will characterize discharge zones, subhydrostatic pressures and pressure gradients will be found in recharge areas. Figure 2.6 shows schematically the relative magnitudes of pore pressures generated by variable fluid density, fluid flow and rapid loading combined with hydraulic isolation (i.e., geopressures).

#### 2.5.1.2 Erosion and Elastic Rebound

The response of strata to unloading is determined by rock compressibility, itself a complex function of prior stress history (Bredehoeft et al., 1968; Freeze and Cherry, 1979; Domenico and Schwartz, 1990). Lithified sediments have a compressibility approximately equal to that of water. Compacted shales are often elastic in compressibility (Tóth and Corbet, 1986, p.48) and may therefore expand when the stress imposed by the weight of overlying sediments is reduced through erosion of overburden. If the expansion of the rock framework results in increased pore volume, then pore pressure will be reduced in the rebounding stratum. This reduction in pore pressure will establish a hydraulic head gradient and water will flow into the expanded stratum until the mass or pressure deficiency is satisfied. Pore pressure anomalies in poorly permeable strata will equalize at a slower rate than in aquifers so that erosional unloading may tend over time to produce foci of subhydrostatic pressure within aquitards. Long-lived transient pressure sinks may develop in and around thick shales.

Shale rebound has been suggested as a cause of the well documented "underpressures" in thin sandstones of the Colorado Shale aquitard of central and southern Alberta (Tóth et al., 1986; Parks, 1989; Corbet et al.,



1992) and may be equally effective in the Peace River Arch region, northern Alberta where the present study area is located. Loading and unloading due to the waxing and waning of Quaternary ice sheets may also induce “underpressures” in subsurface strata.

### **2.5.1.3 Osmosis and Reverse Osmosis**

A semi-permeable membrane permits the passage of water molecules but excludes dissolved salts. When such a membrane separates solutions of different salinity, a gradient of chemical potential will cause water molecules to flow through the membrane from the fresh to the salty solution. This is because the water molecule concentration, and therefore the activity or thermodynamic energy of water, is relatively high in freshwater. In the absence of any additional driving forces, the intensity of flow will be proportional to the salinity contrast between the solutions present on opposite sides of the membrane. As water molecules flow through the membrane the pore pressure, and therefore the hydraulic head of the salt solution rises, setting up a gradient of mechanical potential opposing the osmotic flow. The chemical potential gradient between the two solutions simultaneously falls due to the increased water molecule concentration in the diluting brine. Osmotic flow ceases when the total energy of the two solutions is balanced (i.e., when the declining gradient of chemical potential is exactly balanced by the rising - oppositely directed - mechanical potential gradient). The extra pore pressure in the saline solution at total energy equilibrium is called the osmotic pressure.

It has been suggested that compacted shales in sedimentary basins may behave as natural semi-permeable membranes (Berry, 1969). If a brine saturated sand and a fresh water sand are separated by such a shale then water molecules will spontaneously diffuse across the shale to dilute the brine. The significance of osmosis as a natural flow driving mechanism in sedimentary basins is limited since osmotic flow is a self-stopping process.

The geologic conditions required for osmotic flow could be best satisfied in the western Canada sedimentary basin where the Ireton shale subcrops the sub-Cretaceous unconformity. Here, a thick semi-permeable aquitard (the Ireton Fm.) separates the dilute waters of the basal Cretaceous

sands from the brines of the Cooking Lake Platform. Osmotic flow in this situation should be downward across the Ireton Fm.

Reverse osmosis occurs when the pore pressure of a brine saturated sediment is raised sufficiently by some external force to cause flow across a semi-permeable membrane from the brine saturated sand to the freshwater sand (i.e., in the opposite direction to that in which osmotic flow would be). Reverse osmosis is also called ultrafiltration because salts in the brine are excluded from passing through the shale which concentrates ions in the brine enhancing its salinity. Ultrafiltration may be a significant natural process where topography driven flow drives water across shale aquitards in regions of vertical flow (Bredehoeft, 1963; Roberts, 1981) and may contribute to the enhanced salinity of water in discharge areas.

In conclusion, reverse osmosis due to topography driven flow is probably a geologically significant process that enhances the high salinity of formation waters in discharge areas. Osmosis on the other hand will be a localized phenomenon, both temporally and spatially. In a discharge area, osmosis must oppose topography driven flow. Osmosis as a possible cause of non-hydrostatic pressure in sedimentary basins was studied widely in the 1960's but has been neglected more recently due to the general recognition that most sedimentary basins are open systems in which topography-driven flow is far more significant.

#### **2.5.1.4 Aquathermal Pressuring**

Hydraulic isolation is a required condition for many mechanisms by which anomalous pressure may be generated. Such isolation is probably most effective in regions such as the geo-pressured zones of compacting, depositionally active basins, and may be rare in hydraulically continuous environments where topography driven flow is important. Changes in the physical properties of a fluid saturated sediment that take place without the expulsion of pore water are termed constant mass phenomena. An example is provided by the work of Barker (1972).

Barker (1972) coined the phrase 'aquathermal pressuring' to describe the superhydrostatic pressure that would be generated by the expansion of water contained in a hermetically sealed, constant volume rock body subject to burial in a thermal field. Bradley (1975) favours temperature change as the principal factor in the generation of a

hydrostatic pore pressure. Since the mechanism is fully reversible it will be described in terms of the de-pressuring that would result from erosion and uplift of a sealed rock body which is more relevant to the recent geological history of the present study area.

Uplift results in cooling and the pore fluids in hydraulically continuous sediment contract and increase their density in response to the energy loss associated with temperature decrease. Water in a sealed, non-yielding chamber remains at constant density so its energy loss is manifested as a rapid pressure decline for a given temperature change. Under ideal conditions, the pressure of fresh water will decrease at a rate exceeding 13 MPa/°C (Barker 1972). Barker acknowledges that relatively minor leakage of the rock body or a small change in its volume would increase pressure to the normal hydrostatic value.

Domenico and Schwartz (1990, p.298-301) present an interesting quantitative review of the pressure modifying effects of the thermal expansion of water. They conclude that the mechanism will be more significant in rigid than in soft rocks, that the constant mass case provides an informative upper bound for the true response of natural materials and that in all cases the effectiveness of the mechanism will be determined by the relative rates of pressure production and its dissipation by flow.

Since the WCSB has lost up to 2 km of sediment by erosion in the recent past, aquathermal de-pressuring may be contributing to the observed subhydrostatic pressures in the Cretaceous Colorado shale aquitard.

#### 2.5.1.5 Active Petroleum Generation

Spencer (1987) suggests that the current flow patterns in many Rocky Mountain basins of the USA are controlled by active petroleum generation. Superhydrostatic pressures far exceed the overpressures which could be ascribed to topography. Hedberg (1974) championed the possible role of methane generation in the expulsion of petroleum from source rocks by micro-fracturing. Petroleum generation involves the transformation of solid kerogen into a liquid phase and pore space. Pore pressure will rise only if there is more liquid than pore space created (Bredehoeft et al., undated) the pressure increase involved depends on the difference in density between the kerogen and the petroleum. Bredehoeft modelled pressure development by active oil generation assuming a 10%

volume increase in a recent study in the Uinta Basin. This study confirmed that active oil generation could explain the observed superhydrostatic pressures in the Altamont source/reservoir bed which exhibits pressure gradients up to 0.8 of lithostatic (ibid.). Hedberg (1980) makes the point that the introduction of a petroleum phase liquid into a water-wet rock will immediately reduce the relative permeability of the source rock to either fluid. Free gas or oil will 'plug up' the shale and enhance the build-up of excess pressure which may eventually exceed the lithostatic pressure and cause the rock to fracture, releasing pulses of petroleum from the source rock.

Active petroleum generation may be a significant local source of superhydrostatic pressure sufficient to modify flow patterns in sedimentary basins generally, but is probably not so in the Peace River Arch region at the present time. As shown in Figure 5.1, the present study area is over 60 km from the nearest mature Devonian source rocks. Moreover, these source rocks attained peak oil generative capacity some 60 million years ago (Creaney et al., 1990).

## **2.5.2 Temperature**

The temperature data used for this study are bottom hole temperatures (BHTs) from oil industry wells. The Keg River-Granite Wash reservoir beds in the study area (see Figures 1.4. and 1.5), lie directly on the Pre-Cambrian so virtually all wells penetrate to the basement. Most BHTs were measured in the uppermost Pre-Cambrian crystalline rocks at the base of sediments. The present study will therefore consider factors which can affect:

- 1) the temperature distribution at the top of the basement
- 2) the average vertical temperature gradient between the basement and the ground surface.

### **2.5.2.1 Possible Modes of Heat Transport**

Heat flows from the Earth's interior to the surface where it is dissipated. The possible mechanisms of heat transfer in the Earth's crust are conductive and convective heat flow. Conduction moves heat mainly through the solids of a porous medium whereas convection is achieved by water moving through the pores. In a conduction dominated thermal

regime, heat flow is controlled by the distribution of heat sources and the thermal conductivity of rocks. In a convective thermal regime on the other hand, rates and directions of fluid flow are the controlling factors.

Whether the geothermal regime in the WCSB is dominated by convective or conductive heat transport has been a subject of active research in Alberta for the last decade. An outline of this research is presented in the following section.

### **2.5.2.2 Convective Heat Transport**

Theoretical investigations (Bredehoeft et al., 1965; Domenico et al., 1973) showed that topography-driven groundwater flow systems should exert a demonstrable effect on the conductive thermal regime in a sedimentary basin. Majorowicz and Jessop (1981) were the first to present a coherent convection model in a real basin. They observed a geothermal gradient pattern in Alberta that could not be explained by the regional heat conductivity distribution nor by the known distribution of heat sources in the basement. Upland regions like the Foothills Belt exhibited low gradients whereas lowlands in northeastern Alberta had unusually steep gradients. They attributed this pattern to convective heat transport by a regional flow system in the WCSB that was described earlier by Hitchon (1969). Recharging cool water subdued vertical heat flow in the upland areas. The water flowed down the hydraulic head gradient into and across the basin picking up heat *en route* and steepened geothermal gradients as it discharged in lowland regions. This model of heat flow strongly coupled with topography-driven water flow was developed in a series of publications by Majorowicz et al (1984, 1985) Jones et al (1985) and Hitchon (1984).

### **2.5.2.3 Basement Temperature and Average Geothermal Gradient Trends in a Convective Regime**

In a sedimentary basin with a convection dominated thermal regime coupled to a topography driven flow regime we should theoretically observe:

- 1) An inverse relationship between the geothermal gradient and heat flow on one hand and the topographic elevation of the ground surface on the other. That is, the relationship predicted by Tóth (1980) and observed

by Majorowicz and Jessop (1981): low geothermal gradients in upland recharge areas and high gradients in lowland discharge zones.

2) Temperature isolines at the base of sediments on the top of the crystalline basement may be oriented parallel to equipotentials in the deepest basin aquifers.

#### **2.5.2.4 Conductive Heat Transport**

The alternative view, being that of a conduction dominated thermal regime in the WCSB, has been championed by Bachu (1985). Bachu worked at a finer scale than Majorowicz and Jones, evaluating geothermal gradients over shorter distances and in more lithologically homogeneous units. He concluded that the clearer view of temperature distribution that emerges favours conduction as the dominant heat transport mechanism. Bachu is well aware that most sedimentary basins are hydrodynamic environments but argues that fluid flow rates in the WCSB are simply too slow to compete with conduction. Bachu and Burwash (1991) evaluated evidence for convective heat transport in Alberta at basinal ( $10^3 \text{ km}^2$ ), intermediate and local ( $10 \text{ km}^2$ ) scales and concluded that flow was significant only at the local scale.

#### **2.5.2.5 Basement Temperature and Average Geothermal Gradient Trends in a Conductive Regime**

In a conduction dominated regime the temperature at the base of sediments is affected by three factors. All else being equal, basement temperatures will be high when:

- 1) Overlying sediments are thick
- 2) Overlying sediments are of low thermal conductivity
- 3) Heat flow from the basement is high.

These factors are discussed by Bachu (1988), and Hitchon (1984, p.725). The influence of sediment thickness is easily evaluated by comparing a map of the basement temperatures with an isopach map of the basin fill. Highs on the isopach map should correspond to temperature highs on the basement.

Thermal conductivity is an attribute of lithology. Shale and coal for instance are both poor conductors of heat thus anomalously high basement temperatures may develop under shale basins. Thermally conductive

sediments such as dolomite and halite by transporting heat rapidly away from the source will have a cooling effect. Porosity is also important. Because pore fluids are less conductive than solids thermal conductivity is inversely proportional to porosity. Compacted sediments from deeply buried areas should have enhanced thermal conductivity and may exert a cooling effect.

Heat flow into the Phanerozoic strata of the WCSB from the Pre-Cambrian basement is divided in roughly equal parts between radioactive heat generation in the crust and heat flow from the mantle. Heat flow from the mantle is uniform over large areas whereas crustal heat generation is markedly heterogeneous (Jessop, 1992, p.198). Heat is generated in crustal rocks by the decay of radioactive isotopes of potassium, thorium and uranium. These radiogenic elements are naturally concentrated in the upper crust (Holland et al., 1972) within which heterogeneities are related to basement structure and composition. Granitic intrusions, zones of partial melting or metasomatism may all exhibit anomalously high heat generating capacity. Bachu and Burwash (1991, Figure 7) present a map of the distribution heat generation at the top of basement in the WCSB based on uranium, thorium and potassium concentrations measured in 424 Pre-Cambrian core samples. They conclude that the high heat generating areas have significant impact on both the temperature distribution at the Pre-Cambrian surface and on average geothermal gradients in the basin at large. This map is an updated version of a basement heat generation map presented by Majorowicz and Jessop (1981, Figure 13, p.229). The two maps are broadly similar (i.e., the new data added by Bachu and Burwash does not change the overall pattern in the basin) and yet Majorowicz and Jessop cited their map as evidence for the negative impact of basement heat generation on the thermal regime! Section 4.2.2.1 presents my evaluation of the impact of basement heat sources on the temperature distribution in the present study area.

### 2.5.3 Water Chemistry

Galloway and Hobday (1983) note that water-rock interactions, which both the rock and water are changed, are determined jointly by the chemistry of the invading groundwater and the reactivity of the rock.

The chemistry of the invading water will be determined by its prior history. The major factors affecting matrix reactivity comprise:

Soluble constituents

Those constituents of the matrix that can be leached by the invading groundwater depend on the pore fluid chemistry and the availability and grain size of solid phases within the rock matrix.

Reducing and buffering capacity

Matrix content of elemental oxygen or elements such as iron with variable valence states determine the redox capacity of the matrix. Iron disulfide (pyrite) and organic matter both impart a reducing capacity to the matrix. Buffering is the capacity of the matrix to maintain a steady pH by releasing or absorbing protons during chemical reactions.

Exchange Capacity

Is determined by the reactivity and abundance of colloidal constituents (mostly clays) which can adsorb and release ions from sites within their crystal lattice. Exchange capacities vary for different minerals and are affected by the salinity (ionic strength) and chemical composition of the solution.

Hydration

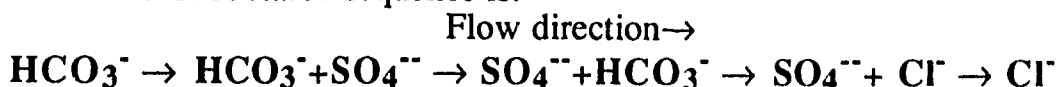
Hydration of an aquifer matrix connotes the structurally bound water which under certain conditions of pressure and temperature can revert to a fluid phase.

The major function of flow may be “keep things moving”. The end result of any reaction or series of reactions in a closed system is chemical homogeneity and equilibrium. Topography driven flow is ideally suited as a mechanism by which subtle imbalances can be maintained. Mass can be introduced or taken away, dilution or concentration can be maintained over geological time spans and chemical reactions of dissolution or precipitation which would otherwise have reached equilibrium and stopped, may be indefinitely prolonged.

Freeze and Cherry (1979) stress the importance of the order of encounter with diverse lithologies for groundwater moving along a lithologically heterogeneous flow path. The ionic strength of the moving groundwater and possible common ion effects due to mineral dissolution are the major factors which determine the chemical evolution.



Chebotarev evaluated 10,000 water analyses from all major continents (Chebotarev, 1955) and discovered a trend characteristic of the general chemical evolution of anions in all groundwater in the direction of flow. The Chebotarev sequence is:



The sequence shows a tendency for all groundwater with increasing age, time, depth and/or distance travelled to evolve from a dilute bicarbonate solution to a saline solution with chloride as the dominant anion. The trend may be apparent at various scales (e.g., in a single flow system moving from recharge to discharge areas, or in flow systems of progressively increasing order - local versus regional). No fixed scale of time or space is implied, and the sequence will often be interrupted or reversed.

The question of why such a trend should exist at all was addressed by Freeze and Cherry (1979). They suggest that the generality of the Chebotarev sequence in a variety of lithological settings can be accounted for by two factors: the differing solubilities of the minerals which yield these anions in solution and their availability along the flow path. Carbonate minerals (e.g. calcite  $\text{CaCO}_3$  or dolomite  $\text{CaMg}(\text{CO}_3)_2$ ) that dissolve to yield  $\text{HCO}_3^-$  are abundant but poorly soluble, whereas chloride minerals (e.g., halite  $\text{NaCl}$  and sylvite  $\text{KCl}$ ) are highly soluble but rare. Groundwater therefore accumulates  $\text{HCO}_3^-$  rapidly and  $\text{HCO}_3^-$  is the dominant ion in young, shallow waters in recharge zones. Halite and sylvite are minor constituents of most common sedimentary rocks, and being highly soluble, are rapidly removed from the bulk flow channels.  $\text{Cl}^-$  subsequently entering the bulk flow pathway (evaporitic strata excepted), must therefore migrate through the solid mineral matter or from dead-end pores by diffusion. Thus  $\text{Cl}^-$  often accumulates slowly in groundwater but since it is an unreactive aqueous ion (i.e., there are no chloride sinks in moderately saline waters) it eventually attains very high concentrations.

#### 2.5.4 Summary

A variety of processes and mechanisms, many unrelated to flow, affect the physicochemical evolution of subsurface water. Where topography driven flow is the dominant control however, the water

pressure, chemistry and temperature should exhibit systematic changes along flow paths and pore water at distinct locations within a basin should display predictable characteristics.

## **Chapter 3 Data Processing for the Field Study - Data Sources and Culling Procedures**

The flow regime in a sedimentary basin is determined jointly by the distribution of fluid potential (i.e., the energy available to drive fluid movement) and by the hydraulic character and spatial distribution of the strata comprising the rock framework through which the fluid moves. This chapter shows what data are required to recognize and characterize these two components and presents methods that may be used to obtain values of hydraulic parameters that are representative at the temporal and spatial scale of interest. Sources and culling procedures for obtaining representative temperature, water chemistry, oil density and petroleum production data are also presented.

### **3.1 Rock Framework Data**

Formations are the basic lithostratigraphic units of geological mapping and provide suitable units for the primary characterization of the rock framework. For flow studies formations are ultimately re-organized into hydrostratigraphic units (HSUs) which comprise aquifers, aquitards and aquicludes, defined on the basis of their ability to permit or retard the flow of water (Maxey, 1964; Tóth, 1978; Seaber, 1988).

#### **3.1.1 Formation Tops**

Formation top elevations were used to create the structural cross-sections (Figures 1.4 and 1.5) and the structure contour maps presented in Chapter 4. There are 1160 wells in the present study area. I personally inspected well logs and picked all formations in 72 wells distributed across the study area and these picks were used to make the cross-sections. The picks I made for the Wabiskaw (Bluesky) to Pre-Cambrian are illustrated on the gamma ray-density log for well 3-8-99-7W5 shown in Figure 3.1. Most formations have a distinctive gamma ray signature. The Keg River and Lower Elk Point Group formations are best identified on density or sonic logs. The caliper log (shown in track 2 for the Muskeg Fm. only on Figure 3.1), is useful for locating halite beds which are often washed out by the drilling fluid.

Since there are too many wells in the study area for my personal inspection of all logs (1160 wells with up to 20 formations per well),

ERCB picks were used for the structure contour maps. These data were obtained in digital form (PUBCO, 1990 a) and comprise picks for 1053 wells in the study area.

ERCB picks were unreliable for the Upper Devonian Grosmont Fm. Unculled ERCB data produced elevation anomalies for the top of the Grosmont Fm. on initial versions of the structure contour map of the Pre-Cretaceous unconformity (the final version of this map is shown as Figure 4.5). Personal inspection of wireline logs for the wells with anomalous elevations revealed that the Grosmont Fm. was often mis-picked. The Grosmont Fm. is fully developed only in the centre of the study area. As shown on Figure 1.4, within the study area, the Grosmont pinches out westward into Ireton shales with a consequent loss of section at the base of the formation. To the east there is a progressive loss of section from the top due to erosional truncation of the Grosmont Fm. at the sub-Cretaceous unconformity. Thus although the gamma ray signature for the Grosmont is distinctive when it is fully developed (Harrison, 1982), recognizing the partially developed section is more challenging.

A second problem was that wireline logging is usually confined to the Mannville Group and deeper strata since there is no exploration interest above the Mannville in the study area. This made it difficult to locate the two important pre-Mannville Cretaceous aquifers: the Pelican (Viking equivalent) and Dunvegan sandstones, and also the base of Pleistocene drift. For the shallow geology on the cross-sections (see Figures 1.4 and 1.5) and for the bedrock structure map (Figure 1.7), published geological maps, hydrogeological maps and cross-sections and water well drillers reports were used.

### 3.1.2 Lithology

Gross formation lithologies are known from literature sources. The Lexicon of Canadian Stratigraphy (Glass, 1990) is an excellent regional reference. For site specific lithological data I obtained 23 lithologs (Canadian Stratigraphic Services), distributed over the study area. These logs provide lithological descriptions based on well cuttings, core analyses and wireline log interpretation. Wireline logs were used to interpolate between wells with Canadian Stratigraphic Services logs. Core analyses

(ERCB, 1991 a) also often provide lithological descriptions of the cored intervals.

### **3.1.3 Porosity, Permeability and Hydraulic Conductivity**

#### **3.1.3.1 Porosity**

Porosity was used in the present study to estimate storativity, thermal conductivity and in Darcy's Law to convert flux to velocity.

Porosity ( $n$ ) is the fraction of total rock volume occupied by voids, usually expressed as a percentage

$$n (\%) = \frac{V_v}{V_t} * 100 \quad (3.1)$$

where  $v$  is volume and the subscripts  $v$  and  $t$  indicate voids and total respectively. A crude correlation with permeability may occur if the porosity is mainly interconnected. Little correlation will exist if most of the pores are closed or dead-end. Porosity varies with lithology: clastic rocks exhibit mainly inter-granular porosity; carbonates more prone to dissolution and re-crystallization during diagenesis develop irregular porosity types such as fracture, pinpoint and vuggy porosity. Evaporites usually display inter-crystalline porosity. Porosity ranges from 50% in unconsolidated sediment to extremely low values in tight evaporites like massive halite.

#### ***Porosity From Core***

Appendix 1 outlines the procedures by which permeability and porosity values are determined from core in the laboratory. The weighted arithmetic mean of plug scale porosities provides a representative value for a formation. Multiple porosity determinations for a single formation tend to exhibit a normal frequency distribution and the weighted arithmetic mean is the best measure of central tendency for such a distribution. Weighted arithmetic mean porosities were included in over 90% of the core reports in my database. Figure 3.2 is a porosity frequency histogram for a 14 m Keg River Fm. core from the Trout field (Geotech core analysis report). Porosities range from 0.5 to 10% and the histogram with a linear

porosity axis exhibits a normal (symmetrical) frequency distribution. The weighted arithmetic mean of 5.8% is a good representation of the central tendency.

### **3.1.3.2 Permeability and Hydraulic conductivity**

Permeability values were used in this study to make hydraulic conductivity and transmissivity maps and to calculate flow rates. These applications are presented in the following chapter.

Intrinsic permeability is a laboratory determined rock property that relates the resistance of the rock to single phase fluid flow caused by the size, shape and geometry of its porous architecture (Appendix 1). When multiple phases coexist in a porous medium the effective permeability of the rock to each individual fluid is reduced. At very low saturations, immiscible fluids are eventually immobilized (wetting phases on the pore walls and non-wetting phases in the pore bodies) as the effective permeability drops to zero. Since the presence of oil reduces the effective permeability to water, oil and gas pools function as barriers to flow, and hence potentially modify the flow field by diverting flowing water around them.

As mentioned in Chapter 2, permeability has directional properties, and permeability anisotropy can strongly influence the direction of flow by refraction towards an axis of increased permeability. Freeze and Cherry (1979) discuss the relationship between anisotropy and flow. The anisotropy of a hydrostratigraphic unit is ideally expressed by 3 orthogonal permeability values, one vertical and two in the horizontal plane. In the present study it is assumed that hydrostratigraphic units are laterally isotropic and that  $k_{max}$  coincides with the orientation of the driving force ( $-\text{grad } h$ ).

This assumption is certain to be invalid locally, particularly since the Keg River Fm. is known to exhibit trending fracture systems in certain regions. An example is an oriented core study combined with DST analysis, interference tests and numerical modeling conducted by Gulf engineers in the Trout Keg River A pool (ERCB, 1986). The study was conducted in a single township Tp.90 R.3 W5, i.e., an area of about 100 km<sup>2</sup>. The investigation indicated that vugs and fractures combine to form the major pore system in the reservoir at this location, with matrix microporosity

forming a second volumetrically minor system. The orientation of  $k_{\max}$  i.e., of the fracture network, was determined to be northwest-southeast and the fractures persisted vertically to link the upper and lower parts of the Keg River Fm.

Unfortunately such detailed local studies are rare. Reports submitted by operators to the ERCB for other fields do not indicate fracture orientation. A report for the Keg River B pool in the Kidney field indicated a dual porosity system with fractures and vugs forming the minor component, and intergranular porosity the major system. In short the information required for a sensible evaluation of the possible effects of permeability heterogeneity on flow directions is simply not available.

Formulations of Darcy's Law (e.g., Equations 2.4 and 2.8) show clearly that although permeability affects the magnitude of flux, the primary determinant of the flow direction is the orientation of the driving force expressed either as the resultant of the two force vectors in Equation 2.4, or as the gradient of hydraulic head in Equation 2.8. Water will certainly take the path of least resistance along a given route, but the directional influence of permeability anisotropy is restricted to local scale options within a regional pattern determined by the force field, that in a mature basin, is controlled ultimately by the topography of the water table. Flow directions certainly cannot be inferred from a permeability distribution without prior knowledge of the distribution of driving forces.

### *Permeability From Core*

The ERCB Core Analysis database (ERCB, 1991 c) yielded 645 core records for the wells in the present study area. Permeability determinations are made at very close intervals along the core (usually three per metre) and a single core interval often comprises well over 100 individual plug or slab sample determinations. There are many reasons why core derived hydraulic parameters may not be representative on the basinal scale (see Appendix 1) but regardless of these shortcomings core is the main source of direct information on deep subsurface hydraulic parameters and core data are widely used in subsurface flow studies.

### ***Up-scaling Plug-scale Permeabilities***

The plug-scale values for different lengths of core are ultimately transformed into values that are representative for hydrostratigraphic units on the scale at which flow is being studied. This is done in two averaging steps. First, a representative average of all the plug-scale values in a single core is found to yield a representative permeability for the formation. Second, the permeabilities of the formations being grouped together in a hydrostratigraphic unit must be combined. The procedure I followed is illustrated in Figure 3.3.

### **Horizontal Permeability**

The geometric mean is usually used to transform plug scale permeabilities to the formation scale. Permeability unlike porosity often exhibits a log normal frequency distribution and the geometric mean is the best measure of central tendency for such distributions (e.g., Davis, 1973; Freeze and Cherry, 1979).

Figure 3.4 is a permeability frequency histogram for the same Keg River Fm. core as shown in Figure 3.2. The measured permeabilities range over 5 orders of magnitude from 0.01 to more than 2000 millidarcies. The histogram in the figure exhibits a symmetrical frequency distribution because the permeability axis is logarithmic - if a linear axis were used the distribution would be highly skewed. Since 70% of the samples for this core have a permeability of 5 millidarcies or less (see the cumulative frequency curve on Figure 3.4) the arithmetic mean of 287 millidarcies is clearly a poor measure of the central tendency whereas the geometric mean of 1.7 millidarcies is reasonable. The geometric mean can be computed by calculating the weighted arithmetic mean of the logarithm of the individual formation permeabilities, the antilog of which is the geometric mean for the HSU.

The arithmetic mean of lateral permeabilities of individual formation weighted by their thickness yield representative values for the lateral permeability of hydrostratigraphic units (Freeze and Cherry, 1979).

### **Up scaling Well-scale Parameters to the Regional Scale**

Having transformed plug-scale parameters to the scale of the hydrostratigraphic units (HSUs) it is assumed that data points are



representative of the entire vertical thickness of the HSU at their location. Lateral heterogeneities are determined by posting the HSU-scale permeabilities and undertaking interpretive contouring based on geological considerations - lithofacies trends. This is reasonable for a regional scale flow study because the lateral extent of an hydrostratigraphic unit is many orders of magnitude greater than its vertical extent. The procedure I followed is described in Chapter 4.

### ***Permeability Anisotropy***

As indicated above it was not possible in the present study to obtain oriented permeability data in order to determine the direction of major and minor lateral permeability axes, so the aquifers are assumed to be laterally isotropic. A crude estimation of the vertical anisotropy was obtained as described below.

### ***Vertical permeability***

To obtain an estimate of vertical permeabilities I selected one core per township (when available) and calculated the  $k_{Hmax}:k_V$  ratio for one randomly selected plug scale sample from each formation within the interval. These ratios are assumed to be provide a very crude estimate of the anisotropy of the whole formation at that location.

### ***3.1.3.3 Estimating Average Parameters***

In order to calculate derived hydraulic parameters such as the storage coefficient, it is useful to have estimates of the average hydraulic properties of hydrostratigraphic units. Table 3.1 shows average (arithmetic mean) values of the core-derived hydraulic parameters (weighted geometric means for permeabilities and weighted arithmetic means for porosities) for each hydrostratigraphic unit. Most cores in the region are from formations in the Keg River - Granite Wash hydrostratigraphic unit (70%), and the Slave Point - Watt Mountain (18%).

### ***3.1.3.4 Permeability From DSTs***

A drill stem test (DST) is a short term production test conducted on a temporarily completed well. Permeability can be calculated from DST analysis; indeed DST derived permeability may be more representative than core-derived values since the DST evaluates the response of a

significant volume of rock around the well bore, based on the in situ flow of reservoir fluids.

I calculated permeabilities for 24 wells for which time and pressure build-up data were given in the DST reports (ERCB, 1991 d). The procedure and equations used in my DST analysis are presented in Appendix 2.

Meaningful comparisons of permeabilities determined by the two methods are restricted to those wells where the core and DST intervals exactly coincide i.e., where the same rock interval is being tested. This was the case for the 5 wells shown in Table 3.2. The permeabilities clearly agree, differing by a maximum of only a factor of four. This is surprising since the Keg River Fm. is known to exhibit significant fracture permeability which might be poorly represented in core. The similarity between the permeability values also suggests that the method of estimating geometric from arithmetic means used in this study is reasonable.

### **3.1.4 Storativity and Transmissivity**

The storage coefficient is a rock-hydraulic property which denotes the amount of water that would be released from a column of unit cross-sectional area within the formation, under a unit decline in hydraulic head (Freeze and Cherry, 1979, p. 59-61). Storativity is the product of the storage coefficient and the formation thickness. Transmissivity is the product of the formation thickness and hydraulic conductivity.

For my production drawdown calculations in Section 3.2, I used constant values of storativity and transmissivity based on representative (average) values of hydraulic parameters for the Keg River - Granite Wash aquifer. Storativity and transmissivity were calculated as indicated in Table 3.3.

### **3.1.5 Thermal Conductivity**

Thermal conductivity is a rock property defining the amount of heat that flows through a specific medium over unit distance in unit time, if there is a temperature gradient. When the temperature in a rock is not uniform, a thermal gradient exists. Heat flow through the rock in any direction is proportional to the thermal gradient and to the magnitude of thermal conductivity in the direction of the gradient. Like its hydraulic

counterpart, thermal conductivity is a tensor property, however for studies using RHT data (see Section 3.3) it is sufficient to assume strata are isotropic.

Thermal conductivity varies with lithology, and a recent study of heat flow in the Alberta Basin (Majorowicz and Jessop, 1992) gives assumed average values of thermal conductivities for different rock types within the basin. Table 3.4 presents these data. Glacial till, coal and shale are the best insulators, limestones, dolomites and sandstones are intermediate and the evaporites, rock salt and anhydrite are the best conductors. Table 3.5 shows crude estimates of the thermal conductivities for the hydrostratigraphic units (values from Table 3.4, were assigned depending on the dominant lithology of the hydrostratigraphic unit). These are crude estimates of the true conductivity, being uncorrected for lithological variation, in situ temperature or porosity. Thermal conductivity varies inversely with porosity since pore fluids are less conductive than rock. Within the depth range of 2 km, thermal conductivity also varies inversely with temperature (Gretener, 1981). The increase in conductivity due to porosity reduction at depth will therefore be offset by a conductivity decrease due to the higher temperature. Halite and dolomite are the most conductive lithologies. Thick halite beds are restricted to the Muskeg Fm. in the eastern half of the basin, so the temperature range to which they are exposed is minimal. Dolomites comprise the Keg River and Grosmont Formations and the Winterburn Group. Each of these will be less conductive in the high temperature regions.

### **3.2 Pressure Data**

For pressure data to be useful in the evaluation of the flow of water they must be:

- a) stabilized i.e., representative of the formation pressure;*
- b) undisturbed by pressure transients caused by fluid extraction or injection, and therefore representative of the "virgin" conditions in the formation;*

*c) representative of the ambient pore pressure in water (if measured in oil, gas or mud).*

### **3.2.1 Source of Pressure Data**

Abundant pressure data for deep basin studies come basically from a single source: drill stem tests (DSTs) which are pressure transient tests conducted in oil industry bore holes. The procedure by which stable formation pressures are determined from DSTs is described in Appendix 2. Accurate pressure data are crucial in any field-based fluid flow study. Ideally all DST interpretation should be done personally. This is a major task since there is much art involved in DST analysis and learning and applying the skills, takes time. Alternatively one can use the pressures supplied by a service company specialized in DST interpretation.

For the present study, interpreted pressure data were obtained from the Canadian Institute of Formation Evaluation (CIFE). In the following section an evaluation of the quality of their data is made. CIFE obtain DST charts from the ERCB, interpret these charts in-house and sell the interpreted data to oil companies. They use standard methods of analysis. A pressure versus time build-up curve on a Horner semi-log plot is extrapolated to infinite time to determine the stable formation pressure, and the shape of the build-up curve is interpreted to assign a qualitative permeability to the geologic interval tested. Many details of the test procedure including the amount and type of fluids recovered are recorded.

### **3.2.2 Evaluation of CIFE DST Interpretation**

CIFE assign an overall quality rating to each test, indicating the reliability of the pressure value. For the present study I used mainly those data classed by CIFE as 'a' and 'b' quality which are defined as:

- 'a' best quality;
- 'b' nearing stabilization.

The categories I did not use are:

- 'c' caution (plugging);
- 'd' questionable;
- 'e' low permeability, low pressure;
- 'f' low permeability, high pressure;
- 'g' mis-run.

The CIFE pressure values used are further restricted to those from tests with a fluid recovery of 100 m or more, and a short (average 15 m) packer interval. A long fluid recovery indicates a high flow rate or long flow periods, both being conducive to a representative test. A short packer interval is desirable for a focussed evaluation of the pressure source.

To evaluate the veracity of the CIFE quality claim I constructed Horner semi-log and log-log plots for 24 DSTs from the CIFE database which had pressure build-up data tabulated in the DST reports (ERCB, 1991 d). Table 3.6 shows the results.

The tests are arranged in descending order of quality as designated by CIFE and for each quality class, in order of increasing pressure value discrepancy (self-extrapolated pressure minus CIFE's). I have included my own ratings of the test quality. For the 10 DSTs which CIFE class as b quality, the pressure value discrepancies are minor. Eight of the extrapolated pressures are virtually identical, and the maximum discrepancy of 147 kPa is relatively insignificant since the average mechanical error for the 24 tests evaluated here is  $\pm 70$  kPa (the expected study area average for mechanical pressure recorders is 75 kPa - see Appendix 3). The reason for the largest discrepancies is that CIFE used the build-up curve that yielded a lower extrapolated pressure in both cases. This is poor interpretive procedure. The DST in the second row (well 3-31-100-22 W4, DST#2) should not be used as that well is supercharged and its inclusion may indicate that CIFE have not screened the DSTs for depletion (see section 2.2.3).

For the 10 tests classed by CIFE as c quality the discrepancies are more serious (maximum difference is 448 kPa or 46 m of fresh water head). Again the discrepancies occur because of analytical confusion by the CIFE interpreter (use of the "wrong" shut-in curve, insufficient data points for the extrapolation) or simply because the interpreter used a different pressure recorder housed higher or lower on the DST tool. I regard 9 of these tests as good quality. For the remaining record (well 6-31-98-22 W4, DST#1) the recorder was apparently reading high since the extrapolated formation pressure exceeds the hydrostatic pressure generated by the mud column which would have resulted in a blow-out. According to the reported mud weight (i.e., the density of the drilling fluid) the mud column would have to have been over 100 m above the ground surface to generate

the reported hydrostatic pressure. Clearly the pressure recorder was miscalibrated, or malfunctioning or both.

In summary it would appear that by accepting only CIFE a and b tests we obtain reliable pressures but discard a lot of potentially useful data. The CIFE interpretation of c and d quality tests is unreliable so personal interpretation is required to cull the non-representative pressures.

### **3.2.3 Evaluation of Production Induced Drawdown (PID) and Injection Build-Up**

Having obtained a set of stable formation pressures it is necessary to consider whether these pressures are disturbed. Petroleum production reduces the fluid pressure of the pumped formation in and around the producing well, modifying the “virgin” hydraulic head distribution by producing closed lows around oil fields. Since the Hydraulic Theory postulates that closed potentiometric lows are the cause of the petroleum accumulation it is crucial to demonstrate convincingly that potentiometric lows are not simply due to production induced drawdown (PID).

#### **3.2.3.1 Previous Work on PID**

Various attempts have been made in the past to identify production affected wells. Some workers restrict their data to those pressures obtained from DSTs in “wildcat” wells which are wells drilled outside the geographic limits of an existing pool or field. However there is no guarantee that wildcat wells are undisturbed since new pools are often discovered on step out wells from pools which have been in production for years.

Another approach is to specify a certain radius beyond which pumping is assumed to have no effect and to eliminate all DSTs conducted within that radius which post-date production (Parks, 1989 p.85-88). The problem is how to define the radius. If it is too small, pressures that are drawn down will be included, too large and undisturbed data will be culled. Parks used a radius of 1.6 km. Tóth and Corbet (1986, p.355) in an earlier hydrogeological study in southern Alberta ignored any active production wells more than 4.8 km distant from a DST well. For production wells within the 4.8 km radius they assessed drawdown by calculating an interference index which is described in detail below.

Other studies (e.g. Bair et al., 1985, p.4), have relied on PID-affected pressures being sufficiently disturbed that they are obviously anomalous (e.g., they might produce closed low “bulls eye” closures around oil fields on a hydraulic head map) and are culled on that basis. No previous study to my knowledge has explicitly considered the production rate and the cumulative effect of multiple pumping wells in the evaluation of PID.

### ***Definition of the Interference Index***

The “interference index” was introduced as a crude PID indicator by Tóth and Corbet (1986). The interference index is defined as

$$I = \log_{10} \frac{t}{r^2}, \quad (3.2)$$

where  $t$  is the pre-DST production time in years and  $r$  is the inter-well distance in miles. Tóth and Corbet calculated  $I$  for DST wells within 4.8 km of an active production well and rejected the pressure if  $I$  exceeded 0.7.

### **3.2.3.2 Overview of Petroleum Production in the Study Area**

The oil field outlines and production well locations in the study area are shown in Figures 4.1 and 3.11.1. Oil production in the study area started in February 1969 with the completion of the discovery well of the Keg River A Pool in the Senex field. To date 407 production wells have been drilled of which three quarters are still active, currently producing from 11 separate fields. Only one gas field (the Liege Field) exists, part of which extends into the eastern edge of the study area. Production activity is intense and over 150 oil wells were completed between 1987 and 1990. A recent Geological Survey of Canada reserves update of Alberta (Podruski et al., 1987) predicts on the basis of an assumed log normal distribution of pool sizes for a given play, that the largest pools in the region remain undiscovered.

Oil production is restricted to the oldest and deepest aquifers on the Peace River Arch: the Keg River-Granite Wash aquifer which mantles the Pre-Cambrian basement at a depth ranging from 1 to 2 km and the Slave Point Formation which is separated from the Keg River Fm. by the Muskeg evaporites. An average well in this region has been active for 3

years and has produced 10 000 m<sup>3</sup> (62 000 bbl) of oil, an equal amount of water and 500 000 m<sup>3</sup> (17 million ft<sup>3</sup>) of gas (see Table 3.7). All oils are undersaturated with gas at reservoir conditions. Bubble point pressures in oil pools at the Trout, Kidney and Senex fields are at least 5 MPa below the initial pressure (ERCB, 1986). Free gas exists only at the Liege field in the Grosmont Fm. The large number of wells and relatively modest production statistics reflects the abundance of small individual pools that characterize the Middle Devonian carbonate and clastic plays on the eastern margin of the Peace River Arch.

The most recent DST pressure in the database of stable pressures for the present study was recorded on 5 April 1987, hence all production initiated after this date was ignored as a potential source of disturbance. Removing the ineffective wells left 243 production wells (including 8 injection wells) to be accounted for. Table 3.8 shows the numbers of wells in the various production zones.

### **3.2.3.3 PID Calculation**

#### ***ERCB production Data***

The ERCB provides detailed production histories for all Alberta oil and gas wells. Using digitized ERCB production data (PUBCO, 1990 b), I calculated drawdown by the procedure described below.

Table 3.9 summarizes the results of the drawdown calculations and shows the categories which were eventually culled. Pressures recorded before the earliest production in the area, in wells more than 10 km from the nearest active production well and in non-producing formations were assumed to be undisturbed which left 151 pressures to be checked. The former and latter assumptions are clearly reasonable and the maximum disturbance radius of 10 km is cautious compared to those applied in previous studies of PID (see Section 3.2.3.1).

#### ***The Theis Equation***

When water is discharged from a well the fluid potential in the aquifer at the well site is reduced. The potentiometric surface at the well site is lowered and a cone of depression centered on the well bore gradually extends outward into the aquifer as pumping continues. The energy loss represented by this growing dent on the potentiometric surface



is manifest as reduced pressure heads within the cone of depression. A DST conducted within such a cone of depression may indicate a stable pressure which is nonetheless disturbed, is lower than the virgin pressure and may cause a misinterpretation of the flow field. Fluid injection will have the reverse affect creating a mound on the potentiometric surface and raising formation pressures above their undisturbed level.

In a classic study which initiated the modern approach to well hydraulics, Theis (1935) developed an equation which can be used to calculate the magnitude of the drawdown (in terms of hydraulic head) as a function of the radial distance to the DST well from the pumped well and the duration of pumping. Using the Theis Equation in this way requires knowledge of two hydraulic parameters for the aquifer (the transmissivity and storativity) and the rate of fluid discharge at to the production well. Hydraulic head drawdown ( $s$ ) which is the difference between the disturbed and the undisturbed elevation of the potentiometric surface can then be calculated as:

$$s = \frac{QW(u)}{4\pi T}, \quad (3.3)$$

where  $Q$  is the well discharge (or fluid production rate) in  $m^3/s$  and  $T$  is the aquifer transmissivity in  $m^2/s$ .  $W(u)$ , known as the well function is defined as

$$W(u) = \int_u^{\infty} \frac{e^{-u} du}{u}, \quad (3.4)$$

where

$$u = \frac{r^2 S}{4Tt}. \quad (3.5)$$

Here  $r$  is the distance from the production well to the DST well in metres.  $S$  is the aquifer storativity,  $T$  is the aquifer transmissivity in  $m^2/s$  and  $t$  is the duration of the pumping interval in seconds. In practice when  $S$  and  $T$  are known, Equations 3.3 to 3.5 are applied in reverse order. A value for  $u$

is calculated first,  $W(u)$  is then computed or read from a  $W(u)$  versus  $u$  table (e.g. Freeze and Cherry, 1979, p.318) and a solution for drawdown is obtained from Equation 3.3.

Numerous idealized conditions are required for the strict application of the Theis Equation (ibid., p.315-317). The most stringent condition is that the aquifer be confined between effectively impermeable aquitards. The ideal conditions are rarely if ever fully met in nature and subsequent workers have devised modifications to Theis' equation to deal with "leaky aquifers", partially penetrating wells and so on (ibid., Chapter 8.3).

### *Justification for Using the Theis Equation in my Study Area*

This section outlines arguments for the confined nature of the aquifers in the present study area on the time scale of production. It is important to note here that a stratum may function as an effective confining bed over a period of a few decades (the life of a pumping well) while transmitting significant quantities of fluid over millions of years. The existence of apparently confined conditions on a human time scale and of regional hydraulic continuity on a basinal scale over geological time periods are not mutually exclusive, rather they indicate the importance of scale definition to the meaningful determination of permeability.

The study area cross-sections (Figures 1.4 and 1.5), show the geometry of the strata concerned. The Keg River aquifer lies on crystalline rocks of the Pre-Cambrian basement and is overlain by the Muskeg-Prairie Evaporite Fm. The Slave Point Aquifer overlies the Muskeg Fm. and is itself overlain by the calcareous shales and argillaceous limestones of the Beaverhill Lake Group. Thus the Pre-Cambrian basement, the Muskeg evaporites and the basal shale of the Beaverhill Lake Group are the proposed confining beds for the two Devonian producing intervals. Table 3.1 shows the low average core permeabilities for these units (all proposed confining beds exhibit permeabilities below one millidarcy).

### *The Pre-Cambrian Basement*

In all previous flow studies conducted in the Western Canada sedimentary basin, the top Pre-Cambrian has been treated as an aquiclude (Tóth 1978; Bachu, 1985; Hitchon et al 1990). Hydrogeologic studies on the Canadian Shield however, (see Section 4.2.3), have demonstrated that

topography driven flow systems are active in fracture and fault systems in Pre-Cambrian crystalline rocks. These discoveries support the possibility of significant fluid transport in the crystalline basement of the western Canada basin. Unfortunately permeability data for the basement are very rare. The geological history of the study area (see Section 1.2.3) provides some constraints on the permeability distribution.

Given the active tectonism of the Peace River Arch, the basement in the present study area is probably more fractured than the basement in tectonically quiescent parts of the basin. If the fractures form a hydraulically continuous network, they will enhance permeability. Weathering, during the pre-Middle Devonian period of subaerial exposure of the Pre-Cambrian surface in the Peace River Arch region, may also have contributed to basement permeability. Because vertical compressive stress increases with depth (i.e., with the thickness of overburden) fracture permeability may decrease with increasing depth. Weathering would obviously be restricted to the exposed basement. It is probable therefore that the basement permeability is greatest in a relatively shallow zone along its upper surface.

If this is the case, the permeable upper surface of the basement will function as a downward extension of the Keg River Aquifer. There are no high elevation basement outcrops which might generate flow systems within the Pre-Cambrian independent of those in the Keg River, so the effect of a permeable layer in the upper basement will be limited to increasing the transmissivity of the Keg River Aquifer. This hypothesis is supported by the fact that formation water samples recovered from drillstem tests conducted in the Pre-Cambrian within the study area show no significant chemical differences from Keg River Aquifer water (see Appendix 5).

#### Muskeg-Prairie Evaporite Fm.

The Muskeg Fm. has been treated in earlier studies as an aquitard (Tóth, 1978) and as an aquitard and partial aquiclude (Bachu 1985, Hitchon et al. 1990). The Muskeg Fm. thickens from 40 m in the southeast to over 300 m in the northwest of the study area. This thickness change reflects increasing basin depth with distance from the palaeo-shoreline to the southwest. The Muskeg-Prairie Evaporite Fm. also exhibits a facies

transition from anhydrite and dolomite in the nearshore environments of the southwest to halite and anhydrite in the northeast. The most permeable beds within this formation are cryptocrystalline dolomites in which anhydrite cement is common. Permeability determinations are rare in the few core samples taken within the Muskeg. Table 3.1 shows the low lateral permeabilities typical of dolomites within the Muskeg Fm. The few permeability data available for the Muskeg Fm. suggest an average permeability just one order of magnitude less than that of the Keg River and Slave Point Aquifers. This reflects the sampling bias, all Muskeg core samples being taken from relatively permeable dolomitic intervals near the base of the formation. The dense, poorly permeable nature of halite and anhydrite strata is widely acknowledged. On the time scale of petroleum production the Muskeg-Prairie Evaporite Fm. is certainly a confining unit.

#### Waterways Fm.

The Beaverhill Lake Group, which overlies the Slave Point Aquifer, comprises interbedded shales and argillaceous limestones. The lowermost unit, the Firebag Fm. (Keith, 1990) thickens westwards from 2 m at the Sawn Lake field in the east, to 25 m at the fifth meridian. The Firebag sediment in cores from the Sawn Lake area is a bitumenous lime-mudstone indicating very slow deposition in a relatively starved basin (Keith, 1990). Core data obtained in the present study (see Table 3.1) indicate an average permeability for the Beaverhill Lake Group of 0.4 millidarcies.

In conclusion the assumption of confined flow in the Keg River and Slave Point aquifers is justified on the basis of the lithology of the confining strata, available core permeabilities and the minor time scale of production. Note moreover that if significant leakage through the aquitards on the time scale of pumping does occur, the Theis Equation will *overestimate* drawdown at DST wells. This ensures that no disturbed pressure data will be overlooked.

There follows a description of the procedure used to compute PID for the 155 potentially disturbed DST pressures in the present study area.

#### ***PID Calculation Procedure***

The following procedure was followed for each DST well in turn.

**1. Identify production (and injection) wells which were active prior to the DST date and calculate the pumping interval.**

Calculate the pumping interval prior to the DST as the DST date minus the Start of Production/Injection date for all production wells. When this is a negative value production post-dates the DST and cannot cause PID. If the calculated pumping interval exceeds the cumulative production time for the well given in the Pubco database - use that instead. This substitution was made for 225 of the 1164 DST-production well interactions. Three assumptions are made in this step. First that production once started is continuous. In reality most production wells halt pumping at intervals to allow the reservoir pressure to recover. Second, that the continuous pumping period ended at the DST date. While this is probably usually the case (over half the production wells remain active today) no check was made for the possible abandonment/suspension of production wells prior to the DST which would diminish the disturbing effect of pumping. Thirdly that the production rate was uniform. Figure 3.5 depicts schematically a case which illustrates these problems.

The main error in this step is to have overestimated the pumping interval by the time that the well was actually idle. The inaccuracy is constrained by the total cumulative production time for the well which the calculated pumping interval cannot exceed.

**2. Identify production (and injection) wells within 10 km radius. Reject those producing from zones other than the aquifer of interest.**

For the production/injection wells which remained from step 1, the radial distance from the DST well was calculated, retaining for further calculation all wells within a 10 km radius. Production wells with a perforated interval mid-point over 200 m above or below the mid-point of the packer interval in the DST well were rejected. This removed wells producing from aquifers other than that in which the DST was conducted. The well location coordinates in the Pubco database are accurately surveyed and are corrected to bottom hole coordinates for deviated wells.

### **3. Calculate $u$ for each active production (and injection) well.**

Using Equation 3.5,  $u$  values were calculated for each DST well with respect to all production wells in a 10 km radius which were active prior to the DST date. The aquifer storativity ( $4.70 \text{ E-}05$ ) and transmissivity ( $9.1 \text{ E-}06 \text{ m}^2/\text{s}$ ) values used are arithmetic averages for the Keg River-Granite Wash aquifer calculated from core data for the study area (see Tables 3.1 and 3.3). The error in the calculated  $u$  values arises from the constant values of  $S$  and  $T$  applied, and the possible non-circularity of cones of depression due to low permeability aquifer boundaries or permeability anisotropy.

It is theoretically possible to obtain more accurate drawdown values by determining local permeability, porosity and aquifer thickness values representative of the 10 km well radius for each DST well, although this would greatly complicate the calculation procedure. The  $S$  and  $T$  calculated for the Keg River aquifer in the present study were also used for the Slave Point aquifer since the hydraulic characteristics of the aquifers are similar. The Keg River and Slave Point Formations exhibit permeabilities of 11 and 5 md and porosities of 6.3% and 6.2% respectively (see Table 3.1).

### **4. Extract $W(u)$ value corresponding to $u$ from Theis Type Curve $u:W(u)$ Table.**

Equation 3.4 was solved (Istok, 1989) for  $u$  values ranging from 0.01 to 20, to cover the data range. Figure 3.6 is a graph of the Theis type curve constructed from these data.  $W(u)$  values were then extracted from the table corresponding to the calculated  $u$  values. The table has a sufficiently high sample density (100 values per log cycle) that it was unnecessary to interpolate between tabled  $W(u)$  values.

### **5. Calculate drawdown caused at a DST well by each individual production well.**

Drawdown in metres, was calculated using Equation 3.3. There were 1196 interactions between the 151 potentially disturbed DST wells in the present study area, and the 243 active producing wells. Of these, 888 generated  $u$  values  $>20$ , hence  $W(u)$  less than  $10^{-10}$  and effectively zero drawdown (see Figure 3.6). The remaining 308 interactions caused disturbance (partial drawdowns) at the DST wells.

**6. Calculate Tóth's Interference Index.**

Tóth's Interference Index (Tóth and Corbet, 1986, p. 355) is:

$$I = \log_{10} \frac{t}{r^2}, \quad (3.2)$$

where  $t$  is the production time in years and  $r$  is the distance between the DST and the production wells in miles.

**7. Calculate total drawdown at each DST well.**

The Principle of Superposition (Freeze and Cherry, 1979, p.327) states that overlapping cones of depression due to multiple pumping (production) wells produce a total drawdown at a given observation (i.e., DST) well which is the sum of the component partial drawdowns. Partial drawdowns caused by all active production wells within a 10 km of each DST well were summed to give the total drawdown.

**8. Calculate a Cumulative Interference Index**

Since total drawdown is actually the sum of the partial drawdowns caused by individual production wells, a cumulative interference index was calculated:

$$\Sigma I = \sum_{i=1}^n \log_{10} \frac{t_i}{r_i^2} \quad (3.6)$$

which is the sum of the individual indices generated for each DST well.

***Evaluation of the Critical Drawdown Parameters***

Equations 3.3 to 3.5 show that there are five variables which affect drawdown. Since constant values of  $S$  and  $T$  were used there are only three variables in my drawdown calculations. Drawdown is proportional to the pumping time and the pumping rate at the production well, and inversely proportional to the square of the distance between the DST and the production well.

Figure 3.7 and Table 3.10 illustrate the relative significance of these 3 variables. The vertical axis of the graphs in Figure 3.7 shows partial drawdown i.e., that component of the total drawdown at a DST well caused by individual production wells. The negative drawdowns were caused by injection wells.

Table 3.10 shows the averages and standard deviations of the 3 variables for different ranges of partial drawdown calculated separately for production and injection wells. The figure and the table comprise the results of 1194 interactions between 155 DST and 235 production wells. The three variables: distance, time and production rate are now discussed in turn.

### 1 Distance

Figure 3.7(a) shows clearly that distance is the dominant variable. All partial drawdowns exceeding 10 m are caused by production wells less than 3 km from a DST well. Further, both the magnitude and frequency of drawdowns diminish as distance increases. However, it is also apparent that minor drawdowns are caused by production wells over distances up to and presumably exceeding 10 km (the maximum distance considered). A sufficient number of these minor partial drawdowns may add up to significant total. Nearly arbitrary disturbance distance cut-offs such as the 1.6 km limit used by Fawcett and the 4.8 km limit by Tóth and Corbet, should be applied with caution and consideration given to the total number of production wells which may contribute to the drawdown at a given DST well. Table 3.10 reinforces these observations. The partial drawdown range increases progressively as the average inter-well distance decreases. Production wells causing over 5 m of partial drawdown at DST wells were on average 1.2 km distant.

### 2 Production Time

Figure 3.7(b) shows that all production wells in a 10 km radius which were active for more than two years before a DST caused drawdown. The maximum disturbances however are caused by production wells with fairly short pumping times (less than 3 years) reflecting the overriding positive influence on drawdown of proximity (Figure 3.7(a)). Table 3.10 shows that the zero drawdowns correspond to the shortest



pumping intervals (average 0.5 years) whereas 1 to 5 m drawdowns occurred when the average pre-DST pumping time was 2.7 years.

### 3 Production Rate

Figure 3.7(c) shows the effect of the pumping rate on PID. Zero drawdowns are concentrated at low pumping rates (less than 50 m<sup>3</sup> per day), but this is also the range within which the maximum drawdowns occur. There is no reliable trend in drawdown related to production rate and this is also apparent from the average values for different drawdown ranges shown in Table 3.10. Overall the variability of production rates is small (only 6 wells exceed 100 m<sup>3</sup> per day) which probably reflects imposed legal production constraints. In conclusion the pumping rate is the least influential of the 3 variables affecting PID.

## *A Refined Interference Index*

### Partial Drawdowns

Figure 3.8(a) is a graph of the drawdowns caused at DST wells by individual production wells (partial drawdowns), versus the interference index of Tóth and Corbet. There is some scatter to the distribution reflecting the influence of the production rate which is not considered and also the fact that (as indicated by Equations 3.3 to 3.5) drawdown is not a log function of  $t/r^2$ . Nonetheless the threshold of PID is well defined at  $I = -0.6$  (see Figure 3.8(b)). This is considerably lower than the threshold of +0.7 used by Tóth and Corbet. Table 3.10 shows that the average individual interference index increases progressively with increasing drawdown. As shown in the table maximum partial drawdowns (62 interactions produced drawdown > 5 m) occur at an average  $I$  value of +0.5.

### Total Drawdowns

Since total drawdown is actually the sum of the partial drawdowns caused by individual production wells, a cumulative interference index was calculated

$$\Sigma I = \sum_{i=1}^n \log_{10} \frac{t_i}{r_i^2}, \quad (3.6)$$

which is the sum of the individual indices generated for each DST well. Figure 3.9 shows the calculated total drawdowns versus the cumulative interference index for the 155 DST wells.

As for the individual index in the previous figure, Figure 3.9(b) shows that the threshold of PID is fairly abrupt. I recognize the threshold of *significant* disturbance at  $\Sigma I = 0.2$  since no zero drawdowns occur at this magnitude whereas all large total drawdowns are included. The discrepancy between my suggested thresholds of  $I$  and  $\Sigma I$  (-0.6 and +0.2 respectively) and the value of +0.7 used by Tóth and Corbet (1983) reflect contrasts between the two study areas: the hydraulic character of the strata (they considered PID in 3 Mesozoic sandstone formations) and the production schedules. Further study in different regions would be required to show whether the thresholds calculated here are applicable outside the present study area.

Table 3.11 shows relevant statistics for these wells, for each of four PID ranges (from zero to over 5 metres drawdown): the number of DSTs; the distance to the closest producing well; the number of active production wells in a 10 km radius and the calculated  $\Sigma I$  values.

Finally in Figure 3.10(a), total drawdown versus the distance to the nearest active production well is graphed while Figure 3.10(b) shows total drawdown versus the number of active production wells within a 10 km radius. From the first graph it is clear that all severe drawdowns are for DST wells <2 km from the nearest active production well. Use of this single culling criterion, which would be very quick and easy to apply would result in the inclusion of only the three seriously disturbed DST wells around the four kilometre distance mark on the figure. Simultaneously however, a large number of undisturbed pressures would be culled (the 10 to 15 points spread along the horizontal axis between 1 and 2 km).

Figure 3.10(a) also shows that no significant total drawdown occurs when the nearest active production well is over 4.5 km distant. This coincides remarkably well with the drawdown limit radius of 4.8 km proposed by Tóth and Corbet. The statistics in Table 3.11 reinforce the relationship, showing progressively smaller average distances to the nearest production well as the total drawdown increases. The differences between

the average values for successive ranges of drawdown are marked and the standard deviations are low.

Figure 3.10(b) shows a very weak positive correlation between total drawdown and the number of active production wells within a 10 km radius. The large standard deviations in Table 3.11 mirror the wide spread of the data points shown in the figure. This criterion is not useful as a disturbance indicator.

### ***Three Methods for Evaluating PID***

In summary, 3 methods of evaluating production disturbance have been evaluated whose refinement is proportional to the time invested in their calculation. In order of increasing refinement these are:

1) Cull all pressures obtained from DST wells <2 km from an active production well (see Figure 3.10(a)). This method would erroneously cull a large amount of undisturbed data.

2) Calculate the cumulative interference index:

$$\Sigma I = \sum_{i=1}^n \log_{10} \frac{t_i}{r_i^2}$$

which considers both distance ( $r$ , in miles) and the pumping interval ( $t$ , in years) and reject those wells for which  $\Sigma I$  exceeds 0.2. (see Figure 3.9(a)).

3) Calculate drawdown using the Theis Equation which considers time, distance, pumping rate and the hydraulic properties of the aquifer.

### ***Conclusions:***

1) Accurate evaluation of PID is fundamental to the meaningful interpretation of subsurface pressure data for detailed flow studies in oil producing regions.

2) Individual production wells in the present study area cause disturbance over distances exceeding 10 km although significant drawdown falls off rapidly with increasing distance. No total

drawdowns exceeding 1 m were calculated for DST wells > 4.5 km from the nearest active production well.

3) Total drawdowns are the sum of the partial drawdowns caused by all contributing production wells. In the present study area each DST well was subject to the influence of an average of 8 production wells within a 10 km radius. One DST well was subject to the effect of 23 production wells.

4) PID can be estimated on the basis of:

*i) Proximity to the nearest single active production well. This factor is the best single indicator of PID.*

*ii) The Cumulative Interference Index. This is a more accurate indicator of PID requiring the same data but more computation effort than i)*

*iii) A relevant "drawdown equation" from well hydraulics.*

### **3.2.4 Culling of Production Disturbed Pressure Data**

The total drawdown values I calculated are precise but inaccurate given the certainty of local deviations from the S and T constants used, plus the possible violation of some of the ideal assumptions underlying the Theis Equation. For this reason rather than recalculate undisturbed heads, I culled all the pressure data for which total calculated drawdowns exceeded 1 m and identified the remaining data with varying confidence levels. This resulted in the culling of 63 of the 301 stable pressures from the database.

Figure 3.11.1 shows the distribution of production wells that were active prior to the most recent DST in my data base. Different symbols distinguish Keg River-Granite Wash aquifer wells from those in the Slave Point. Figure 3.11.2 is a contour map of calculated drawdown in the Keg River Aquifer. The drawdowns represent conditions at the time of the individual DSTs which were conducted over a period of 30 years. The map illustrates the maximum error that could exist in the Keg River Aquifer potentiometric surface if PID were unaccounted for.

### 3.2.5 Rationale for Using Non-Water Recoveries

#### 3.2.5.1 Mud Recoveries

Mud recoveries may indicate either a packer seat failure or production of mud filtrate from the formation. In the former case the pressure recording is useless but in the latter case it may be perfectly valid. A packer seat failure will normally generate a range of effects including an abnormal build up curve which make it immediately recognizable and the DST will be classed as mis-run. Extensive mud invasion of the formations penetrated by the borehole during drilling is common and may cause supercharging if the reservoir is small. The pre-flow period of a DST is intended to bleed off any excess pressure due to supercharging and if it does not the DST will usually show depletion. Depletion is indicated when the extrapolated pressure for the initial shut in is over 3% higher than that for the final shut in (Ehrmann, undated). Supercharge and depletion are causally related because a reservoir that is small enough to experience a significant pressure increase from mud invasion will also experience a significant pressure decline during the main flow period of a DST. In practice, since supercharge can be recognized from the test results (by depletion) reliable and dubious mud recovery DSTs can be distinguished.

#### 3.2.5.2 Oil Recoveries

Pore pressures in oil pools are often higher than those in adjacent water saturated rock. The pressure difference increases with the height of the vertically continuous oil column, and with the density contrast between oil and water. This is a simple consequence of hydrostatics. It would be erroneous to take pressures recorded in oil pools as representative of the ambient water pressure if the oil is significantly over-pressured. The potential magnitudes of excess pressure in the oil pools of the present study area can be calculated using the data in Table 3.12. Presented in the table are the arithmetic mean averages and standard deviations of pool heights (b) and oil and water densities ( $\rho_o$  and  $\rho_w$  respectively) for the Keg River Formation. The fluid densities are from ERCB data (ERCB, 1991 a), (ERCB, 1991 b). Both fluid densities are corrected to reservoir conditions.

Assuming that all of these data are from populations with approximately normal distributions, the mean  $\pm 2$  standard deviations will

cover the range of 95% of the population (Davis, 1973) This range is included in Table 3.12.

The excess pressure ( $P_{ex}$ ) generated in the oil at the top of a pool can be calculated as

$$P_{ex} = (\rho_w - \rho_p) b g, \quad (3.7)$$

where  $\rho_w$  is the water density,  $\rho_p$  is the oil density,  $g$  is gravitational acceleration ( $9.82 \text{ m s}^{-2}$ ) and  $b$  the height of the oil column (thickness of net pay). Thus the maximum excess pressure possible for the oil pools in the present study area is:

$$P_{ex \text{ max}} = (1228-729)*15*9.82 = 74 \text{ kPa} \quad (3.8)$$

whereas the average excess pressure (using arithmetic mean values for all variables) is:

$$P_{ex \text{ avg}} = (1156-765)*7*9.82 = 27 \text{ kPa} \quad (3.9)$$

Although these are relatively insignificant magnitudes (average mechanical error of pressure recorders is  $\pm 75 \text{ kPa}$  - see Appendix 3), oil recovery pressures were not used to construct hydraulic head maps.

### **3.2.6 Review of the Culled Data Set**

A total of 913 DSTs are tabulated in the CIFE database for the 1160 wells in the present study area of which 74% were eventually culled. Only 301 were stabilized of which a further 63 were seriously affected by production drawdown. Table 3.13 is a summary of the 238 stable, undisturbed pressures in my database which remained after culling. The oldest DST used was recorded in January 1953, the most recent in April 1987.

## **3.3 Temperature Data**

The most abundant source of deep subsurface temperature data are bottom hole temperatures (BH'Ts) recorded during the routine geophysical

logging of petroleum wells. These are the data used in the present study. BHTs are obtained mainly by maximum temperature mercury thermometers mounted on geophysical tools. After drilling has stopped the mud is circulated for a few hours to “treat” the hole. Geophysical logging then proceeds, the BHT being recorded when each tool is pulled back to the surface. Obtaining an accurate temperature reading is unfortunately not a major priority of the logging operation and BHTs comprise a data base of notoriously variable quality. As noted in Appendix 3 the theoretical limits of temperature resolution imposed by the accuracy of the temperature sensors and by thermal convection in the mud column are at best  $0.1^{\circ}\text{C}$ . However the actual error in reported temperatures, collected as a low priority task under uncontrolled conditions is frankly unknown. Leblanc et al (1982) assume an absolute error of  $\pm 5.5^{\circ}\text{C}$  in reported BHTs, but this is an arbitrary value.

### 3.3.1 Thermal Disequilibrium and Correction Methods

A more tractable problem than the accuracy of the reported BHTs is that of the thermal disequilibrium caused by drilling. In a well, circulating drilling mud cools the lower portion and warms the upper portion of the borehole as shown in Figure 3.12. The actual shape of the disturbed temperature curve depends on many factors including the mud composition and circulation rate, the ground surface temperature and the local geothermal gradient (Gretener, 1981, p.67). When circulation stops the rock adjacent to the borehole slowly recovers its undisturbed ‘formation temperature’ which is transmitted to the mud. It is the stable formation temperature at the bottom of the hole that we seek. Since most BHTs are measured before thermal equilibrium is attained, the recorded temperatures are too low. The problem then is how to derive true formation temperatures from BHTs.

Over the last four decades some 30 different methods to correct petroleum well BHTs for the effects of thermal disequilibrium have been devised, many of which are reviewed and compared by Hermanrud (1986). Early models based on fairly simple assumptions have been succeeded by models attempting a more sophisticated description of the borehole conditions. However the latter models require several parameters (e.g., thermal conductivities and heat capacities of the mud and the strata) which

are only approximately known, so do not necessarily yield better results (ibid, p.925).

To account for thermal disequilibrium effects, Horner corrections were calculated (Horner, 1951) for those BHT measurements with recorded times of cessation of drilling and of circulation. These data were subsequently used to calibrate the corrections applied to the remaining data (see Section 3.3.1). Dowdle and Cobb (1975) show that although temperature build up is not strictly analogous to pressure build up, Horner extrapolation gives reasonable estimates of static formation temperature when the circulation time is short (i.e., less than a day) and the geothermal gradient is not exceptionally high. A practical description of how to use Horner plots for BHT correction is given by Fertl and Wichmann, (1977).

Horner plots require multiple temperature measurements at the same depth in the same well, the total mud circulation time after cessation of drilling plus the times elapsed since circulation stopped for each temperature measurement. Often, the circulation time is not available and in such cases I have used an assumed value. This introduces error of unknown magnitude.

### **3.3.2 Culling and Correcting BHT data**

BHT data were read from the headers of well logs in the ERCB microfiche collection (ERCB, 1990 b). Dr. Bachu of the Basin Analysis Group at the Alberta Research Council provided guidance and assistance in the culling and correction of these data. Figure 3.13 is a flow chart which outlines the procedure used.

#### **3.3.2.1 First Stage**

A total of 4202 BHT records consisting of between 1 and 5 temperature readings per record, were tabulated for the wells in the study area. Initial culling removed 145 clearly contradictory records (e.g. different temperatures reported at the same time in the same well). The remaining raw data were arranged into three classes:

*Class 1: 3196 records with two or more temperature readings including the time elapsed since circulation stopped*



*Class 2: 574 records with single temperature readings including the time elapsed since circulation stopped*

*Class 3: 287 records with single temperature readings without time elapsed since circulation stopped*

For Class 1 and 2 records a circulation time of 6 hours was assumed where the circulation time ( $t_c$ ) was not recorded. This comprises 4 hours for circulation after drilling stopped (as used by Chapman, 1984), plus an extra 2 hours for the average time required to drill to TD below the point of temperature measurement. Two hours is my estimate based on the location of the thermometers (normally positioned 9 m above the bottom of the tool), and assuming a penetration rate of 14 minutes per metre for the lower Elk Point Group sediments or weathered Pre-Cambrian (Helander, 1983). The necessity of including this calculation in the circulation time was pointed out by Gretener (1981, p.70).

### **3.3.2.2 Second Stage**

Corrected formation temperatures for the Class 1 data were obtained by extrapolating to origin (i.e., to infinite time) a Horner plot of the BHTs versus the dimensionless time variable  $\log[(t_c+t_e)/t_e]$  where  $t_c$  is the circulation time and  $t_e$  is the time elapsed since circulation stopped. The calculation was performed using software written and implemented by Dr. Bachu at the Alberta Research Council (Bachu, 1988).

Horner analysis of the Class 1 data yielded 25 records with positive slope (temperatures decreasing over time), 1256 records with zero slope and 1815 records with negative slope. The positive slope records yielding a static temperature lower than the measured temperatures were discarded since none of the temperatures were recorded at shallow depth in a deep well, which could explain a cooling trend. Example Horner plots are shown in Figure 3.14. The zero slope data (i.e., two or more temperature readings all the same value) were added to the Class 2 data for later processing, retaining only the first temperature reading and time elapsed. It is assumed here that the temperature was measured once (on the first logging run), that value being copied for subsequent runs. The negative slope data were scanned for records where:

*i) The temperature correction  $\Delta T$  (Horner corrected temperature minus final BHT) exceeded  $8^{\circ}\text{C}$*

*ii) The correlation coefficient was less than 0.5*

Log headers of these records were reexamined for data entry errors, and considering the time and temperature data for each case individually, 168 records were rejected, leaving 1747 corrected Class 1 records.

### **3.3.2.3 Third Stage**

Following the procedure developed by AAPG (1976) and used by Chapman (1984), and Bachu (1988), regression analyses were performed on the 1747 Class 1 temperature corrections (the Horner corrected temperature minus the final BHT reading). The regression analysis was conducted by Dr. Bachu at the ARC using software developed by Bachu for this purpose. First, least squares regression equations were solved for  $\Delta T$  as a function of depth alone. Solutions were obtained to polynomials of the form:

$$\Delta T = a_1d + a_2d^2 + a_3d^3 \dots + a_nd^n \quad (3.10)$$

where  $\Delta T$  is the temperature correction in  $^{\circ}\text{C}$ ,  $a_1, a_2, \dots, a_n$  are the polynomial coefficients and  $d$  the depth (in km) of the BHT. The correlation coefficient was calculated for each solution as an indication of the goodness of fit, and  $n$  was increased until no significant increase in correlation coefficient was achieved. A reasonable fit (correlation coefficient  $r^2$  of 0.593) was obtained for the third order polynomial:

$$\Delta T = 42.1384d - 41.616d^2 + 11.7738d^3 \quad (3.11)$$

This equation was used to calculate corrections for the 287 Class 3 records which had no information beyond the depth and the BHT. Next regression equations were solved in the same manner for  $\Delta T$  as a function of depth

and time. A correlation coefficient  $r^2$  of 0.54 was obtained for the polynomial:

$$\Delta T = (92.7675d - 86.5754d^2 + 25.6326d^3) * \log[(t_c+t_e)/t_e] \quad (3.12)$$

where  $t_c$  = circulation time and  $t_e$  is the time elapsed since circulation stopped. This equation was used to correct the Class 2 BHTs.

### 3.3.3 Temperature Data Quality Classes

Of the original 4202 BHTs approximately 90% were retained with the following breakdown of data quality:

*Class 1: 1747 Horner corrected BHTs*

*Class 2: 1830 BHTs corrected by a polynomial in time and depth*

*Class 3: 287 BHTs corrected by a polynomial in depth*

### 3.3.4 Review of the Culled Data Set

The temperature data are used in the following chapter to construct a temperature map and an average geothermal gradient map. The distribution of the data are shown on these maps. The data are almost exclusively from the Pre-Cambrian.

## 3.4 Water Chemistry Data

### 3.4.1 Source and Type of Water Chemistry Data

A large database (on microfiche) of major ion analyses is available from the ERCB for formation waters sampled from oil wells. Water samples are routinely taken during drillstem tests. They may be caught at the surface as the pipe is broken down or isolated at depth in a special chamber in the DST tool (the down hole sampler). Samples may also be obtained at the surface during production tests. Chemical analyses are conducted by commercial labs (e.g. AGAT, Core Lab, Geotech etc.) all of which use standard procedures and produce uniform results (Johnson,

1988, p.9). Major ion analyses report concentrations (in mg/L) of the cations  $\text{Na}^+$ ,  $\text{K}^+$ ,  $\text{Ca}^{++}$  and  $\text{Mg}^+$  and the anions  $\text{Cl}^-$ ,  $\text{HCO}_3^-$ ,  $\text{CO}_3^{--}$  and  $\text{SO}_4^{--}$ . Trace elements (F, Ba, Sr, I and Br) are occasionally reported.

### **3.4.2 Culling Criteria**

All water samples in the ERCB database (ERCB, 1990 a) are contaminated to some degree (Johnson, 1988), the purpose of culling is to remove those analyses which are so contaminated that they are unrepresentative of the true formation water composition. The most common contaminants are mud filtrate derived from the drilling fluid and acids used in well stimulation. Certain checks can also be made for serious analytical errors. The Opus Engineering publication Belly River Water Study (Johnson, 1988) is a very useful practical guide to the interpretation of water chemical analyses from the ERCB database.

#### **3.4.2.1 Initial Culling**

For the wells in the present study area, 1568 analyses were available all of which were viewed on a microfiche reader. Initial culling removed 764 analyses. These comprised duplicated records, incomplete analyses ( $\text{Cl}^-$  concentration or resistivity only), battery (multiple well) samples and samples with pH greater than 12 and less than 4 (severely mud and acid contaminated respectively). A few analyses of these severely contaminated waters were recorded to help define the criteria by which to recognize less contaminated formation waters. For the remaining 804 samples, the following information was entered into a spreadsheet: the major and minor ion concentrations; TDS (calculated); water density and pH (both at 15.6 °C and one atmosphere); sampling date; the recovery method (DST, swab, production test etc.) recovery description and lab comments. I also recorded well data including the wellhead elevation, the reported formation name, and the DST packer interval depth range.

#### **3.4.2.2 Detailed Culling Criteria**

Two approaches to detailed culling were made: numerical comparisons of selected parameters on a spreadsheet, and graphical comparisons of overall composition using Stiff and Piper diagrams. Different criteria were developed for the determination of analytical errors, recognition of acid and mud contamination.

### 3.4.2.3 Analytical Error Recognition

Gross analytical errors can be in some cases be determined by calculating the ion balance error (IBE) for the analysis. Since electrolyte solutions are electrically neutral on a macroscopic scale, ionic imbalance indicates either that chemical species were present in significant quantity -- that were not included in the analysis or that the concentrations determined are in error. The ion balance error is calculated as (Freeze and Cherry 1979, p.97):

$$\text{IBE (\%)} = \frac{\sum \varepsilon m_c - \sum \varepsilon m_a}{\sum \varepsilon m_c + \sum \varepsilon m_a} * 100, \quad (3.13)$$

where  $\varepsilon$  is the valence and  $m$  the molality of the major ions. The subscripts  $c$  and  $a$  represent cations and anions respectively. Major ions only (no trace elements) were used for this computation. Freeze and Cherry (1979) suggest a tolerance of  $\pm 5\%$ . Johnson (1988) suggests that this should be relaxed for waters with low TDS where small errors in calculated concentrations can cause large calculated imbalances. All analyses in my database with  $\text{IBE} > \pm 5\%$  were deleted. This check does not apply to many pre-1980 analyses for which Na concentration is not determined by analysis but is calculated by difference in order to achieve electroneutrality.

### 3.4.2.4 Selected parameter comparisons

Table 3.14 shows the criteria used to characterize the ERCB analyses of Keg River Formation water which comprised the majority (70%) of the data for the present study. The rationale for each criterion is given in the second column. The criteria are not individually definitive, rather each was considered as a warning and samples were accepted or rejected on the basis of the sum of acid or mud warnings they scored. Samples were accepted as "pure" Keg River waters with one (of a possible three) acid warnings or two (of six) mud warnings. The majority (85%) of samples accepted had zero warnings.

I found the most useful culling criteria to be the Na/Cl ratio and the pH. The Na/Cl mole ratio is sensitive to both acid and mud contamination. Hydrochloric acid (HCl) is the acid usually used to enhance the

permeability of carbonate formations. Cl is added to the formation water directly from the acid while only Ca and Mg are added from the induced dissolution of dolomite. An acid wash will usually force the Na/Cl ratio in the formation water below 0.5. Typical Keg River muds are Na Cl saturated for drilling through the overlying Muskeg Fm. evaporites and therefore have Na/Cl ratios  $\geq 1.0$ . Gel chem muds used in Cretaceous formations contain more sodium and the tie ratio is therefore even higher. The Keg River Fm. is dolomite so formation waters naturally contain appreciable Ca and Mg. The anions are strongly dominated by Cl so the Na/Cl ratio is always less than unity. This is also true for Cretaceous formations. The pH of most formation waters ranges from 5.5 to 8.3, acid contamination may push the pH below 4.0 while muds often exhibit a pH over 9.0.

#### 3.4.2.5 Graphical comparisons

Major ion concentrations were converted into thermodynamically meaningful units by dividing the reported concentrations in mg/L by the equivalent weights listed in Table 3.15 to yield meq/L and constructed Stiff diagrams (Stiff, 1951; Freeze and Cherry 1979) for each water sample.

Stiff diagrams display the water chemistry in a visual form which aids culling once an appreciation has been developed for the shapes characteristic of specific formation waters, muds and acids. Figure 3.15 shows Stiff diagrams for the arithmetic mean average water chemistry of all formations in my culled data base. Figure 3.16 shows Piper diagrams for the same data. Table 3.16 gives the average major ion concentrations for each formation.

In summary, the most critical information for culling purposes comprises:

- 1) *Origin of sample (geological formation)*
- 2) *Pattern of Stiff diagram*
- 3) *pH*
  - $>8.3$       *mud contamination*
  - $5.5-8.3$     *formation water*
  - $<5.5$       *acid contamination*
- 4) *Na/Cl molar ratio*
  - $>1.0$       *mud contamination*

1.0-0.5      *formation water*  
 <0.5         *acid contamination*

### **3.4.3 Review of the Culled Data Set**

Through detailed culling 401 of the 804 analyses in the ERCB database that remained after primary culling were removed. The water chemistry database therefore comprises 403 representative formation waters. Since there were initially 1568 analyses, 75% were culled. Regarding the stratigraphic distribution of the data it is again predominantly from the Keg River and other Devonian formations. According to a recent USGS publication (Hem, 1989, p.163) major ions can be determined under optimum conditions with an accuracy of  $\pm 2\%$  for solutes present at concentrations exceeding 100 mg/L, and with an accuracy of  $\pm 10\%$  for solutes at less than 1 mg/L.

## **3.5 Oil Density Data**

### **3.5.1 ERCB Oil Analyses**

The ERCB (1991 a) have tabulated the average densities ( $\text{kg/m}^3$ ) of individual oil and gas pools for the fields in the study area. Densities are determined at 15 °C and 101 kPa abs from laboratory analyses of reservoir fluid samples taken early in the pools production history. The ERCB also provide the initial solution gas-oil ratios (GOR), and formation volume factors for oils (OFVF) determined by pressure-volume-temperature (PVT) analysis. These data were used in the present study to correct the oil densities to reservoir conditions.

### **3.5.2 Correcting Oil Densities to Reservoir Conditions**

The oil density in the reservoir differs from that at STP because the temperature and pressure at depth exceed STP and solution gas is dissolved in the reservoir oil. The gas content of the oil pools in the study area is relatively low with an average initial solution gas-oil ratio of 40  $\text{m}^3$  gas per  $\text{m}^3$  of stock tank oil, but is sufficient to significantly reduce the reservoir oil density. I used the method of Dake (1978) to correct oil densities to reservoir conditions.

Dake uses the principle of mass conservation to determine reservoir oil density. The oil formation volume factor (OFVF) is the volume of reservoir oil (containing dissolved gas) which yields 1 m<sup>3</sup> of stock tank oil plus GOR m<sup>3</sup> of gas at the well head. Knowing the density of each phase at STP, we calculate their total mass. Dividing this number by the OFVF yields the density of the oil in the reservoir. The simplicity of this method depends on knowing the OFVF. The ERCB do not indicate the density of the solution gas produced from the oil pools in the present study area so I used the average value given for the Liege gas field.

### **3.5.3 Review of the Data Set**

Oil density data are summarized in Table 3.17. Oil density data were also used to construct oil pool density maps for the Keg River and Slave Point Formations (Figures 4.26 and 4.27) and to evaluate the static “over-pressure” in oil recovery DSTs (see Table 3.12).

## **3.6 Production Data**

### **3.6.1 ERCB Production Records: PUBCO CD-Rom**

Production data to December 1990 were obtained in digital form (PUBCO, 1990 b) for the 391 production and 16 injection wells in the study area. The ERCB provide production dates and perforation depths. They give the formation name, field and pool names and well type (wildcat, production well etc.). They provide monthly and cumulative fluid production statistics (for oil, gas and water) and also give the monthly and cumulative production times. From these I calculated an average production rate for each well which was used in the evaluation of production induced drawdown of DST pressures. Production activity in the study area is described in Section 3.2.3.2.

### **3.6.2 Review of the Data Set**

The production data are presumed to be accurate. Some of the limitations in the accuracy of the data were discussed in Section 3.2.4. The geographic distribution of production wells is shown in Figure 3.11.1.

In the following chapter the culled data are manipulated to make a hydrogeological evaluation.



## **Chapter 4 Presentation of the Culled Data - Representation of the Rock Framework and Indicator Patterns**

In this chapter the culled data are manipulated to make a hydrogeological evaluation. This chapter provides methods and techniques of mapping, graphical analysis and interpretation.

### **4.1 Representation of the Rock Framework**

Most data in the study area are concentrated in the Keg River and Slave Point Aquifers which are the focus of this study. A sketchy outline will be drawn for various other units where sufficient data is available in an attempt to understand how the above mentioned aquifers interact hydraulically with the basin as a whole. Figure 4.1 shows the distribution of wells in the study area and the producing formations in the different oil fields. Also shown on Figure 4.1 are the reef edges in the Keg River and Slave Point Formations (Podruski et al., 1987). The displacement of the Slave Point reef margin relative to that of the Keg River Fm. reflects the Devonian transgression, the coastline shifted to the southwest over time, as the sea advanced up the Peace River land mass.

Note that the Slave Point Formation is producing oil at the Senex and Kidney fields which are 60 km east of the reef edge. This suggests that oil has migrated through the Slave Point Fm. east of the Sawn Lake field and that the sparsely drilled area between Sawn Lake and Panny, may contain additional oil pools. The Keg River fields conform closely to the reef edge. The Keg River formation is a poorly permeable reservoir at Senex and Kidney and becomes even tighter as the reef facies pass into thin shaley basinal facies. It is clear from the paucity of wells west of the reef margin that there is little expectation of Keg River production beyond it. The Liege gas field in the southeast corner of the study area is accumulated in the Grosmont and lower Mannville sands. I do not have much data for these units beyond the region in which the gas field lies, so will devote little attention to it.

#### **4.1.1 Computer Contouring**

Most of the contour maps for this study were generated using the graphics program Surface II (Sampson, 1975) on the University of Alberta mainframe computer. The Surface II contouring algorithm takes an x, y, z

data set of irregularly spaced oilwell data (where  $x$  and  $y$  are location coordinates and  $z$  is the variable to be contoured) from which it calculates estimated values of the  $z$  variable at each node of a regular grid. The estimated values are then contoured to produce a map. The procedure for calculating the estimates can be modified by changing: the search radius; the number of nearest neighbor data points used for averaging; weighting factors for distance from the node etc. Two extrapolation procedures are available whereby estimated  $z$  values can be constrained by the range of the input data or allowed to exceed that range. The program is therefore quite flexible and allows the user considerable control over the appearance of the final map. Furthermore the grids can be saved and subsequently manipulated (e.g., one subtracted from another to produce isopach maps).

The advantages of machine contouring are speed and uniformity of procedure. The latter quality is also a limitation however since informed interpretation may dictate a variety of ways treating the data in the production of a single map. For some maps, dummy data points were added to attain a desired interpretive effect. Computer contouring is least reliable when data are sparse.

#### **4.1.2 Structure Contour Maps**

Structure contour maps were generated for the Keg River and Slave Point Aquifers and also for the underlying Pre-Cambrian basement and the overlying sub-Cretaceous unconformity. Table 1.1 shows the stratigraphic relationships between the various formations discussed in this section. The cross-sections (Figures 1.4 and 1.5) illustrate the geometric relations.

The Pre-Cambrian surface (Figure 4.2) shows marked structural relief, commensurate with the active tectonic history of the Peace River Arch, the northern limit of which (O'Connell et al., 1990) is shown on the figure. Also shown is the outline of a 1600 Ma granite intrusion in the basement called the Trout Mountain Batholith (Burwash, 1990). The granite is less dense than the ambient ferromagnesian gneisses (Burwash, 1990) and extensional faulting in the late Pre-Cambrian and Early Palaeozoic (Cant, 1988) probably caused block faulted portions of the batholith to rise isostatically above the level of the surrounding Arch. The resulting horsts were submerged during the Middle Devonian transgression and were consequently colonized by robust stromatoporoids and corals to

form the high energy portions of the Keg River fringing reef and subsequently the most permeable, structurally elevated portions of the Keg River Formation. This may partly explain the location of the Keg River oil fields in the study area over the batholith (compare Figures 4.1 and 4.2)

The regional dip of basement is about 3 m/km (less than 0.2 ° dip WSW). There is a clear correlation between the positions of the known oil fields and positive structural elevations of the basement. There are a number of structural basement highs (open and closed) in the study area which have been only sparsely drilled. These areas have been highlighted and represent regions within which potential exploration targets will be sought in the overlying aquifers.

The next surface mapped, is the top of the Keg River Aquifer (Figure 4.3) which comprises the dolomitic Keg River Fm. and the feldspathic sands and conglomerates of the Granite Wash Fm. The Keg River Aquifer top has a regional slope of 4.2 m/km (less than 0.25 ° dip) and the relief is similar to that of the underlying basement. The Keg River Fm. reef margin is shown and I have indicated a number of structural highs on its shoreward side on the map. In the northeast, four pinnacle reefs can be discerned. To date no oil has been discovered north of east of the reef edge. The aquifer transmissivity is significantly reduced beyond this limit, and although the pinnacle reefs in the basin do have reasonable permeability, oil apparently cannot traverse the intervening area. Separate conceptual plays exist for the carbonates and clastics in this unit (Podruski et al., 1987). For the Granite Wash, the following trap types are recognized:

- 1) Stratigraphic traps at the up-dip (northeast) edge of deposition.
- 2) Stratigraphic-structural traps where local pre-Devonian structures influence sandstone deposition.
- 3) Structural traps where younger structures pool oil in continuous sheet sands.

For the Keg River Fm., a single trap type has been recognized, i.e.:

- 1) Structural-stratigraphic traps where Keg River reef facies are developed over pre-existing basement fault blocks.

The reservoir properties of the pools discovered so far, indicate that lithofacies trends within the reef are important. The eastern shelf edge, as at the Senex oilfield, comprises muddy wackestones and recovery factors are low. Higher energy trends as in the Panny field have better permeability and higher recovery factors.

The three triangles drawn on the map identify the groups of wells used to calculate gradients (hydraulic head and structure) as described in Section 4.2.1.1.

The Slave Point Aquifer is separated from the Keg River by the Muskeg-Prairie Evaporite Fm. The evaporites filled in much of the relief on the top of Keg River Fm. which is clear from Figure 4.4. The Slave Point Aquifer shows considerably less relief than the Keg River Fm., dipping WSW at 3.75 m/km. As indicated earlier, oil production in the Slave Point has been established 60 km east of the Slave Point reef margin in western parts of the Kidney and Senex fields. The high-graded areas on Figure 4.4 indicate prospective structures up-dip of the Sawn Lake field. These are clearly comparable in magnitude to the structure at Sawn Lake. Greater resolution (i.e., a smaller contour interval and a finer grid) would undoubtedly reveal structural closure at most of these sites.

The last structure contour map shows the Pre-Cretaceous unconformity and basal Mannville sands which corresponds to the top of the Upper Devonian Aquifer (Figure 4.5). Different well symbols and patterns distinguish the basal Mannville sands and the various Paleozoic formations that subcrop the unconformity where the sands are absent. The unconformity has a very gentle WSW dip of 0.6 m/km (contour interval for this map is 10 m). The map shows that Bluesky sand is absent over the subcrops of the two dolomitized formations, the Grosmont and Winterburn in the east. The Wabamun and Banff limestones are largely sand covered. The sand distribution may reflect differential relief at the time of deposition (the dolomites forming elevated ridges on the sea floor) possibly indicating that dolomitization occurred prior to Bluesky deposition. The high permeability of the Upper Devonian carbonates and the sandstone renders this surface an important conduit for lateral flow.

### 4.1.3 Isopach Maps

One objective of this study is to determine the degree of hydraulic communication between aquifers separated by thick aquitards. The Keg River and Slave Point aquifers are separated by the Muskeg Aquitard. It is reasonable to suppose that such communication will be enhanced where the aquitard is thin. Figure 4.6 is an isopach map of the Muskeg. The Muskeg Fm. thickens to the northeast (from 40 to 300 m) reflecting the increased basin depth with distance from the shoreline in the southwest. Interrupting this general trend are a number of anomalous "hollows". The two in the northeast are due to Keg River Fm. pinnacle reefs but all of those in the southern half of the area are associated with structural highs on the Pre-Cambrian (open circles on the map) and no unusual development in the Keg River Fm.

Figure 4.7 shows the well logs for the two wells indicated on the isopach map which form a short transect across the hollow in Tp.93 R.2 W5. The Muskeg Fm. in well 16-23 is devoid of halite as indicated by the caliper log (track #2). The compensatory thickening of the Watt Mountain Fm. fixes the timing of the dissolution as a very early event, possibly even syndepositional. It has been suggested that fluid migrating through the Pre-Cambrian caused dissolution of soluble salts in the Muskeg to produce these hollows which are well-known in this area (Anderson et al., 1988). Possibly meteoric water recharging the Peace River peninsula, discharged offshore creating a freshwater plume in the hypersaline evaporating basin thereby preventing local salt accumulation. Regardless of their origin these hollows are optimal locations for hydraulic communication between the Keg River and Slave Point Aquifers.

### 4.1.4 Hydraulic Conductivity Maps

Figures 4.8 to 4.10 are computer-generated hydraulic conductivity maps of the three Paleozoic aquifers. Hydraulic conductivity (K) was calculated from core permeability using:

$$K = k * \frac{\rho_o g}{\mu_w}, \quad (2.7)$$

where, in consistent units, hydraulic conductivity is in m/s,  $k$  is permeability in  $m^2$ ,  $\rho_o$  is freshwater density in  $kg/m^3$ ,  $g$  is the gravity constant (9.82 m/s) and  $\mu_w$  is the dynamic viscosity in Pa.s. ERCB core permeabilities are given in millidarcies which are converted to  $m^2$  by (Freeze and Cherry, 1979):

$$\text{millidarcy} * 9.87e-10 = m^2 \quad (4.1.1)$$

Where available, local values of temperature (to determine viscosity) were obtained, otherwise average values for the relevant formations were used. For the Keg River Aquifer, the average water temperature is 38 °C (see Table 3.17). Bear (1972) gives a viscosity value of  $6.5e-4$  Pa.s for water at this temperature, hence:

$$\frac{\rho_o g}{\mu} = \frac{1000*9.82}{6.5e-4} = 15.11e+6 \quad (4.1.2)$$

Thus for the Keg River Fm. where local values of the fluid parameters were not available the following conversion was made:

$$k \text{ (millidarcies)} * 9.87e-10 * 15.11e+6 = K \text{ (m/s)} \quad (4.1.3)$$

which accounts for the in situ viscosity of the Keg River formation water. Except for the Keg River Aquifer, the data abundance and distribution is very poor.

For the Keg River Aquifer the area of maximum conductivity is where the Granite Wash sands are thickest, in the southwest (Figure 4.8). The high permeability of these sandstones combined with low water viscosity due to high temperatures yields a conductivity in the  $10^{-6}$  m/s range. Moving northeast onto the Keg River reef, conductivities remain fairly high ranging from  $10^{-6}$  m/s down to  $10^{-8}$  m/s where the very high density brines are located. Beyond the reef, conductivities decline basinward. Anticipated lithofacies trends along the reef (high and low energy depositional environments) are not apparent on Figure 4.8. This

may indicate a more complex pattern of permeability in the Keg River Fm. than simple reef models suggest, or that the core data for this aquifer do not accurately reflect the true permeability distribution. The hydraulic head distribution (described below) indicates that the latter is probably the case.

Lacking a permeable clastic facies in the study area, the Slave Point aquifer (Figure 4.9) has a lower hydraulic conductivity than the Keg River aquifer. The conductivity in the Sawn Lake field is probably the highest in the region ( $10^{-6}$  m/s in the Joan field is suspect). If that data point is excluded then the  $10^{-8}$  m/s contour roughly parallels the reef margin. Note that conductivity does not decrease appreciably in the Slave Point aquifer between Sawn Lake and the wells at the Senex and Kidney fields.

Hydraulic conductivity in the Upper Devonian-Basal Cretaceous Aquifer (Figure 4.10) is clearly much higher than in the older Paleozoic aquifers. Because this hydrogeologic unit is very thick compared to the Keg River and Slave Point aquifers its transmissivity is huge.

#### **4.1.5 Transmissivity in the Keg River Aquifer**

Data are most abundant for the Granite Wash and Keg River Formations, so transmissivity was calculated for this aquifer alone (Figure 4.11). The transmissivity calculation procedure is described in Appendix 4. There is generally an inverse relationship between thickness and permeability in the Keg River Fm. since the dolomites are most permeable over structural highs where the aquifer is thin, so the transmissivity range is somewhat muted compared to the range of hydraulic conductivities (compare Figures 4.11 and 4.8). Transmissivity varies over just three orders of magnitude versus five orders of magnitude for the conductivity. The transmissivity value of  $10^{-6}$  m<sup>2</sup>/s used in the calculation of production induced drawdown (Section 3.2.3) is clearly a representative average. The lowest transmissivities are in the west central area (Tp.94 R.12 W5) and in the east (Tp.100 W4). Figure 4.11 does not indicate a drop in transmissivity at the reef margin, rather transmissivity increases to the north. This is at variance with geological expectation and probably reflects the paucity of core in the northern part of the study area and the bias to permeable (potential reservoir) intervals in both the sampling and analysis of core.

## **4.2 Representation of Indicator Patterns**

### **4.2.1 Pressure**

#### **4.2.1.1 Hydraulic Head Maps**

Conventional hydrogeological interpretation of a freshwater equivalent hydraulic head map as a potentiometric surface assumes confined flow in a horizontal aquifer with isotropic permeability. When there is no vertical motion and no water density contrast it can be safely inferred that flow is in the direction of decreasing head.

#### ***Keg River Aquifer***

Figure 4.12 shows the freshwater equivalent hydraulic head distribution for the Keg River Aquifer. Hydraulic heads were calculated using the best quality DST pressures as described in Chapter 3. Oil recovery pressures were excluded and only water and a few carefully screened mud recoveries were used. The dip of the Keg River Aquifer is slight but the formation water comprises brines of variable density. Before inferring flow directions from freshwater equivalent head gradients, the possible influence of buoyant forces must be evaluated.

#### ***Variable Density Water***

By using freshwater equivalent heads to infer flow directions in gently dipping aquifers saturated with variable density brines we implicitly assume that since the flow is quasi-horizontal, buoyant forces are negligible. Bear (1972) discusses instability in variable density brines and presents the correct formulation of Darcy's Law for evaluating the flux of an inhomogeneous fluid in which convective currents may arise due to variations in solute concentration. Bear's formulation, for an anisotropic medium (1972, p.654, Equation 10.7.45), can be written for flux in the x direction, using partial derivative notation as:

$$q_x = -\frac{k_x}{\mu} \left( \rho_o g * \frac{\partial h}{\partial x} \right) - \frac{k_x}{\mu} \left( g (\rho_w - \rho_o) \frac{\partial z}{\partial x} \right). \quad (4.2.1)$$



For the point under consideration,  $k_x$  is the permeability of the brine saturated aquifer in the x-direction,  $\mu$  the fluid viscosity,  $\partial h/\partial x$  is the freshwater equivalent head gradient and  $\partial z/\partial x$  the gradient of the aquifer in the x-direction. The point water density is  $\rho_w$  and  $\rho_o$  is a hypothetical reference fluid density (i.e., freshwater). Motion is thus caused by two driving forces: the first term in brackets in Equation 4.2.1, proportional to the negative gradient of the freshwater equivalent hydraulic head distribution at the point; and the second term in brackets that constitutes the buoyant force. The latter force impels a fluid particle of density  $\rho_o$ , immersed in a fluid of density  $\rho_w$ , vertically upwards. This term is the x-direction component of the total buoyant force for petroleum given as Equation 2.1:

$$E_b = - \text{grad } z_a * g (\rho_w - \rho_p). \quad (2.1)$$

Davies (1987) simplified Equation 4.2.1 by assuming a medium with isotropic permeability, and substituting hydraulic conductivity (K):

$$K = \frac{k \rho_o g}{\mu_w}, \quad (2.7)$$

for the relevant rock-fluid properties. Equation 4.2.1 can be rewritten as:

$$q = - K (\text{grad } h) - \frac{k}{\mu_w} (g (\rho_w - \rho_o) \text{grad } z) * \frac{\rho_o}{\rho_o}, \quad (4.2.2)$$

which simplifies to, (Davies, 1987, p.4):

$$q = -K \left( \text{grad } h + \frac{\rho_w - \rho_o}{\rho_o} \text{grad } z \right) \quad (4.2.3)$$

or since  $\rho_o$  is unity ( $1.0 * 10^{-3} \text{ kg/m}^3$ ):

$$\mathbf{q} = -K \left( \mathbf{grad} h + (\rho_w - 1) \mathbf{grad} z \right) \quad (4.2.4)$$

The first term within the brackets is the freshwater equivalent head gradient at the point considered. The second represents the buoyant force that is usually assumed to equal zero. The real flow direction is the resultant of these two vectors.

Equation 4.2.4 shows clearly that it is not the absolute magnitude of the buoyant term that determines whether density-related effects are significant but rather its magnitude relative to the head gradient. The ratio of the density-related buoyancy term to the freshwater head term (Bear, 1972, p.654), is termed the driving force ratio (DFR) by Davies (1987, p.6):

$$DFR = (\rho_w - 1) \frac{|\mathbf{grad} z|}{|\mathbf{grad} h|} \quad (4.3)$$

Bear (1972, p.654) states that when  $DFR \gg 1$ , buoyant forces dominate and the flow regime is one of *free convection*. When  $DFR \ll 1$ , on the other hand, the flow is governed mainly by external head gradients and the flow regime is one of *forced convection*. Davies (1987) showed that buoyant forces were significant in a gently dipping confined aquifer saturated with variable density water for a study area in New Mexico. Flux vectors computed from the freshwater equivalent heads distribution alone (Equation 2.9) were compared with those accounting for buoyant forces (Equation 4.2.4). Davies determined that the approximate threshold at which a buoyant force became significant in the New Mexico study area was at  $DFR=0.5$ . This threshold corresponded to a possible deviation between the orientations of the freshwater and buoyancy modified flux vector of up to 30 degrees. Davies noted that this threshold could vary depending on local flow conditions.

### *Calculation of DFR for the Keg River Aquifer*

The average fluid density for the Keg River Aquifer corrected to reservoir conditions (Table 3.17) is  $1.156 \times 10^3 \text{ kg/m}^3$ .  $\text{Grad } z = 0.00325$  is the regional dip on the top of the Keg River Fm. scaled from the Keg River structure contour map between Tp.90 R.12 W5 and Tp.102 R.23 W4. Finally  $\text{grad } h = 0.00116$  is the average freshwater equivalent head gradient scaled over the same interval from Figure 4.12. Substituting these regional values into Equation 4.3 yields:

$$\text{DFR regional} = 0.44 \quad (4.4)$$

which is close to Davies' threshold value. Local areas in which the freshwater head gradient will not represent the true flow direction will be where the head gradient is slight, the water density is high and the aquifer is steeply dipping.

Inspection of Figure 4.12 (hydraulic head) reveals the lowest head gradients in the southwest and northeast quadrants of the study area. The greater salinity of the water (Figure 4.24) and the local steep dip of the aquifer (Figure 4.3) in the northeast quadrant suggest that the freshwater head vector in this area (oriented northeast) is directly opposed by a buoyant force vector oriented down dip.

To investigate further, the specific discharge or water flux was determined by Equation 4.2.3 for three regions in the study area centred on: Tp.92 R.9 W5; Tp.97 R.2 W5 and Tp.100 R.6 W5 respectively (locations shown on Figure 4.12). Table 4.1 shows the head and elevation data used to determine the gradients  $\text{grad } h$  and  $\text{grad } z$ . Figures 4.13.1 to 4.13.3 are scaled plan view vector diagrams illustrating these component gradients and their vector sum representing the buoyancy modified driving force (labelled  $F$  on the Figures). The deviations due to buoyancy both in terms of the magnitude and orientation of the driving force are tabulated in Table 4.2, which also shows the driving force ratios (Equation 4.3) calculated for the three locations. In the southwest  $\text{DFR}=0.1$  and buoyancy is unimportant. In the northeast where the local dip is steep and the water density is high,  $\text{DFR}=3.4$ . At this location, the downdip flow of heavy brine dominates and the true driving force exceeds that inferred from the

freshwater head by a factor of three while the force orientation deviates  $123^\circ$  from  $-\text{grad } h$ . Finally in the north,  $\text{DFR}=0.7$ . Figure 4.13.3 shows how at this location, the buoyancy-modified flow force is greatly diminished since the local head and buoyant forces are almost directly opposed.

Table 4.3 presents the calculated lateral flow rates for the three areas. Locally representative hydraulic parameters from my core database were used. Flow rates vary from nearly 2 m/y at the southwest site in permeable Granite Wash sands, to just 15 mm/y in the northeast. Here buoyancy driven flow is retarded by the head gradient. In the northern region where the component forces are nearly balanced, flow is very sluggish attaining a flux of less than 3 mm/y with a northeasterly orientation. The final column in the table shows the time period required for a unit volume of fluid to move laterally 10 km, i.e., to cross one township. This time varies from about 6 000 y in the south to 66 000 y in the northeast and over three million years in the north.

In summary, water in the Keg River Aquifer is therefore entering the study area from the south (flowing north) and leaving across the northern boundary. Flow to the northeast is retarded because of the heavy brine occupying updip locations which is impelled downdip against the regional head gradient. In areas of relatively steep dip the buoyancy driven flow dominates.

### ***Hydraulic Head for the Keg River Aquifer***

In marked contrast to the hydraulic conductivity and transmissivity maps (Figures 4.8 and 4.11) the head map indicates a tremendous barrier to flow which coincides exactly with the reef margin (see Figure 4.1). The steep head gradient flexure striking northwest to southeast, reflects the huge expenditure of energy required to force water from the transmissive reef into the relatively thin and shaley basin facies. The head map therefore reveals a transmissivity barrier known from lithofacies analysis (Campbell, 1987), that was invisible from core permeability data. This immediately demonstrates the utility of the fluid potential distribution as an exploration tool. Potentiometric surface analysis has been used in a similar fashion to successfully locate coarse sand lenses encased in shale in the Belly River Fm. of central Alberta (Parks, 1989; Rostron and Tóth, 1991).

***Comparison of Hydraulic Head to Ground Surface Topography for the Keg River Aquifer***

Comparison of Figure 4.12 (hydraulic head) with Figure 4.14 (ground surface topography) shows a reasonable correspondence between the ground surface and the head distribution in the southwest, and a flatter surface in the northeast. Trout Mountain in the southeast and the southern Buffalo Head Hills in the southwest are reasonably well represented by the 700 m equipotential, but the northern Buffalo Head Hills and Birch Mountain have no influence. There is a linear NNE oriented zone of low heads running across the southern half of the study area which creates a re-entrant in the 700 m equipotential in the south and includes the closed low at the SW corner of the Panny field at Tp.94 R.7 W5. This linear low directly underlies my interpreted extrapolation of the Misaw pre-glacial channel (see Figure 1.7) which Hitchon et al. (1990), considered effective in focussing discharge from this aquifer further south.

In the south and west then, overhead ground surface topographic elements are well represented. In the north and east the potentiometric surface is flatter, as formation fluids drain towards the outcrop. This reinforces Tóth's (1978) conclusion that flow in the deepest aquifers is not at steady state. Rather a decaying palaeoflow system exists in the Keg River Aquifer that is currently adjusting to the modern boundary conditions established during the Pleistocene. It appears that the study area straddles the interface between the fossil (southern) system and the modern system in the north.

This map is similar in most respects to Tóth's, Figure 16 (Tóth, 1978, p.822) which was constructed from much less data than subsequently became available for the present study. The main difference is that I have not included three very high pressures that Tóth accepted but could not really explain to his own satisfaction (*ibid.*, p.823). Accepting these pressures Tóth envisaged a large potentiometric mound in the Keg River Aquifer under Birch Mountain with fluid potential elevations some 200 m above the present ground surface (*ibid.*, Figure 16). I consider two of the three DSTs to be supercharged and the third to have a faulty pressure recorder (my analyses of the high pressures are presented in Appendix 2). With the Birch Mountain high potential mound removed, the "bleeding off" of potentials in the northeast half of the study area to the low elevation

outcrop becomes more apparent. It is interesting to speculate that Tóth's misinterpretation of this pressure data (assuming that my interpretation is correct) played a role in stimulating his profoundly important conceptualization of palaeoflow systems.

### ***Lateral Flow Rates***

Table 4.3 shows that lateral flow rates in the Keg River Aquifer are subdued. Average linear velocities range from 1.7 m/year in the southwest down to 3 mm/year in the northeast. The main controls on flow velocity are the hydraulic conductivity (two orders of magnitude higher in the Granite Wash Fm. than in the Keg River Fm.), the freshwater head gradient and the aquifer dip.

### ***Slave Point Aquifer***

Figure 4.15 shows the hydraulic head distribution in the Slave Point Aquifer. A number of unreliable data were included for this map since the good data were so restricted and the map is rather unsatisfactory. It does suggest however that the Slave Point heads are uniformly lower than the Keg River and thus the closed lows on the Keg River head map may be discharging upwards through the Muskeg evaporites into the Slave Point. Also heads appear to decrease to the north where the potentiometric surface is "deflated" due to the proximity of the low elevation outcrop shown in Figure 1.6.

### ***Upper Devonian-Basal Cretaceous Aquifer***

Figure 4.16 shows the hydraulic head distribution in the Upper Devonian-Basal Cretaceous Aquifer. The map comprises mainly Cretaceous data in the west and Upper Devonian in the east. The high heads around Tp.98 W4 probably indicate upward flow from the Devonian to the unconformity rather than a barrier to eastward flow. Note that these heads are all higher than the surface water elevations shown on Figure 1.9 and water at the unconformity is certain to be moving east and north.

#### **4.2.1.2 Oil Heads: Application of the UVZ Method**

##### ***Theory of the UVZ Method***

Using Hubbert's UVZ method (Hubbert, 1953, p.1986-1988<sup>1</sup>; Dahlberg, 1982, Chapter 6) we can calculate oil equipotentials to determine the hypothetical flow directions and accumulation sites that would exist for petroleum particles of a given density that were placed in the flow field. The Keg River Aquifer has sufficient data for the application of the method.

Conceptually, the UVZ method accounts for the buoyant impelling force acting on an isolated oil particle and for the hydraulic impelling force also acting upon it which is determined by the local direction and rate of water flow. The shape of the upper surface of the aquifer of interest then determines the locations of potential accumulation sites which will be in regions where the slope of the aquifer top exceeds the tilt of the total impelling force vector. In practice this means that oil pools will form in structures whose downstream dip is greater than the hydrodynamically maintained tilt of the oil-water interface. Where hydraulic gradients are low and flow is weak, buoyant forces will be dominant and accumulations will occur at the culminations of structures as in a hydrostatic environment. Where gradients are high and water flow is strong, all potentially oil-bearing structures may be "flushed out", and the oil will be transported further downstream. Intermediate conditions will produce accumulations in positions of hydrodynamic equilibrium on the downstream flanks of structures. Such accumulations will exhibit inclined oil-water contacts, tilted in the direction of water flow.

##### ***Limitations of the UVZ Method***

The UVZ method considers the migration and accumulation of minute oil particles. The migration of tiny oil particles is probably relatively unimportant in secondary migration since even if oil enters the carrier bed in such a form, the small particles will naturally coalesce.

---

<sup>1</sup> Note the typographic error on p.1986: , the denominator of the second term in Equation 47 should be  $\rho_o$  and not  $\rho_w$  as written. There is a second typographic error on p.1991 of this paper: Equation 55' should read  $u=v-z$  and not  $u=v+z$  as written.

Unless some force exists to create tiny volumes initially and to prevent these from amalgamating within the carrier bed, the greater part of migration will be as continuous phase stringers of oil. The buoyant force as defined in Hubbert's UVZ method does not account for the vertical extent of an oil stringer (Tissot and Welte 1978, p.343, present a formulation that does account for the height of the stringer).

Furthermore, the method does not account for the capillary gradients which exist even in a relatively homogeneous aquifer (Davis, 1987). Nor does it account for the varying water and oil flow fields that evolve in response to changes in relative permeability of the medium to each fluid as an oil accumulation forms (Rostron and Tóth, 1991). With these limitations in mind, the UVZ method is still useful for identifying prospective accumulation sites in a region of active fluid flow.

### *Application of the UVZ Method*

Hubbert devised the UVZ method as a graphical procedure. The method requires two maps (freshwater equivalent hydraulic head and a structure contour map of the top of the reservoir bed) plus knowledge of the local water and petroleum density ( $\rho_w$  and  $\rho_p$  respectively). The hydraulic head map is redrawn onto the structure contour map with each hydraulic head contour multiplied by a so-called tilt-amplification factor:  $\rho_w / (\rho_w - \rho_p)$  (Hubbert, 1953, p. 1987). The modified heads are values of the  $v$  function, so we have thus far produced a map of the structure of the top of the reservoir on which  $v$  contours are superimposed. Going over this map, wherever the two sets of contours intersect, a  $u$  value is calculated by subtracting the elevation of the top of the reservoir ( $z$ ) from the  $v$  value. Finally the  $u$  values are contoured. Low closures of the  $u$  map indicate regions of fluid potential minima for oil i.e., hydrodynamic oil traps.

Mathematically the UVZ method can be stated as:

$$u = v - z \quad (4.5)$$

where



$$u = \frac{\rho_p}{\rho_w - \rho_p} h_p \quad (4.6)$$

and

$$v = \frac{\rho_w}{\rho_w - \rho_p} h_w \quad (4.7)$$

In the present study a UVZ map, was created using the Surface II graphics program (Sampson, 1975). Using the best quality hydraulic head data (stable and undisturbed DST pressures) for the Keg River Aquifer, I generated a hydraulic head grid (see Section 4.1.1 for an outline of the Surface II method of grid construction). Figure 4.12 is a contoured representation of this grid. The grid was stored for later use. I used PUBCO formation tops data (PUBCO, 1990 b) to generate a grid of z values (Figure 4.3), which was also stored. I next obtained average values of Keg River oil and water density, corrected to reservoir conditions (Table 3.17) to calculate the following ratios:

$$\frac{\rho_p}{\rho_w - \rho_p} = \frac{764}{1156 - 764} = 1.95, \quad (4.8)$$

$$\frac{\rho_w}{\rho_w - \rho_p} = \frac{1156}{1156 - 764} = 2.95. \quad (4.9)$$

I then applied Equation 4.7 to obtain a matrix of v values. Next, applying Equation 4.5 I created a u matrix by simply subtracting the z matrix from the u matrix (all the grids were spatially identical so that corresponding values in the matrices represented the same map location). Finally I multiplied the u matrix array by 1/1.95 to obtain a matrix of oil heads. This matrix served as the grid for the construction of the oil head map shown as Figure 4.17.

### ***Keg River Aquifer UVZ Map***

The map shows the same trend as the hydraulic head map with a large minimum closure at the southwest corner of the Panny Field. A number of smaller closures exist in the relatively flat areas upstream (southwest) of the high gradient flexure. This whole zone is highly prospective for future discoveries and constitutes a new petroleum play in this region: the Keg River Hydrodynamic Play. The northward oil head gradient in the southern map area may have important implications for the regional pattern of migration on the Peace River Arch and this will be discussed in the next chapter.

#### **4.2.1.3 Pressure versus Depth**

Decreasing hydraulic heads in the three aquifers just described clearly indicate an upward directed hydraulic gradient for the entire sub-Cretaceous section. However freshwater heads do not directly indicate vertical flux (Luszczynski, 1961). To investigate the nature of vertical flow I constructed a pressure-depth plot of all stable, undisturbed pressure data grouped by ranges of wellhead elevation for the study area (Figure 4.18).

Figure 4.18 shows the data split into two groups. The shallow wells tested the Bluesky, Winterburn and Grosmont Formations. The deeper pressures are from the Keg River and Slave Point Aquifers. Very clearly both groups show that the low elevation wells (i.e., those wells situated in lowland areas) have higher pressures and steeper pressure gradients than those from upland areas. Topography driven flow and the dynamic pressure increment as described in Chapter 2 (Section 2.6.1.1) provide an explanation for these phenomena. The fact that the phenomena exist throughout the study area confirms the hydraulic continuity of at least this part of the western Canada basin. Figure 4.19 expresses the same relationship in a slightly different way. Pressure versus depth ratios were calculated for each DST and these were then plotted against wellhead elevations. Again the data fall naturally into two groups, each of which shows that the P/D ratio increases as the wellhead elevation declines. It is difficult to conceive of any process other than the dynamic pressure increment that would cause such a systematic trend over a region as large as the study area.

Note that the shallow pressures (group A in Figure 4.18) regardless of the overlying ground surface elevation are significantly subhydrostatic. This could be due to downward flow (from Cretaceous strata) towards the highly permeable aquifer straddling the sub-Cretaceous unconformity in response to the exposure of low elevation outcrop outside the study area as discussed in Section 4.2.1. Alternatively the low pressures may reflect shale rebound in response to the erosion of overburden or the wasting of Pleistocene ice sheets. Tóth and Corbet (1986), Parks (1989) and Corbet and Bethke (1992) have investigated rebound phenomena in the WCSB.

### *Vertical Flow Rates*

To evaluate the possibility of upward flow from the Keg River Aquifer, across the Muskeg Formation to the Slave Point Aquifer, a pressure versus depth plot was constructed for the region of Twps. 94-95, Rs.6-7. The potentiometric surfaces for the Keg River, Slave Point and Basal Cretaceous-Upper Devonian Aquifers (Figures 4.12, 4.15 and 4.16) suggest that water is converging laterally toward this site in each aquifer. Since heads also decrease progressively upwards this may be the site of an upward flowing discharge plume. From the water density profile for this area (Table 4.4) the hydrostatic pressure gradient was calculated and is plotted on Figure 4.19.1, along with the culled DST pressures measured in the area. The observed vertical pressure gradient exceeds the hydrostatic gradient indicating that upward flow across the Muskeg Aquitard does occur. Applying Equations 2.10 and 2.11, indicates upward average linear flow rate of about 0.2 m/year in the Keg River Fm. Table 4.5 presents the data used in this calculation.

### **4.2.2 Temperature**

The purpose of reviewing the temperature distribution is to gain understanding of the thermal regime (see Section 2.6.2). In a convective thermal regime flowing water is the agent of heat transport. Since water is also the agent of petroleum transport we expect that petroleum may accumulate in regions with distinct thermal characteristics (“hot spots”, positive geothermal anomalies etc.). If we can show in a given region that convective heat transport is important, then patterns of temperature distribution may help to elucidate flow paths, migration paths and

accumulation sites. In a conduction dominated thermal regime there is no such active relationship between petroleum migration and heat transport.

#### **4.2.2.1 Basement Temperature and Average Geothermal Gradients**

The bottom hole temperatures (BHTs) are contoured in Figure 4.20. I have also contoured the average geothermal gradient i.e., the BHT and surface temperature difference divided by BHT depth (Figure 4.21). The temperature map shows a fairly erratic distribution. There is a westerly warming trend but temperatures fluctuate significantly in every direction.

It is difficult to see how the flow pattern in Figure 4.12 could contribute to such a distribution. The influence of convection should be apparent in a bending of isolines in the direction of flow. Considering other possible causes of the temperature distribution, basement heat flux variations seem an unlikely cause since the Trout Mountain Batholith (see Figure 4.2) which is potassium feldspar-rich should be an excellent heat generator and yet underlies the relatively cool central area. According to the heat generation map in Bachu and Burwash (1991) the pattern of heat generation on the Peace River Arch is complex so there are probably many other heat sources in the area. More knowledge of their distribution is required to evaluate this factor. The scale of the map of Bachu and Burwash (1991, Figure 7) precludes close comparison.

Thermal conductivity variations in the overlying sediments may be influential. The eastern half of the study area has the most thermally conductive cover due to the presence of Cold Lake salt, the thick development of the Muskeg Fm. (halite and anhydrite facies) plus the Grosmont Fm. (dolomite) in place of Ireton shale to the west. Thermal conductivities for halite and dolomite are 5.7 and 4.7 Wm/°C respectively (see Table 3.4). In the west the Muskeg is thin (and lacks halite) and the Grosmont Fm. pinches out into Ireton Fm. shale. The thermal conductivity of the well compacted Ireton shale is probably less than 1.6 Wm/°C. Thus with a more thermally conductive cover, the basement in the east should be cooler than that in the west which indeed it is. Comparison between the average geothermal gradient map and Figure 4.22, the maximum thickness (i.e., upper limit of possible thickness) of halite in the Muskeg Fm. shows some remarkable local scale correlations. Note for example the elongate

high (30 °C/km plus) between Tps. 90 to 95 on the Fifth Meridian and the halite low in the same position in Figure 4.22. Similarly the gradient high in Tp.101 R.24 W4 and its adjacent low in R.1 W5 correspond to thick and thin halite closures on Figure 4.22 in precisely the same locations. The fact that gradients in the east on Figure 4.21 are generally higher than those in the west (contrary to expectation considering the bulk conductivity of the overlying section) is rather perplexing. Local conductivity variations apparently affect the average geothermal gradient between basement and land surface in fine detail and yet the bulk conductivity of the cover has no discernible effect. This must indicate the influence of an additional factor.

Figure 4.23 shows the thickness of sedimentary cover or the depth to basement for all wells that penetrated the Pre-Cambrian. All else being constant, basement temperatures will be higher where the cover is thicker. The cover is thickest under the Buffalo Head Hills. Next is Trout Mountain in the south then Birch Mountains in the east. These are also the hottest parts of the basement in the study area. In the centre of the study area and to the northwest cover is thin and the basement is cool. This factor then would seem to have the strongest correlation with temperature. Where the cover is thick (i.e., where the depth is greatest) the basement is hot.

One final remark. I would suggest that the temperature and geothermal gradient highs north of Tp.99 and between Rs. 5 and 10 are either bad data or indicate the presence of a basement heat source, since their location does not correlate with absent halite or cover thickness.

#### **4.2.2.2 Temperature Anomalies and Oil Fields**

Convective heat flow is unimportant in this area, so the temperature data do not reveal any anomalous characteristics with respect to oil field locations. Basement temperatures range from below 40 °C for most of the Panny field to over 50 °C for Sawn Lake. Isolines do not cluster around the oil field areas. The same is true of the geothermal gradient distribution. Gradients range from 25 °C/km at Sawn Lake and Red Earth to 30 °C/km at Trout and Kidney and up to 35 °C/km at Redfish. Comparing the Keg River hydraulic head map (Figure 4.12) to the geothermal gradient map none of the closed head lows correspond with geothermal gradient highs. At the scale of investigation possible for this study, no convective effect is

apparent and the conclusion is that heat transport in this part of the basin is very clearly conduction dominated.

### 4.2.3 Water Chemistry

#### 4.2.3.1 TDS Maps

My objectives in mapping hydrochemical trends are:

- 1) to discern what role flowing water plays in modifying the water chemistry within the aquifers in the study area;
- 2) to evaluate the hydrochemical composition of oil field brines and to recognize if possible some distinctive hydrochemical characteristics by which oil field waters on the Arch and possibly elsewhere can be distinguished from 'barren' waters;
- 3) to identify hydraulic links between discrete aquifers and evidence of active cross-formational flow.

Figure 4.24 is a map of the total dissolved solids (TDS) in the Keg River Aquifer. First what trends exist in the TDS distribution? Maximum total ion concentrations (over 300 g/L) occur in the south at Trout field, and also in the east and northeast in the Keg River basin facies. There are two closed salinity lows in the central area aligned with the Keg River reef margin. The lowest salinities occur in the west where the salinity drops below 100 g/L.

Chebotarev (1955) and Tóth (1984, p.15) postulated that a downstream salinity increase should occur within a flow system due to increased residence time and total area of rock-water contact. Inspecting the Keg River Aquifer TDS distribution (Figure 4.24) in relation to freshwater heads (Figure 4.12) no TDS increase is apparent along the northerly flow path. Instead, there is a general trend of salinity increase from less than 200 g/L in the west to over 300 g/L in the east. This trend is interrupted by a linear northwest-southeast oriented body of relatively dilute brines (the closed lows referred to above) located roughly over the Keg River reef margin. If the TDS lows represent dilution due to mixing the source of relatively fresh water is problematic.

The average compositions of water samples from the Keg River Fm., Granite Wash Fm. and the Pre-Cambrian show no significant differences despite the lithological diversity of the host rocks (see Figure 3.15 and especially 3.16 where the three waters plot at a single point in the combined field of the Piper diagram). All are Ca Cl or Na Cl brines with an average TDS around 200 g/L. So where else could the dilute water come from?

Juvenile water from the crystalline basement is a possibility, although Hitchon and Friedman (1969) determined that the isotopic character of all formation waters in the WCSB could be explained as mixtures in various proportions of isotopically light meteoric water and diagenetically modified sea water. Recent hydrogeological studies on the Canadian Shield sponsored by the Canadian Nuclear Fuel Waste Management Program (Fritz and Frape eds., 1987) have proven the existence of active topography-driven fluid flow systems in fractured zones of crystalline rocks. Gascoyne et al., (1987) describe active local flow systems within each of four widely separated plutons on the Canadian Shield extending to depths of at least 300 m, possibly underlain by more deeply circulating regional scale systems (*ibid.*, p.60). The estimated compositions of "parent brines" in these crystalline rocks however are Ca Cl solutions with TDS values ranging from 378 to 418 g/L. In view of these discoveries on the Shield we cannot rule out the possibility of significant fluid transport in the crystalline rocks underlying the WCSB, however they would not appear to be a likely source of fresh water.

An obvious explanation for the observed trend is the presence of halite in the Muskeg Fm. overlying this aquifer. I made a simple map (Figure 4.22) by picking the first and last occurrence of halite in the Muskeg Fm. in about 70 wells for which I had a caliper log for the relevant interval. I then contoured the calculated thicknesses which represent the upper limit of possible halite thickness in the Muskeg for each well.

The map correlates remarkably well with the observed TDS distribution. The 250 g/L TDS low centred on Tp.93 R.2 W5 correlates with the dissolution hollow (i.e., absence of halite) at the same location. This is the same solution hollow that featured in Figure 4.7. The lowest TDS values in the aquifer occur around the zero edge of halite in the west,

and the TDS maxima correspond to halite thickness maxima in the east and northeast. Given that halite dissolution appears to be the source of the TDS<sup>c</sup> it would seem reasonable to expect, that the existing flow system would redistribute the salt mass and that there might be some saline plumes visible, especially in highly transmissive areas. It is particularly surprising that there are no TDS maxima associated with the closed lows on the head map. If water is converging in these locations why is there no increase in concentration? In summary halite dissolution appears to control the pattern of salinity but flow is ineffective in transporting the dissolved mass.

In terms of distinctive major ion hydrochemical characteristics for oil field waters I attempted to discern some unique chemical signature for oilfield versus barren formation waters by using the petroleum indicator criteria proposed by Palmer, Sulin, and Bojarski as reported by Collins (1975). These included:

- 1) Schoeller's index of base exchange (IBE)
- 2) Schoeller's approximation of CaSO<sub>4</sub> saturation
- 3) Schoeller's SO<sub>4</sub> classes (VERY HIGH through NORMAL)
- 4) Schoeller's Cl Concentration Classes (VERY HIGH through NORMAL)
- 5) Palmers Water Classes (1, 3 and 5)
- 6) Sulin's Water Types (Cl-Ca, SO<sub>4</sub>-Na, HCO<sub>3</sub>-Na and Cl-Mg)
- 7) Sulin's Cl-Ca Type Classes (S1S2S3, S1S2A2, S1A2S2 and S2S1S3)
- 8) Bojarski's modified Cl-Ca Water Types (I through V)

Although all the oil field waters are indeed of the various petroleum indicator types so too are the barren waters. The range in composition of the waters co-produced with oil from the various Keg River and Granite Wash oilfields is equal to the total range of all waters sampled. None of these parameters could be used to predict on the basis of major ion chemistry whether a given Keg River or Granite Wash water sample was obtained from a producing well or a dry hole. Hitchon et al., (1974, p. 469-470) suggested that iodide is an petroleum indicator for Palaeozoic strata in the WCSB. Analytical determination of Iodide concentrations in my database were to sporadic to be useful, and I could not evaluate the utility of this ion as a hydrochemical indicator.



I also mapped various major ion ratios (Na/Cl, Ca/Mg, and SO<sub>4</sub>/Cl) for both the Keg River and Slave Point Aquifers. Again I was unable to discern distinctive characteristics for the oil fields. The situation is adequately illustrated by Figure 4.24. The TDS range of the oil field brines (from 150 g/L in Tp.89 R.11 W5 adjacent to the Otter and Ogston fields, to 300 g/L at Tps.89-90, Rs.3-4 W5 in the Trout-Kidney Field region) incorporates virtually the total range of salinities in the aquifer. The TDS map for the Slave Point Aquifer (Figure 4.25) though lacking data within the Sawn Lake oilfield suggests that its salinity is below 150 g/L. In summary I was unable to discern any hydrochemical characteristics distinctive to the oil fields. I was therefore unsuccessful regarding the second objective.

Finally what of evidence for cross-formational flow between the Keg River and Slave Point Aquifers? Because hydraulic heads throughout the Keg River are higher than in the Slave Point Aquifer, there exists a potential for upward flow. Vertical flow through the Muskeg evaporites with consequent dissolution of soluble chloride and sulfate minerals should create a high TDS anomaly where the water enters the Slave Point. Inspection of Figure 4.25 reveals an isolated TDS high (300 g/L) in the Slave Point Aquifer at Tp.94 Rs.6-7 W5. The Keg River head map (Figure 4.12) shows that this is the location of a major local depression on the Keg River potentiometric surface which is also a local minimum in the Slave Point (Figure 4.15) and in the overlying Upper Devonian-Basal Cretaceous Aquifer (Figure 4.16). Moreover this is the location at the ground surface of the intersection of the two large pre-glacial channels (Figure 1.7) and of two present day surface drainage channels the Loon and Wabasca Rivers (Figure 1.6). This feature would appear to be a major discharge zone funnelling water from the base of sediments towards low water table elevations at the land surface. Note that the oil pools in the southwest part of the Panny oilfield are clustered in the region of the fluid potential minimum.

Luszczynski (1961), Tóth (1979) and Maccagno (1991) have shown that freshwater equivalent heads cannot be used to determine vertical flux. Instead a pressure versus depth plot can be used. Using the vertically changing densities of formation waters from the surface to and across the interval of interest, we construct a nominal pressure versus depth curve

(applying Equation 1.1). Field data are then posted, and their position in relation to the nominal curve will reveal their static or dynamic state. If a data point plots on the nominal curve this means that the pore pressure is perfectly balanced by the weight of the overlying fluid column. Hence there is no possibility of vertical fluid motion at the point in the subsurface where the pressure was recorded although there may be vigorous lateral flow. If a data point plots above the curve, this indicates the water has energy in excess of the weight of the overlying fluid column and hence upward flow at that location. If a point plots below the nominal curve downward flow is inferred. Because a hydrostatic pressure in a hydraulically continuous environment requires fluid movement, (or rather because fluid motion driven by the potential field causes the pore pressure at various locations to be ahydrostatic) Tóth (1978) coined the phrase “dynamic pressure increment” to describe the difference between nominal and observed pore pressures (see also Section 2.6.1.1).

#### **4.2.3.2 TDS Anomalies and Oil Fields**

Although the GHT predicts that hydrocarbons should occur in association with high TDS waters (and there are many good reasons why this association should exist) it is clearly not the case that most of the oil field waters in the present study area are so enriched.

Salinity patterns in the Keg River and possibly also in the Slave Point, appear to be controlled by halite dissolution in the intervening Muskeg Aquitard but flow is apparently ineffective in distributing the dissolved mass within the aquifers. I was unable to discern any major ion hydrochemical characteristics distinctive to the oil fields. None of the petroleum indicators proposed by Palmer, Sulin or Bojarski successfully distinguished waters co-produced with oil from those recovered in dry holes.

The most favourable indicator of the mechanism by which TDS highs and oil fields are linked (i.e., cross-formational discharge) may exist at the present time as the ascending “plume” or “chimney”, emanating from the Keg River Fm, and channeling water vertically through Muskeg Aquitard to the Slave Point Aquifer. The plume may extend through the Upper Devonian platform rocks to the Bluesky Fm. and even to the topographic lows on the land surface overhead. Oil pools in Tp.94 R.5-6

W5, at the southwest corner of the Panny Field are clustered at the base of the plume in the Keg River Fm. This feature is arguably an example of the main trap type postulated by the GHT: a vertically extensive regional discharge zone. Clearly the Slave Point Fm. and overlying units should be considered prospective (notwithstanding the difficulty of moving petroleum through aquitards). The Slave Point structures highlighted in Figure 4.4, would be suitable receptacles for any oil that migrated “up the chimney” or laterally through the Slave Point Aquifer towards the potentiometric depression.

#### **4.2.4 Oil Density**

##### **4.2.4.1 Oil Density Maps**

When separate phase oil migrates along a carrier bed due to buoyancy, the lightest components will accumulate in the first traps encountered. This will result in an increase in the average density of the pools in the direction of transport. The traps may be structural, stratigraphic or hydrodynamic. Migration in aqueous solution should theoretically produce the reverse trend because the lightest fractions are also the most soluble and would tend to exsolve last. More complex migration fractionation patterns than those described above have been conceived by various authors (e.g., Silverman, 1965; Illich et al., 1981) but these will not be considered here, since my knowledge of the oil character in the study area is limited to its density and dissolved gas content.

Figure 4.26 is a contour map showing average oil pool densities for the Keg River Aquifer fields, obtained from the (ERCB, 1991 a). Figure 4.17 (Keg River Aquifer oil heads) showed that the present migration direction in the study area is northward across the southern boundary and then towards the northeast Figure 4.26 shows that average oil pool densities decrease towards the northwest. This would favour a solution migration mode if transport was from the south as my head data suggest. Other alternatives are limited. Possibly migration was from the north and we are simply viewing the trend from the wrong end? The Duvernay equivalent Muskwa Fm. occurs north of the Peace River Arch where it will be mature if it is indeed a source rock. Podruski et al., (1987) consider that north to south migration is unlikely because all pools discovered so far are on the

southern and eastern sides of the Arch. Also the northern Arch has a narrower shelf because its margin dips more steeply than the southern side. Figure 4.27 shows the oil density distribution of Slave Point oils. Again a northward density decrease is apparent, although here the sample (only three fields) may be too small to be meaningful. Maps of the initial solution gas-oil ratio (not shown) show that the density variations are caused by differences in gas content. In both the Keg River and Slave Point Aquifers, the heaviest oils (density of  $790 \text{ kg/m}^3$ ) exhibit a gas-oil ratio of  $30 \text{ m}^3/\text{m}^3$  whereas the lightest oils ( $<750 \text{ kg/m}^3$ ) contain up to  $55 \text{ m}^3$  of solution gas per  $\text{m}^3$  oil.

It could be that the variations we see are minor and essentially random. The effectiveness of processes such as the adsorption of polar components by clays, dissolution of light components by water, biodegradation by oleophilic bacteria etc., are determined by heterogeneities in the reservoir. For example clays are not present in all pore channels; water washing may be limited to bulk flow pathways while bacterial colonies will be excluded from excessively hot or saline environments. Thus fractionation processes may affect one pool and not its neighbor. I suspect that local phenomena of some sort are important in this area because oil density variations between individual pools (posted at a larger scale and not shown here) are even more erratic than suggested by the contours in Figure 4.26. For instance the maximum and minimum density oils for the entire region occur in two pools in the Kidney field that are less than 15 km apart. In conclusion oil density distribution patterns do not seem to throw much light on the migration pattern.

## **Chapter 5 Interpretation of Results - Ramifications for Oil Migration on the Peace River Arch**

In this final chapter I will consider how topography induced flow influenced the migration and accumulation of petroleum on the Peace River Arch. As mentioned in Chapter 1, Allan and Creaney (1989) have produced geochemical evidence that the Duvernay Fm. an Upper Devonian (Leduc age equivalent) shale of starved-basin type, is the source rock for all petroleum in the Middle Devonian aquifers of the Peace River Arch region. Their argument for buoyancy-driven migration structurally up and stratigraphically down, into Middle Devonian aquifers was outlined in Chapter 1. Piggot and Lines, (1991) pointed out that the Duvernay Fm. was not deposited on the Arch which would consequently have been bypassed by up-dip migration parallel to its axis. Piggot suggested that Duvernay oil was somehow drawn into the dolomitized portion of the Slave Point Fm. on the Arch and thence into the reservoir beds where it is now found. The migration pattern suggested by Piggot seems rather contrived: downwards from the Duvernay, then laterally along basin strike into the dolomitized Slave Point Fm. around the Arch. Even though the dolomitized Slave Point may be relatively permeable, permeability does not cause flow, and Piggot gives no explanation of the forces which could have caused downward and horizontal flow. The Slave Point Fm does not seem the most logical choice as carrier bed. His main point though is sound: that buoyancy alone cannot explain the presence of petroleum in the present study area or elsewhere on the Arch.

Figure 5.1 illustrates the problem. The Leduc reef complex fringing the Peace River Arch is shown in dark stipple (Dix, 1990) surrounded by the lighter stipple outline of the Granite Wash coarse permeable clastic apron which is developed directly on the Pre-Cambrian surface (Trotter, 1989). The Granite Wash Fm. achieves a thickness in excess of 100 m in fault bounded structures on and adjacent to the arch and is two orders of magnitude more permeable than the Keg River Fm. Thick Duvernay shale accumulated in deeper water environments to the south. The up-dip limit of oil maturity for the Duvernay source rock (Piggot and Lines, 1991) and its northern equivalent the Muskwa Fm is shown superimposed on Figure 5.1. This line follows the -1200 m structure contour on Pre-Cambrian basement

(O'Connell et al, 1990) and is thus parallel to basin strike. Clearly, pure up-dip migration from south of the Arch would have bypassed the present study area. The question is then, what force diverted the oil generated to the south of the Arch driving it northwards onto the Arch to form the oil fields in the present study area?

Figure 5.2 reveals a second element to the problem. This is a cross-section along the axis of the Arch (location shown on Figure 5.1). Note at the base of section that the Keg River and Slave Point aquifers diverge eastwards as the Muskeg Fm. thickens between them. Clearly if oil is to access to Slave Point it must do so early i.e., any oil that migrates within the Granite Wash Fm. far enough to the east to be below the Muskeg Fm. will be effectively isolated from the Slave Point Fm. Returning to the plan view, this is why I have shown the oil migration arrows converging near the northeast tip of the Leduc platform. If they did not do so all oil would have bypassed the Slave Point Aquifer.

At the present time there is a strong northward-dipping hydraulic gradient in the southern part of the study area (see Figure 4.12). Oil heads in the study area decrease to the northeast (see Figure 4.17) The bold arrow in Figure 5.1 represents the general direction of oil migration. There are a number of UVZ closures in the study area which correspond to known and potential oil pools.

If the present pattern of flow existed at the time of oil migration this would fully explain the northward movement of oil onto the Arch. Water was the agent that diverted the northeast buoyant rise of oil and drove the oil north into the permeable near shore facies of the Middle Devonian aquifers which are now oil reservoirs.

## **Conclusions**

I will describe the conclusions to my thesis in relation to the working hypotheses listed in the Introduction.

### *1 The pore water is in motion.*

Pore water motion is inferred from the hydraulic head distribution in three major aquifers and the observed hydraulic continuity of the sedimentary strata. Calculations for the Keg River Aquifer indicate lateral flow rates (average linear flow velocities) on the order of millimetres to metres per year depending on the local magnitude of hydraulic conductivity. Vertical flux in the Keg River Aquifer is of a similar intensity.

### *2 Gravity-driven flow generated by the topographic relief of the water table is the main force causing fluid motion.*

As shown by a regional pressure versus depth plot (Figure 4.18) and a pressure:depth ratio versus wellhead elevation plot (Figure 4.19) subsurface pressures are linked to the topographic relief of the overlying ground surface. This indicates that the relief of the water table drives flow in the study area. However the relationship is complex and boundary conditions both within and beyond the study area are influential.

The low elevation outcrop of the sub-Cretaceous unconformity and of Devonian strata to the north and east exerts a strong influence on flow patterns in all formations in the northeastern half of the study area. In the southwest, at greater depth, the influence of the overlying ground surface topography is more apparent. The potentiometric surface of the Keg River, and possibly also the Slave Point Aquifers exhibit characteristics of both surfaces. Close to the present day outcrop the potentiometric surfaces in the Devonian aquifers flatten out as formation fluids drain towards the low water table elevations in the outcrop region. This finding reinforces Tóth's (1978) conclusion that flow in the deepest aquifers is not at steady state. Rather a decaying palaeoflow system exists in the Keg River Aquifer that is currently adjusting to the modern boundary conditions established during the Pleistocene. It appears that the study area straddles the interface between the fossil (southern) system and the modern system in the north.

Density-driven flow is also locally significant. Heavy brines are produced in the Keg River Fm. by the dissolution of halite in the overlying Muskeg Fm. These brines are impelled down-dip by buoyancy and in areas where the aquifer dip is steep, override freshwater head gradients, which generally impel water up-dip.

*3 Flow paths within and between aquifers can be determined using existing oilwell data.*

Flow patterns were determined from existing oilwell data, but improved recording procedure in the field would yield more better quality data, facilitating clearer resolution of basin hydraulics. Most historical oil industry data are unrepresentative. Particular effort should be made to determine permeabilities and DST pressures for low permeability strata. As noted above, the three potentiometric surfaces I constructed reflect the progressively increasing influence of the low elevation outcrop proceeding from the deepest aquifers to the unconformity (compare Figures 4.12, 4.15 and 4.16). Flow in all aquifers is directed to the north and east of the study area (see Figure 1.9). The southwest parts of the Keg River and Slave Point aquifers retain the high fluid potentials imprinted by the land surface prior to the exhumation of the outcrop. The high TDS contents of the waters of the Slave Point Fm. in the southeast (see Figure 4.25) mirror very generally the TDS distribution in the Keg River (see Figure 4.24) and may reflect upward flow from the Keg River in the past. Upward, cross-formational flow from the Keg River to the Slave Point Aquifer across the Muskeg Aquitard was demonstrated in the central study area.

*4 The flow pattern will reflect aquifer heterogeneities.*

Core permeability data did not reveal the presence of the Keg River reef edge, which was however clearly indicated by hydraulic head gradients. This demonstrates the utility of the hydraulic head map as an exploration tool. Alone, the hydraulic head distribution can reveal transmissivity variations in aquifers which are not apparent from contoured point values of permeability measured in rock core.



*5 The geothermal regime is convective: average vertical temperature gradients and subsurface temperatures are influenced by forced convective heat transport via topography-driven flow systems.*

Regarding temperature distribution at the Pre-Cambrian surface, and the pattern of average geothermal gradients, my conclusions are in general in agreement with Hitchon et al (1990). The geothermal regime in the Peace River Arch region is dominated by conductive heat flow, thus thermal conductivity (i.e., lithology) and the thickness of sedimentary cover are the main controls. Flow rates in this region are apparently too low for convective heat transport to be effective.

*6 Distribution patterns of major ions are influenced by flow patterns: water salinity (total dissolved solids) increases downstream.*

Salinity in the Keg River and Slave Point Aquifers is controlled by proximity to halite in the Muskeg Aquitard, with halite dissolution producing local TDS highs. Salinity does not generally increase along the flow path. One major exception is the chemical anomaly in the Slave Point Fm. caused by a vertically ascending plume at Tp.94 Rs. 6 and 7 (see Figure 4.25). The discharge plume transports water upwards from the Keg River across the Muskeg evaporites to 'contaminate' the Slave Point Aquifer. This plume may extend to the sub-Cretaceous unconformity and is associated with a closed potentiometric low and a large oil pool in the Keg River Fm. (see Figure 4.12). The plume is within the fossil flow system and suggests that in the past, when the current low elevation outcrop of the Devonian aquifers was buried under Cretaceous strata, vertical flow across aquitards to low elevations of the land surface overhead was more significant.

*7 Average oil pool mass density increases downstream.*

This hypothesis was disproven. The average densities of oil pools in the study area vary within a narrow range (810 to 870 kg/m<sup>3</sup> or 43 to 31° API) and no clear control on oil pool mass density was determined. It was concluded that in the study area, variations in oil density are unaffected by water flow.

*8 Oil pools are concentrated in regional discharge zones.*

Much evidence supports this hypothesis. Inspection of the freshwater head distribution in the Keg River Aquifer (Figure 4.12) reveals that the southwest portion of the Panny Field, the northeast part of Kidney and all of the Ogston, Red Earth and Joan fields lie within closed lows or at least in regions of locally reduced head. The oil head map for the Keg River Aquifer (Figure 4.17) reveals 9 closed lows, 7 of which correspond with the positions of known oil fields. Closed oil head lows occur at Panny (Tp.94 R.5 W5 and Tp.96 R.5 W5), Kidney (Tp.92 R.6 W5), Joan (Tp.91 R.9 W5), Red Earth (Tp.89 R.7 W5) and also at northwest Trout (Tp.90 R.2 W5) and southeast Senex (Tp.92 R.2 W5). The oil head map indicates that a region of flat hydraulic gradient on the southwest (high transmissivity) side of the steep gradient flexure, extending from Tp.96 R.10 W5 to Tp.94 R.8 W5. These are the most favourable regions for exploration and constitute what may be termed a hydrodynamic play for the Keg River Fm. in the study area.

*9 Petroleum migration paths and accumulation sites are being/have been influenced by topography-driven flow systems.*

My work indicates that the present northward directed water flow is a potential agent for driving petroleum onto the Peace River Arch which would have been by-passed by purely buoyancy driven migration. I also demonstrate that accumulation sites on the Arch are often (but not exclusively) in regions of fluid potential minima, and have identified a potential hydrodynamic petroleum play in the region.

In summary, this work started by outlining the scientific theory underpinning hydraulic theories of petroleum migration. From a theoretical point of view, it is as erroneous to ignore water flow as a potential agent of petroleum transport, as it would be to ignore buoyancy. Where hydraulic gradients are steep, petroleum will not necessarily accumulate in structural apices and hydrogeologic understanding is required to determine where true accumulation sites will be. Converging flow can create petroleum traps independent of structure. Evaluation of hydrodynamic effects would be considerably enhanced if subsurface data were recorded in the field with greater care. The present research has demonstrated:

- 1 the inadequacy of the conventional rock-trap oriented approach to migration;
- 2 the need to consider both the driving forces for fluid flow and the permeability pathways available for migration;
- 3 that most of the known oil accumulations in the study area are in regions of hydrodynamic stability;
- 4 the existence of a hydrodynamic oil play in the study area.

124

**Tables**

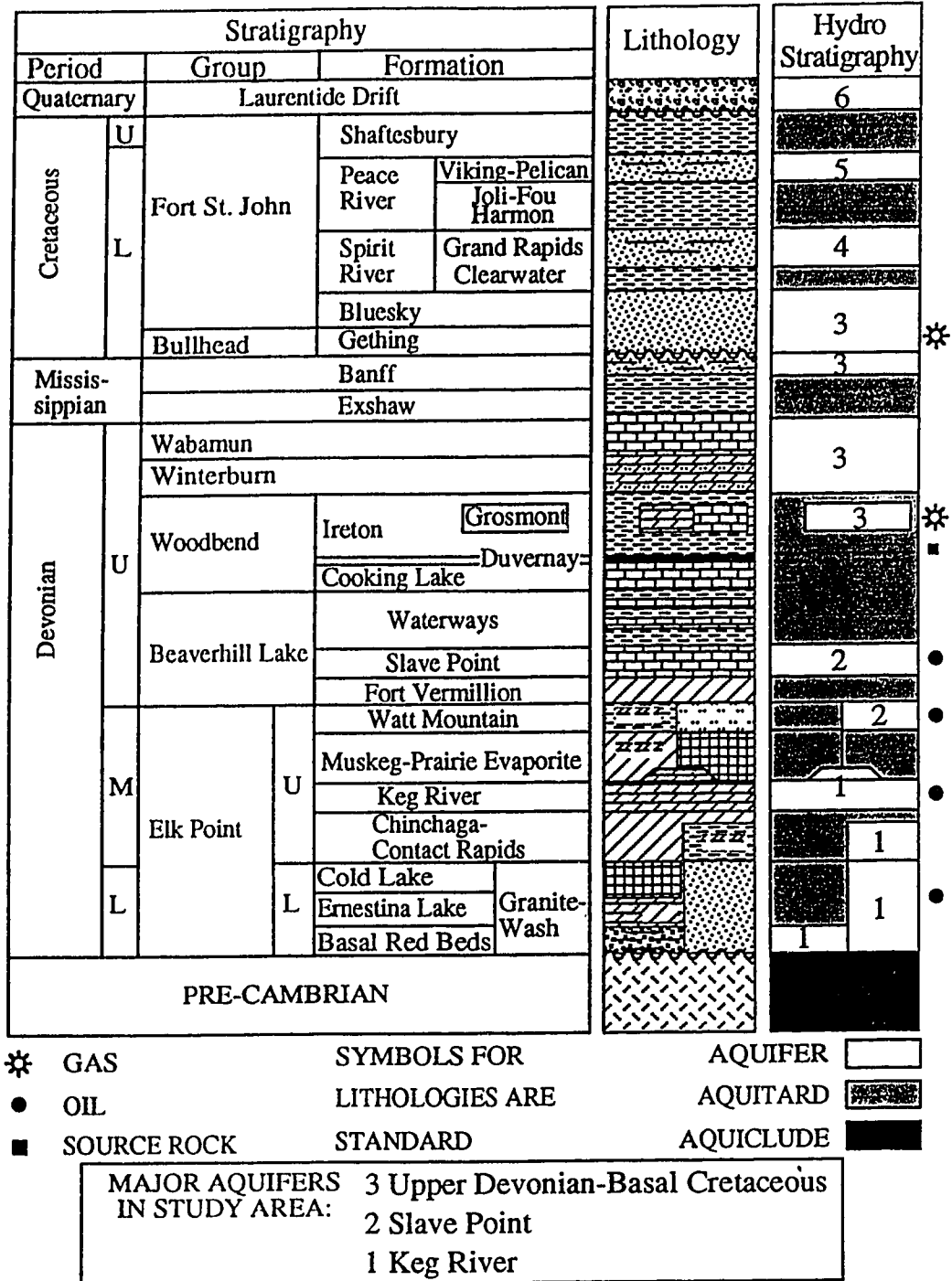


Table 1.1 Stratigraphic Table With Hydrostratigraphy and Petroleum Geological Features

HYDRO-STRATIGRAPHIC UNIT	n		w.g.m. Permeability (mD)		% Porosity		Ratio		kH/kV	
	n		kH	STDEV	%	STDEV	Ratio	STDEV	kH	STDEV
Basal Cretaceous	20		961	1123	7	24.2%	11	4	3	
Lower Wabamun Fm.	2		0.6 e	nd	0	9.0%	11	12	2	
Winterburn-Woodbend Fm.	10		8.4 e	nd	0	14.7%	11	22	7	
Grosmont Fm.	18		172	225	12	11.0%	623	1155	13	
Beaverhill Lake Gp.	19		0.4	0.5	14	5.5%	1	nd	1	
Slave Point-Watt Mtn. Fm.	110		5	42	84	6.2%	50	172	26	
Muskeg Fm.	11		0.8	1.3	6	6.7%	6	3	7	
Keg River Fm.	383		3	6	333	5.5%	88	380	73	
Granite Wash Fm.	70		83	120	38	12.6%	10	9	16	
Pre-Cambrian	2		0.9	nd	1	8.0%	1	nd	1	
<b>TOTAL</b>	<b>645</b>				<b>495</b>				<b>595</b>	<b>149</b>
Winterburn-Grosmont Fm.	28		172	225	12	12.3%	409	966	20	
Keg River-Granite Wash Fm.	453		11	46	371	6.3%	74	345	89	

n total # of analyzed core intervals, each comprising up to 100 measurements.

kH mean horizontal permeability (maximum) determined for whole core intervals

kH/kV horizontal/vertical permeability ratio for individual samples

w.g.m. weighted geometric mean

STDEV standard deviation

nd not determined

e geometric mean estimated from arithmetic mean

aquitar

Table 3.1 Average Hydraulic Properties of Hydro-Stratigraphic Units From Core Analyses

Well Location	DST#	Formations		DST packer interval (m)		Core interval (m)		Permeability (md)		Perm. ratio max/min
		depth from	depth to	thick	depth from	depth to	thick	DST calculated	CORE E.g.m.	
7 33 92 4 5	2	1236	1251	15	1222	1251	29	1.3	1.0	1
8 1 92 4 5	1	1251	1280	30	1251	1274	23	0.7	0.5	1
6 36 92 4 5	1	1288	1312	25	1289	1312	23	0.4	1	2
9 6 95 4 5	1	1210	1227	17	1212	1226	14	1.1	2.7	2
7 27 92 4 5	1	1243	1263	20	1245	1270	25	2	8	4

See Appendix 2 for DST analyses.

Core permeabilities from ERCB core analysis reports

E.g.m. geometric mean average permeability for the core interval estimated from arith. mean

Table 3.2 Permeability Determination: Drillstem Test Versus Core

Parameter	Value	Units	Source	st. dev.	n	
<b>Storage Coefficient</b>						
<b>Ss=rho g (alpha + por beta)</b>						
rho	1156	kg/m3	Table 3.17	36	295	
g	9.82	m/sec^2				
alpha	5.25E-11	m^2/N	Literature* alpha =f(Porosity)			
por	0.063	fraction	Table 3.1	0.04	423	
beta	4.80E-10	m^2/N	Literature** ( water at 25 deg C)			
Ss=	9.40E-07	/m	calculated			
<b>Storativity</b>						
<b>S=Ss*b</b>						
b	50	m	ERCB (a.m. of HSU thickness in 683 wells)	21	683	
S=	4.70E-05		calculated			
<b>Hydraulic conductivity</b>						
<b>K=(k rho g/mu)</b>						
k	0.011	darcy	Table 3.1	0.046	371	
mu	6.76E-01	cP	Literature*** (water at 38 deg C)			
K=	1.82E-07	m/sec	calculated			
<b>Transmissivity</b>						
<b>T=Kb</b>						
T=	9.1E-06	m/sec^2	calculated			
<b>Abbreviations:</b>						
rho	water density	b	aquifer thickness	Sources:		
g	gravitation constant	mu	dynamic viscosity	* Hall, 1953		
alpha	aquifer compressibility	k	permeability	** Domenico & Schwartz, 1992		
por	porosity	Conversion factors:			*** Bear, 1972	
beta	water compressibility	k(darcy) x 9.87e-13 = k(m^3)				
		mu(cP) x 0.001 = mu( N sec/m^2)				

Table 3.3 Storativity and Transmissivity Calculation for the Keg River Aquifer



Lithology	Thermal Conductivity (W/m/oC)	Error ( $\pm$ )
Limestone	2.8	1.5
Marlstone	2	1.1
Dolomite	4.7	0.8
Rock salt	5.7	1
Anhydrite	5.4	0.4
Shale	1.4	0.4
Siltstone	2.7	0.3
Sandstone	3.7	1.2
Conglomerate	2.1	1
Chert	1.4	0.5
Coal	0.2	0.2
Glacial Till	1.5	0.2

(Data From Majorowicz and Jessop, 1991)

Table 3.4 Thermal Conductivity Values for Lithologies in the Alberta Basin

Hydrostratigraphic Unit	Lithology	Thermal Conductivity (W/m/oC)
<b>Quaternary Aquifer</b>	glacial till, sandstone, gravel	1.5
<b>Shaftesbury Aquitard</b>	shale	1.4
<b>Peace River - Spirit River Aquifer</b>	sandstone, sandy shale	3.7
<b>Clearwater Aquitard</b>	shale	1.4
<b>Bluesky Aquifer</b>	sandstone	3.7
<b>Upper Banff Aquifer</b>	sandstone	3.7
<b>Lower Banff Aquitard</b>	shale	1.4
<b>Wabamun-Grosmont Aquifer</b>	dolomite	4.7
<b>Ireton Aquitard</b>	calcareous shale	1.4
<b>Beaverhill Lake Aquitard</b>	limestone - shale	2.8
<b>Slave Point Aquifer</b>	limestone, sandy shale	2.8
<b>Muskeg Aquitard</b>	anhydrite, halite	5.7
<b>Keg River Aquifer</b>	dolomite, arkosic, sandstone/conglomerate	4.7

Table 3.5 Thermal Conductivity Values for Hydrostratigraphic Units in the Study Area

I	s	t	r	m	DST#	MY ANALYSIS			CIFE ANALYSIS			DISCREPANCY			Reason for
						PI (kPa)	Head fw (m)	Quality	PI kPa	head (m)	quality	rec. z (m)	PI (kPa)	head (m)	
6	36	92	4	5	1	13314	687	1	13356	691	b	0	-41	-4	CIFE typo?
3	31	100	22	4	2	14383	1062	3	14390	1063	b	0	-7	-1	
9	6	95	4	5	2	10649	663	1	10653	663	b	0	-4	0	
7	27	92	4	5	1	13425	693	1	13425	693	b	0	0	0	
11	11	91	11	5	1	16258	705	1	16258	705	b	0	0	0	
9	6	95	4	5	1	12580	616	1	12576	616	b	0	4	0	
7	27	92	4	5	2	13611	693	1	13604	693	b	0	7	1	
7	33	92	4	5	2	13631	708	1	13618	707	b	0	14	1	
8	1	92	4	5	1	13266	664	1	13169	654	b	0	97	10	CIFE extrap. FSI
7	24	101	12	5	1	12710	458	1	12563	443	b	0	147	15	CIFE extrap. ISI
4	31	99	9	5	2	13101	544	1	13142	552	c	-4	-41	-8	CIFE diff. recorder
16	22	92	4	5	2	14252	707	1	14259	708	c	0	-7	-1	
16	2	96	2	5	1	11378	566	1	11384	566	c	0	-6	-1	
4	3	100	7	5	4	12383	576	1	12383	576	c	0	0	0	
16	22	92	4	5	1	13245	683	1	13232	682	c	0	14	1	
6	31	98	22	4	1	14024	1040	3	13997	1037	c	0	28	3	CIFE fewer points
10	34	91	24	4	1	11577	616	1	11494	607	c	0	83	8	CIFE extrap. ISI
7	26	91	9	5	1	15652	711	1	15500	695	c	0	152	15	CIFE extrap. ISI
7	11	98	3	5	1	11763	537	1	11535	564	c	0	228	23	CIFE used ISI
7	33	92	4	5	1	14169	779	1	13721	733	c	0	448	46	CIFE fewer points
3	7	101	5	5	1	11915	629	3	11811	612	d	7	103	18	CIFE diff. recorder
2	17	91	7	5	7	16707	826	3	16707	826	d	0	0	0	
3	7	94	3	5	3	11065	727	2	ne	ne	f	nd	nd	nd	
11	33	94	22	4	1	14873	1030	3	nr	nr	/	nd	nd	nd	

ne: no extrapolation; nr: no record; nd: not determined 1: good; 2: dubious; 3: bad

ISI: initial shut in  
FSI: final shut in

Table 3.6 Evaluation of CIFE DST Interpretation

Initial Prod. Date	Total Prod. Time	Prod. (Mgda. Prod.)	Gas Production	Water Production	Oil Production
Minimum 17 Feb 69	11 h	-685	0	-1099	0
Maximum 5 Apr 87	16 y	398	10.3	610	96
Average 22 Feb 84	3 y	21	0.5	11	10
St. Dev. 5 y	3 y	35	1.0	48	13
Total			112	2622	2376
			3968	16491	14946

Wells active prior to 5 April 1987

†(gas not incl)

Table 3.7 Petroleum Production Statistics for the Study Area

Production Zones	# of Production wells to April 5 1987	# of Production wells to March 1990
Lower Mannville	0	4
Grosmont	0	5
Slave Point	65	72
Gilwood	0	1
Keg River (carbonate)	151	290
Keg River (sandstone)	6	7
Granite Wash	18	22
Undefined	3	6
Total	243*	407**

\*Includes 8 injection wells

\*\* Includes 16 injection wells

Table 3.8 Production Zones and Number of Production Wells

	number of DSTs
Stabilized DST pressure records	301
DST's which pre-date earliest production (17 Feb. 1969)	54
DST's > 10 km from nearest active production well	88
DST's > 200 m above or below any active production zone	8
Calculated drawdown (Theis equation)	
0 to ±1 metre	88
±1 to ±5 metres	22
> ±5 metres	41
Total undisturbed pressures	238

Table 3.9 Summary of Production Induced Disturbance Calculations

Partial Drawdown at DST Wells	#DST-Production Well Pairs	Inter-well Distance (km)		Pre-DST Production (years)		Production Rate* (m <sup>3</sup> /day)		I (log[t(r <sup>2</sup> )])	
		avg	stdev	avg	stdev	avg	stdev	avg	stdev
positive (production wells)									
> 5 m	62	1.2	0.7	1.3	1.3	26	19	0.5	0.3
1 to 5 m	60	2.3	1.5	3.7	5.3	20	30	0.1	-0.1
< 1m	165	3.9	2.4	3.2	4.3	22	36	-0.5	-0.8
0 m	876	6.5	2.3	0.5	0.6	24	40	-1.5	-1.4
negative (injection wells)									
> 5m	1	2.7	na	4.8	na	-25	na	0.2	na
1 to 5 m	7	4.9	1.1	8.2	3.4	-109	254	0.0	-0.3
< 1 m	11	7.8	1.2	7.4	2.6	-20	13	-0.5	-0.8
0 m	12	5.4	2.4	0.2	0.2	-156	249	-1.5	-1.4
	total								
	1194								

\*gas not included

Abbreviations na: not applicable st dev: one standard deviation r: inter-well distance in miles  
 avg: arithmetic mean t: pre-DST production time in years

Table 3.10 Partial Drawdowns - Inter-well Distances, Pumping Intervals and Production Rates

Total Drawdown	# DSTs	Closest Production Well (km)		#Production Wells Within 10 km		Cumulative I (Interference Index)	
		avg	stdev	avg	stdev	avg	stdev
> ±5 metres	41	1.0	0.9	11	7	0.8	0.6
±1 to ±5 metres	22	1.2	0.5	9	7	0.2	0.0
0 to ±1 metres	56	3.0	1.9	8	7	-0.3	-0.3
0	32	5.7	2.5	2	2	-1.2	-0.7
total DSTs	151						

Table 3.11 Total Drawdown Versus Closest Production Well, Number of Wells and Cumulative Interference Index



	Arithmetic Mean	Standard Deviation	Mean $\pm$ 2 Standard Deviations	Units	No. of Samples
water density*	1156	36	1084 to 1228	kg/m <sup>3</sup>	295**
oil density*	765	18	729 to 801	kg/m <sup>3</sup>	163
b	7	4	1 to 15	m	165

\*corrected to average reservoir conditions

\*\* Pre-Cambrian, Granite Wash and Keg River Fm. water samples culled from ERCB data

Table 3.12 Static Oil "Overpressure" Evaluation

HSU	No. of DSTs	RECOVERY	No. of DSTs
Keg River Aquifer	176	gas	9
<i>Muskeg Aquitard</i>	3	<i>water</i>	<i>143</i>
Slave Point Aquifer	11	oil	55
<i>Ireton Aquitard</i>	<i>1</i>	<i>mud</i>	<i>31</i>
Upper Devonian Aquifer	14		
Mannville	32		
Viking	1		
<b>TOTAL</b>	<b>238</b>		<b>238</b>

Table 3.13 Summary of DSTs Undisturbed By Production

CULLING CRITERIA		EXPLANATION	of 232 analyses accepted
ACID INDICATORS			
1	$pH \leq 5.5$	Acid wash lowers pH HCl acid adds Cl. No Na added Dolomite dissolution adds Ca and Mg May also see: High Fe: drill pipe/casing dissolution IBE > 5%	9%
2	$Na/Cl \text{ (mols)} \leq 0.5$		2%
3	$Ca+Mg \geq 30\% \text{ tot.cations (mols)}$		1%
<b>MUD FILTRATE INDICATORS</b>			
1	$K > 0.75\% \text{ of total cations (mols)}$	KCl mud/completion fluid All muds are low in Ca and Mg All muds maintained at high pH High SO <sub>4</sub> may indicate: Surface water added to well Sodium sulphate added to well <i>Gypsum/Anhydrite are possible natural sources</i> Typical Keg River mud is Na Cl saturated for drilling through Muskeg evaporites Na Cl mud has Na/Cl=1.0 and high SO <sub>4</sub> otherwise similar to fm wr NaOH added as a mud dispersent This criterion indicates high concn of CO <sub>3</sub> or SO <sub>4</sub> (both indicate mud) Unreliable criterion	15%
2	$Ca+Mg \leq 4\% \text{ tot.cations (mols)}$		2%
3	$pH \geq 8.3$		3%
4	$SO_4 > 2\% \text{ tot.anions (mols)}$		0%
5	$Na/Cl \text{ (mols)} \geq 1$		0%
6	$Cl < 98.5\% \text{ anions (mols)}$		0%
<i>"mud" in recovery description</i>			49%
<b>HYDROCARBON INDICATORS</b>			
<i>hydrocarbons in recovery</i>		Any recovery of hydrocarbons Iodine used as hc proximity indicator	46%
<i>Iodide measured</i>			8%
<b>ANALYTICAL RELIABILITY</b>			
$IBE = 0.0\%$		Probably indicates Na calculated by difference Analytical error or presence of "exotic" ions pH measurement error pH measurement error IBE: Ion Balance Error	43%
$IBE > 5\%$			0%
$CO_3 \text{ present at } pH < 8.3$ $HCO_3 \text{ present at } pH < 4.5$			3%
Analyses accepted with at most: 1 acid or 2 mud indicators			

Table 3.14 Culling Criteria for Major Ion Analyses (Keg River Formation)

ION	IONIC WEIGHT	EQUIVALENT WEIGHT
Na+	22.99	22.99
K+	39.1	39.1
Ca <sup>2+</sup>	40.08	20.04
Mg <sup>2+</sup>	24.31	12.155
Cl <sup>-</sup>	35.45	35.45
HCO <sub>3</sub> <sup>-</sup>	61.02	61.02
CO <sub>3</sub> <sup>2-</sup>	60.01	30.005
SO <sub>4</sub> <sup>2-</sup>	96.06	48.03

Table 3.15 Equivalent Weights Used in Calculation of Equivalents per Litre

FORMATION	MAJOR IONS (mg/l)											Relative Density	pH	No. of Analyses
	Mg	Ca	Na	K	HCO <sub>3</sub>	CO <sub>3</sub>	SO <sub>4</sub>	Cl	TDS calc					
Bluesky Fm.	111	162	4982	658	1713	10	363	7665	16273	1.01	7.9	23		
Wabamun Fm.	93	160	4616	32	1441	89	395	6564	13390	1.02	8.4	10		
Winterburn Fm.	757	4877	28913	1141	435	23	1075	55354	105783	1.07	8.1	8		
Grosmont Fm.	153	444	8733	21	1564	0	616	13482	25026	1.02	7.8	16		
Ireton Fm.	320	579	15969	74	1271	0	3356	24433	46002	1.03	8.0	8		
Slave Point Fm.	2306	11867	57505	666	227	86	1828	117218	191411	1.13	6.9	26		
Muskeg Fm.	1484	8056	82412	700	238	0	2963	142696	238023	1.16	7.5	4		
Keg River Fm.	3411	20092	72321	1040	133	26	833	159286	256983	1.18	6.7	232		
Granite Wash Fm.	2676	16026	54879	699	91	22	1187	120285	195447	1.14	6.6	65		
Pre-Cambrian	2250	18969	59927	727	104	38	1032	134917	217925	1.15	6.5	13		
											<b>TOTAL</b>	<b>405</b>		

Table 3.16 Average Formation Water Compositions for the Culled Database

RESERVOIR PARAMETERS						
	Mean	St. dev.	Max	Min	# Samples	
Depth	1350	126	1630	1037	165	
Elevation	-739	80	-539	-961	165	
Initial Pressure	13375	1369	16410	6462	163	
Temperature	38.0	2.9	49.0	30.0	164	
Bo (OFVF)	1.13	0.03	1.19	1.05	165	
Initial Solution GOR	41	12	70	16	164	
Average Pay Thickness	7	4	28	1	165	
FLUIDS AT STP (15 C, 101 kPa abs)						
water density†	1166	36	1284	107†)	295	
oil density	831	8	879	810	164	
FLUIDS AT RESERVOIR CONDITIONS						
water density*	1156					
oil density	764.5	18.2	819.3	733.2	164	
water specific weight	11.4					
oil specific weight	7.5	0.2	8.0	7.2	164	

†from my culled wc file (Pre-Cambrian, Granite Wash and Keg River Fms)

\*avg water density at surface corrected to reservoir conditions using Schowalter's (1979) nomogram

Data Source: ERCB (1991 a)

STP: surface temperature and pressure  
OFVF: Oil Formation Volume Factor

Table 3.17 Keg River - Granite Wash Fluid Densities at Reservoir Conditions

Well Location		FWE Head (m amsl)	Aquifer Top Elev. (m amsl)	Average Water Density (10 <sup>3</sup> kg/m <sup>3</sup> )	Hydraulic Conductivity (m/sec)	Average Porosity (fraction)
L	S T R M					
2	25 91 9 5	684	-850			
10	16 92 9 5	697	-855	1.154	2.3 E-06	0.12
10	10 93 8 5	661	-784			
16	2 96 2 5	566	-580			
4	8 97 2 5	569	-586	1.202	4.0 E-08	0.09
6	6 98 1 5	567	-518			
6	10 100 5 5	548	-633			
3	7 101 5 5	546	-632	1.190	2.4 E-08	0.11
10	6 101 6 5	555	-677			

FWE: fresh water equivalent

Table 4.1 Data Used For Three-Point Determinations of Buoyancy-Modified Flux in Keg River Aquifer

Well Location L S T R M			-Grad h (FWE)		Buoyancy-Modified Driving Force (F)		Driving Force Deviation* (degrees)	DFR†		
			Magnitude (m/m)	Orientation (degrees)	Magnitude (m/m)	Orientation (degrees)				
2	25	91	9	5	3.1E-3	88	2.8E-3	90	2	0.1
10	16	92	9	5						
10	10	93	8	5						
16	2	96	2	5						
4	8	97	2	5	3.9E-4	107	1.0E-3	230	123	3.4
6	6	98	1	5						
6	10	100	5	5						
3	7	101	5	5	1.2E-3	54	4.1E-4	37	17	0.7
10	6	101	6	5						

h: hydraulic head

FWE: freshwater equivalent

\*Deviation between -Grad h and F

† see text

Table 4.2 Freshwater Head Gradient and Buoyancy-Modified Driving Force in Keg River Aquifer



Well Location			Lateral Specific Discharge [m/sec]	Average Linear Flow Velocity		Time to move 10 km (1 Tp.) [years]
L	S	M		[m/sec]	[m/year]	
2	25	91	5	5.4E-8	1.7	5.9E+3
10	16	92	5	6.4E-9		
10	10	93	5			
16	2	96	2			
4	8	97	2	4.2E-11	1.5E-2	6.6E+5
6	6	98	1			
6	10	100	5	9.6E-12	8.7E-11	3.6E+6
3	7	101	5		2.8E-3	
10	6	101	6			

Table 4.3 Lateral Water Flow Rates in Keg River Aquifer

Geologic Unit	Unit Thickness (m)	Water Density ( $10^3 \text{ kg/m}^3$ )	Data Source	Specific Weight (kPa/m)	Nominal Hydrostatic Pressure at Base of Unit (kPa)
Quaternary-Bluesky Fm.	399	1.01	sa.avg	9.92	3957
Winterburn Fm.	93	1.10	sa.avg	10.80	4962
Grosmont Fm.	206	1.02	local	10.05	7031
Ireton-Waterways Fm.	312	1.03	sa.avg	10.11	10187
Slave Point-Watt Mtn Fm.	45	1.18	local	11.55	10707
Muskeg Fm.	178	1.17	e(250 g/l)	11.51	12756
Keg River-Granite Wash Fm.	34	1.17	local	11.53	13148
Pre-Cambrian					

sa.avg	study area average from water chemistry data base
local	based on local water chemistry analyses
e	estimated
Geologic unit depths from ERCB for well 10-8-95-6W5	

Table 4.4 Water Density Profile for Townships 94-95, Ranges 6-7

Parameter	Value	Source
Vertical Hydraulic Conductivity (m/sec)	1.14E-10	Hydraulic Conductivity Map (Figure 4.8) and Kh/Kz Ratio (Table 3.1)
Vertical Pressure Gradient (kPa/m)	11.92	Figure 4.19.1
Water Density ( $10^3 \text{ kg/m}^3$ )	1.17	Table 4.4
Porosity (fraction)	0.05	ERCB data
Vertical Specific Discharge (m/sec)	-2.71E-10	Equation 2.10
Average Linear Vertical Flow Velocity (m/sec)	-5.42E-09	Equation 2.11
Average Linear Vertical Flow Velocity (m/year)	-1.71E-01	

Table 4.5 Calculation of Vertical Flux in Keg River Fm. at Townships 94-95, Ranges 6-7W5

148

**Figures**

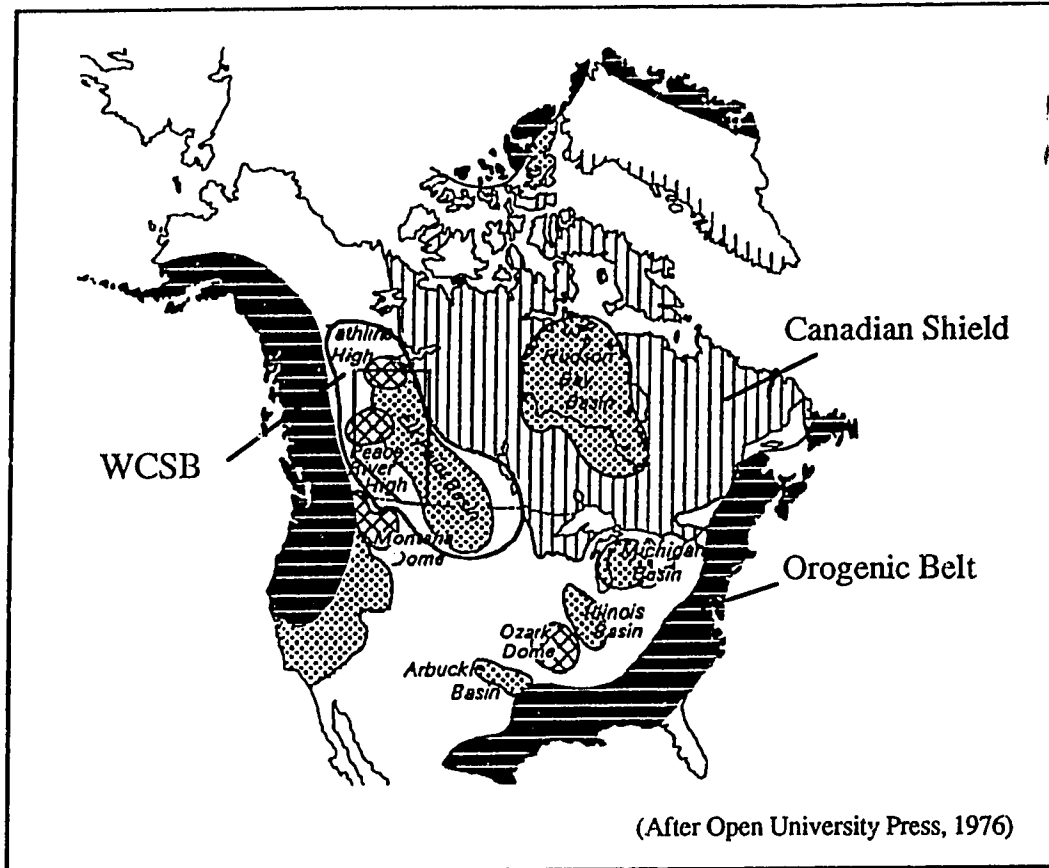
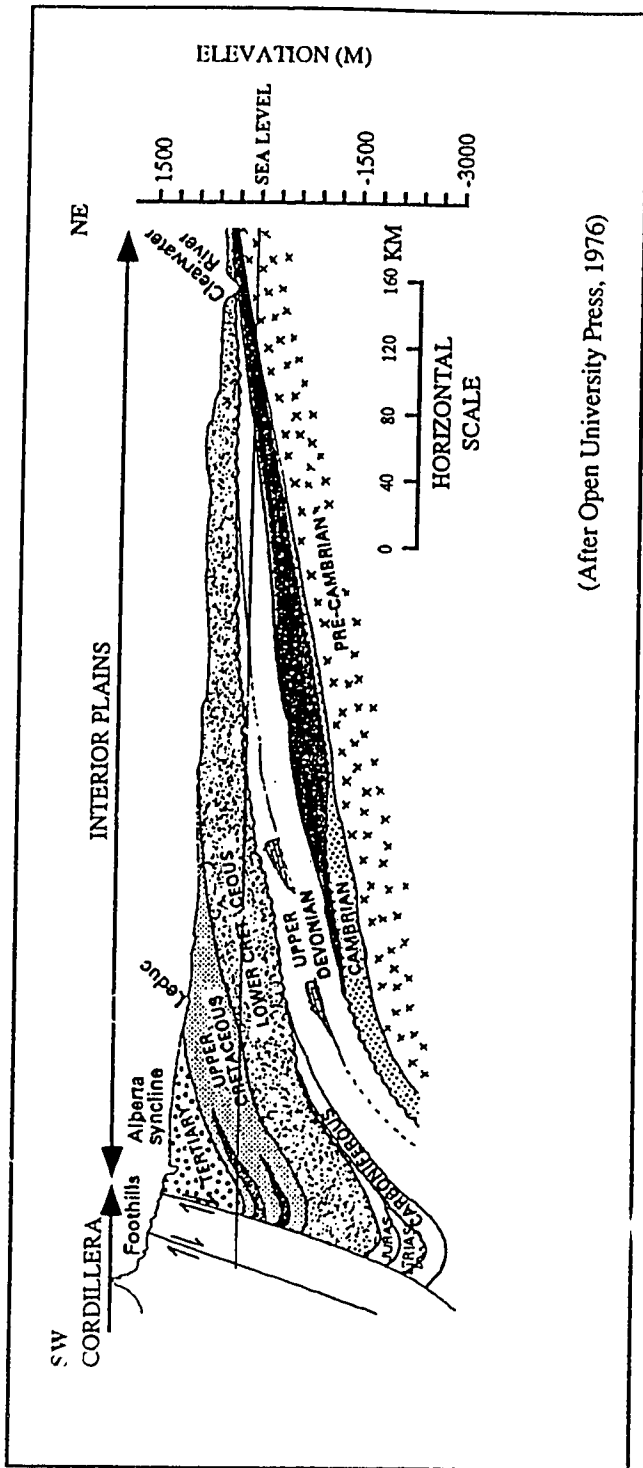


**Figure 1.1 Tectonic Elements of North America and Location of Western Canada Sedimentary Basin**

Shows present extent of western Canada sedimentary basin (WCSB), extent of basin during Middle Devonian (Elk Point Basin) and Middle Devonian craton uplifts including the Peace River Arch.



(After Open University Press, 1976)

Figure 1.2 Western Canada Sedimentary Basin, Regional Dip Section Across Central Alberta

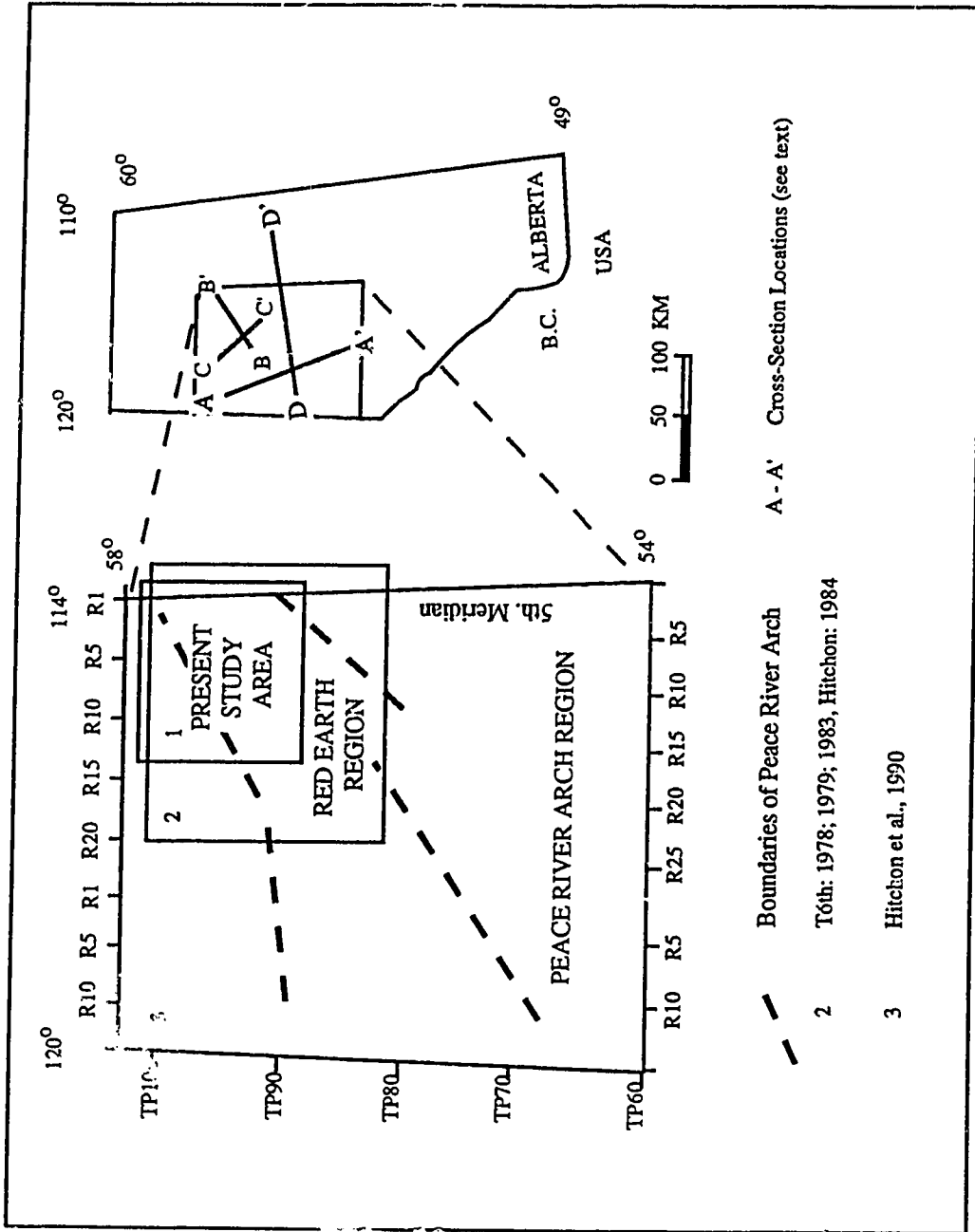


Figure 1.3 Location Map of Present and Previous Study Areas in the Peace River Region

**SW**      **STRUCTURAL CROSS-SECTION**      **NE**  
**B**      **PANNY REGION**      **B'**

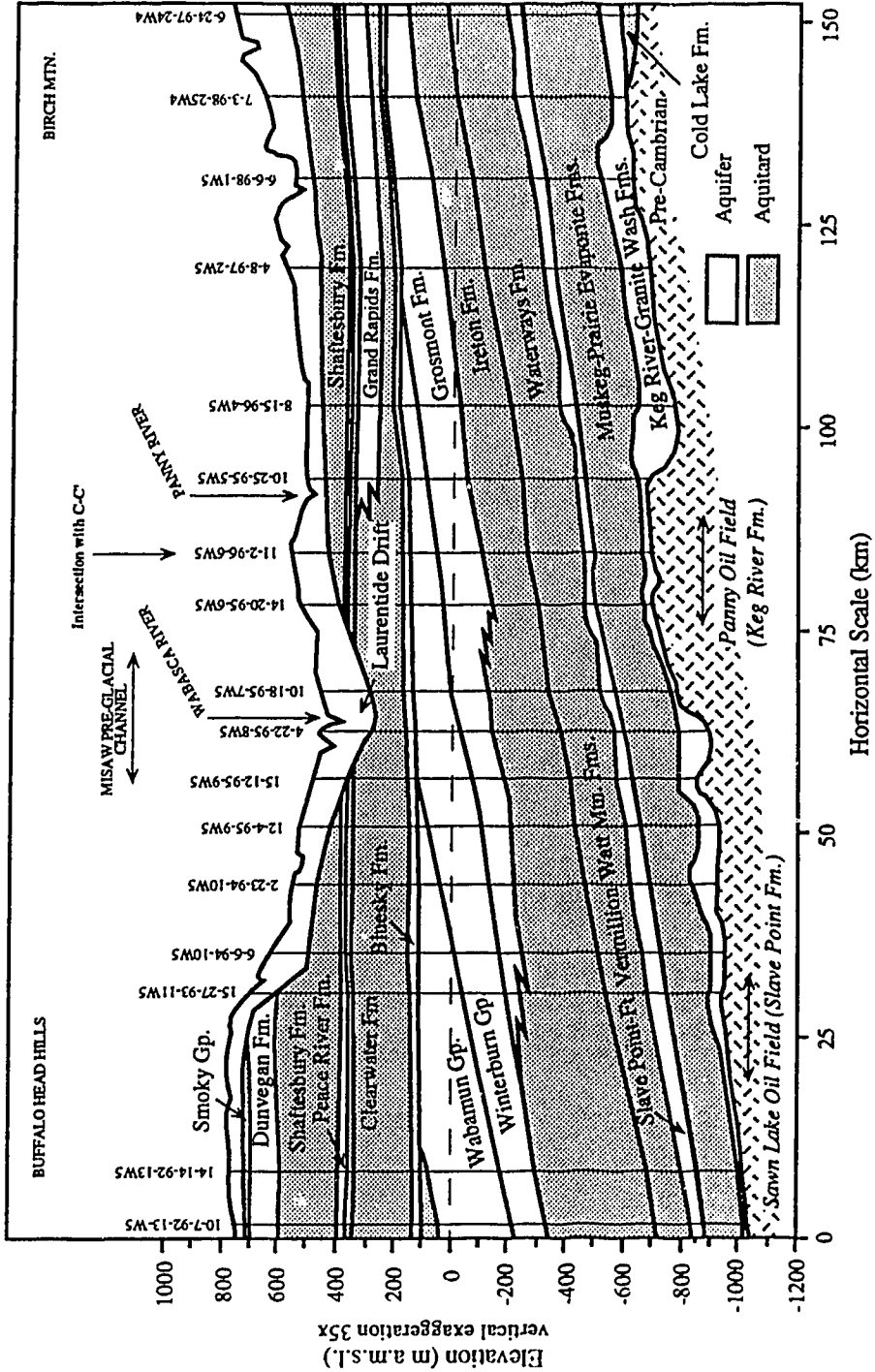


Figure 1.4 Structural Cross-section of Study Area Parallel to Basin Dip





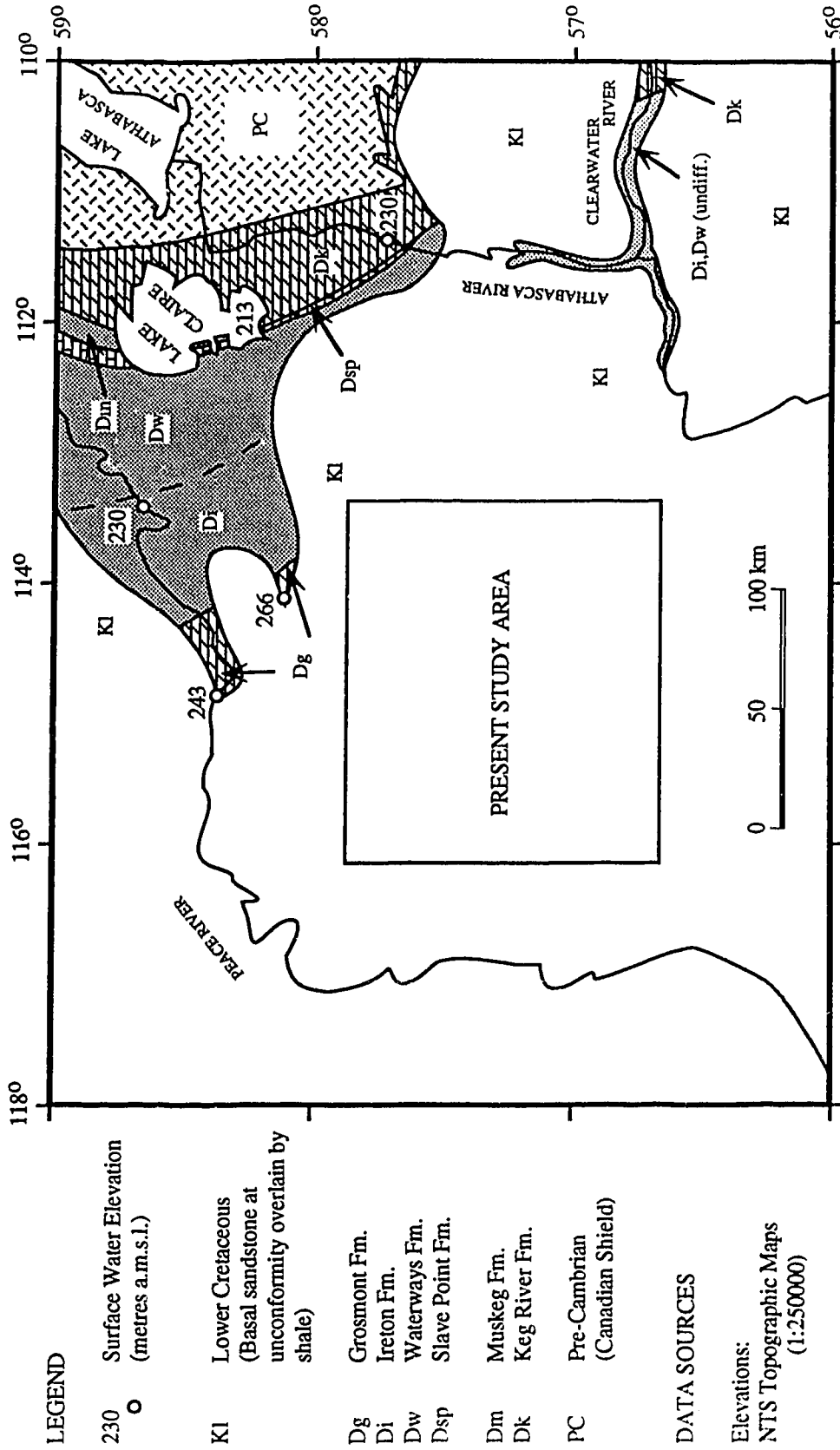


Figure 1.6 Devonian Outcrop Adjacent to Study Area

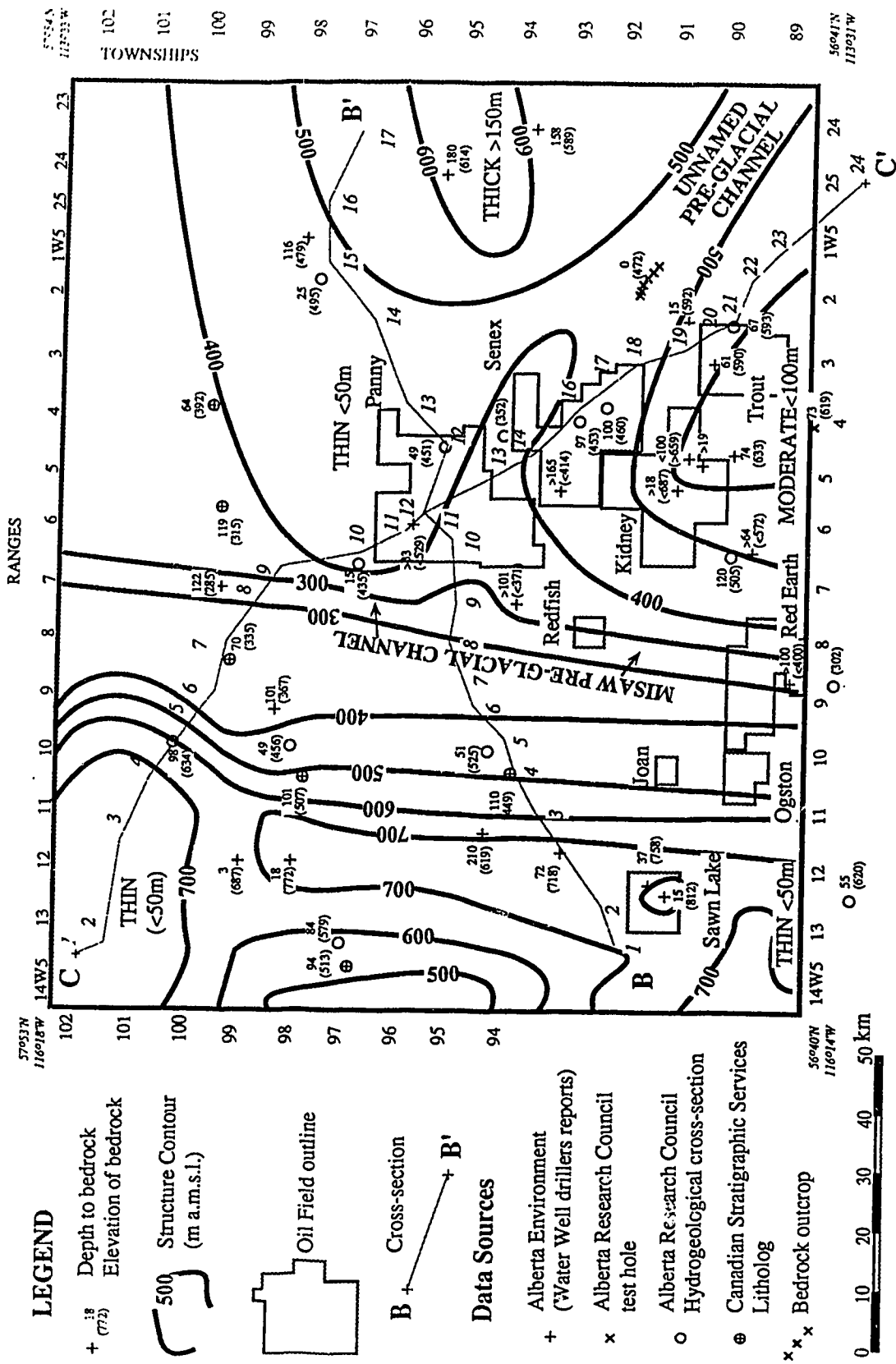


Figure 1.7 Structure Contours on Bedrock and Thickness of Drift

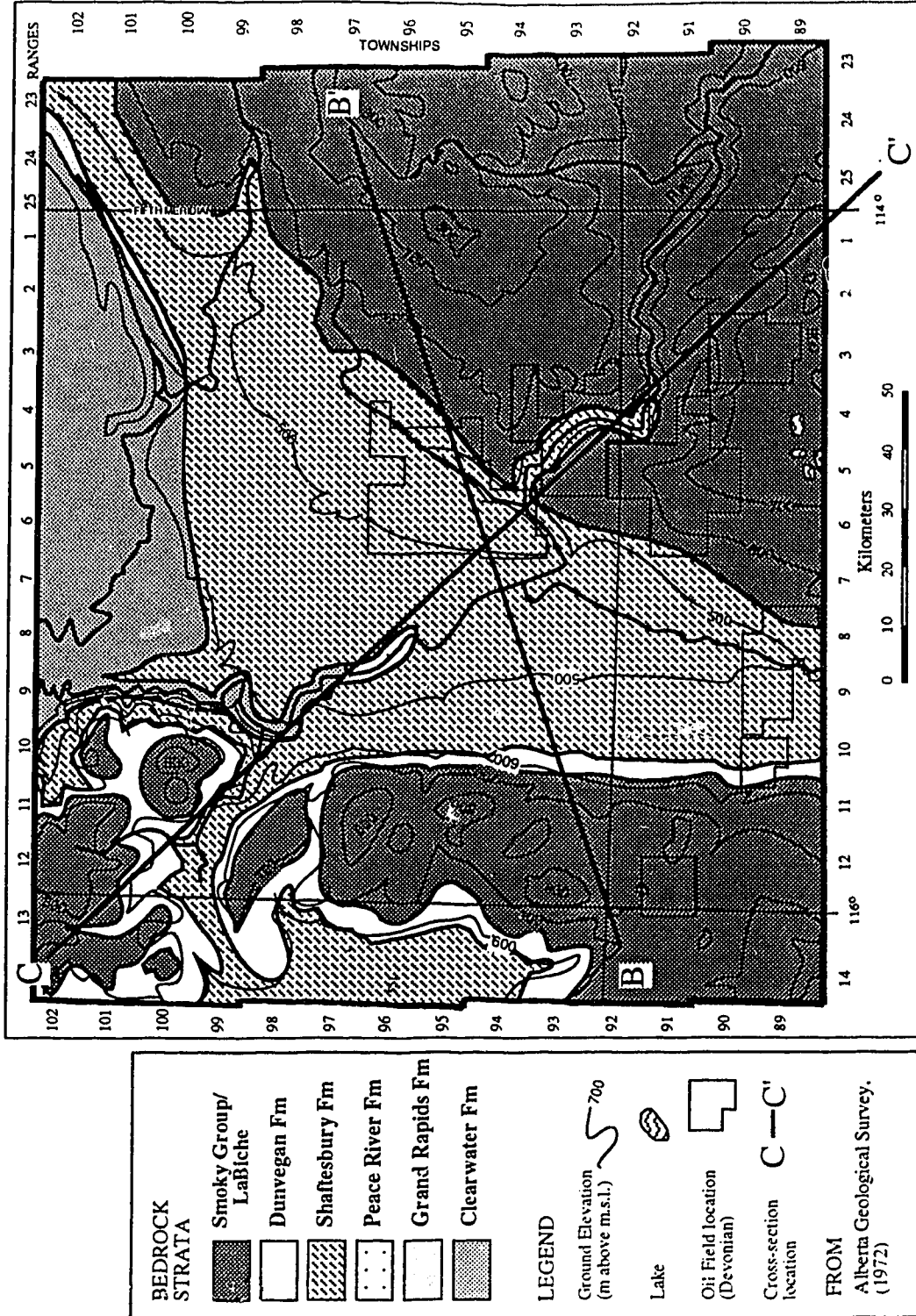


Figure 1.8 Study Area Bedrock Geology



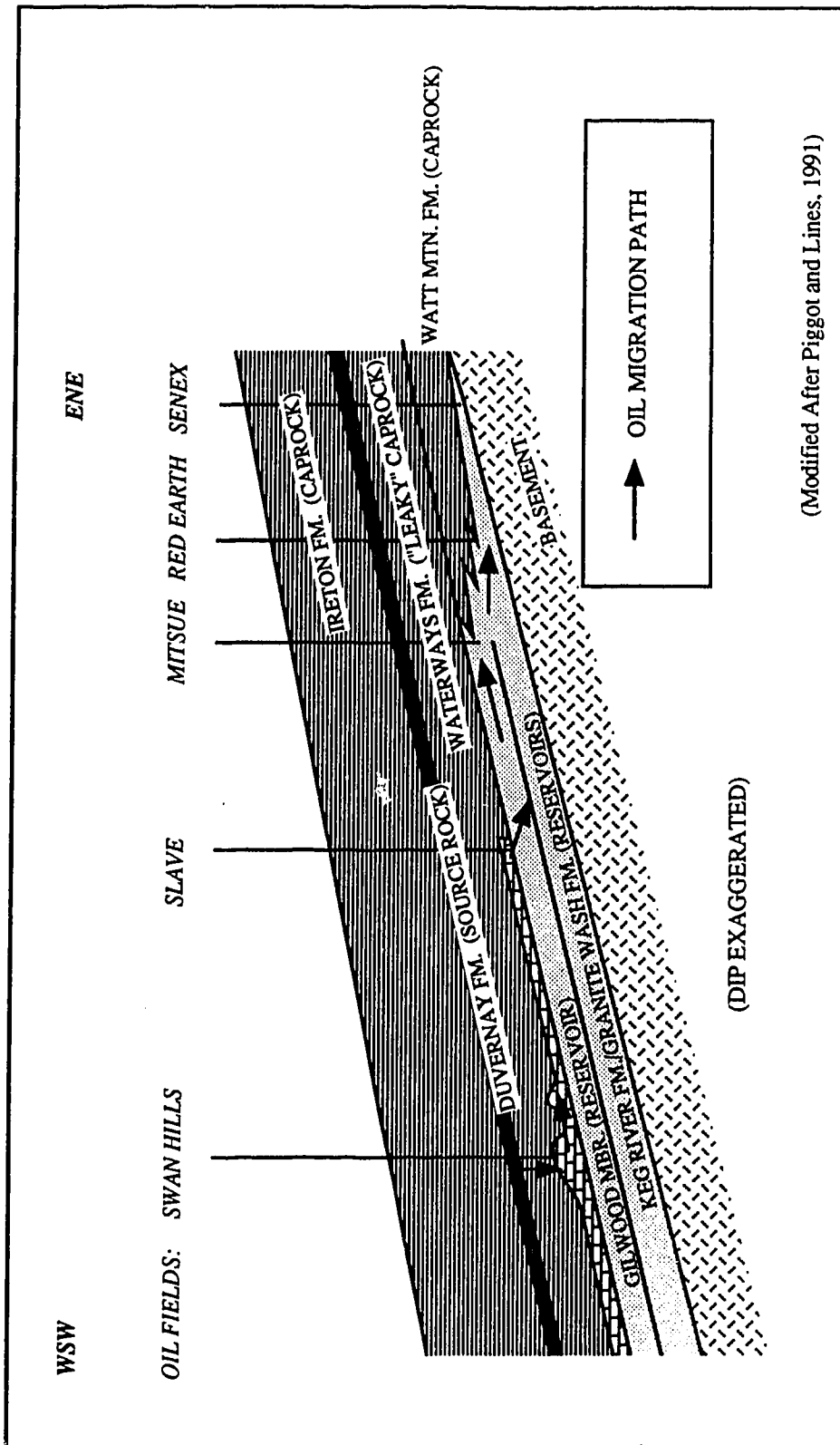
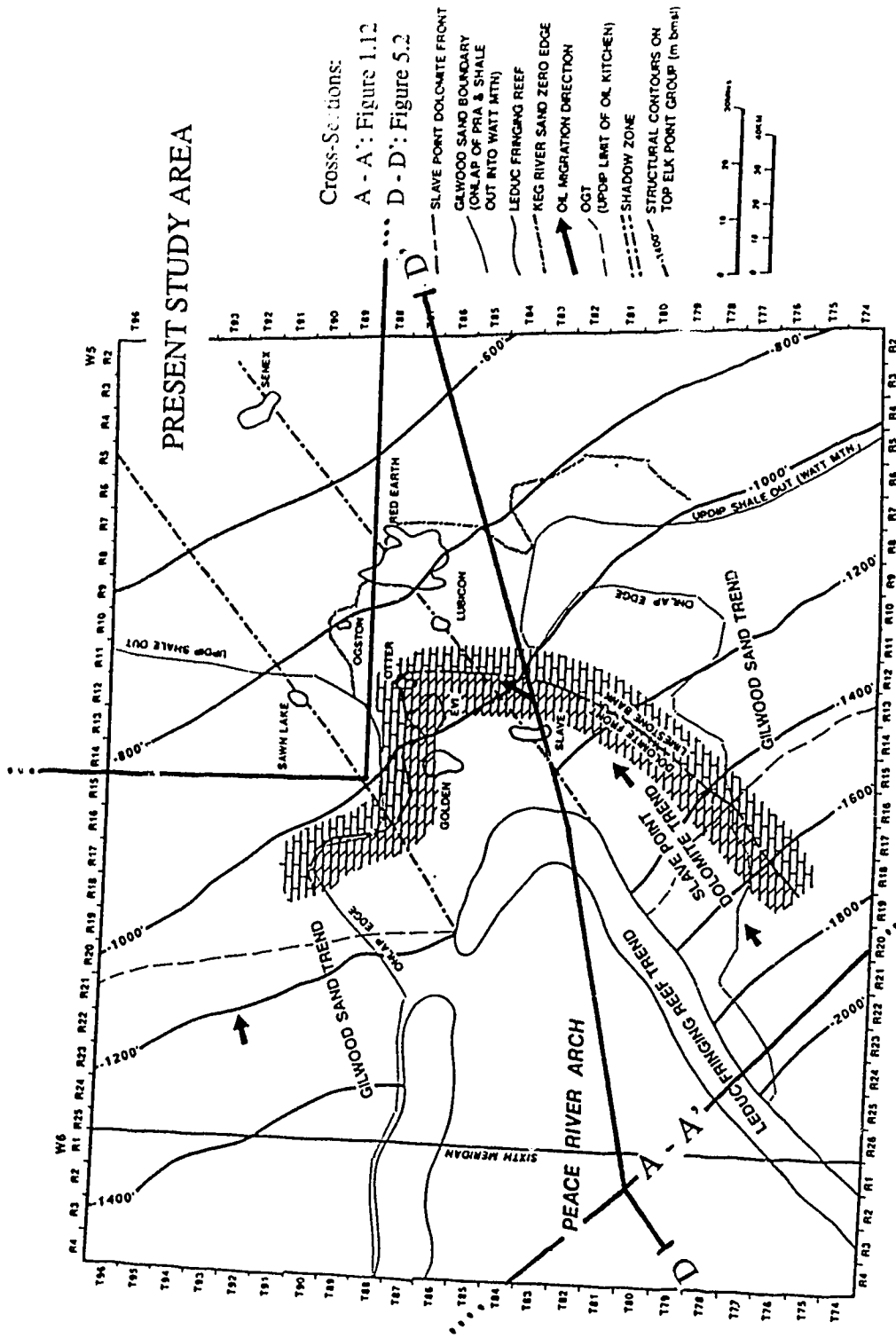


Figure 1.10 Schematic Cross-Section Illustrating the Conventional (Buoyancy Driven) Oil Migration Model in the Peace River Arch Region



(After Piggot and Lines, 1991)

Figure 1.11 Slave Point Fm. Facies Distribution and Inferred Oil Migration "Focusing" in Peace River Region

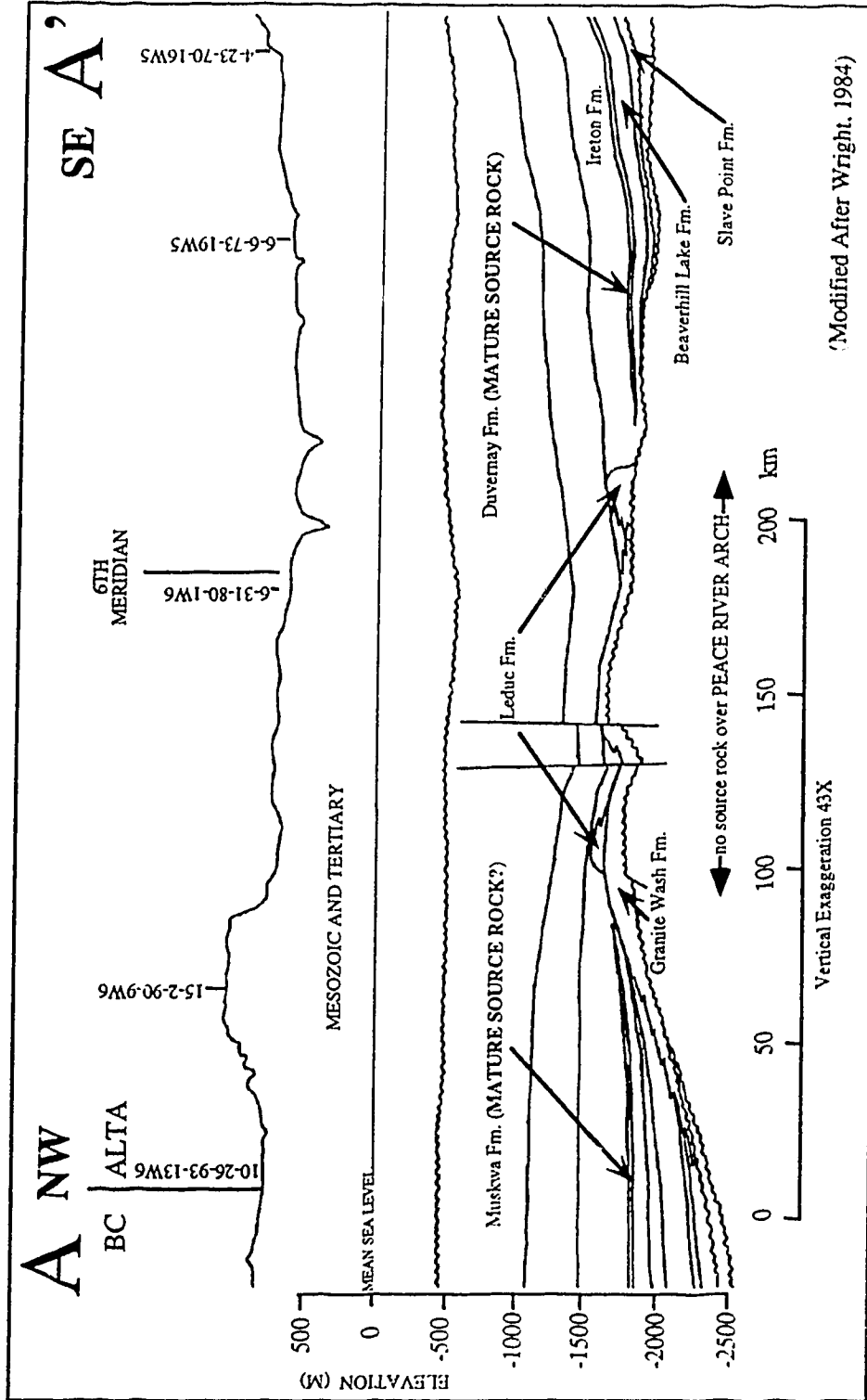


Figure 1.12 Strike Section Across Peace River Arch



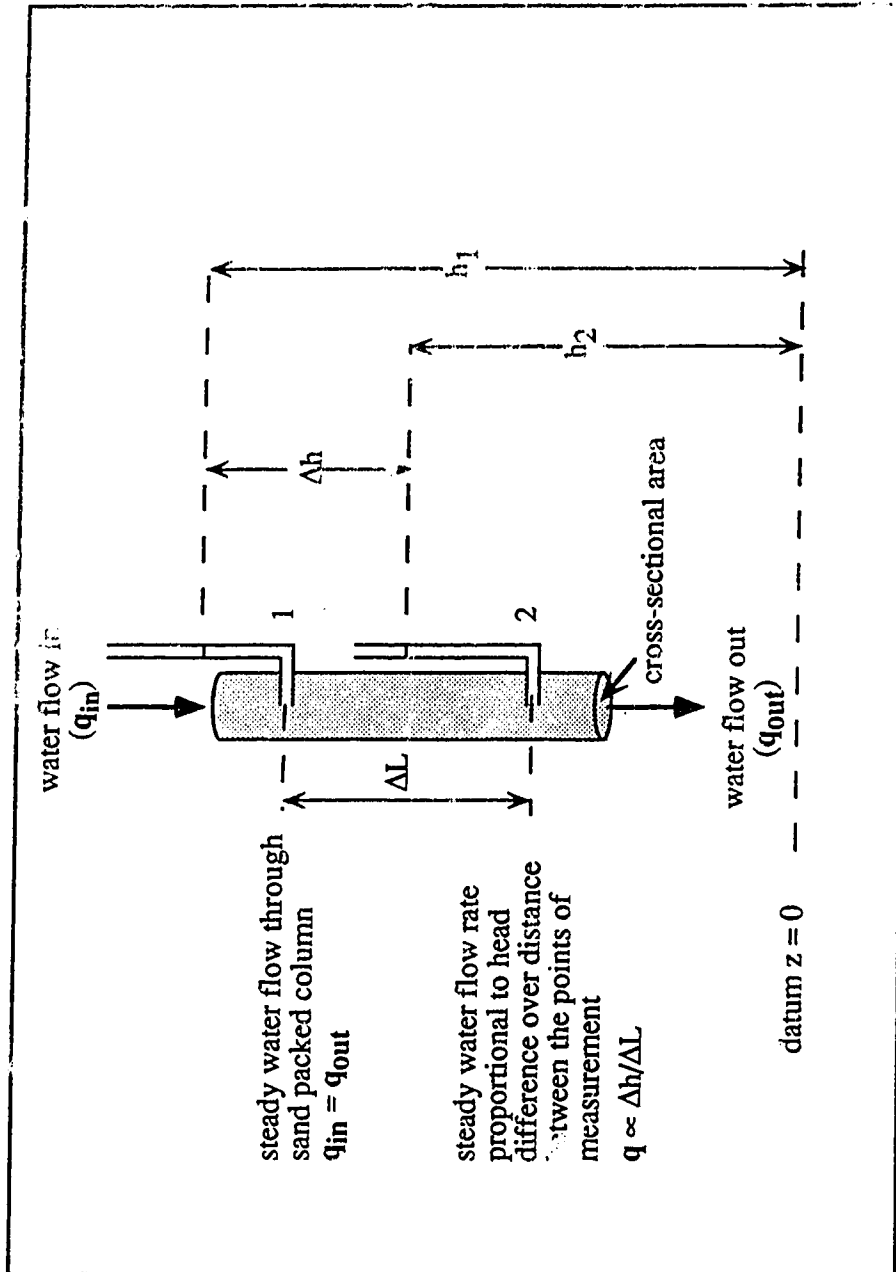


Figure 2.1 Schematic Diagram of Darcy's Fluid Flow Experiment

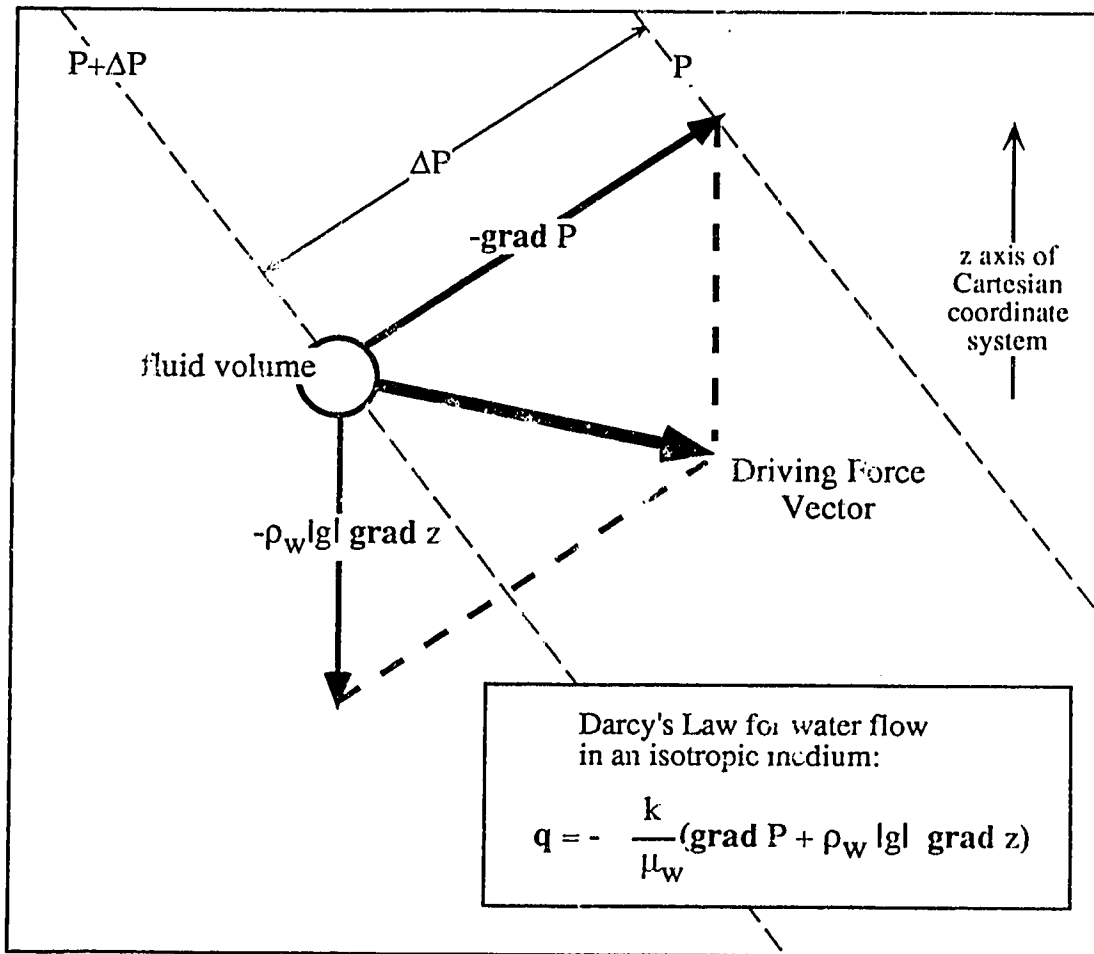


Figure 2.2 Vector Diagram Illustrating the Twin Components of the Driving Force for Water Flow

Valid forms of Darcy's Law in terms of the freshwater head gradient in variable density systems

For horizontal flow:

$$q_x = -K_x \frac{\partial h}{\partial x}$$

For inclined flow in direction 's':

$$q_s = -K_s \left( \frac{\partial h}{\partial s} + (\rho_w - 1) \frac{\partial z}{\partial s} \right)$$

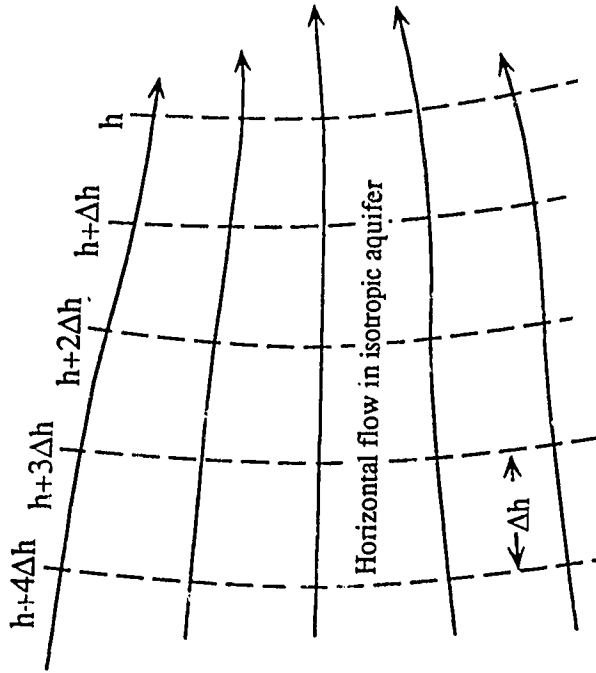
For vertical flow:

$$q_z = -K_z \left( \frac{\partial h}{\partial z} + \rho_w - 1 \right)$$

or, in terms of the vertical pressure gradient  $\partial P / \partial z$ ,

$$q_z = -K_z \left( \frac{1}{\rho_0 g} \frac{\partial P}{\partial z} + \rho_w \right)$$

where  $\rho_0$  is the density of freshwater and  $\rho_w$  is the density of the water at the point



Flow lines are orthogonal to freshwater head contours when permeability is isotropic and flow horizontal. Flow lines are not generally orthogonal when the medium is anisotropic or when the flow is inclined and the water density is variable.

Figure 2.2.1 Water Flow in Response to the Freshwater Head Gradient

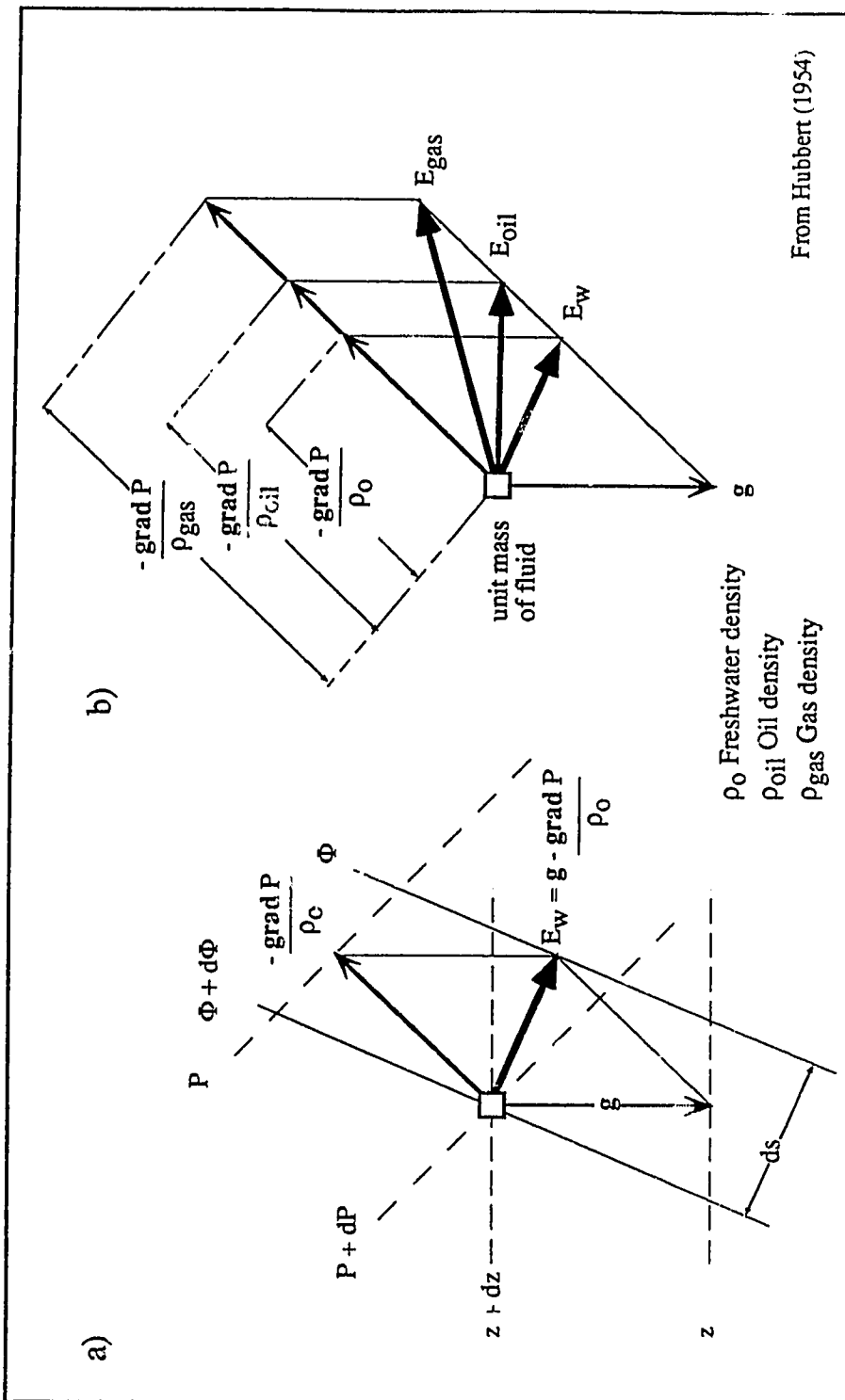


Figure 2.3.2 Vector Diagrams Illustrating:  
 a) the Components of the Driving Force for Water Flow in terms of Fluid Potential  
 b) the Unique of Direction and Magnitude of Driving Forces for Water, Oil and Gas

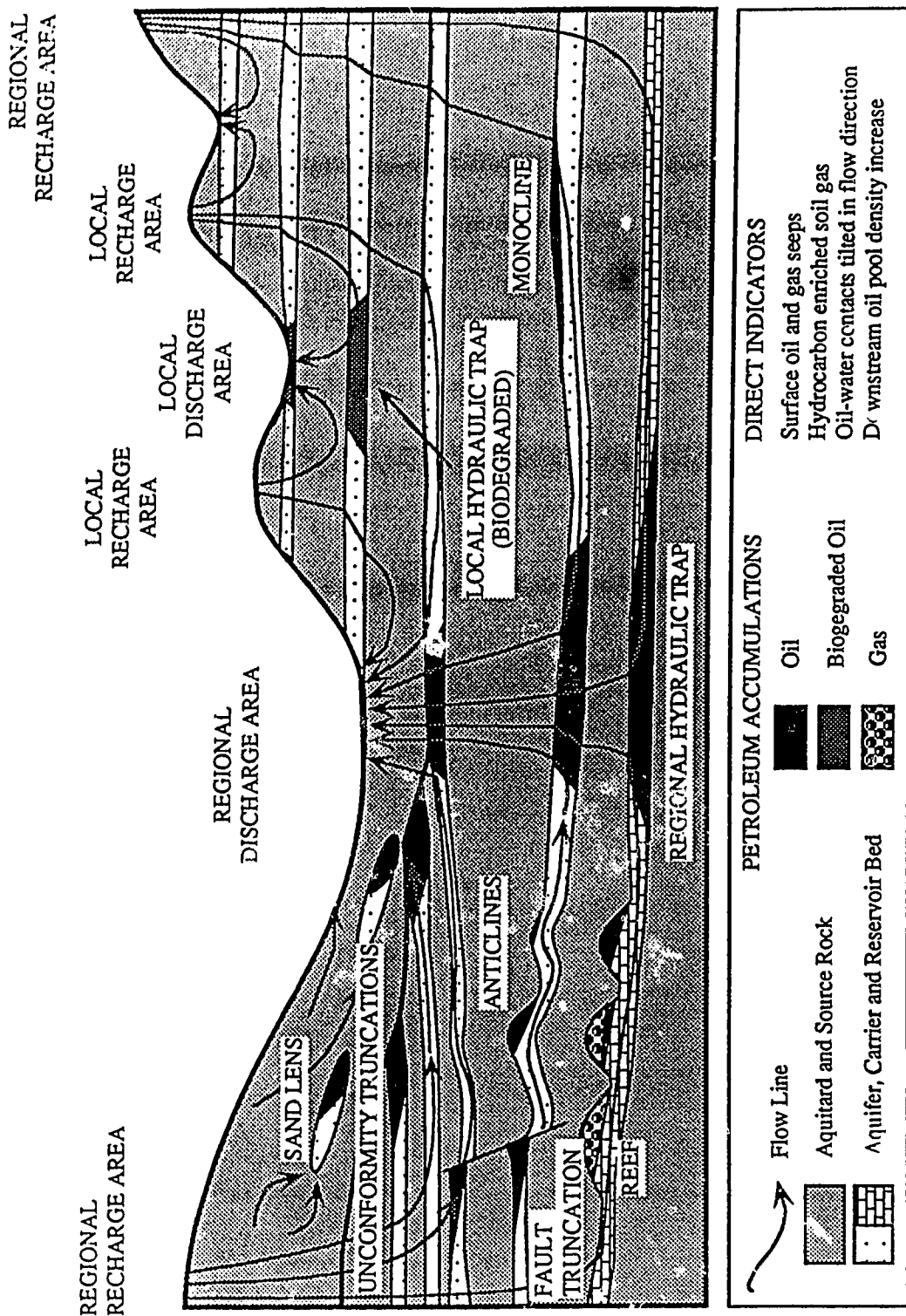


Figure 2.4 Conceptual Geologically Mature Basin Cross-Section Illustrating Potential Petroleum Accumulation Sites (modified after Tóth, 1980)

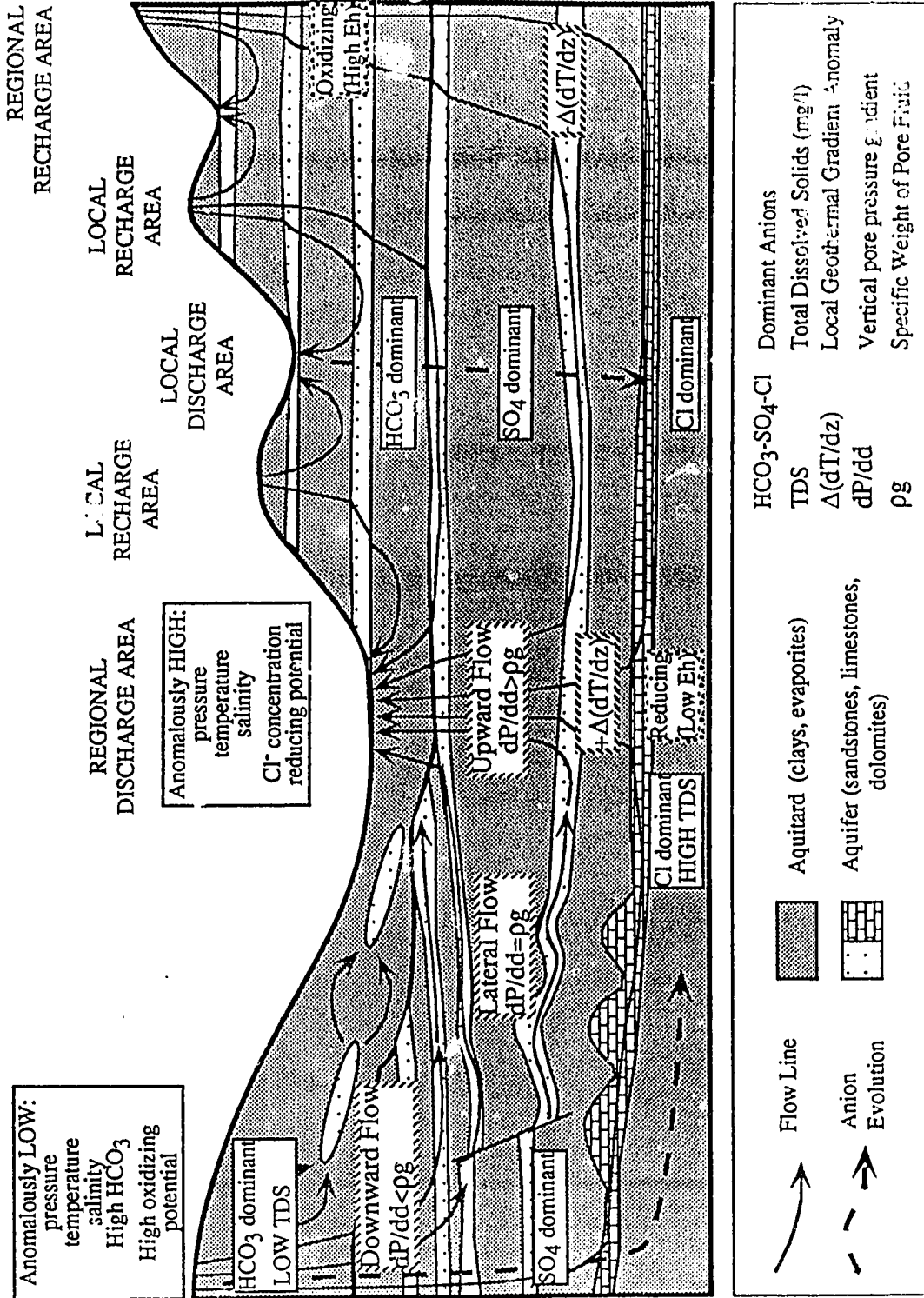


Figure 2.5 Conceptual Geologically Mature Basin Cross-Section Illustrating Hydrogeological Indicators of Various Regions of the Flow Field (modified after Toth, 1980)

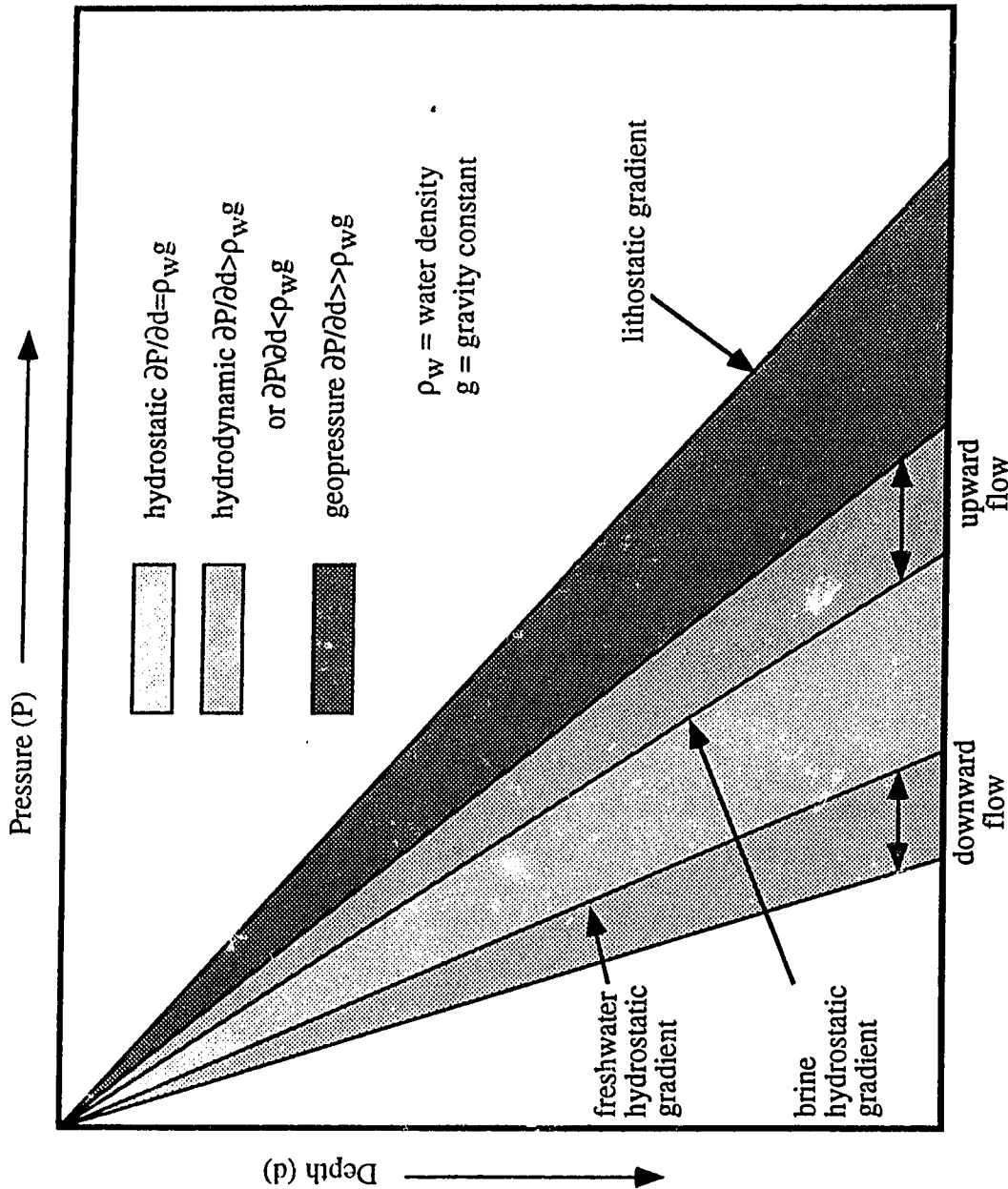


Figure 2.6 Pressure-Depth Relations: Hydrostatic, Hydrodynamic and Lithostatic

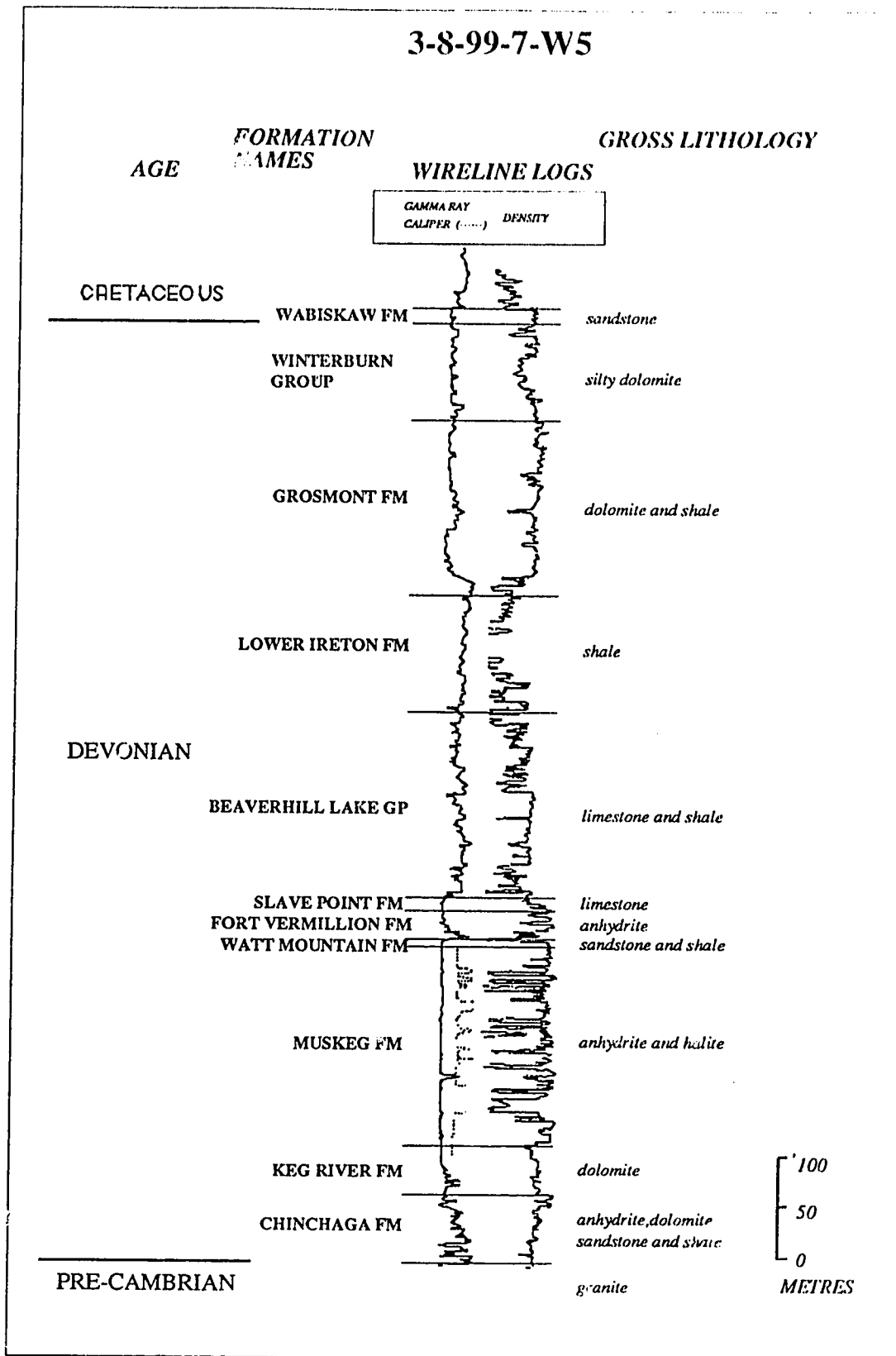


Figure 3.1 Characteristic Log Signatures for Palaeozoic Formations

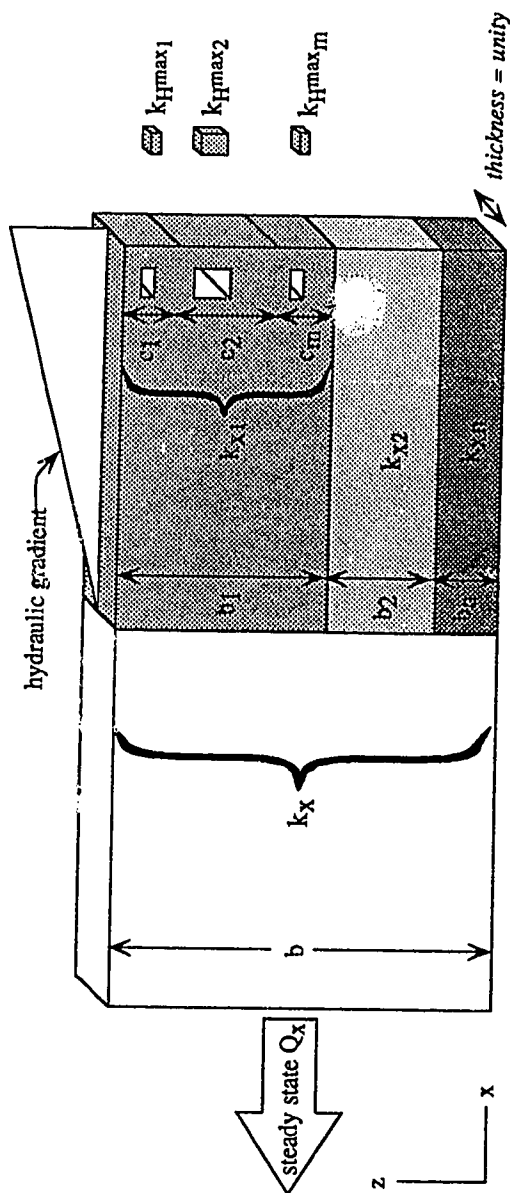


The material on this page has been removed for the National Library of Canada microfilm copy of the thesis, because of copyright restrictions.

Figure 3.2 is a GEOTECH core analysis report histogram, showing the normal (bell-shaped) frequency distribution of porosity in a core sample from the Keg River Formation.

Reference: ERCB, 1991

Figure 3.2 Porosity Frequency Histogram



REPRESENTATIVE LATERAL PERMEABILITY

<p><b>HYDROSTRATIGRAPHIC UNIT</b></p> $k_x = \sum_{i=1}^n \frac{k_i b_i}{b}$ <p>the weighted arithmetic mean of formation permeabilities, derived from Darcy's Law for lateral flow (Freeze and Cherry, 1979)</p>	<p><b>FORMATION</b></p> $k_{xi} = \frac{\sum_{j=1}^m \log k_{Hmax,j} c_j}{b_i}$ <p>the weighted geometric mean of constituent core plug permeabilities is derived as the best estimate of the central tendency of <math>k_{Hmax}</math> variance</p>	<p><b>CORE PLUG</b></p> <p><math>k_{Hmax}</math>, the maximum horizontal permeability. Orientation assumed parallel to the hydraulic gradient.</p>
---	--	--

Figure 3.3 Representative Lateral Permeabilities at Various Scales

The material on this page has been removed for the National Library of Canada microfilm copy of this thesis, because of copyright restrictions.

Figure 3.4 is a GEOTECH core analysis report histogram, showing the log-normal frequency distribution of horizontal permeability in a core sample from the Keg River Formation.

Reference: ERCB, 1991 c.

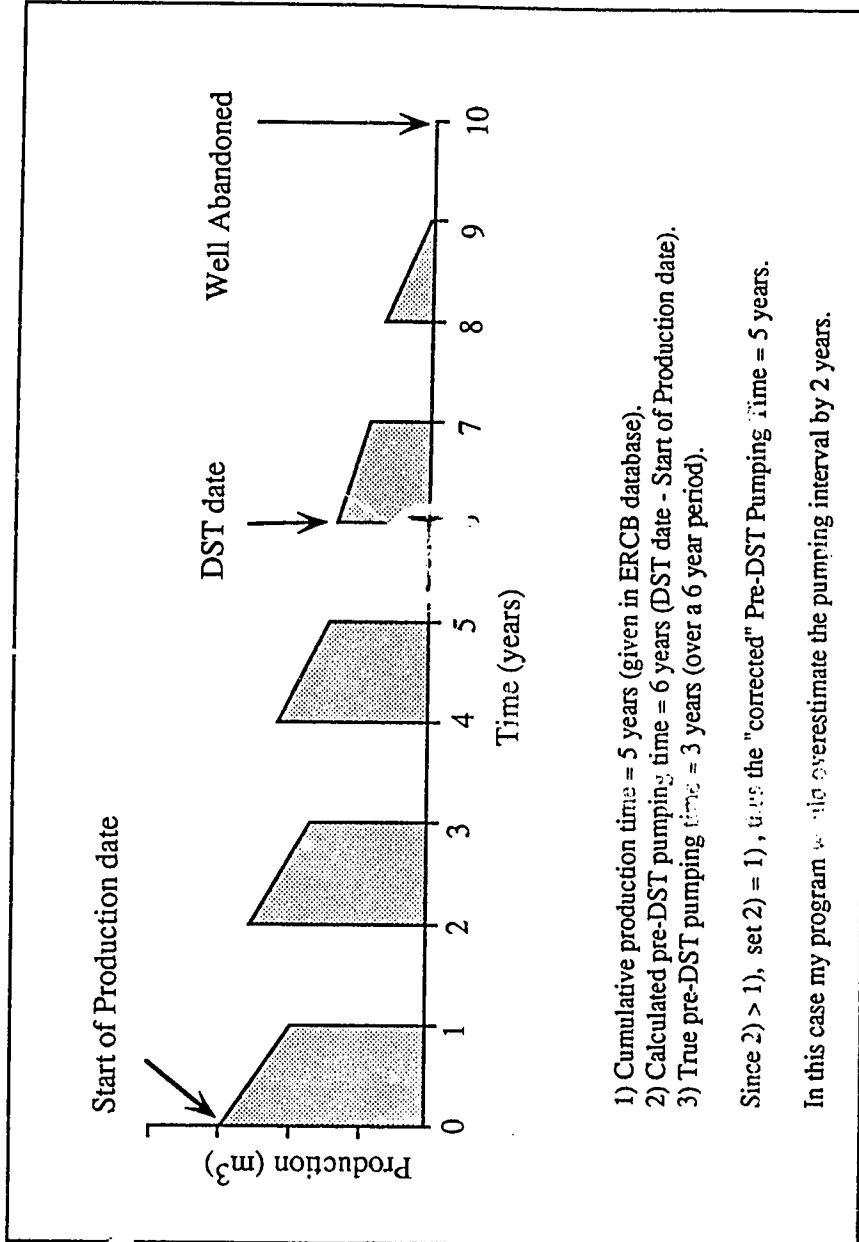


Figure 3.5 Schematic Production History Graph

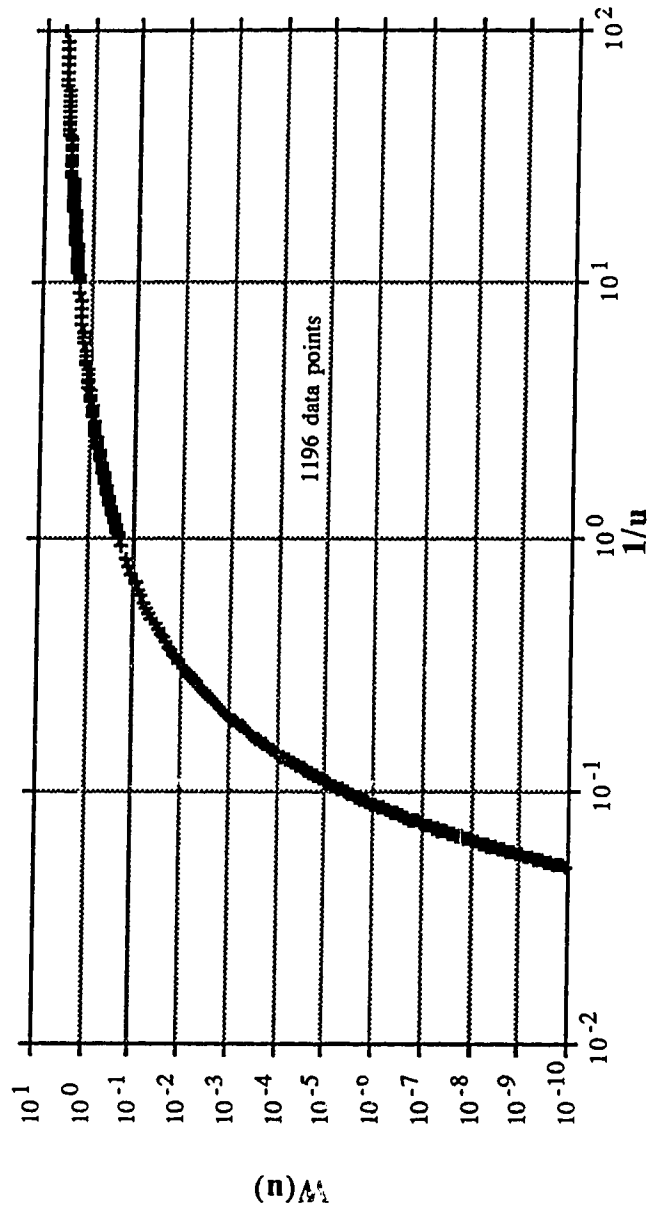
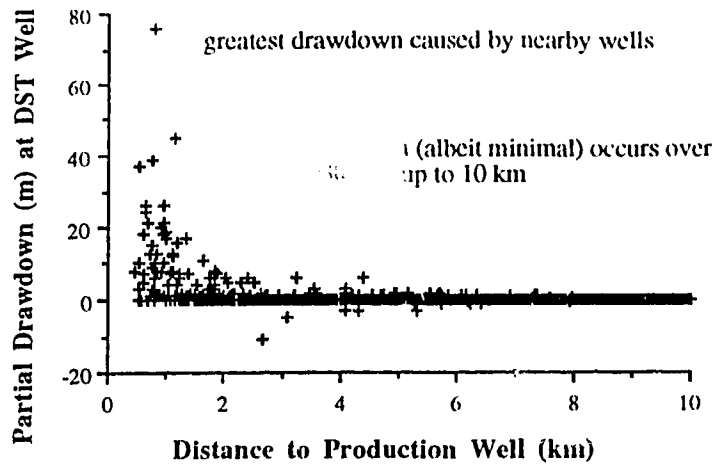
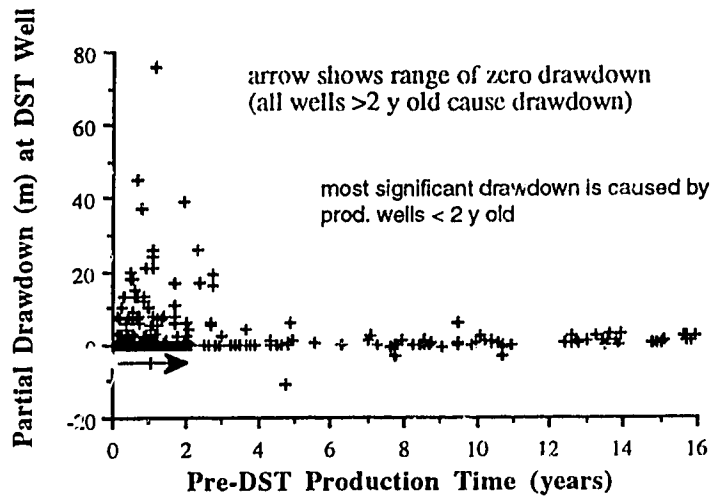


Figure 3.6 Graph of  $W(u)$  versus  $1/u$  - the Theis Type Curve

a)



b)



c)

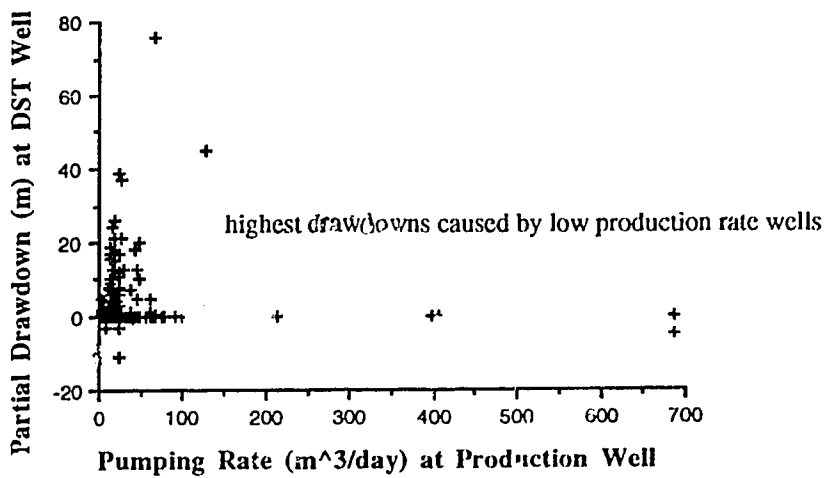


Figure 3.7 The Influence on Drawdown of:  
 a) Distance; b) Production Time and c) Production Rate

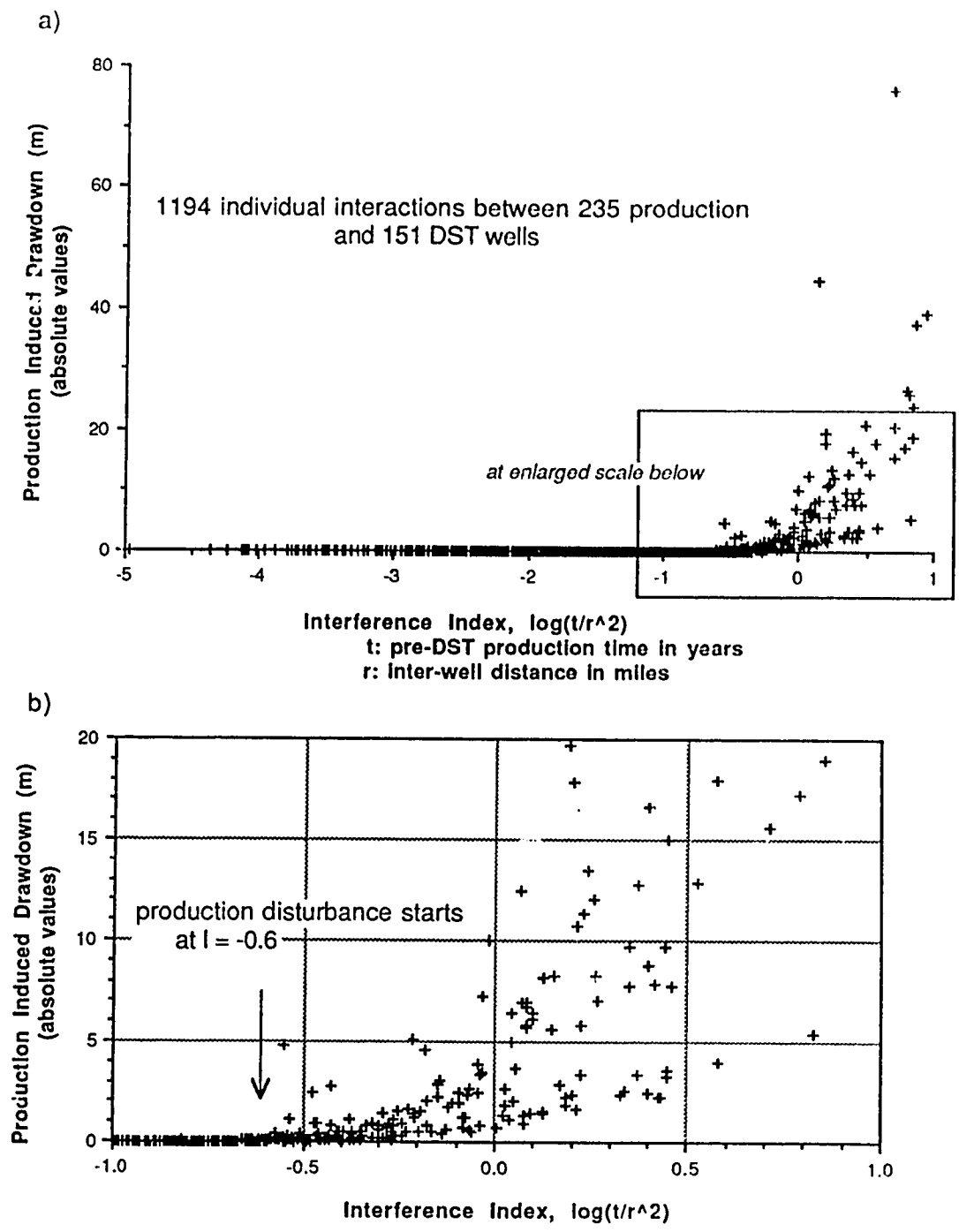


Figure 3.8 Partial Drawdown Versus:  
a) All Data; b) Disturbed Wells at Enlarged Scale

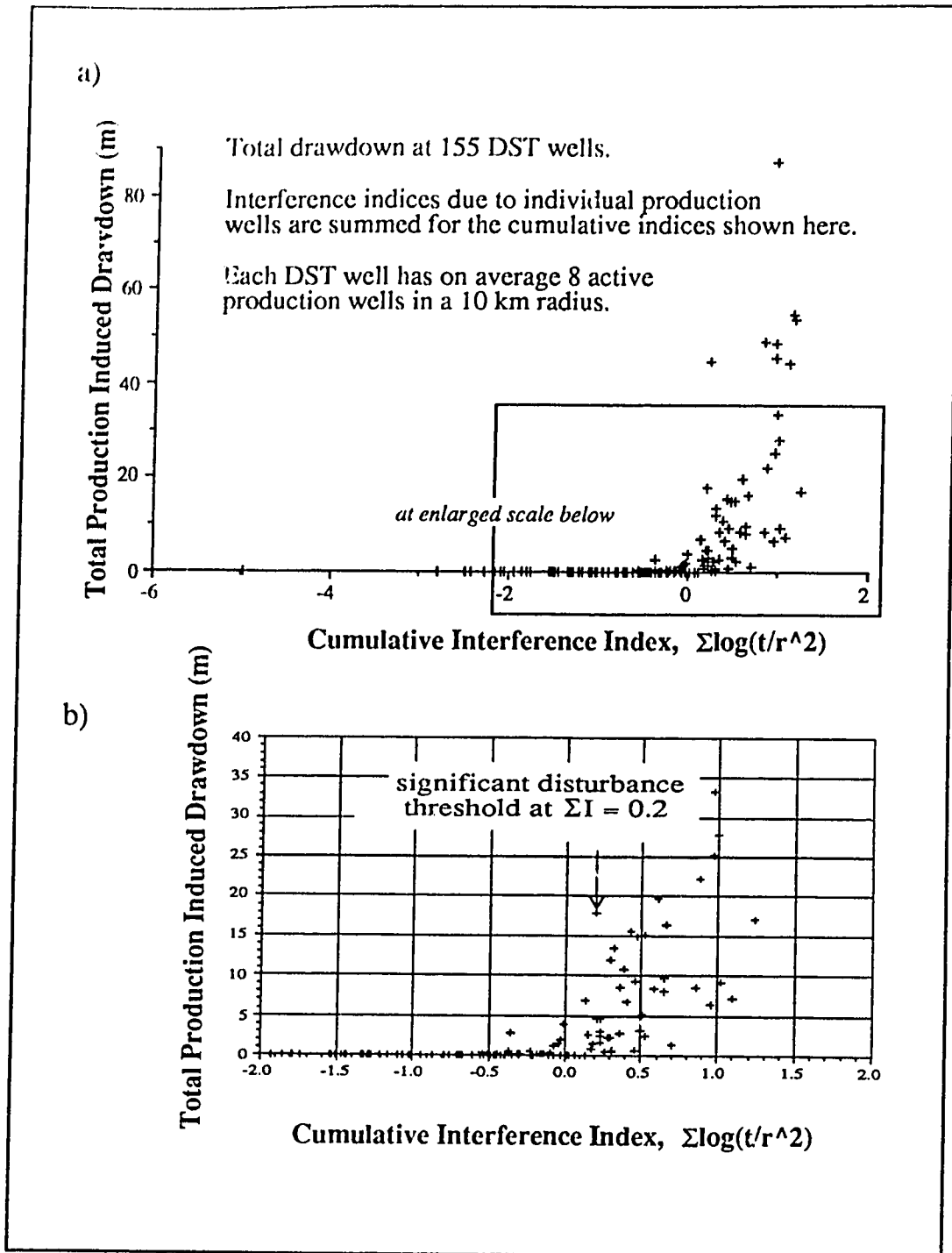


Figure 3.9 Total Drawdown Versus Cumulative Interference Index

a) All Data

b) Disturbed Well Data at Enlarged Scale



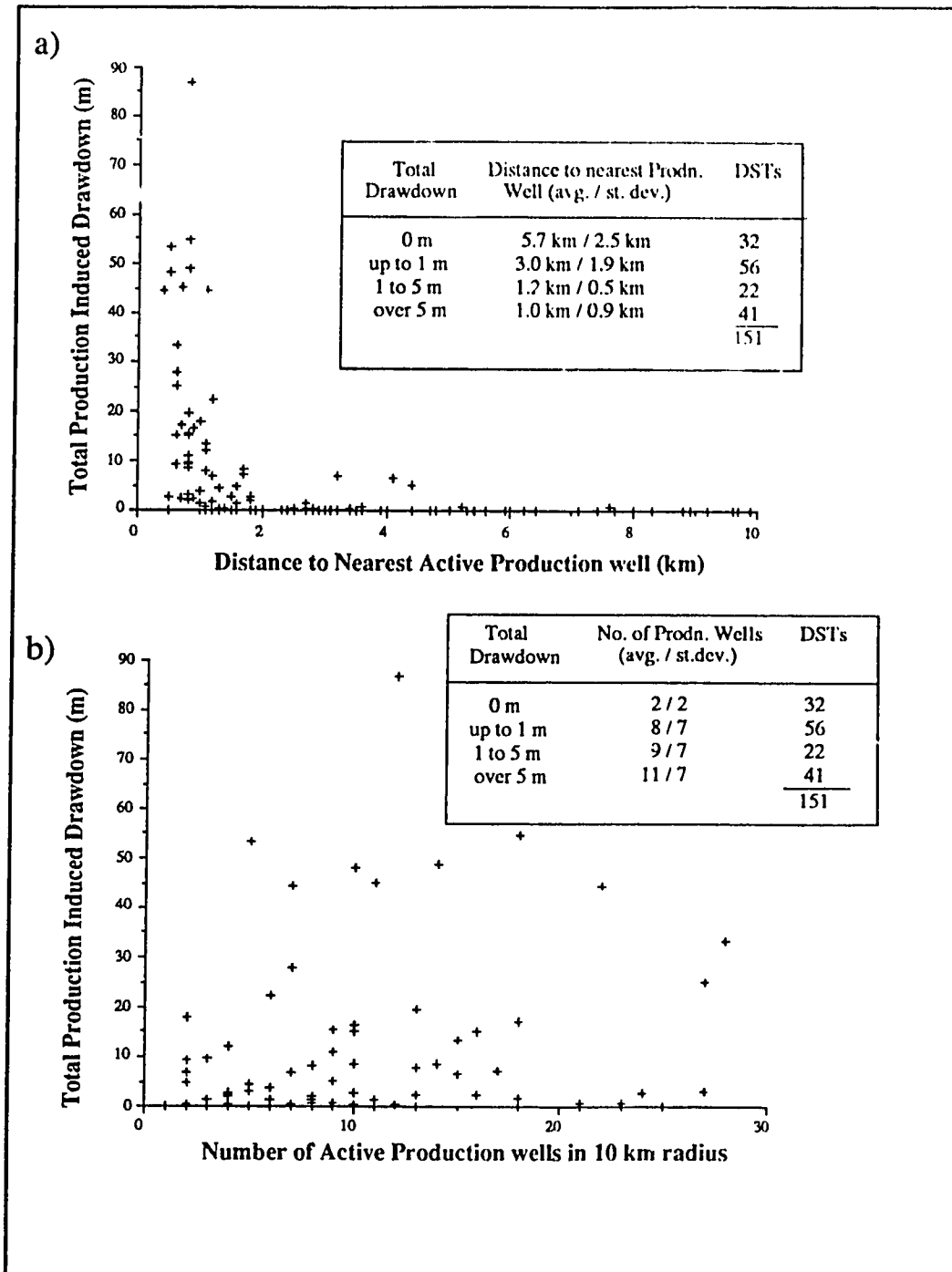


Figure 3.10 Total Production Induced Drawdown Versus:  
 a) Distance to Nearest Active Production Well  
 b) Number of Active Production Wells Within 10 km Radius

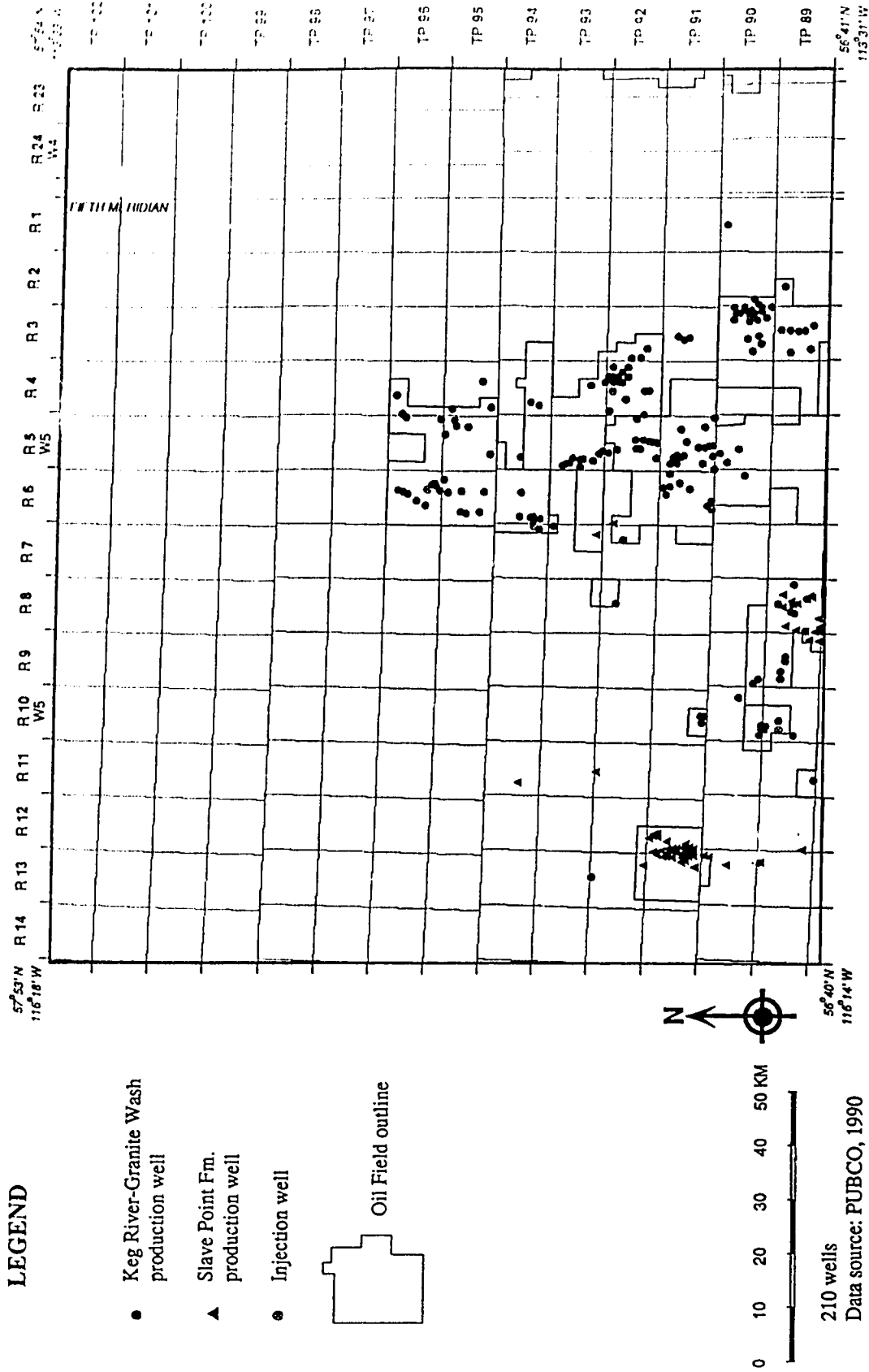


Figure 3.1.1.1 Production and Injection Wells Active Prior to Most Recent Drillstem Test

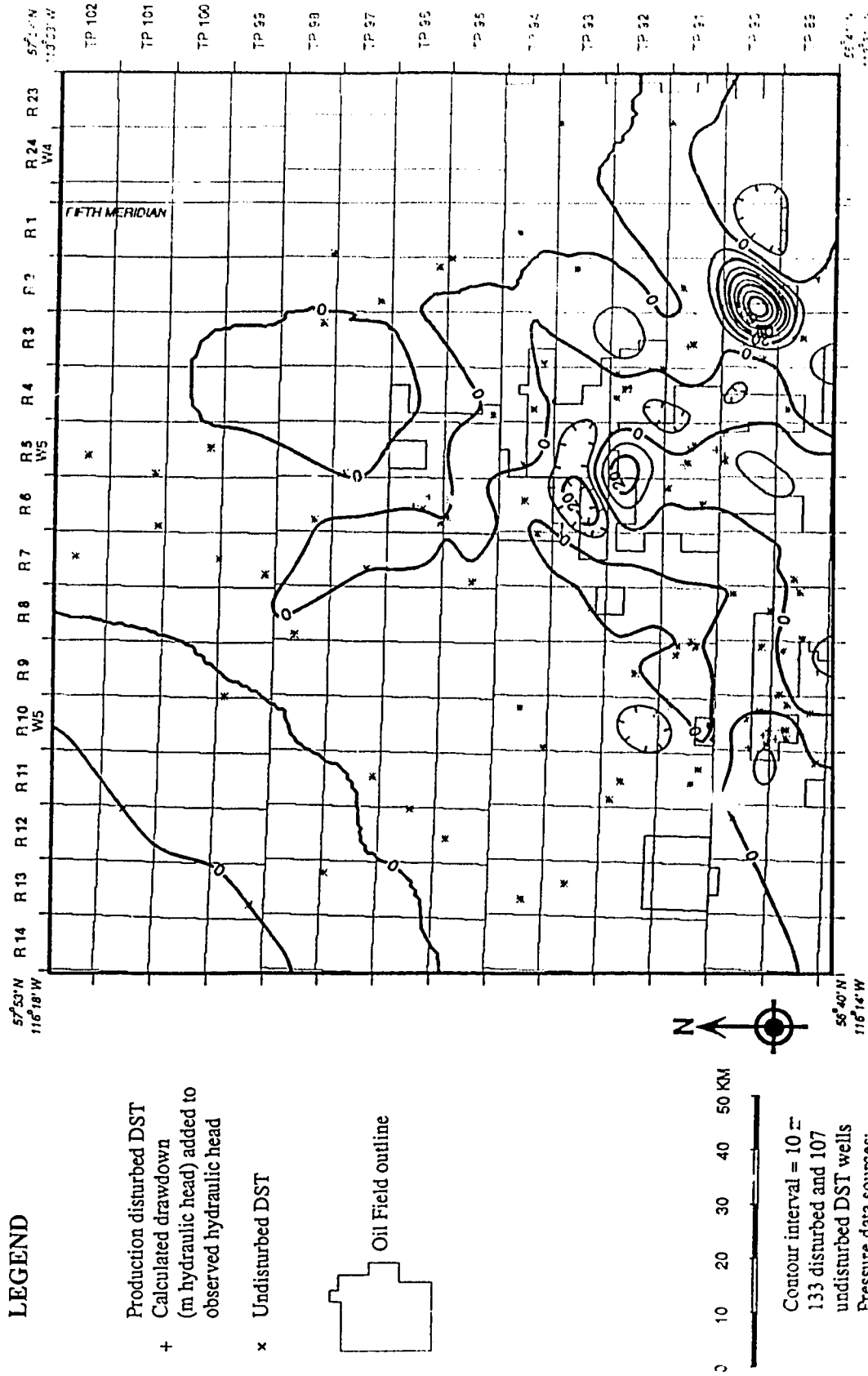
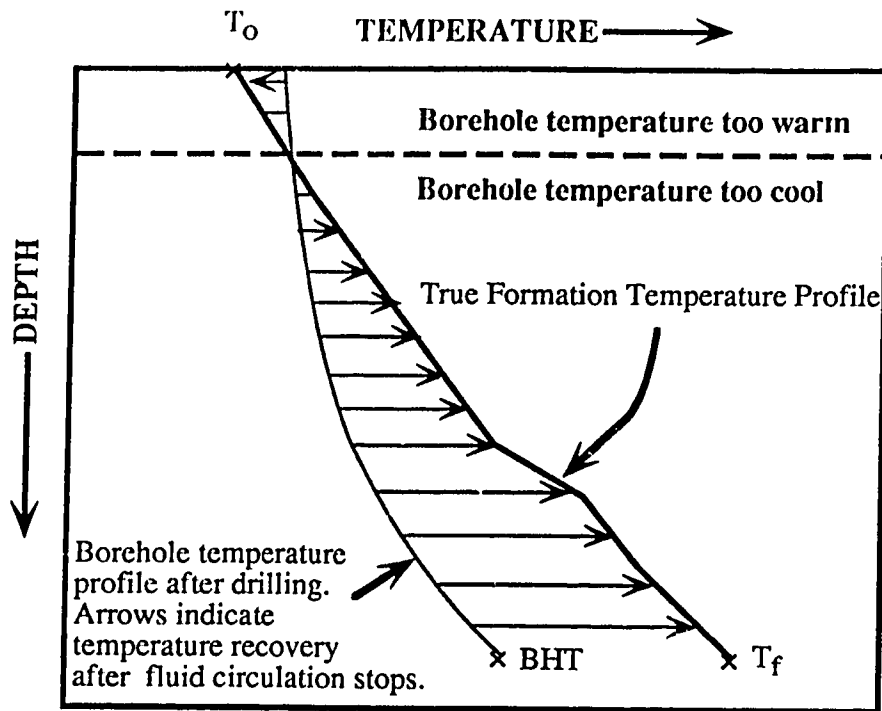


Figure 3.11.2 Calculated Production Drawdown in the Keg River Aquifer



LEGEND	
$T_0$ :	Ground Surface Temperature
$T_f$ :	True Bottom Hole Temperature
BHT:	Measured Bottom Hole Temperature

Modified after Gretener (1981)

Figure 3.12 Thermal Disequilibrium in a Borehole After Drilling



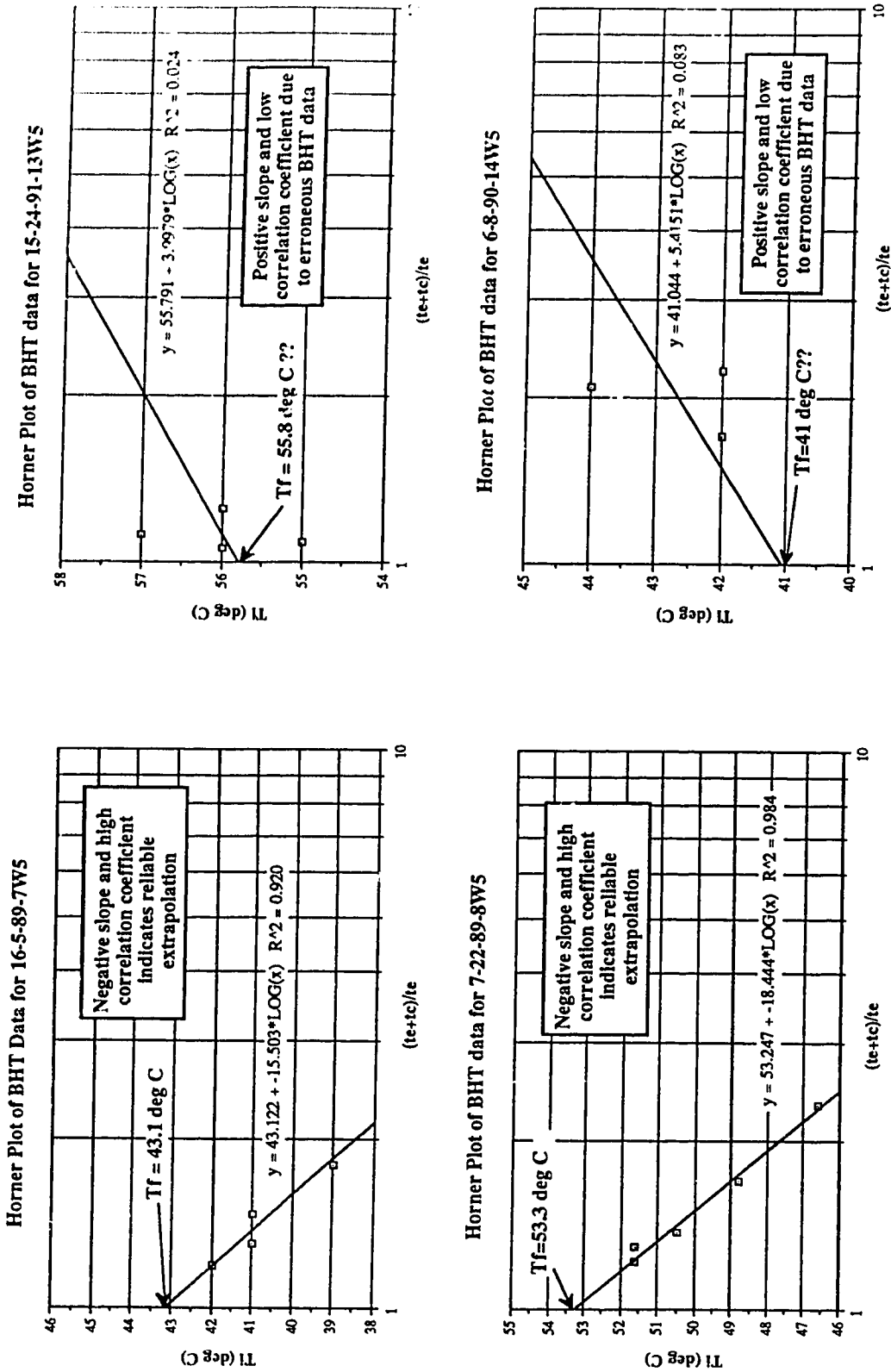


Figure 3.14 Examples of Horner Plots of BHT Data - Used to Estimate Undisturbed Formation Temperature

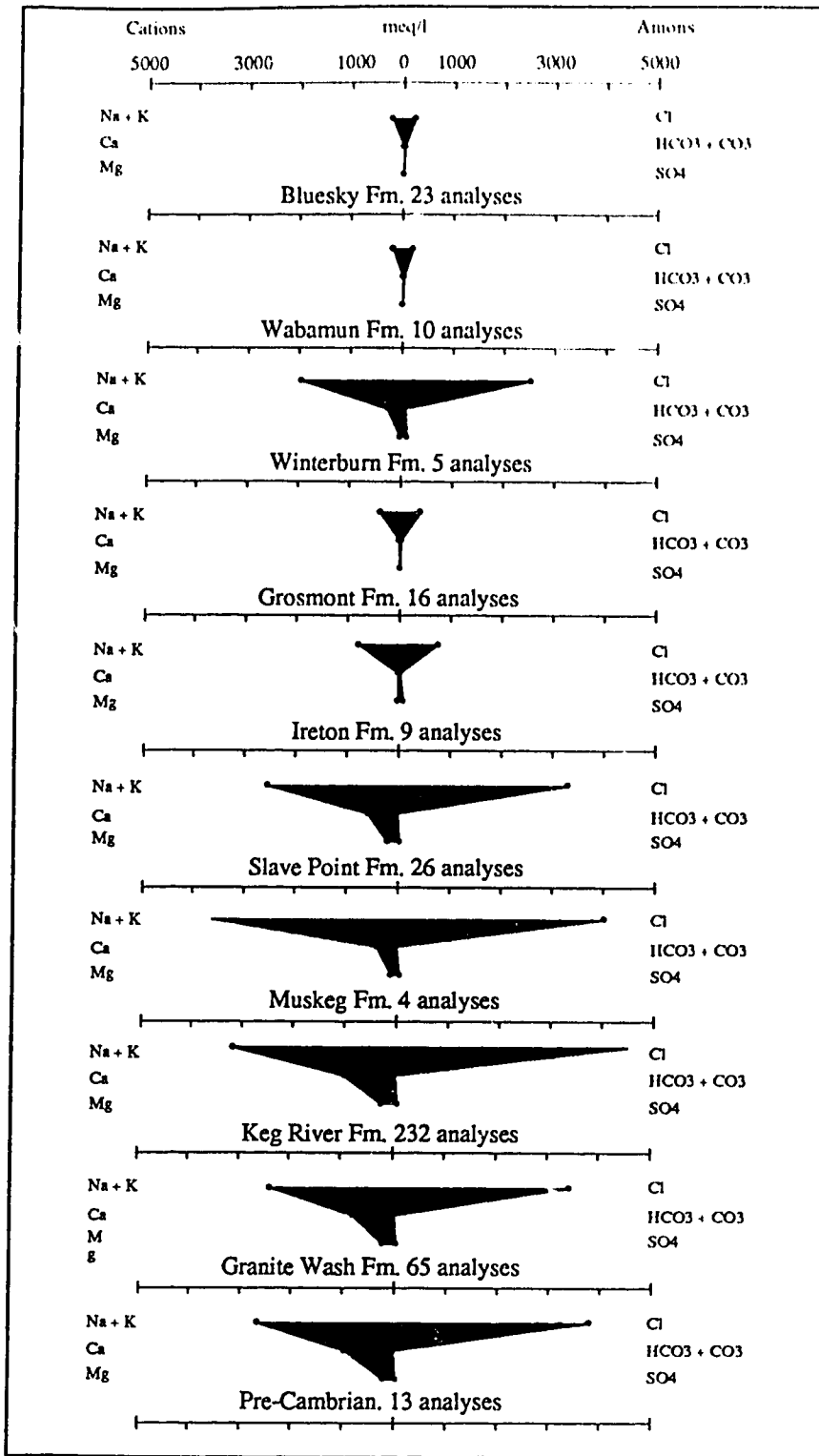
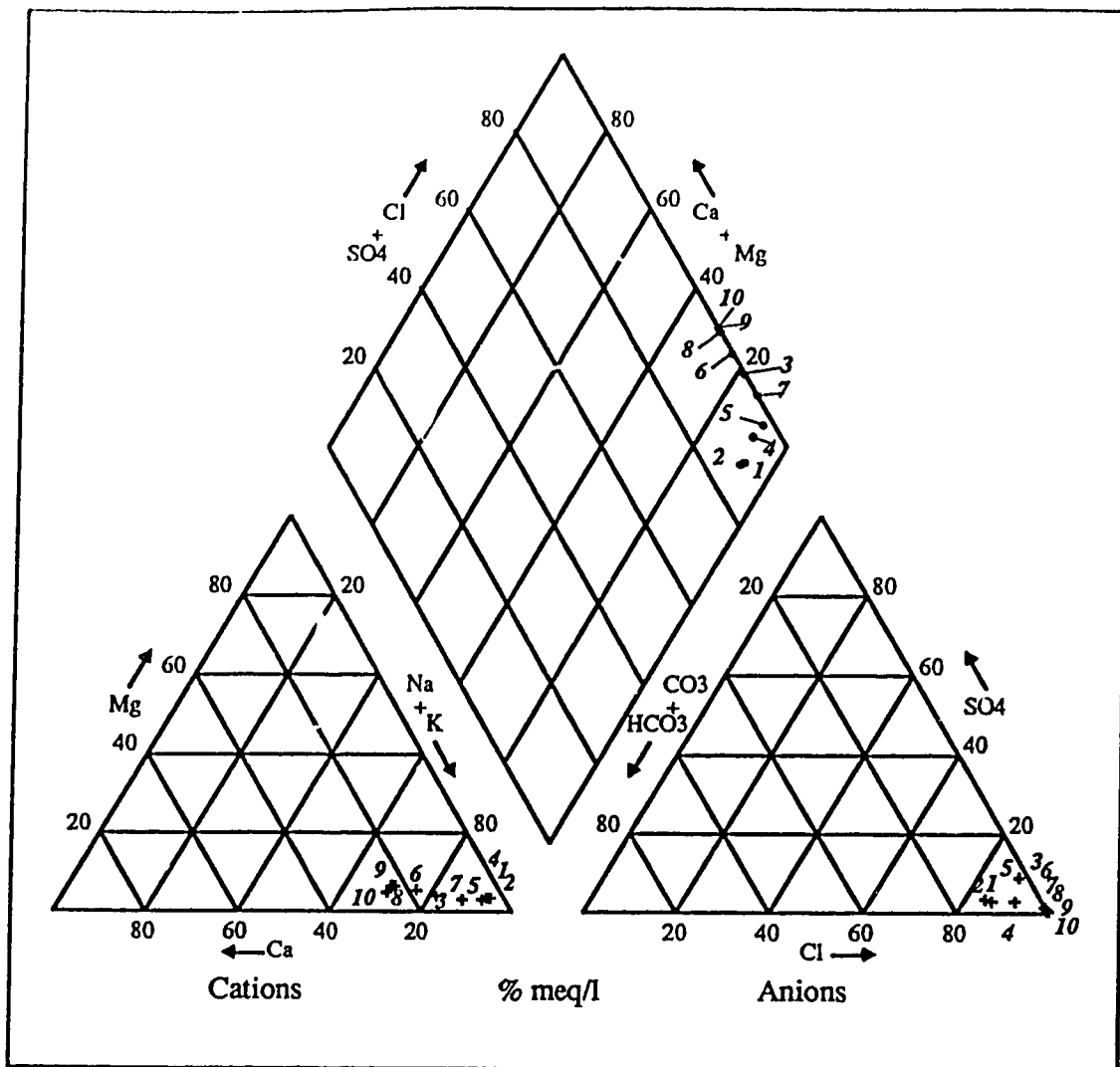


Figure 3.15 Stiff Diagrams Showing Average Formation Water Compositions



No.	TDS (mg/l)	Formation Name	No. of Analyses
1	15664	Bluesky	23
2	13390	Wabamun	10
3	144357	Winterburn	5
4	25013	Grosmont	16
5	50537	Ireton	9
6	191703	Slave Point	26
7	238549	Muskeg	4
8	257142	Keg River	232
9	195865	Granite Wash	65
10	217964	Pre-Cambrian	13

Figure 3.16 Piper Diagram Showing Average Composition of Formation Waters in the Study Area



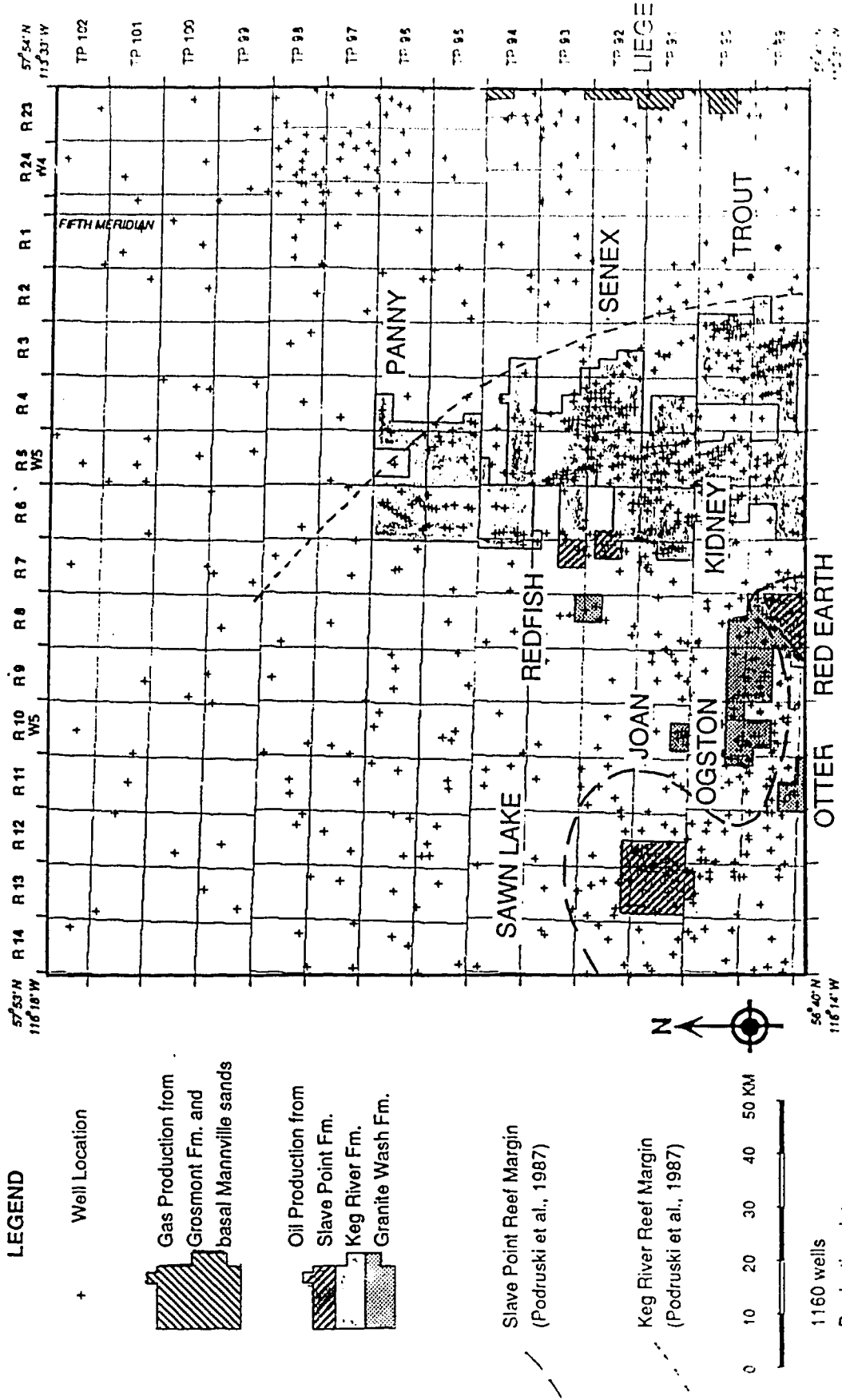
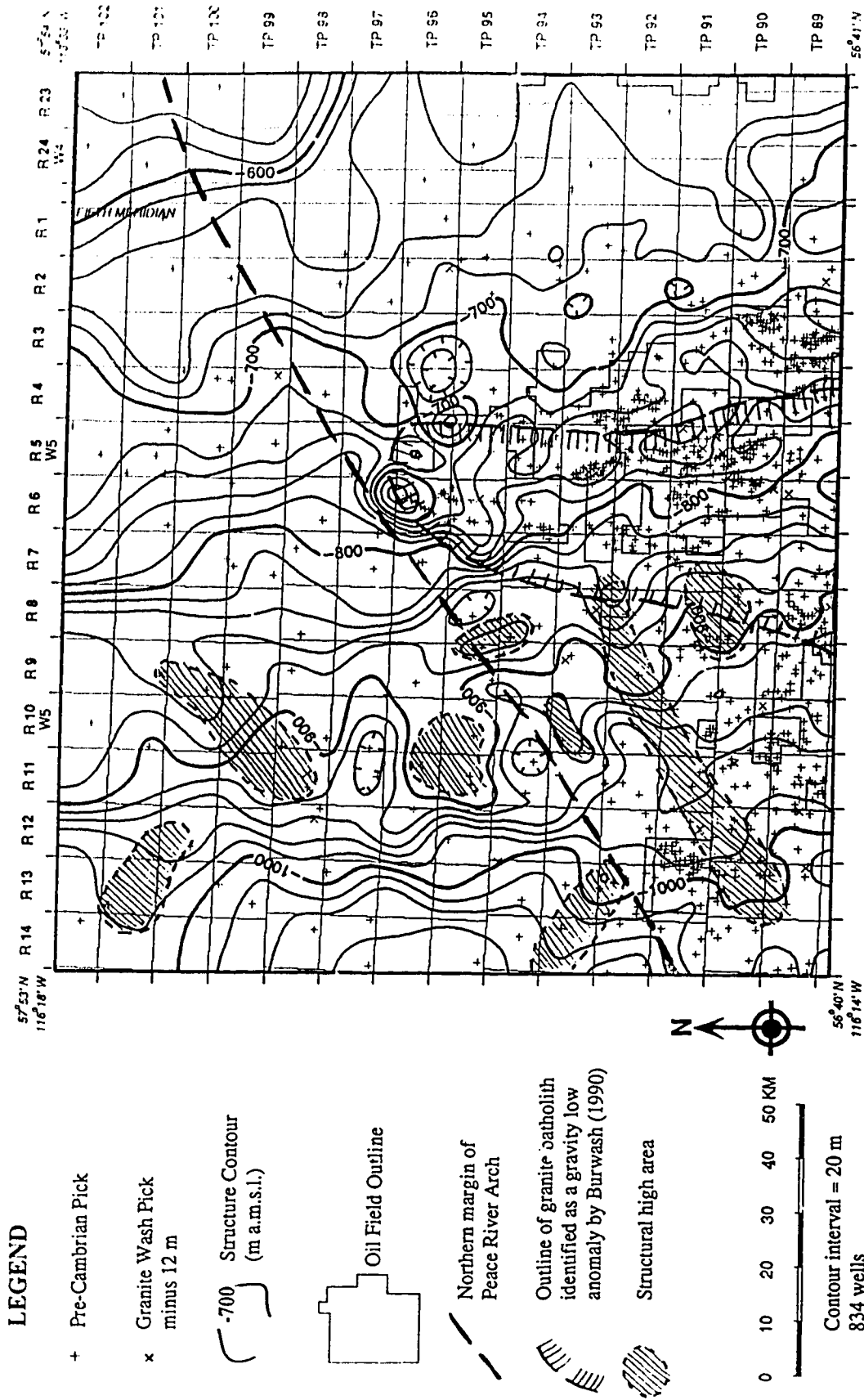
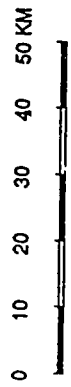


Figure 4.1 Well Locations, Oil Fields and Reef Margins



**LEGEND**

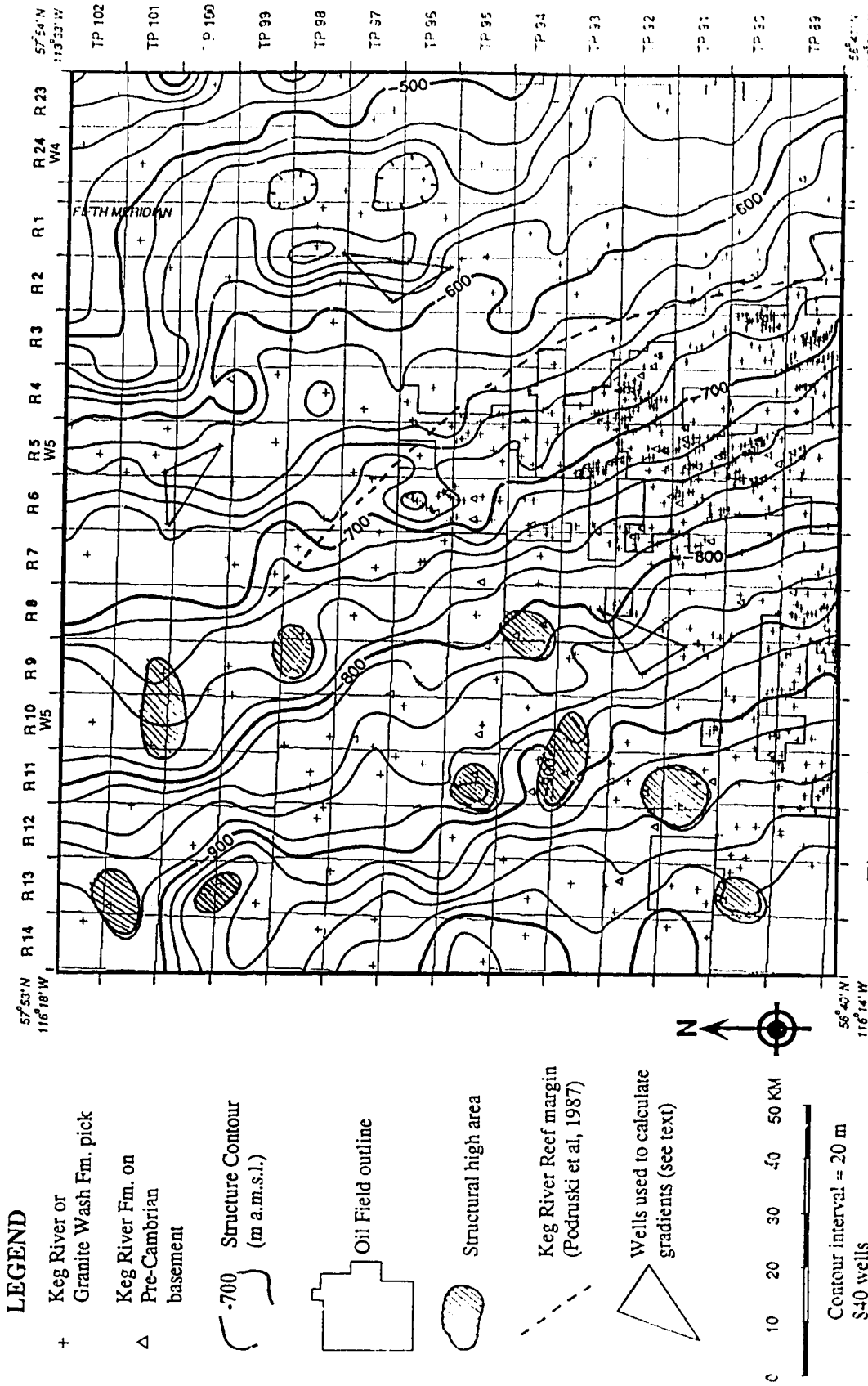
- + Pre-Cambrian Pick
- x Granite Wash Pick minus 12 m
- 700 Structure Contour (m a.m.s.l.)
- Oil Field Outline
- Northern margin of Peace River Arch
- Outline of granite batholith identified as a gravity low anomaly by Burwash (1990)
- Structural high area



Contour interval = 20 m  
834 wells

Data source: PUBCO (1990)

Figure 4.2 Structure Contours on Top of Pre-Cambrian Basement



**LEGEND**

- + Keg River or Granite Wash Fm. pick
- Δ Keg River Fm. on Pre-Cambrian basement
- .700 Structure Contour (m a.m.s.l.)
- [ ] Oil Field outline
- ▨ Structural high area
- - - Keg River Reef margin (Podruski et al, 1987)
- △ Wells used to calculate gradients (see text)

0 10 20 30 40 50 KM  
 Contour interval = 20 m  
 S40 wells

Data source:  
 PUBCO (1990)

Figure 4.3 Structure Contours on Top of Keg River Aquifer

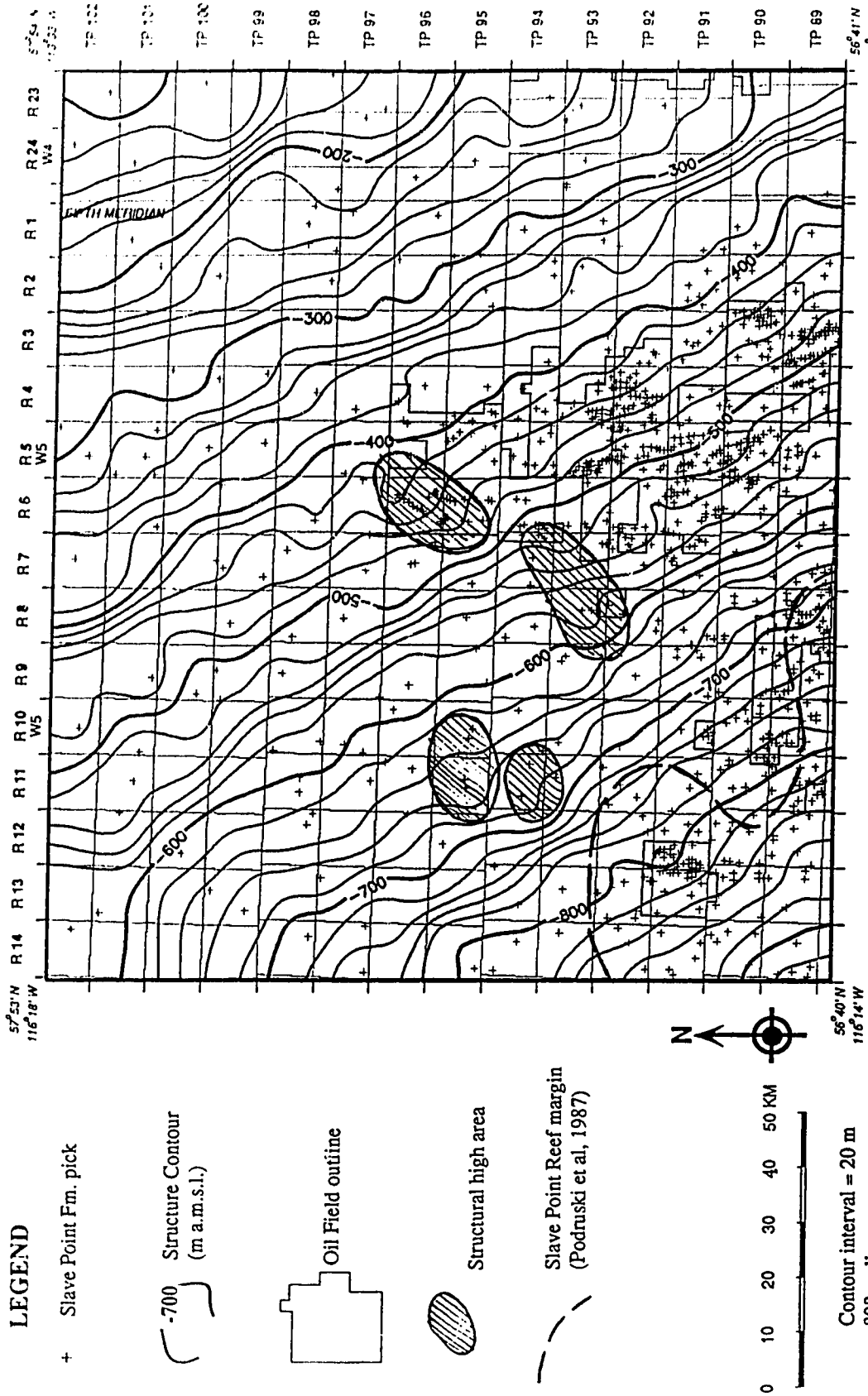


Figure 4.4 Structure Contours on Top of Slave Point Aquifer

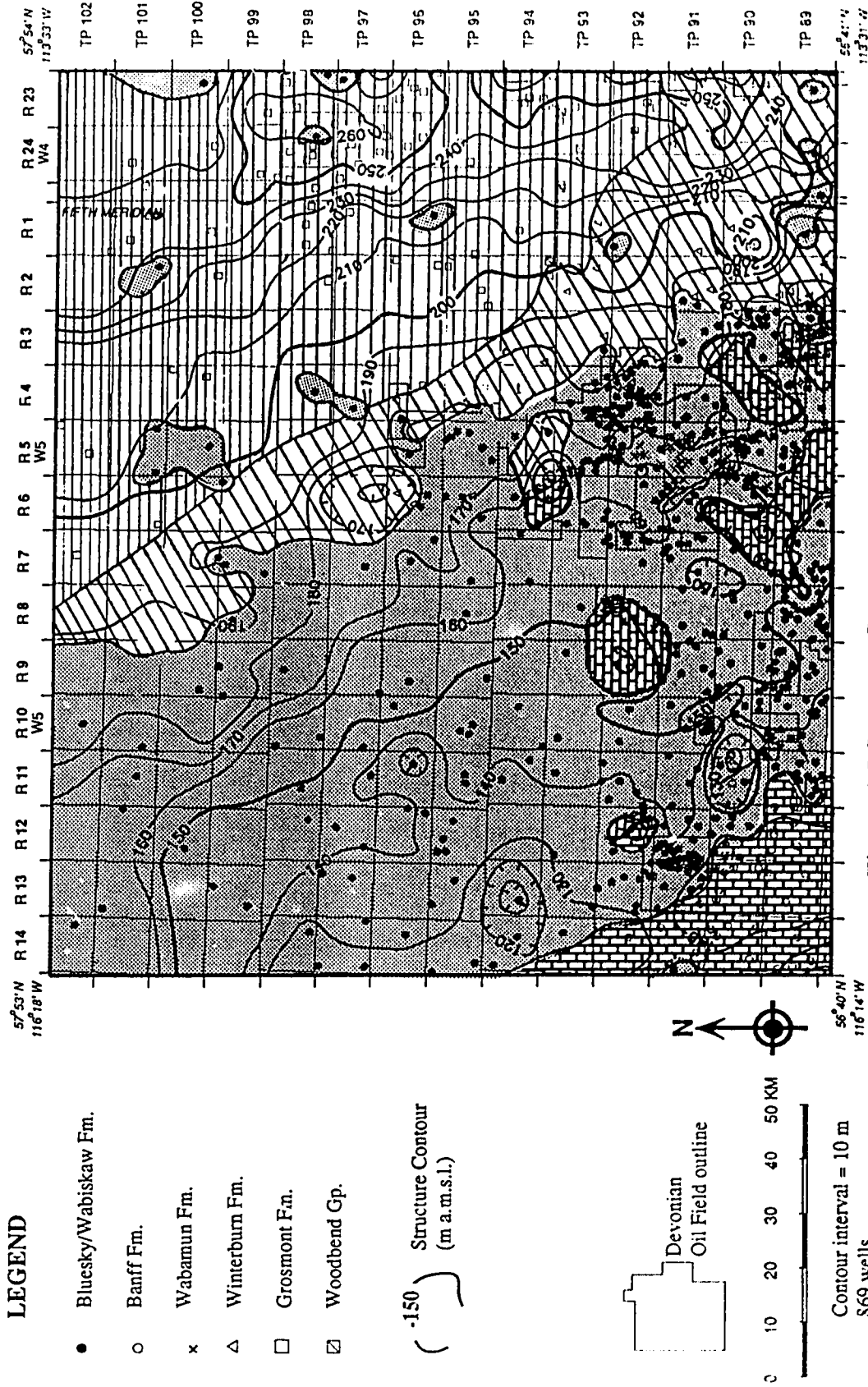
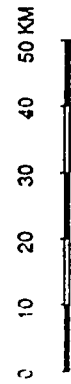


Figure 4.5 Structure Contours on Top of Upper Devonian-Basal Cretaceous Aquifer Showing Palaeozoic Fm. Subcrops

**LEGEND**

- Bluesky/Wabiskaw Fm.
- Banff Fm.
- × Wabamun Fm.
- △ Winterburn Fm.
- Grosmont Fm.
- ▣ Woodbend Gp.

( ) -150 Structure Contour  
(m a.s.l.)



Contour interval = 10 m  
S69 wells  
Data source: PUBCO (1990)



56°40'N  
116°14'W

57°53'N  
116°18'W

57°54'N  
113°33'W

56°41'N  
113°31'W

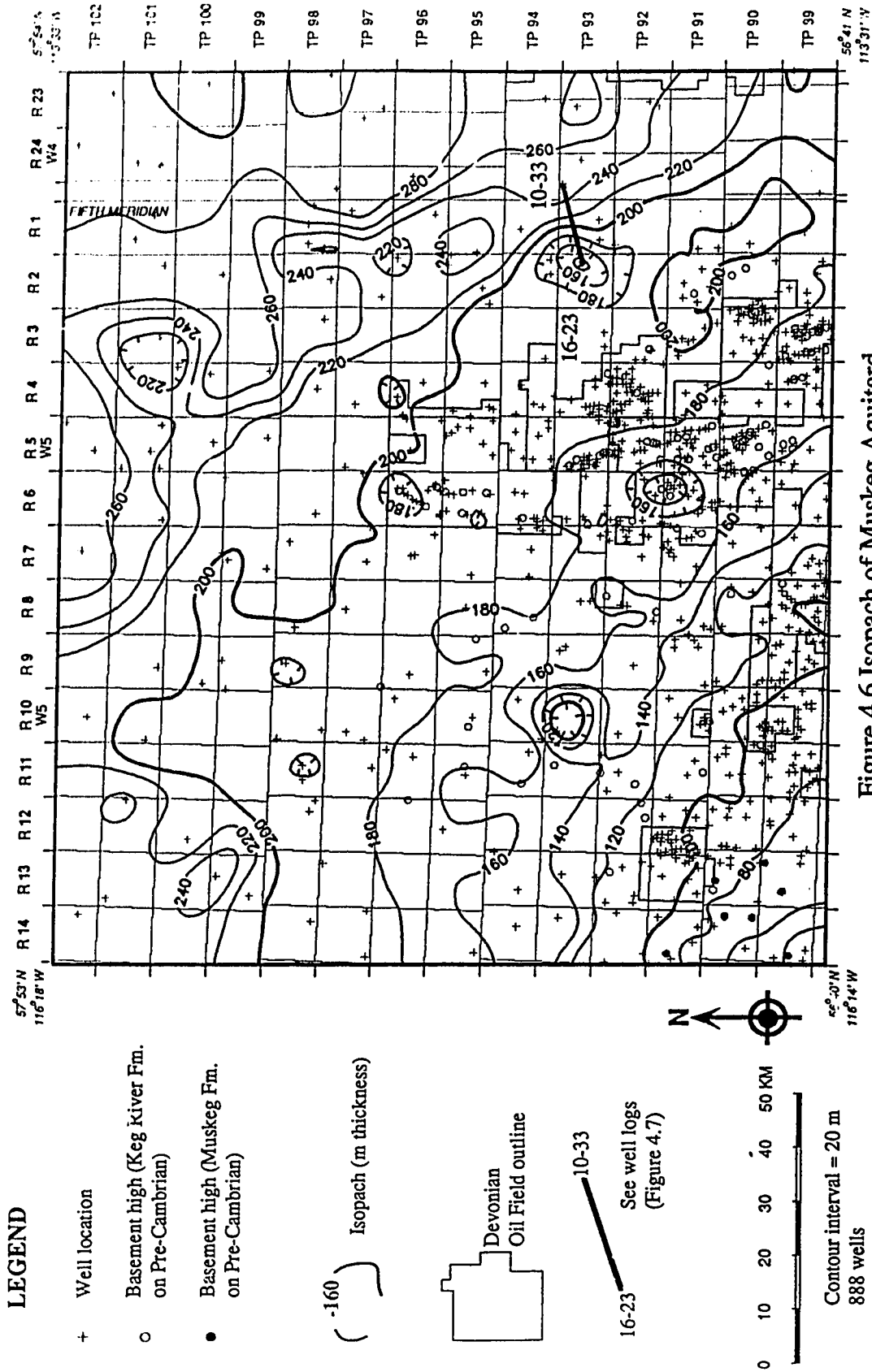


Figure 4.6 Isopach of Muskeg Aquitard

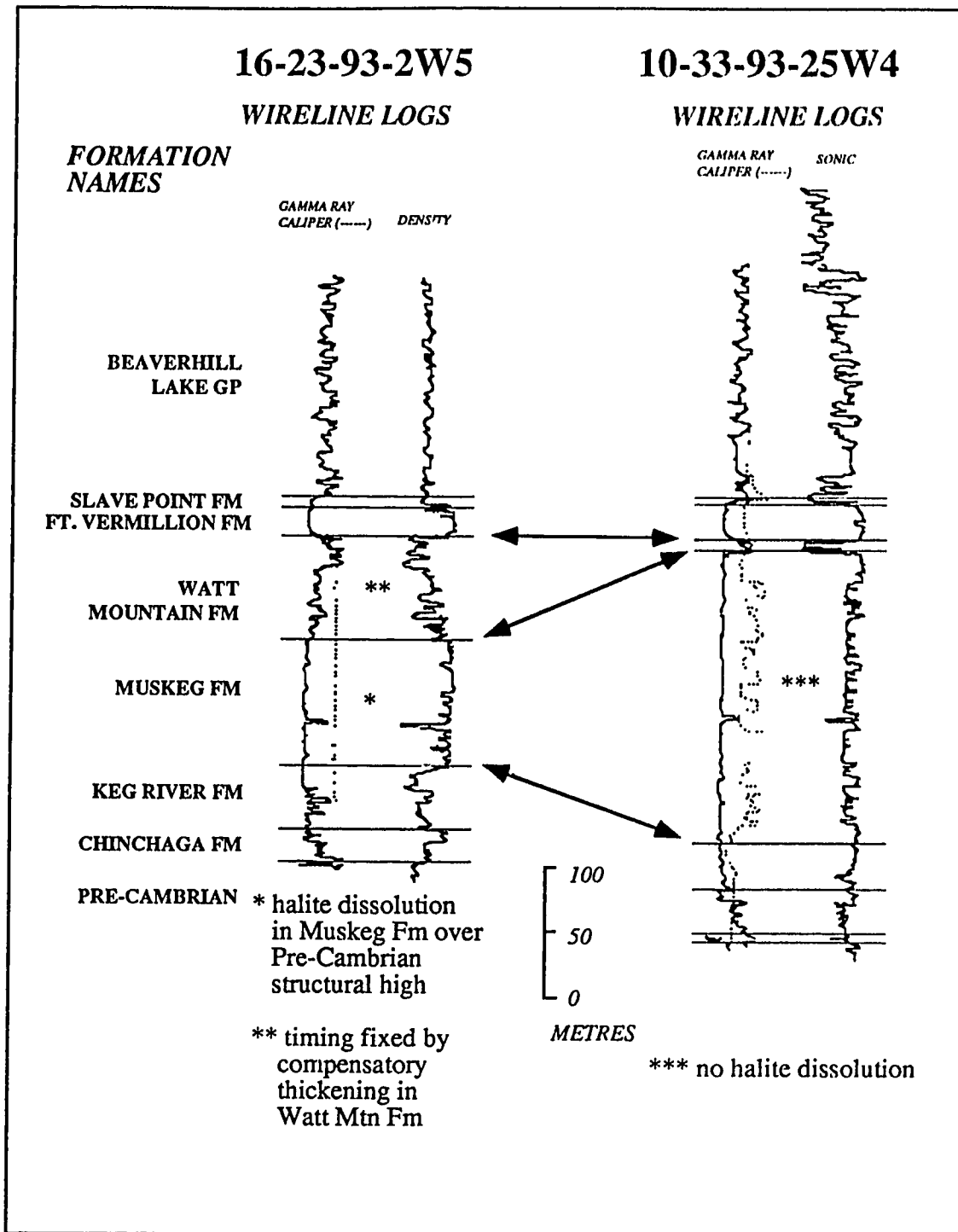


Figure 4.7 Muskeg Fm. Salt Distribution in Adjacent Wells - Probable Halite Dissolution

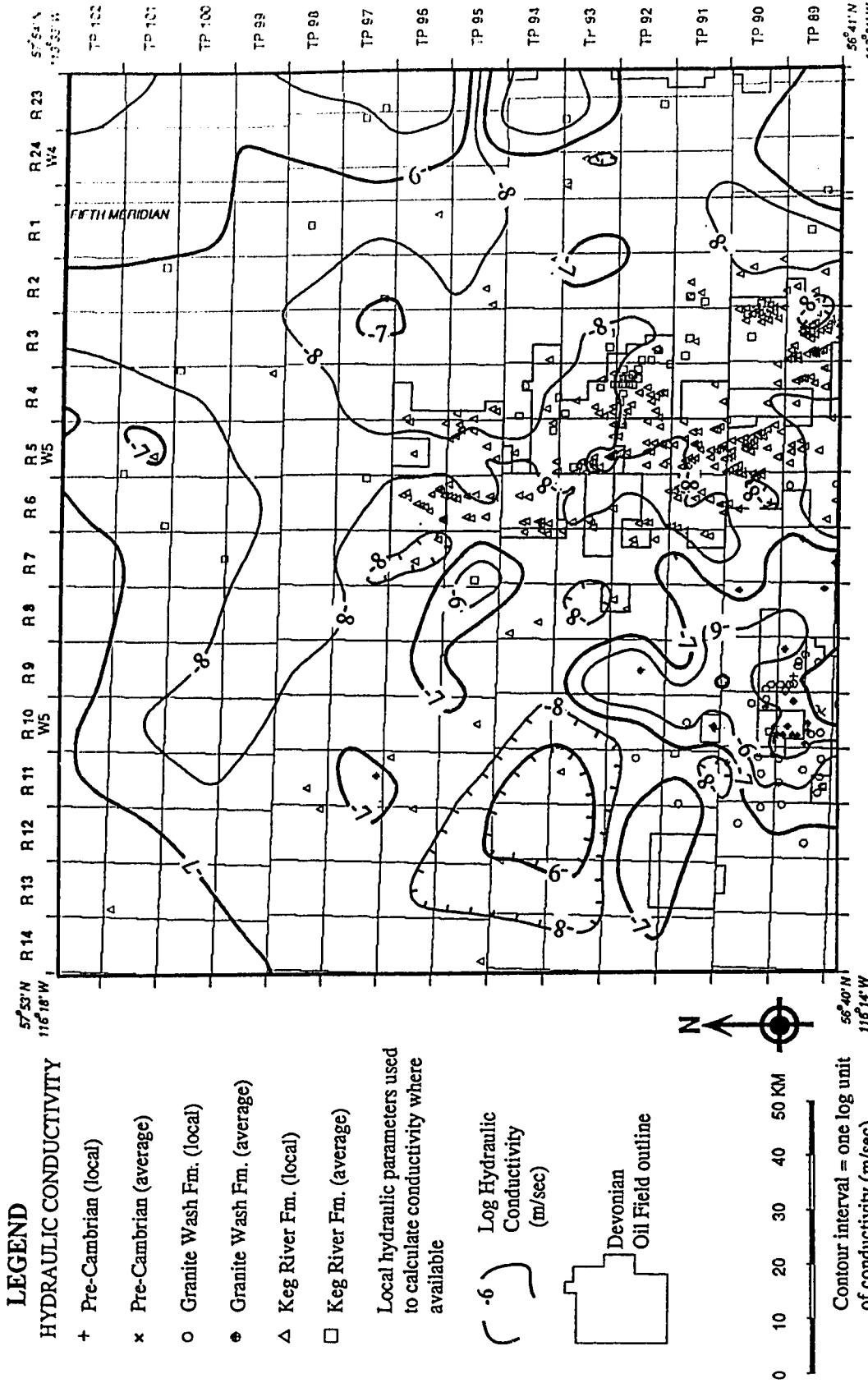


Figure 4.8 Hydraulic Conductivity Distribution in Keg River Aquifer



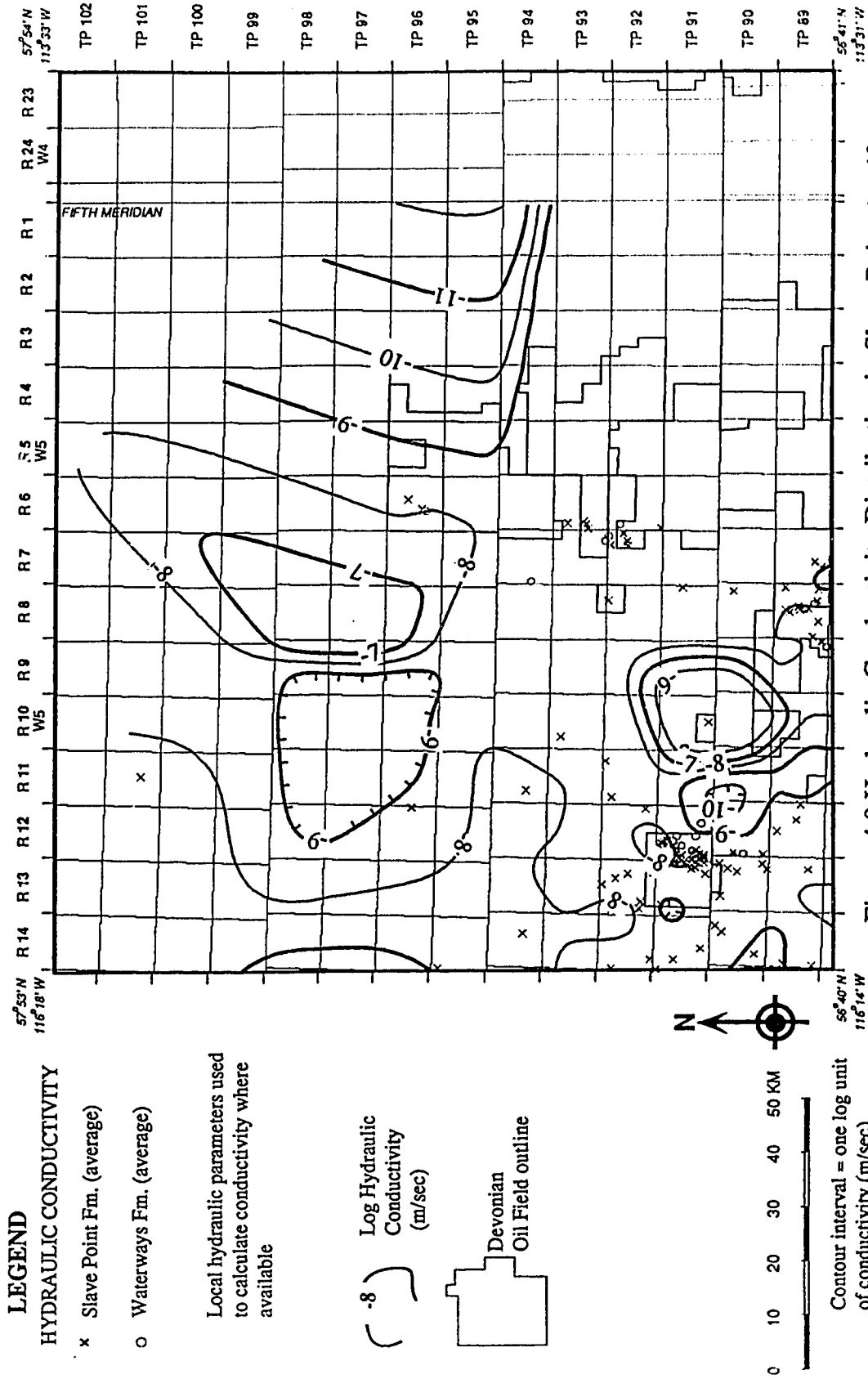


Figure 4.9 Hydraulic Conductivity Distribution in Slave Point Aquifer

**LEGEND**  
**HYDRAULIC CONDUCTIVITY**

- x Slave Point Fm. (average)
- o Waterways Fm. (average)
- Local hydraulic parameters used to calculate conductivity where available
- ( -8 ) Log Hydraulic Conductivity (m/sec)
- Devonian Oil Field outline

0 10 20 30 40 50 KM

Contour interval = one log unit of conductivity (m/sec)  
 126 wells  
 Data source: ERCB (1991c)



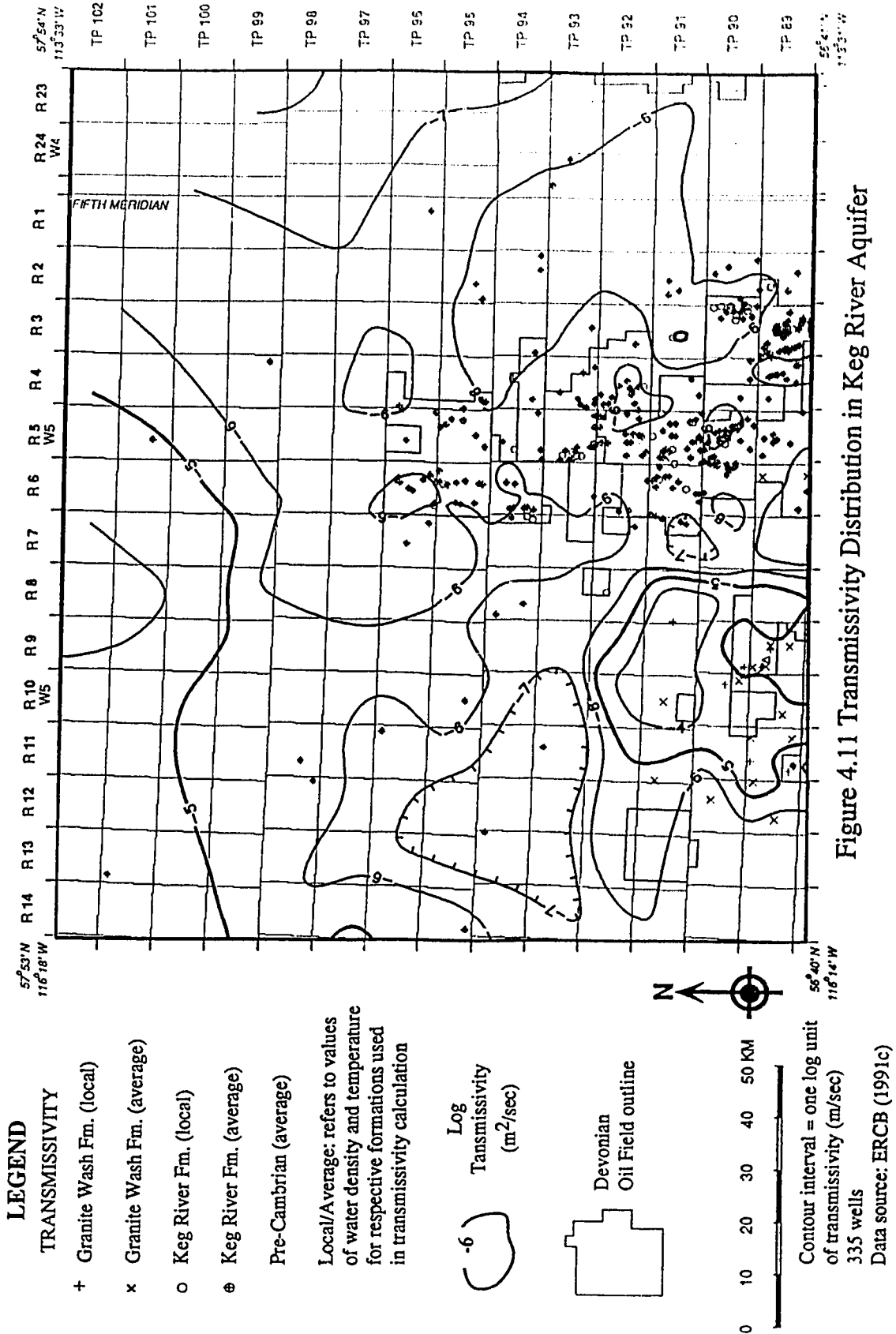
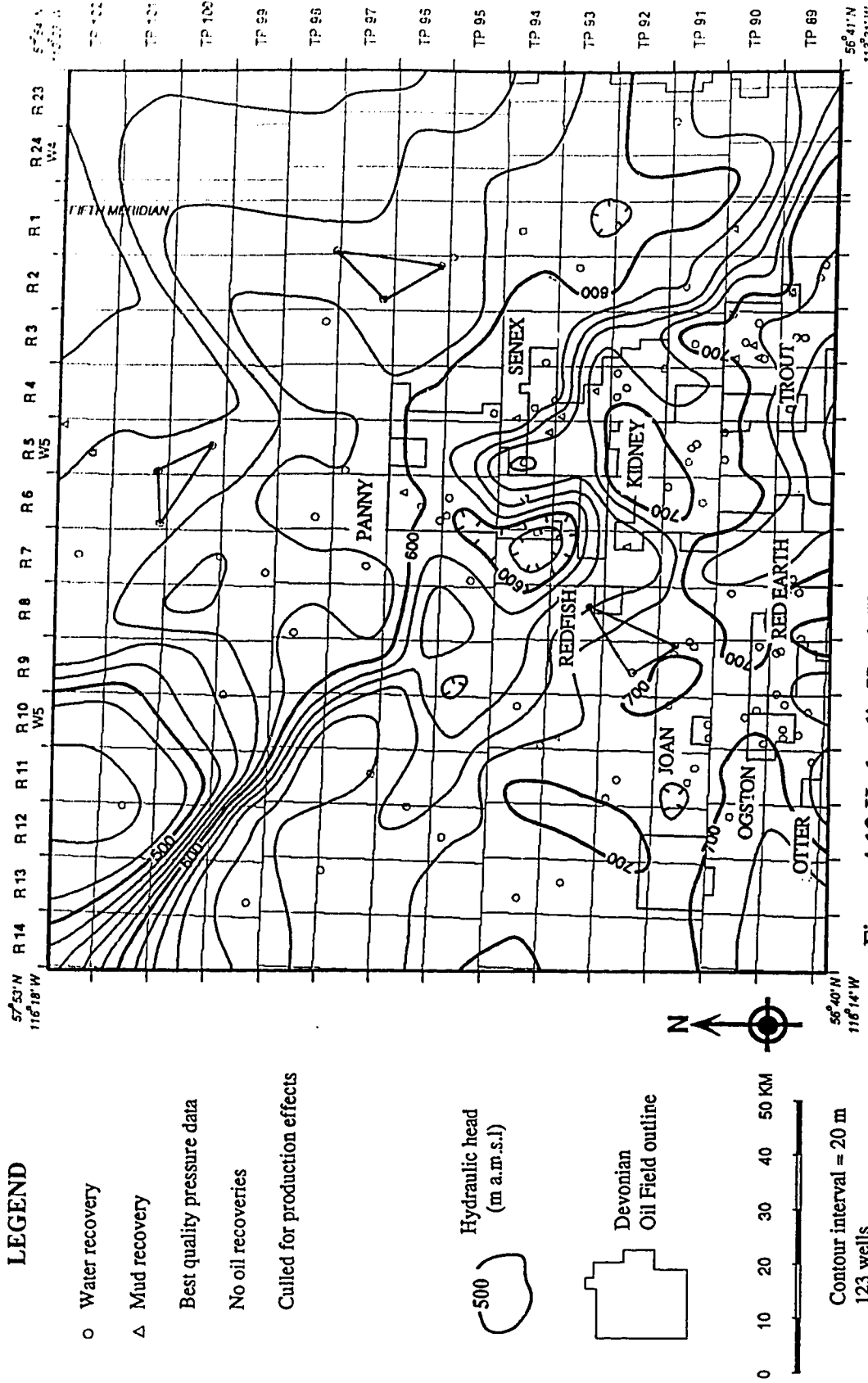


Figure 4.1.1 Transmissivity Distribution in Keg River Aquifer



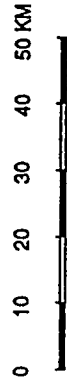
**LEGEND**

- Water recovery
- △ Mud recovery
- Best quality pressure data
- No oil recoveries
- Culled for production effects

Hydraulic head  
(m a.m.s.l)



Devonian  
Oil Field outline



Contour interval = 20 m  
123 wells

Data source: CIFE, ERCB (1991d)

Figure 4.12 Hydraulic Head (Freshwater Equivalent) in Keg River Aquifer

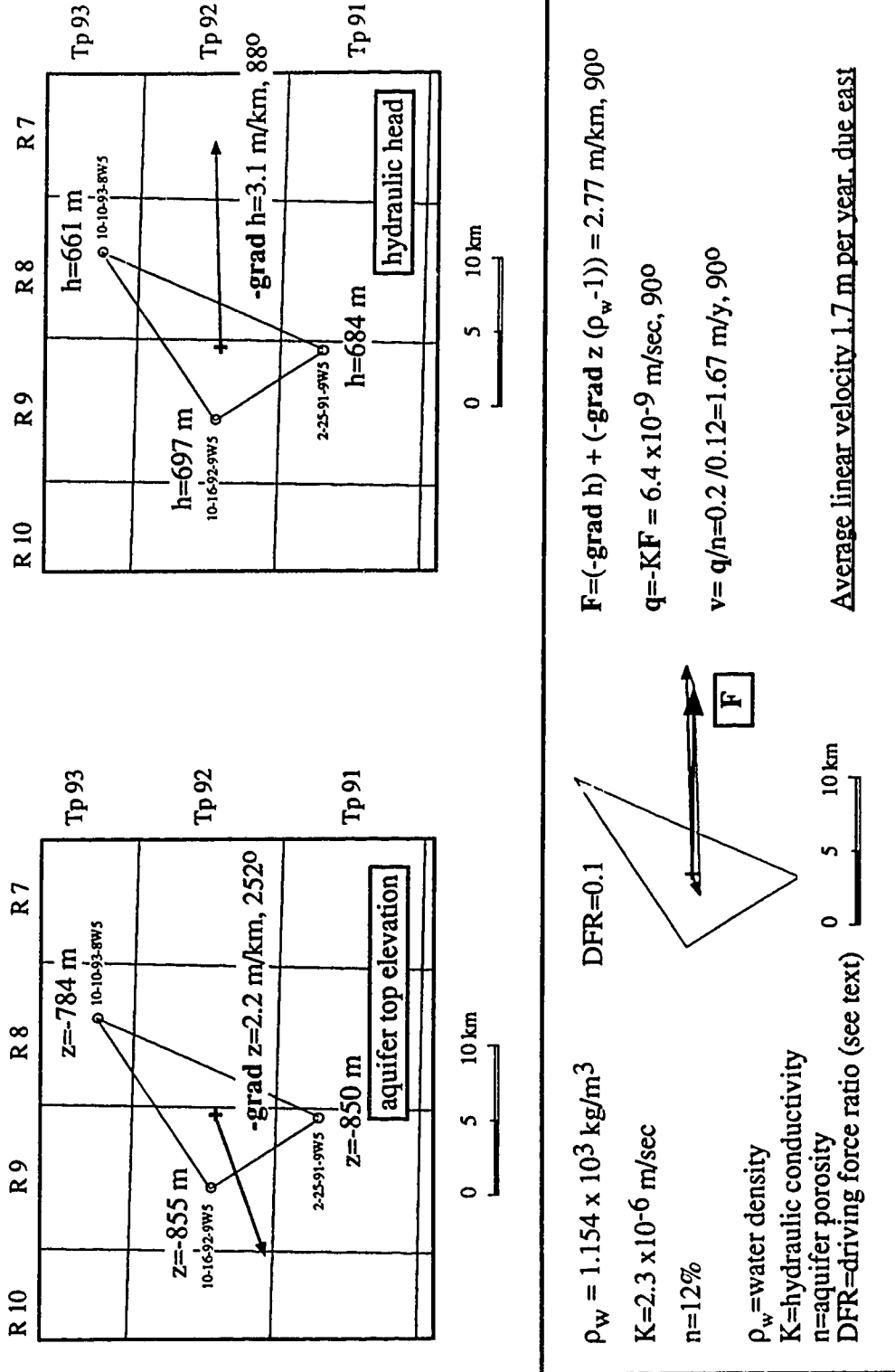
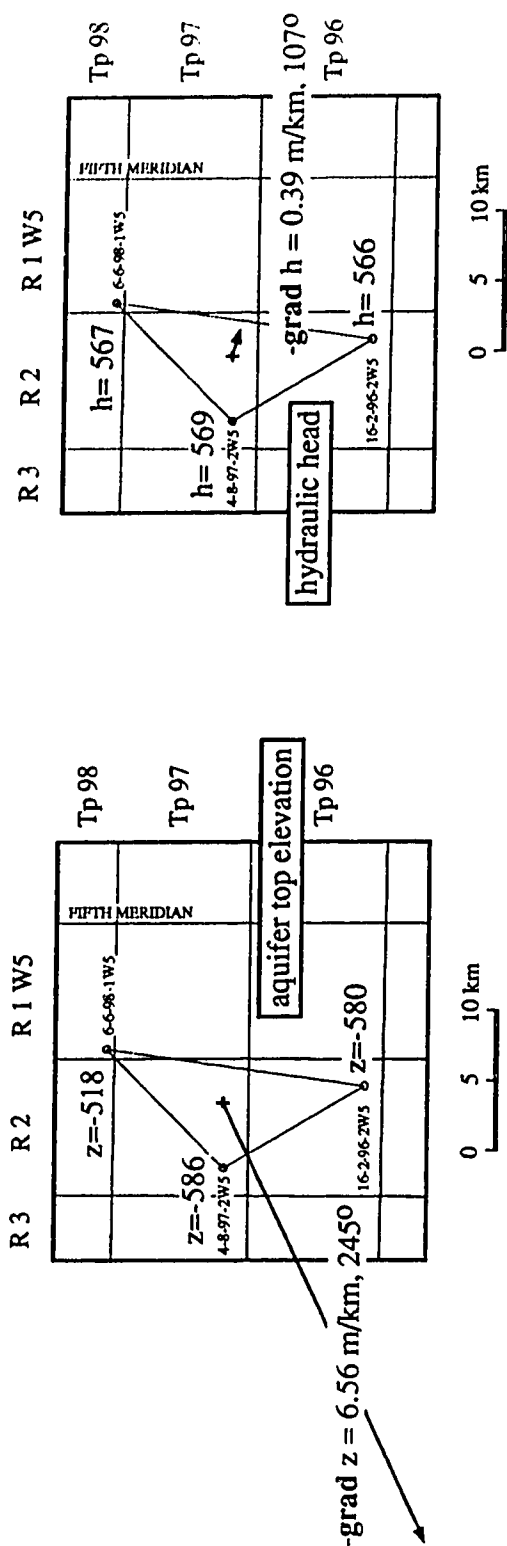


Figure 4.13.1 Buoyancy Modified Flow in Keg River Aquifer, Southwest Region



$\rho_w = 1.202 \times 10^3 \text{ kg/m}^3$

$K = 4.0 \times 10^{-8} \text{ m/sec}$

$n = 9\%$

$\rho_w$ : water density

$K$ : hydraulic conductivity

$n$ : aquifer porosity

DFR: driving force ratio (see text)

DFR=3.4

$F = (-\text{grad } h) + (-\text{grad } z (\rho_w - 1)) = 1.05 \text{ m/km}, 2300$

$q = KF = 4.0 \times 10^{-11} \text{ m/sec}, 2300$

$q = 1.3 \times 10^{-3} \text{ m/y}, 2300$

$v = q/n = 1.3 \times 10^{-3} / 0.09 = 14.4 \times 10^{-3} \text{ m/y}, 2300$

Average linear velocity 14 mm per year, southwest

Figure 4.13.2 Buoyancy Modified Flow in Keg River Aquifer, Northeast Region

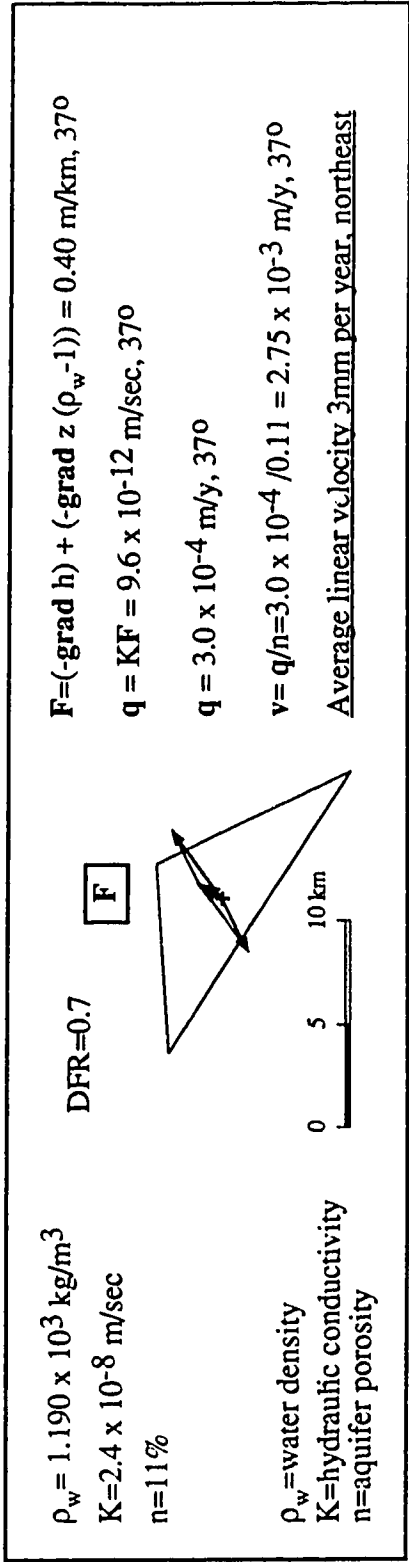
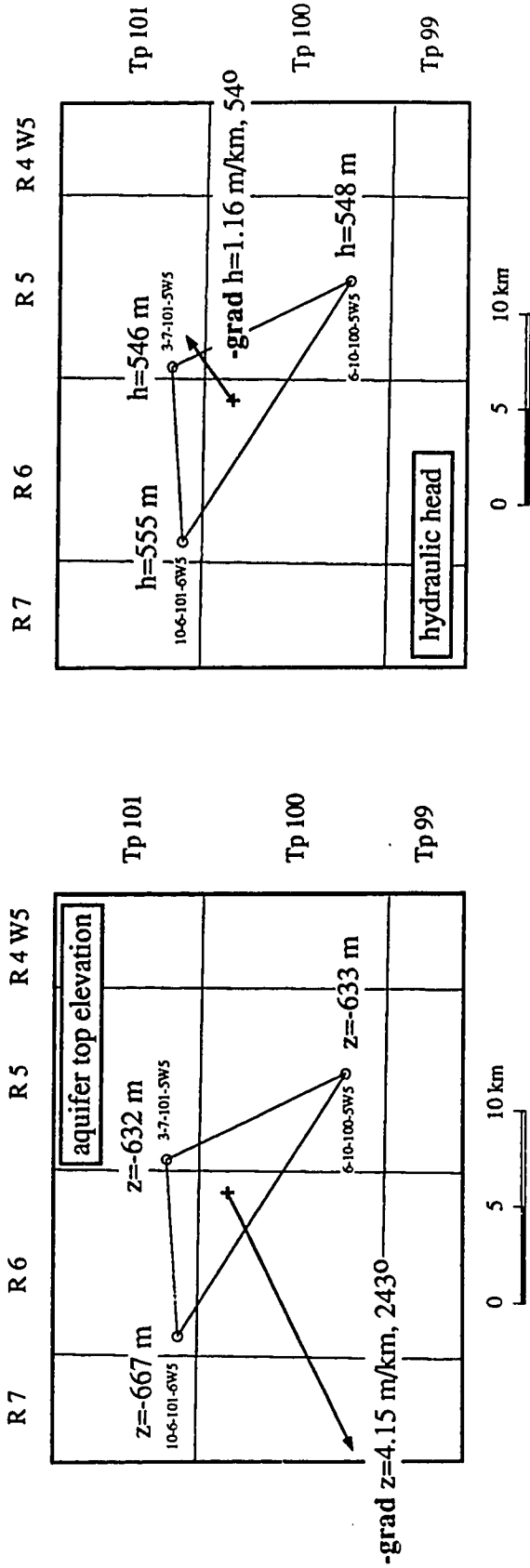


Figure 4.13.3 Buoyancy Modified Flow in Keg River Aquifer, North Region

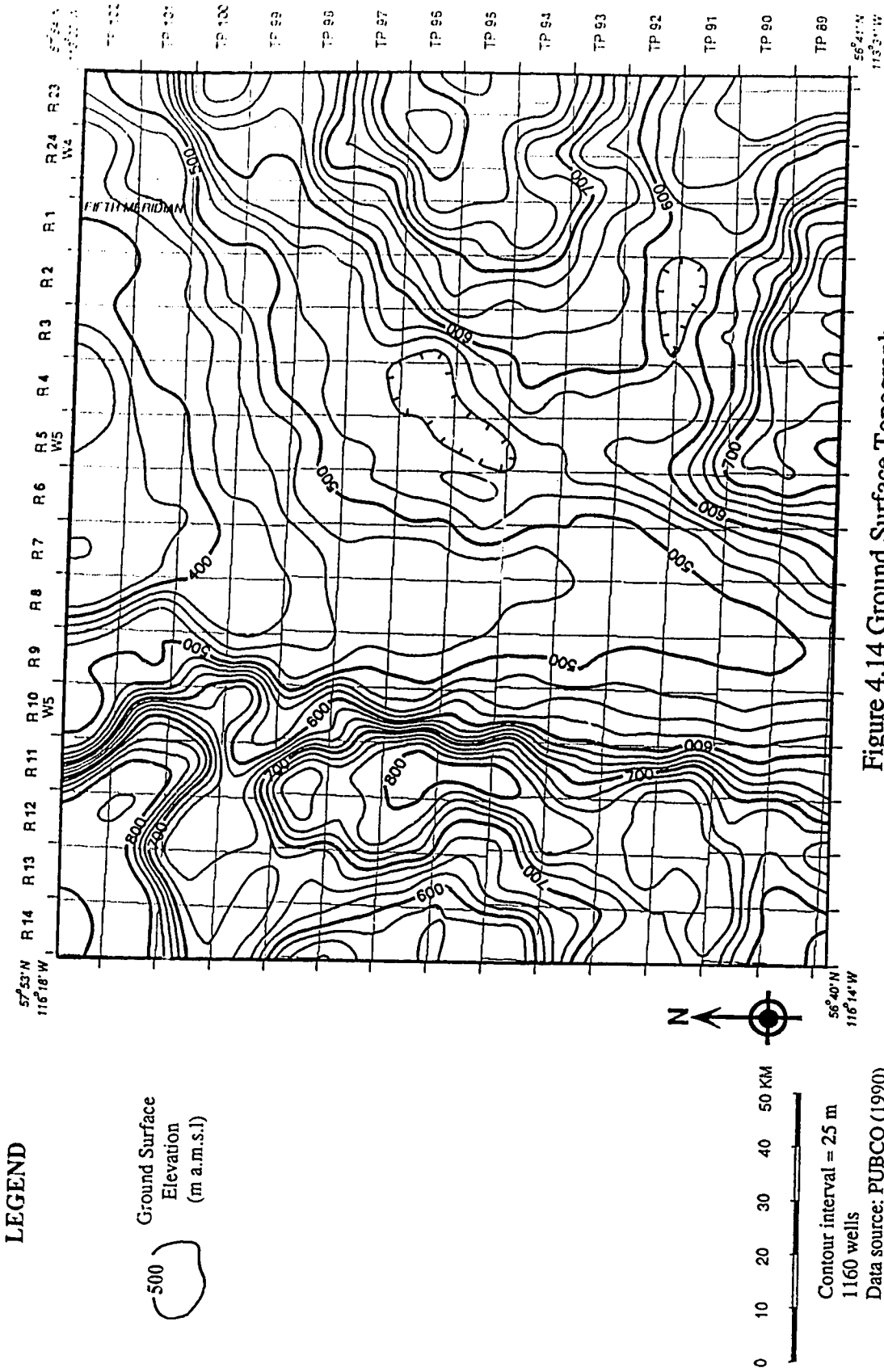


Figure 4.14 Ground Surface Topography



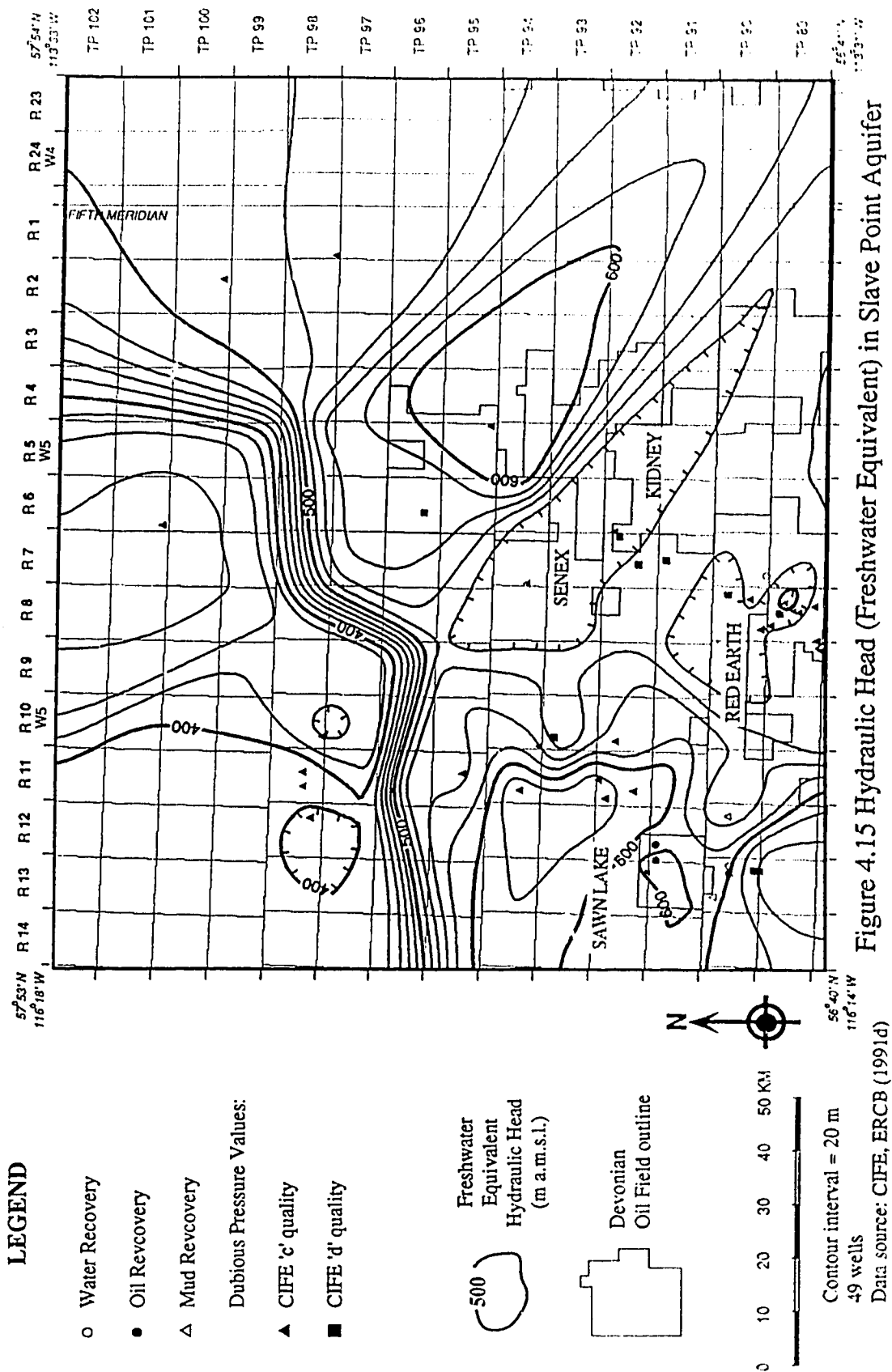
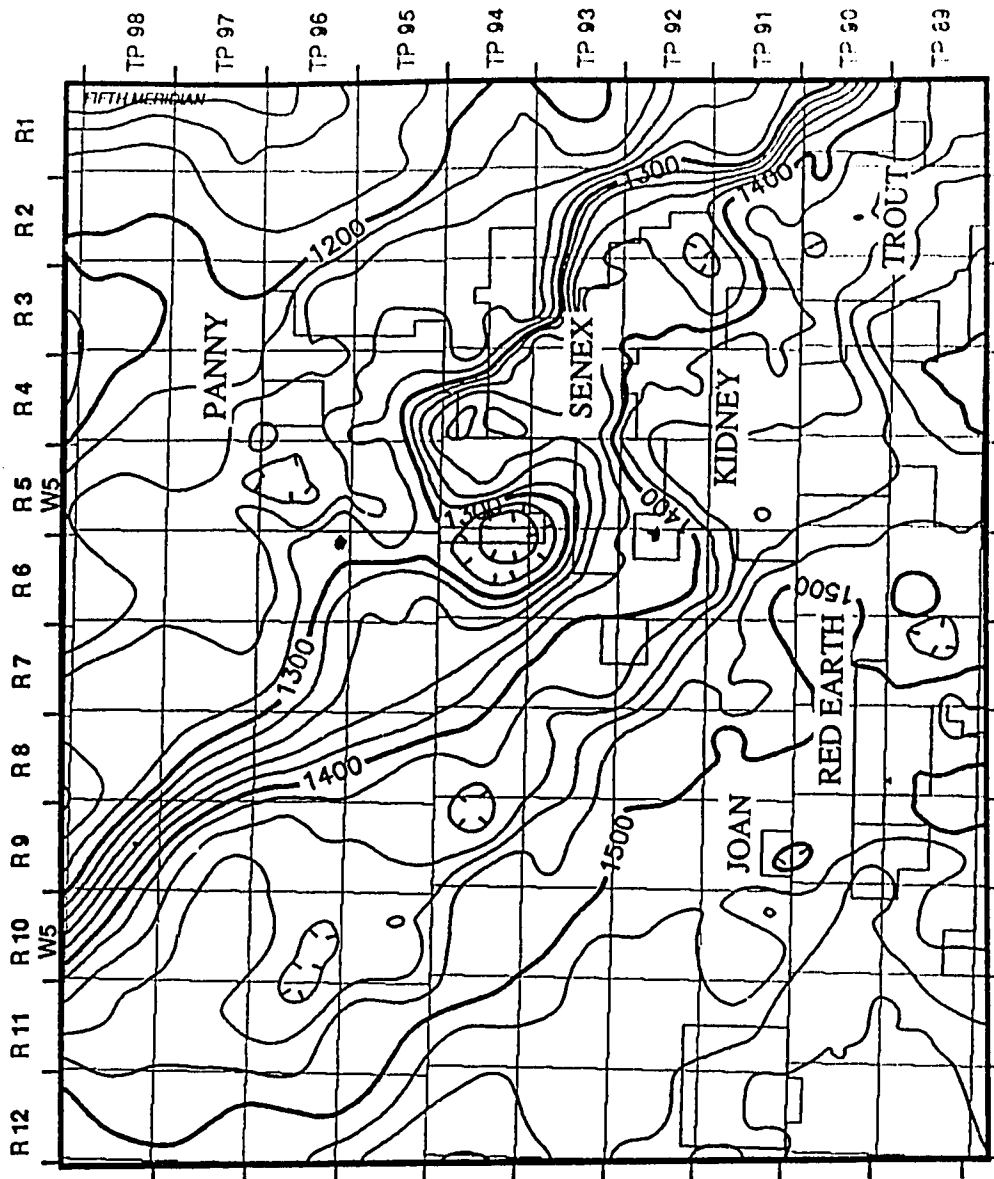




Figure 4.15 Hydraulic Head (Freshwater Equivalent) in Slave Point Aquifer





**LEGEND**

-  Oil Head Contour  
(m a.m.s.l.)
-  Devonian  
Oil Field outline



Contour interval = 20 m  
 126 wells  
 Pressure Data sources:  
 CIFE (1989), ERCB (1991 d)  
 Production Data Source:  
 PUBCO (1990 b)

Figure 4.17 Oil Head in Keg River Aquifer

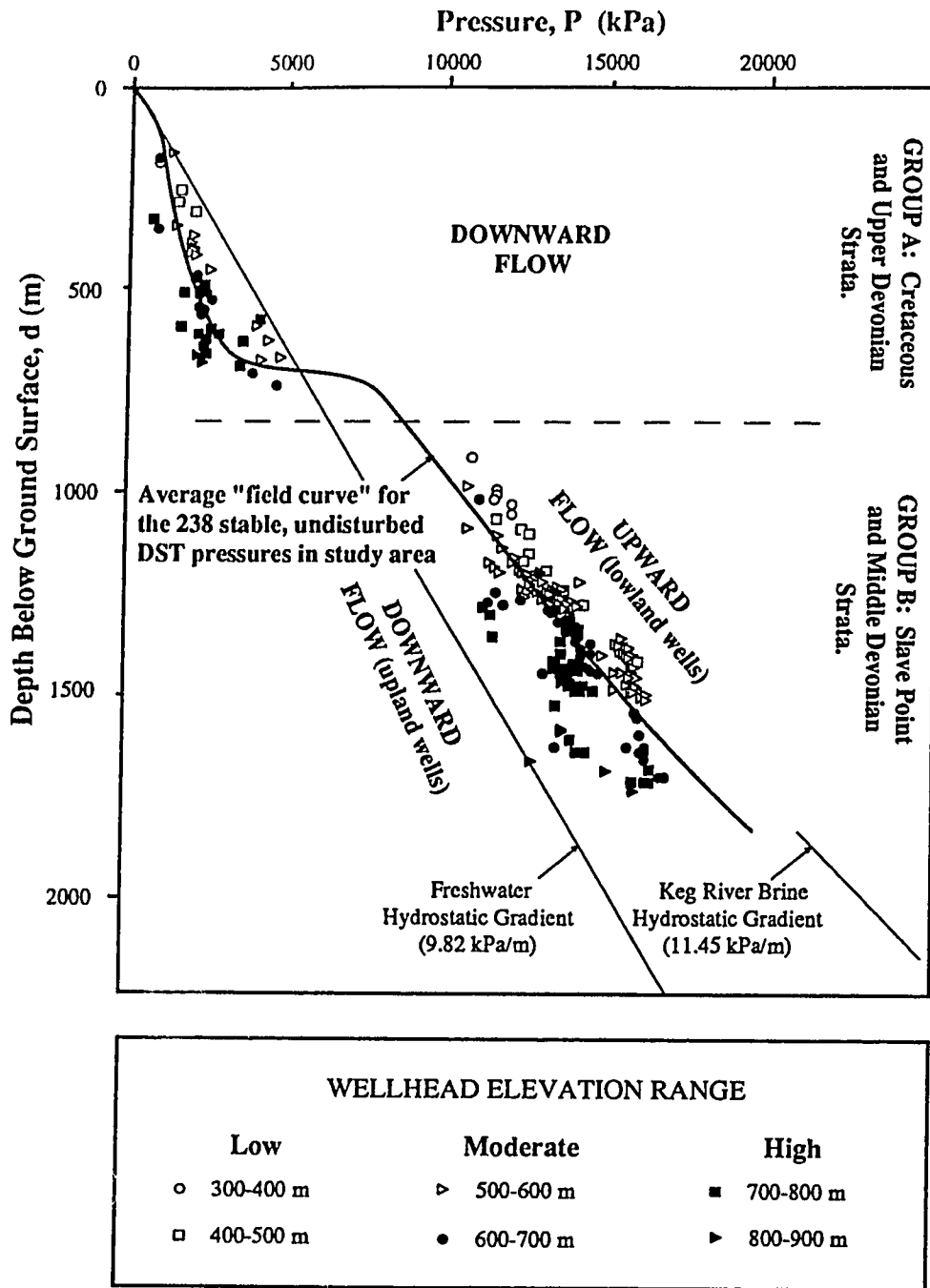


Figure 4.18 Pressure-Depth Plot for all Stable, Undisturbed Pressures, Grouped by Wellhead Elevation Range

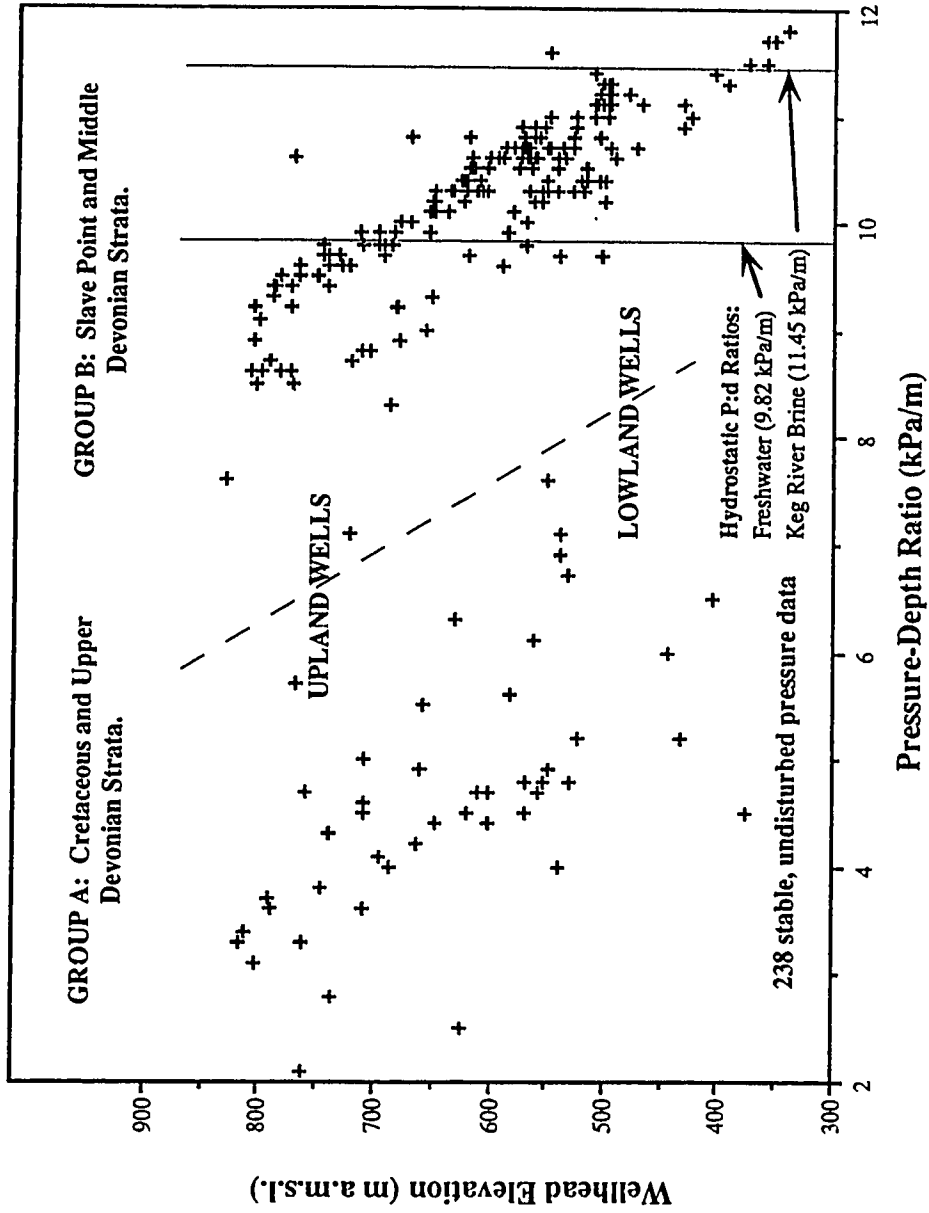


Figure 4.19 Pressure-Depth Ratio Versus Wellhead Elevation for all Stable, Undisturbed Pressures

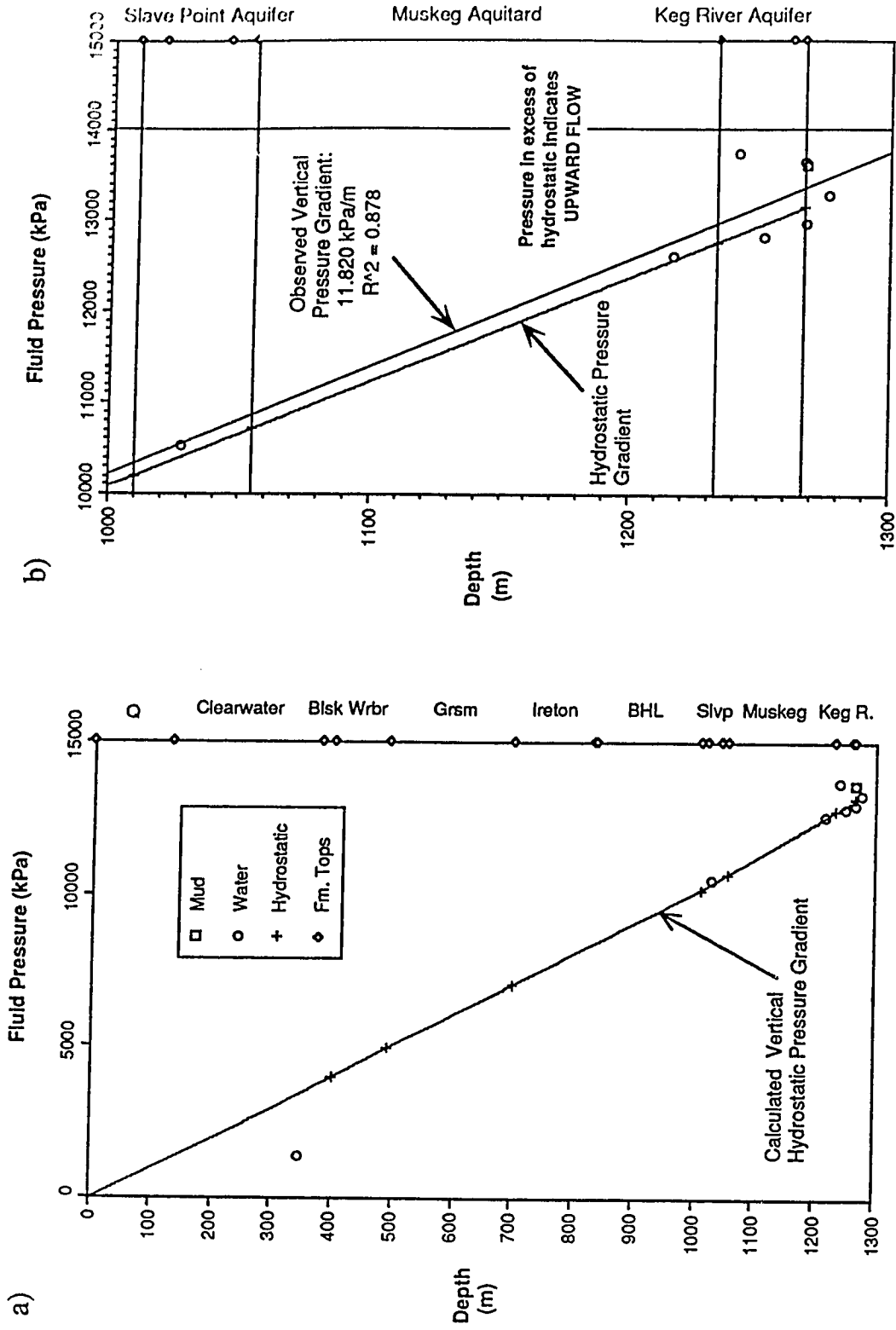


Figure 4.19.1 Pressure Versus Depth Plot for Townships 94-95, Ranges 6-7:  
 a) Ground Surface to Basement; b) Detail: Devonian Aquifers

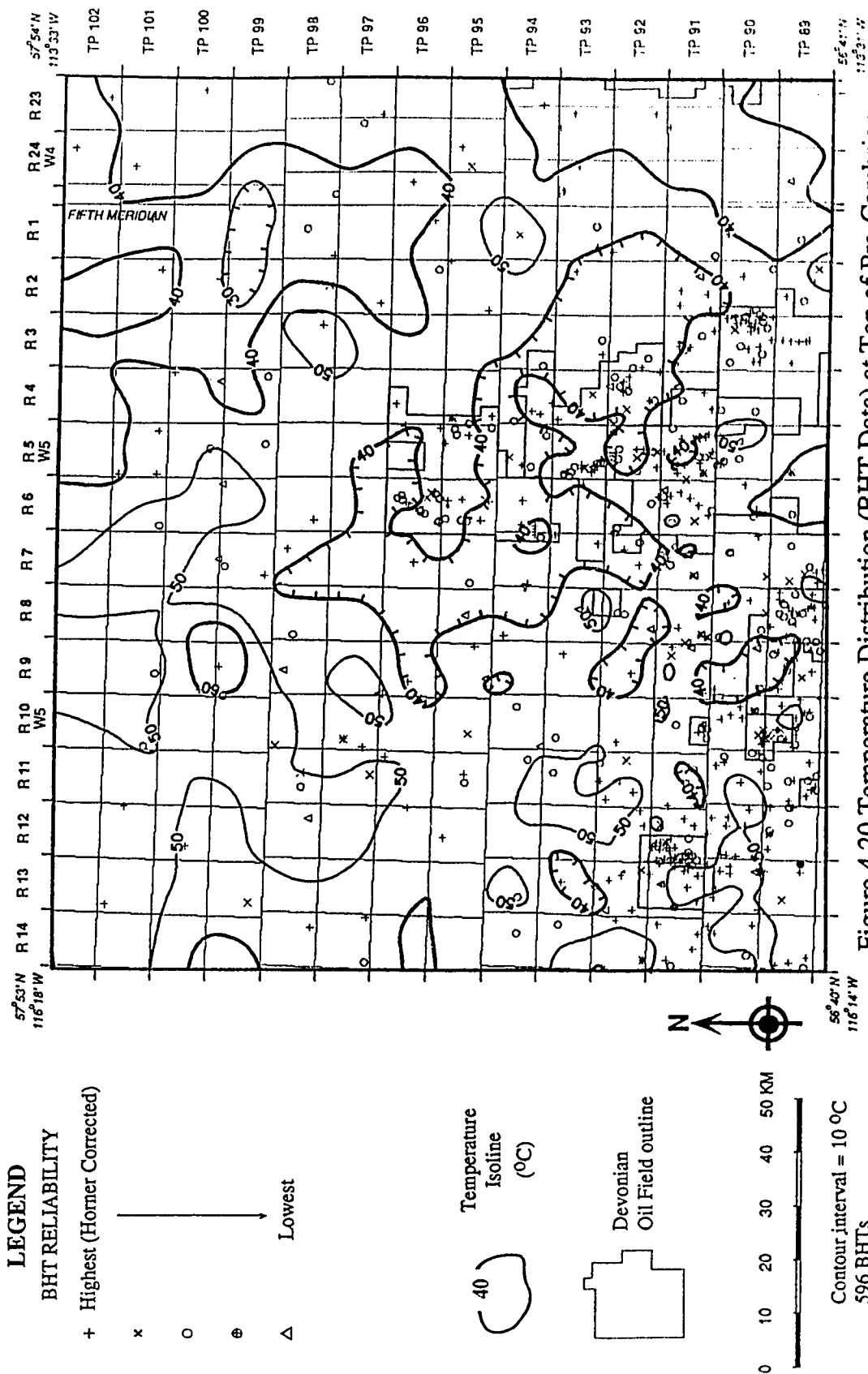


Figure 4.20 Temperature Distribution (BHT Data) at Top of Pre-Cambrian

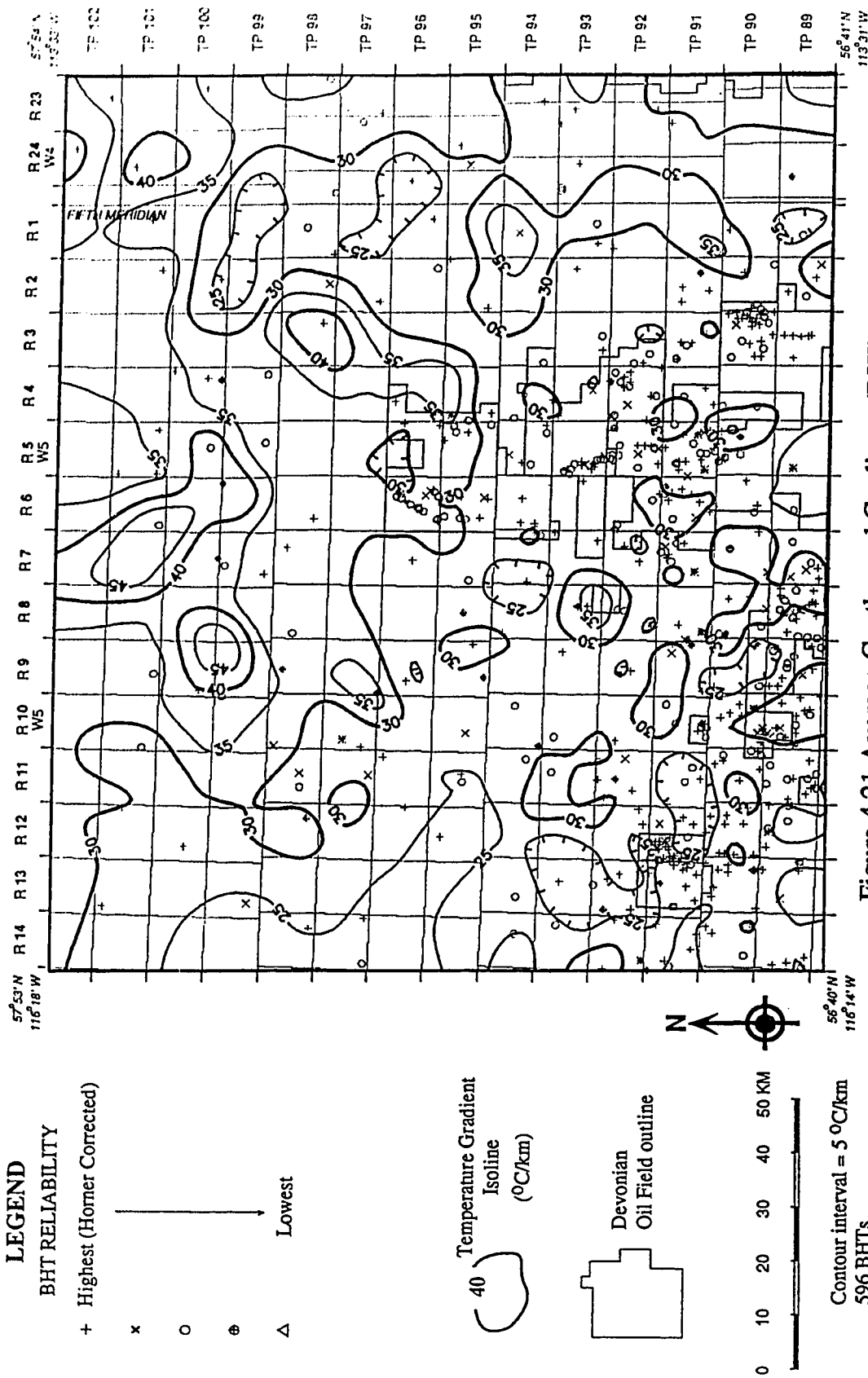
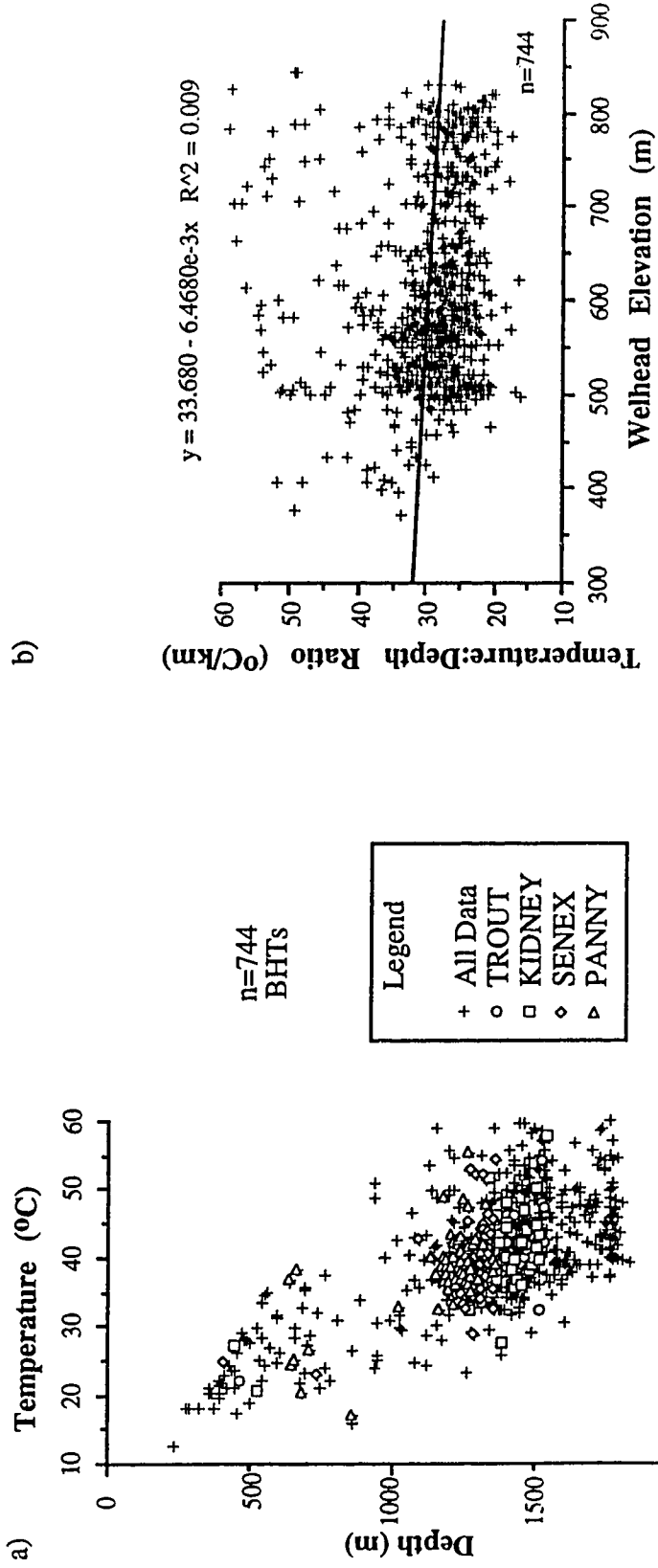


Figure 4.21 Average Geothermal Gradients (BHT Data) Between Ground Surface and Pre-Cambrian Basement





Wells within oilfield limits are not identified by anomalous characteristics such as exceptionally high temperatures

Very weak linear correlation between wellhead elevation and average temperature gradient. Compare with Figures 4.18 and 4.19 (Pressure-Depth relations)

Figure 4.21.1 BHT Data Analysis: a) Temperature Versus Depth, with Oilfield Wellhead Elevation Versus Temperature:Depth Ratio.

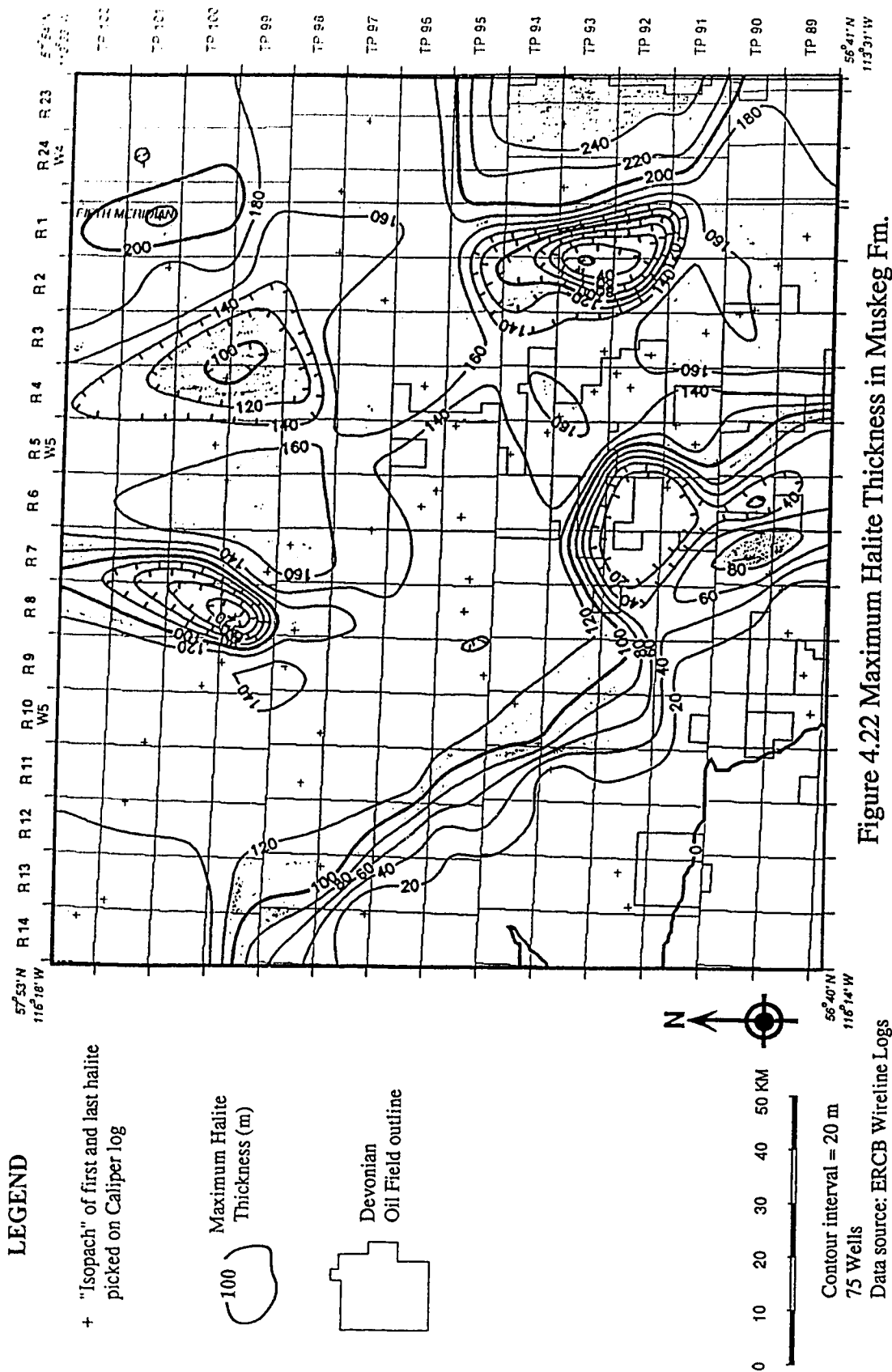
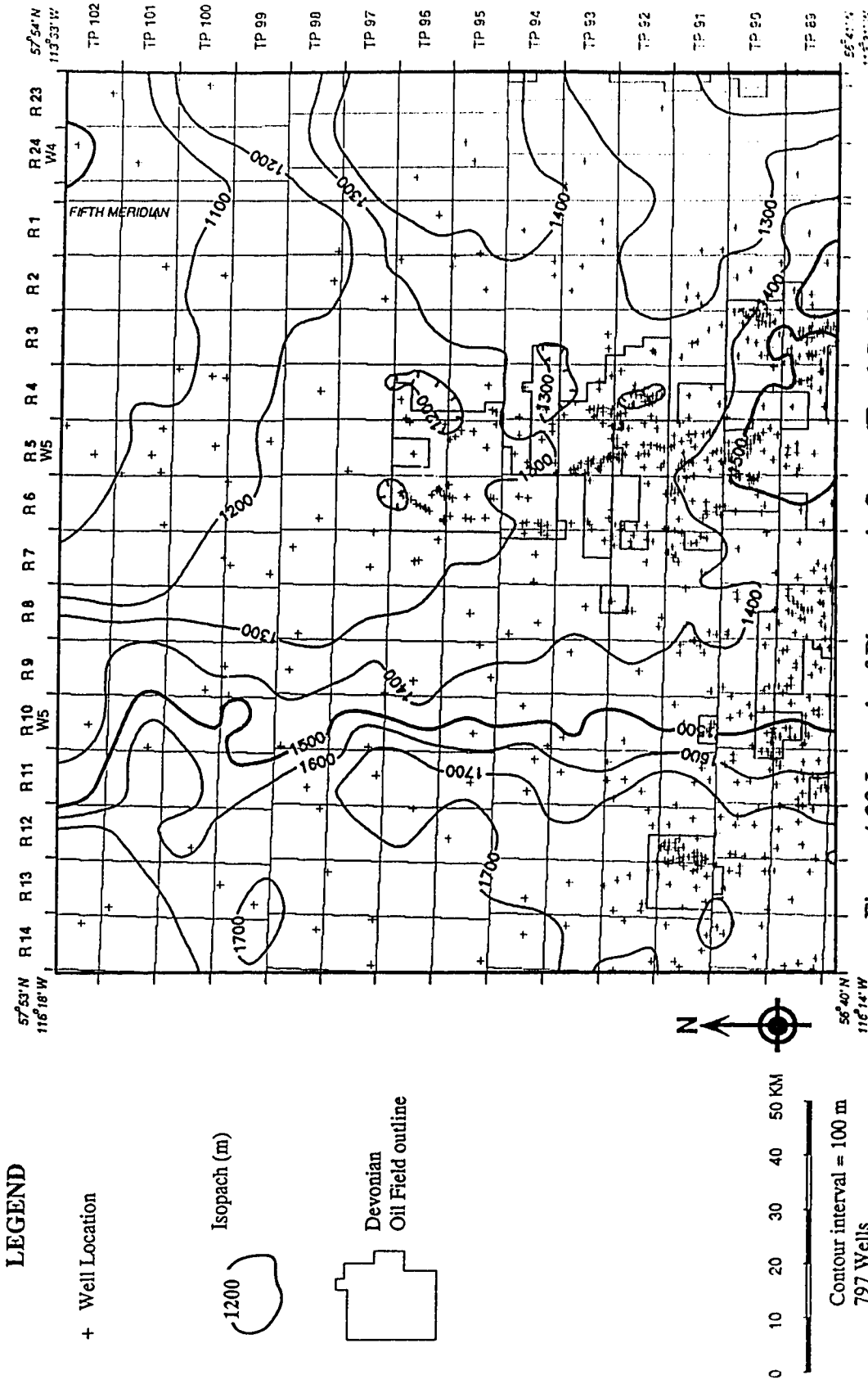


Figure 4.22 Maximum Halite Thickness in Muskeg Fm.



**LEGEND**

+ Well Location

Isopach (m)



Devonian Oil Field outline



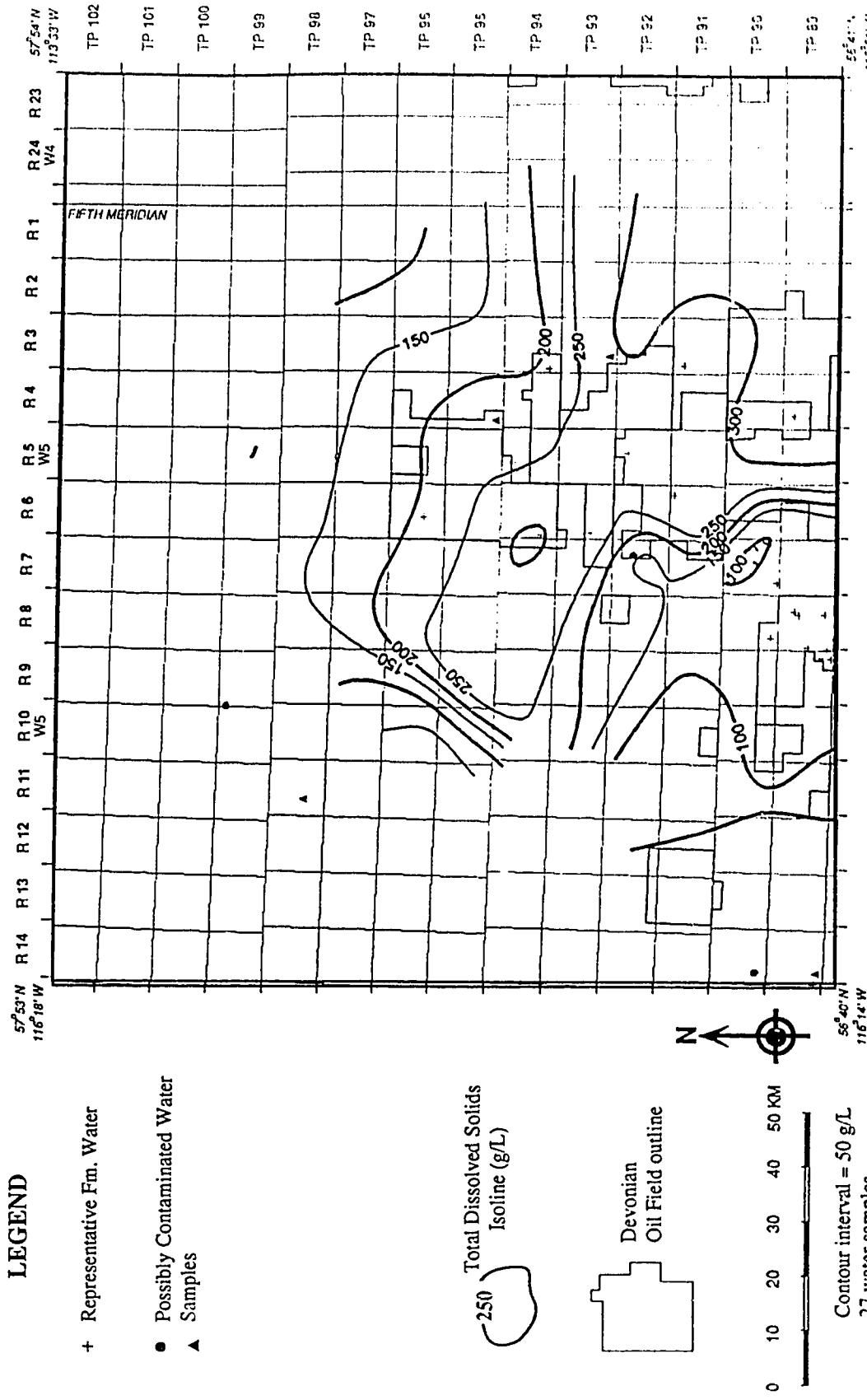
Contour interval = 100 m

797 Wells

Data source: PUBCO (1990)

Figure 4.23 Isopach of Phanerozoic Strata (Total Sediment Thickness)



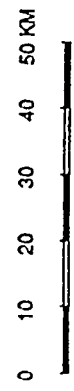


**LEGEND**

- + Representative Fm. Water
- Possibly Contaminated Water
- ▲ Samples

Total Dissolved Solids  
Isohaline (g/L)

Devonian  
Oil Field outline



Contour interval = 50 g/L  
27 water samples  
Data source: ERCB (1991 b)

Figure 4.25 Salinity (Total Dissolved Solids) in Slave Point Aquifer

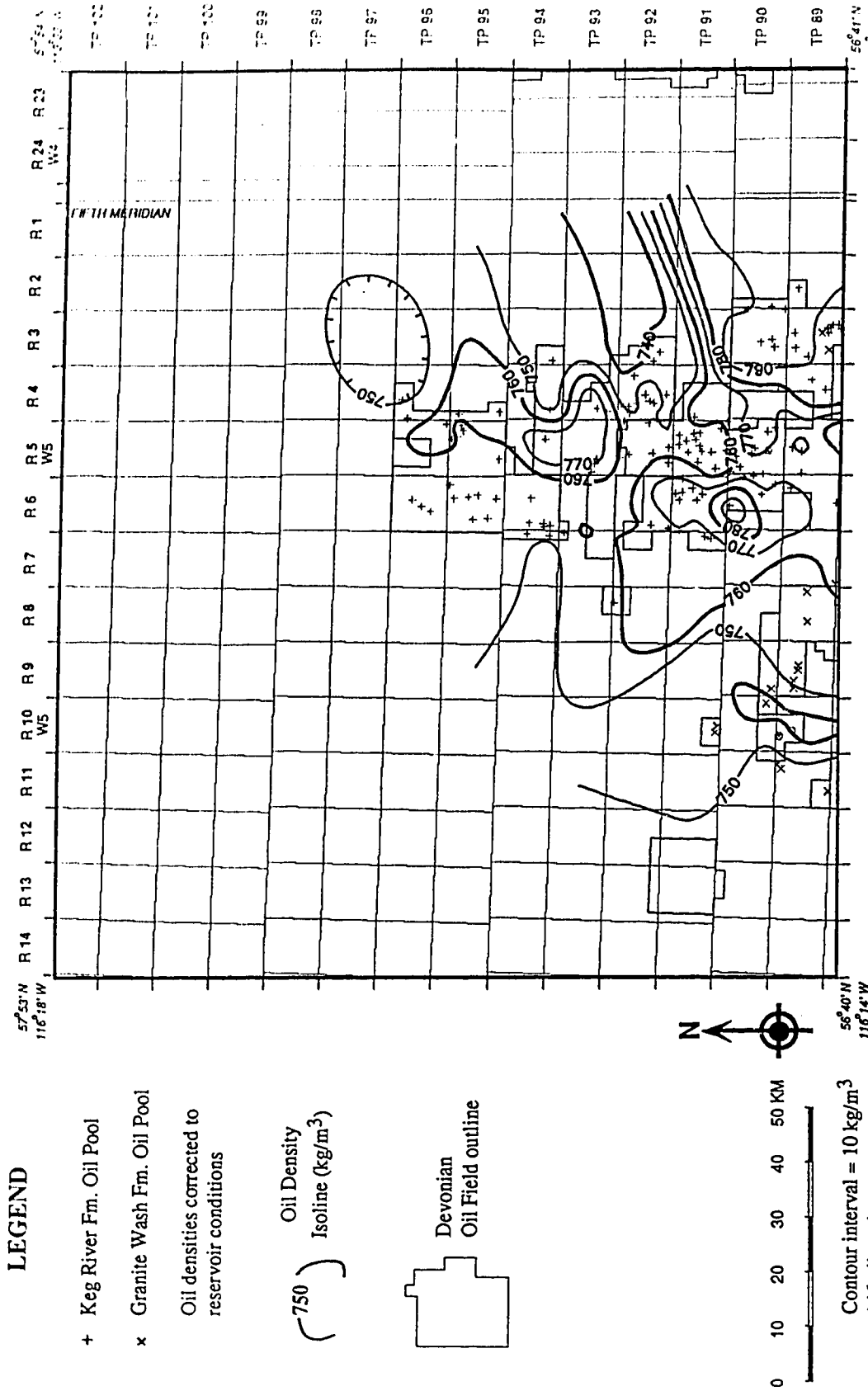


Figure 4.26 Oil Density (Corrected to Reservoir Conditions) in Keg River Aquifer

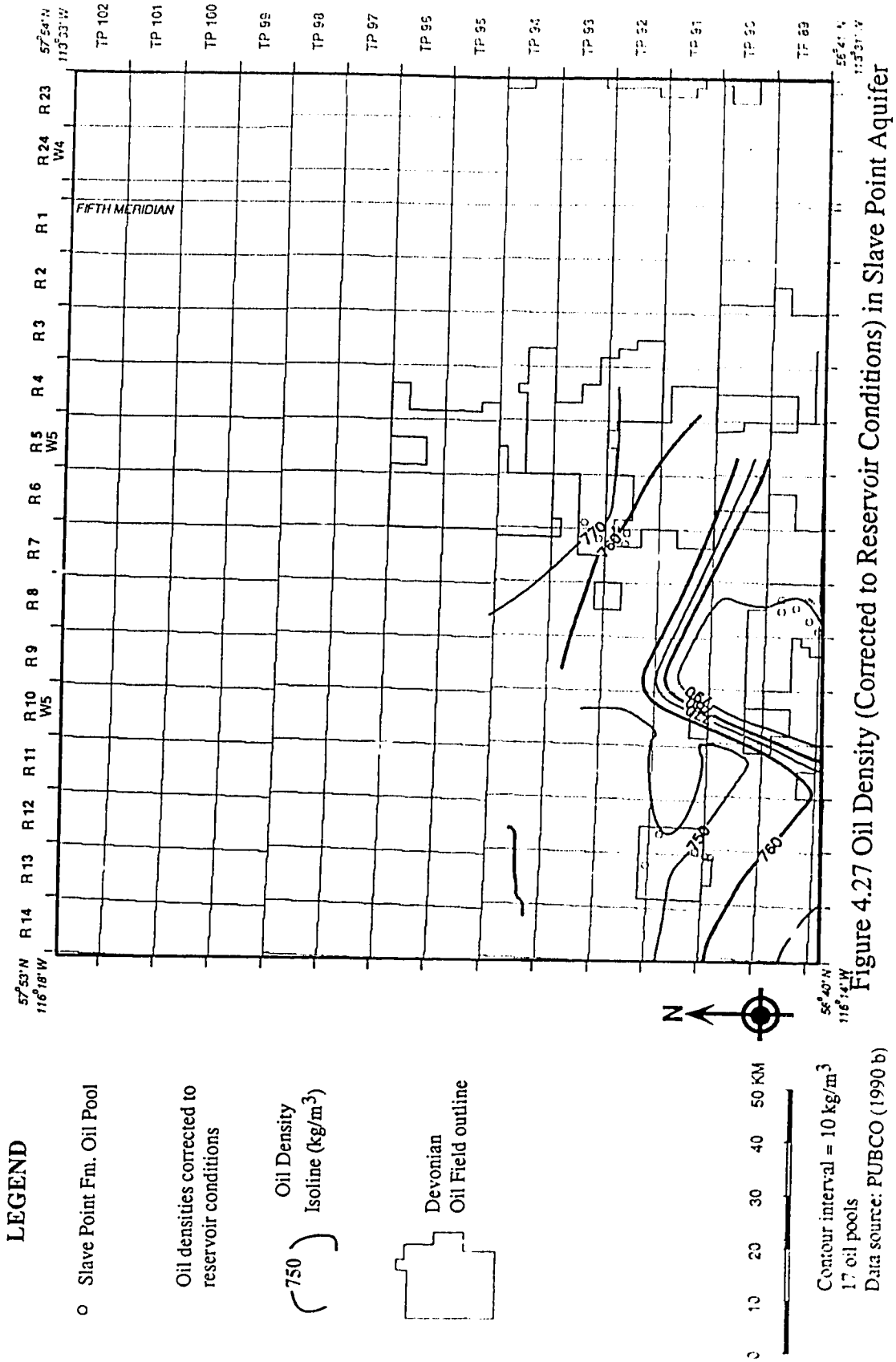


Figure 4.27 Oil Density (Corrected to Reservoir Conditions) in Slave Point Aquifer

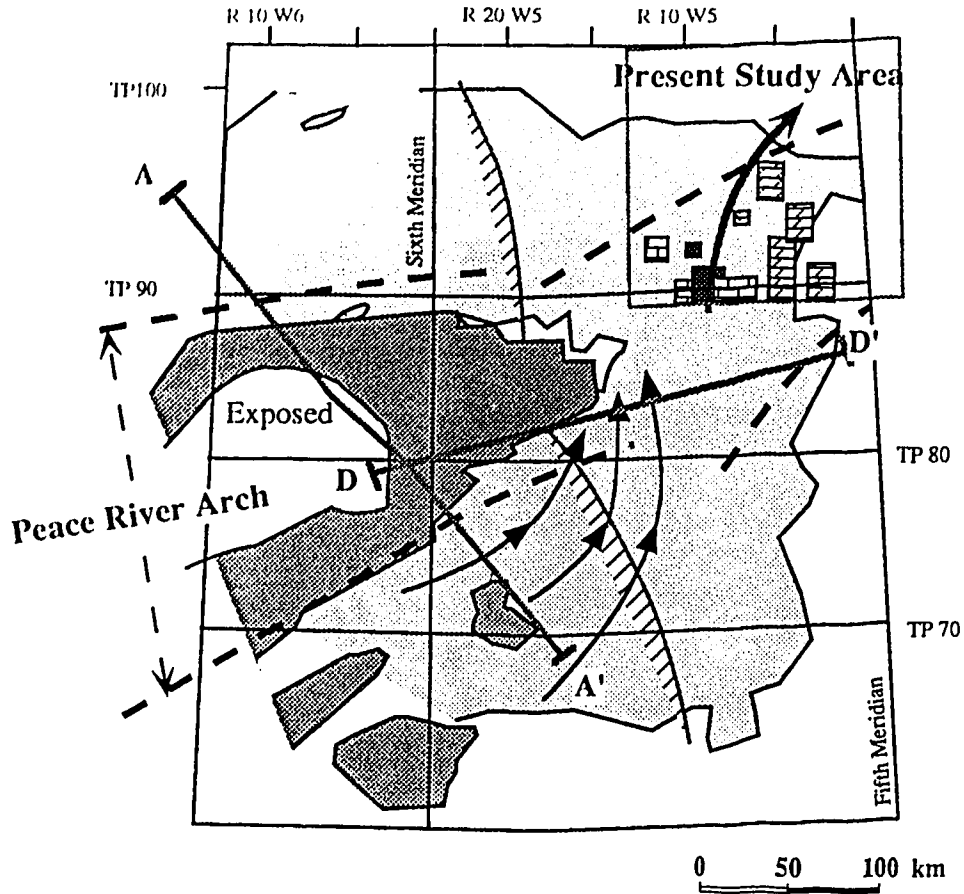
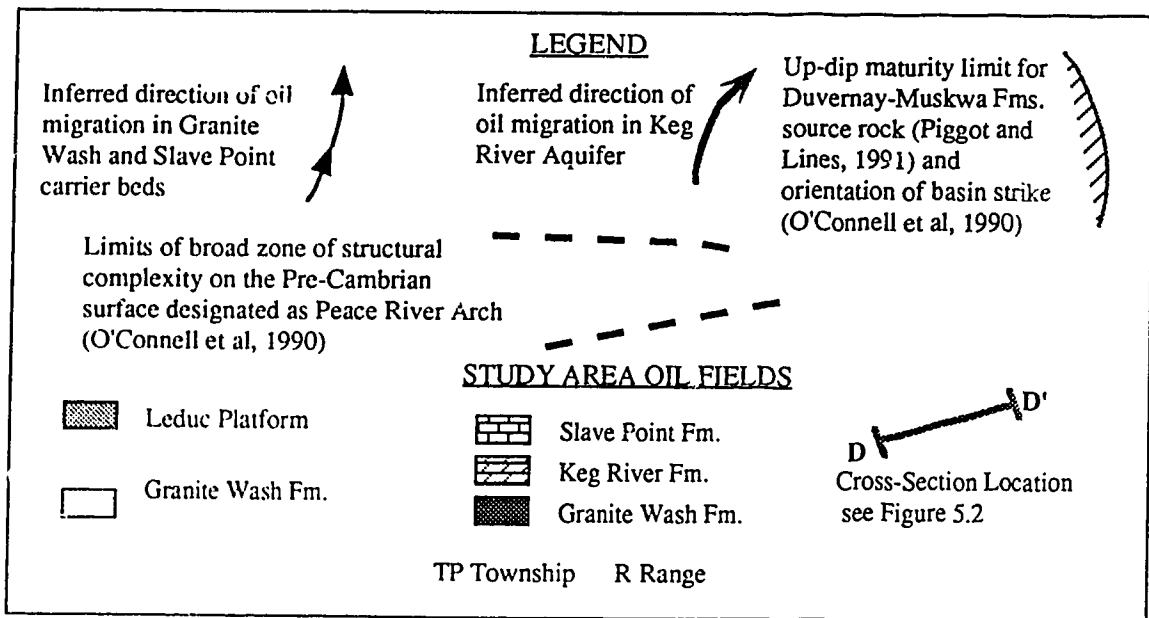
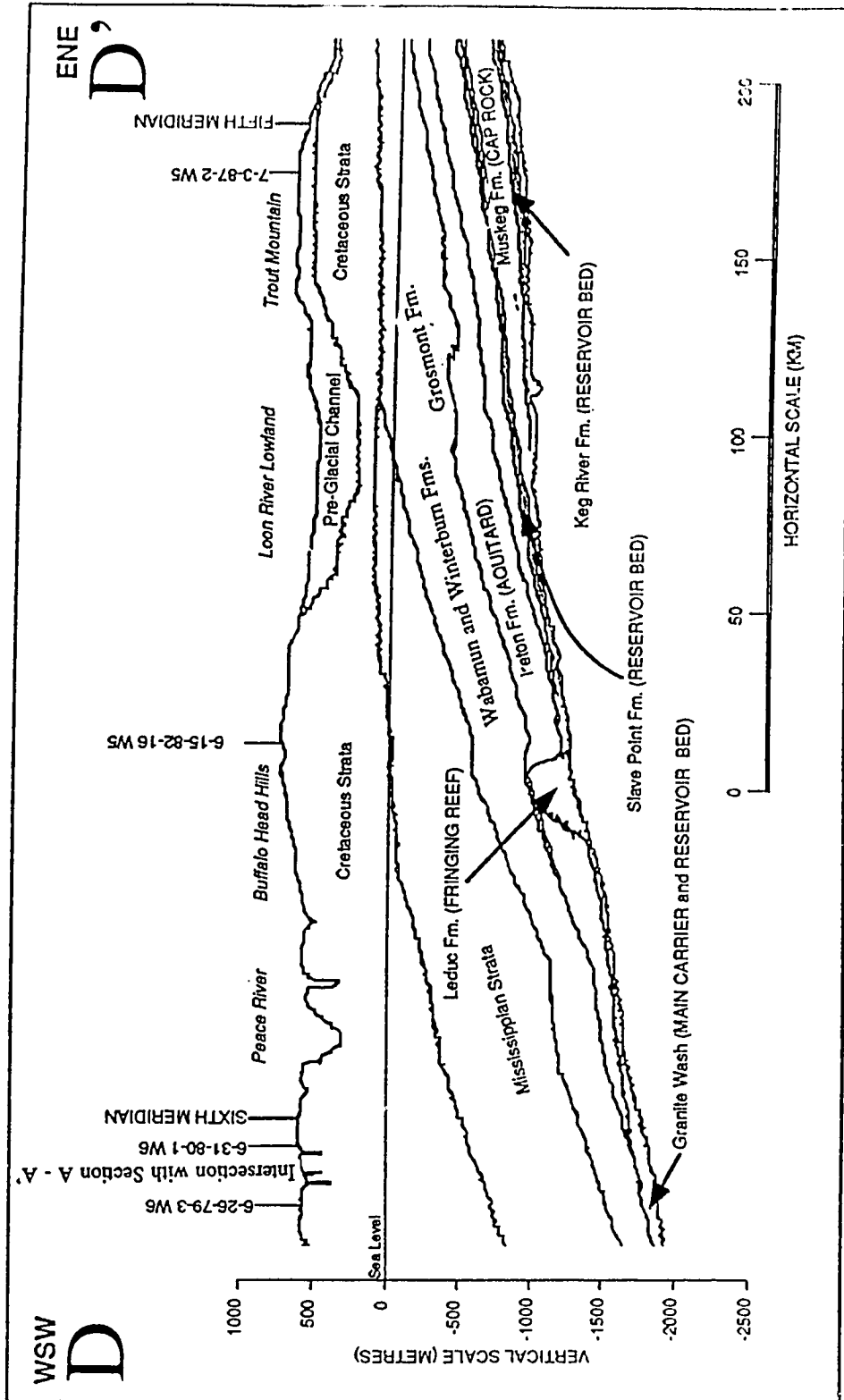


Figure 5.1 Possible Hydrodynamic Oil Migration in Peace River Arch Region

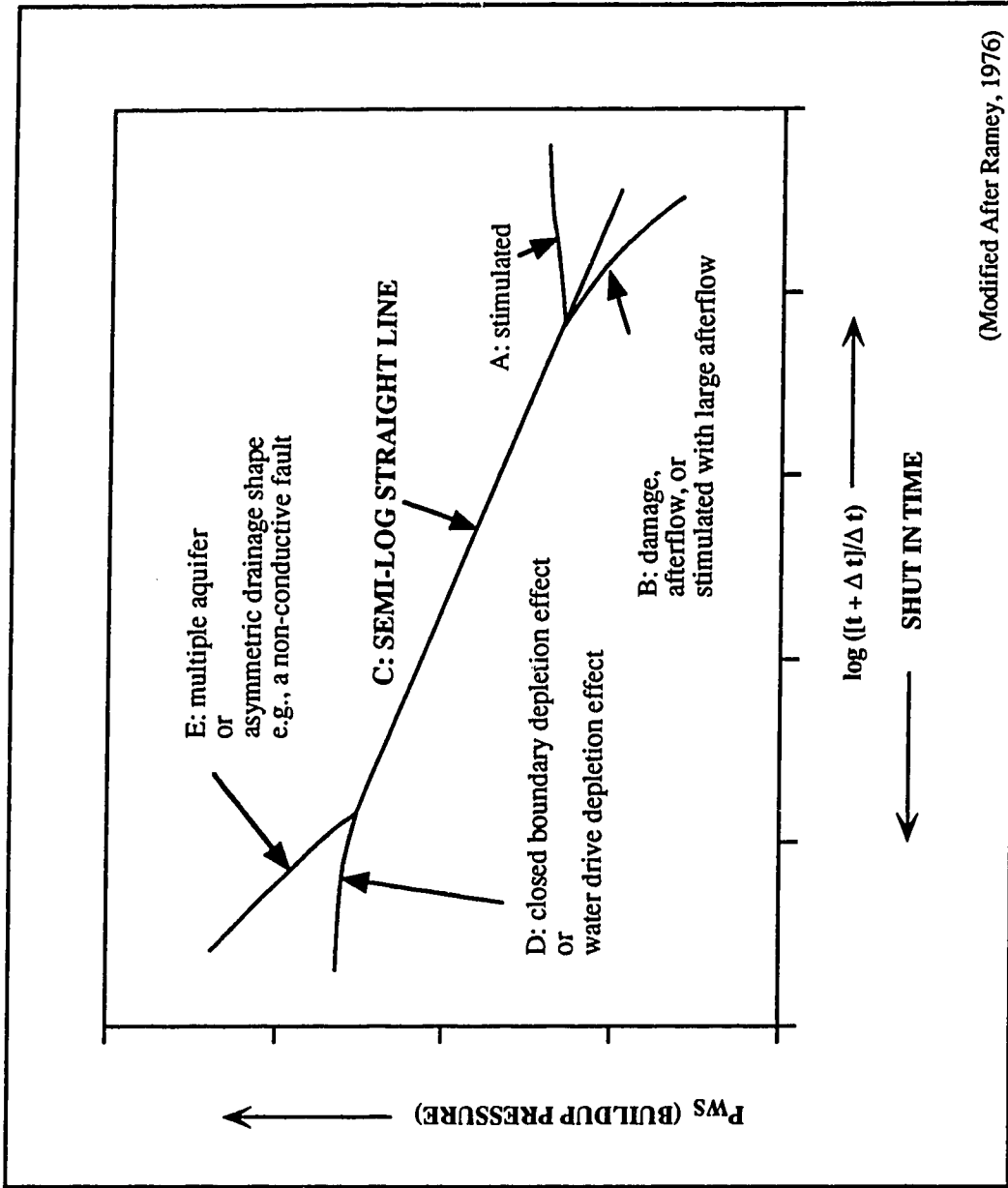






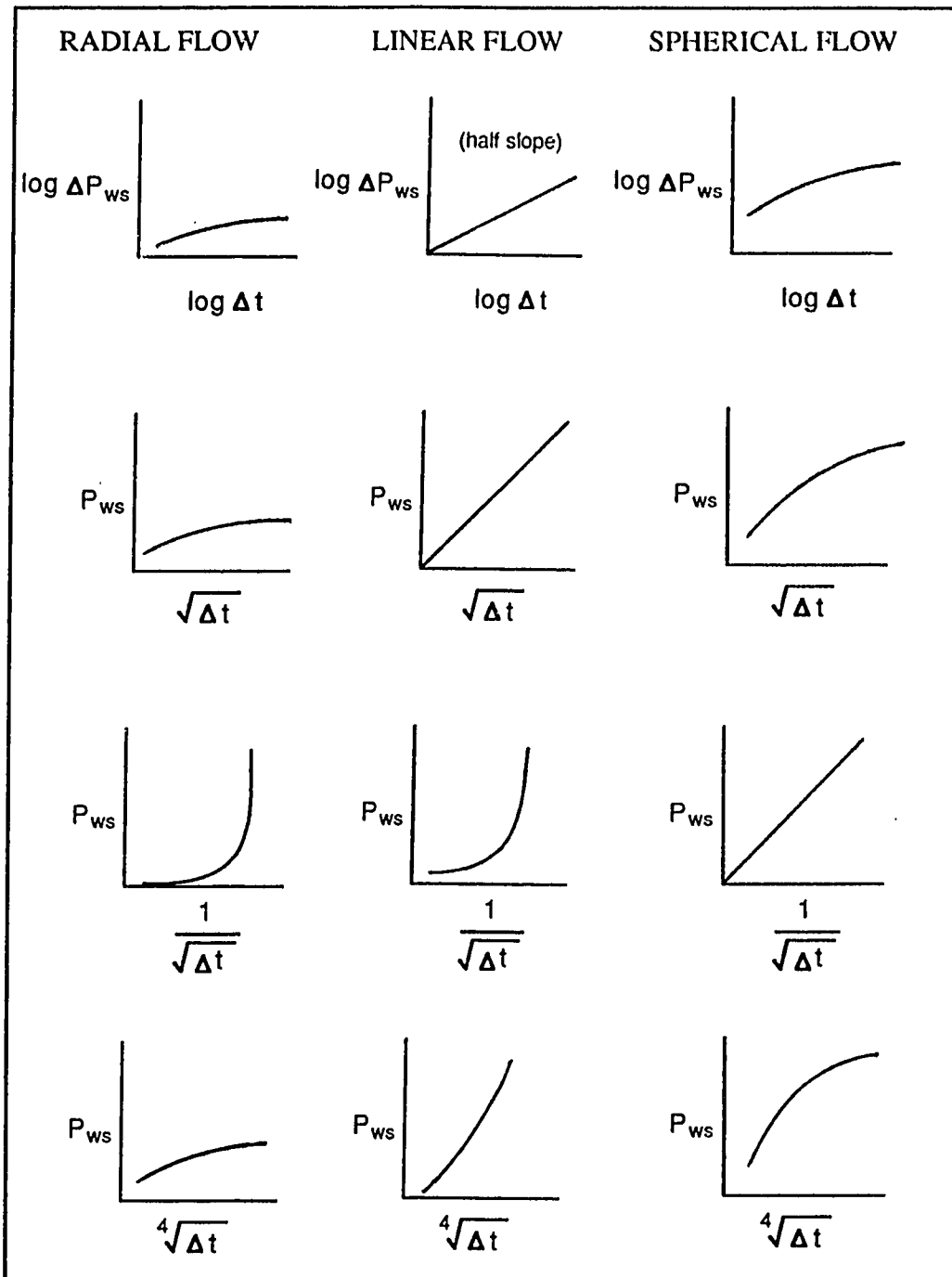
Cross-Section simplified from Wright (1924);

Figure 5.2 Regional Structural Cross-Section Along Axis of Peace River Arch, Parallel to Basin Dip



(Modified After Ramey, 1976)

Figure A2.1 Possible Causes of Characteristic Buildup Curves on an Idealized Homer Plot



(Modified After Ershaghi and Woodbury, 1985)

Figure A2.2 Characteristic Curves for Radial, Linear and Spherical Flow on Various Pressure Versus Time Plots

## References

AAPG (American Association of Petroleum Geologists), 1976. *Basic data file from the AAPG geothermal survey of North America*. University of Oklahoma.

Allan, J. and S. Creaney, 1991. *Oil families of the western Canada basin*. Bulletin of Canadian Petroleum Geology, 39 (2), p. 107-122.

Anderson, N.L., R. Brown J. and R.C. Hinds, 1988. *A seismic perspective on the Panny and Trout fields of north-central Alberta*. Canadian Journal of Exploration Geophysics, 24, p. 154-165.

Aprahamian, F. (ed.), 1976. *Sedimentary basin case study - the western Canadian sedimentary basin*. Earth Science topics and methods, The Open University Press, Milton Keynes, 68 p.

Bachu, S., 1985. *Influence of lithology and fluid flow on the temperature distribution in a sedimentary basin: a case study from the Cold Lake area, Alberta, Canada*. Tectonophysics, 120 (3-4), p. 257-284.

Bachu, S., 1988. *Analysis of heat transfer processes and geothermal pattern in the Alberta basin, Canada*. Journal of Geophysical Research, 93, (B7), p. 7767-7781.

Bachu, S. and R.A. Burwash, 1991. *Regional-scale analysis of the geothermal regime in the western Canada sedimentary basin*. Geothermics, 20 (5/6), p. 387-407.

Bachu, S. and J.R. Underschultz, 1992. *Regional-scale porosity and permeability variations, Peace River Arch area, Alberta, Canada*. American Association of Petroleum Geologists, Bulletin, 76, p. 547-562.

Bair, E.S., T.P. O'Donnel and L.W. Picking, 1985. *Potentiometric mapping from incomplete DST data: Palo Duro Basin area, Texas and New Mexico*. Groundwater, 23 (2), p. 198-211.

Bally, A.W., P.L. Gorgy and G.A. Stewart, 1966. *Structure, seismic data and evolution of the southern Canadian Rocky Mountains*. Bulletin of Canadian Petroleum Geology, 14 (3), p. 337-381.

Barker, C., 1972. *Aquathermal pressuring: role of temperature in development of abnormal-pressure zones*. American Association of Petroleum Geologists, Bulletin, 56 (10), p. 2068-2071.

Barton, R.H., E.A. Christiensen, W.O. Kupsch, W.H. Matthews, C.P. Gravenor and L.A. Bayrock, 1964. *Quaternary*. In: Geological history of western Canada. R.G. McGrossan and R.P. Glaister (eds.). Alberta Society of Petroleum Geologists, Calgary, Alberta, p. 195-200.

Bear, J., 1972. *Dynamics of fluids in porous media*. Elsevier, New York, Environmental Science Series, 764 p.

Beaumont, C., 1981. *Foreland basins*. Royal Astronomical Society Geophysical Journal, 65, p. 291-329.

Bebout, D.G. and W.R. Maiklem, 1973. *Ancient anhydrite facies and environments, Middle Devonian Elk Point Basin, Alberta*. Bulletin of Canadian Petroleum Geology, 21, p. 287-343.

Berg, R., 1975. *Capillary pressure in stratigraphic traps*. American Association of Petroleum Geologists, Bulletin, 59 (6), p. 939-956.

Berry, F.A.F., 1969. *Relative factors influencing membrane filtration effects in geologic environments*. Chemical Geology, 4, p. 295-301.

- Bethke, C.M., J.G. Reed and D.F. Oltz, 1991. *Long range petroleum migration in the Illinois basin*. American Association of Petroleum Geologists, Bulletin, 75, p. 925-945.
- Brace, W.F., 1980. *Permeability of crystalline and argillaceous rocks*. Journal of Rock Mechanics, Mineral Science and Geomechanics, 17, p. 241-251.
- Bradley, J.S., 1975. *Abnormal formation pressure*. American Association of Petroleum Geologists, Bulletin, 59, p. 957-973.
- Bredehoeft, J.D., 1963. *Possible mechanism for concentration of brines in subsurface formations*. American Association of Petroleum Geologists, Bulletin, 47 (2), p. 257-269.
- Bredehoeft, J.D. and B.B. Hanshaw, 1968. *On the maintenance of anomalous fluid pressures: I. Thick sedimentary sequences*. Geological Society of America, Bulletin, 79 (9), p. 1097-1106.
- Bredehoeft, J.D. and S. Papadopoulos, 1965. *Rates of vertical groundwater movement from the earth's thermal profile*. Water Resources Research, 1 (2), p. 325-328.
- Bredehoeft, J.D., J.B. Wesley and T.D. Fouch, undated. *The hydrodynamics of the Uinta basin: the role of hydrocarbon generation*.
- Campbell, C.V., 1987. *Stratigraphy and facies of the Upper Elk Point subgroup, northern Alberta*. In: Devonian lithofacies and reservoir styles in Alberta. Publication for Second International Symposium on the Devonian System. F.F. Krause and O.G. Burrowes (eds.). Canadian Society of Petroleum Geologists, Calgary, p. 243-286.
- Cant, D.J., 1988. *Regional structure and development of the Peace River Arch, Alberta: a Paleozoic failed rift system?* Bulletin of Canadian Petroleum Geology, 36, p. 284-295.

- Ceroici, W., 1979. *Hydrogeology of the Peerless Lake area, Alberta*. Alberta Research Council, Earth Sciences Report 79-5.
- Chamberlain, V.E., R.S.J. Lambert and W.S. McKerrow, 1989. *Mesozoic sedimentation rates in the western Canada basin as indicators of the time and place of tectonic activity*. Basin Research, 2, p. 189-202.
- Chamberlin, T.C., 1885, *Requisite and qualifying conditions of artesian wells*. U.S. Geological Survey, 1885, 5th. Annual Report.
- Chapman, D.S., 1984. *Heat flow in the Uinta Basin determined from bottom hole temperature (BHT) data*. Geophysics, 49, p. 453-466.
- Chebotarev, I.I., 1955. *Metamorphism of natural waters in the crust of weathering, parts 1-3*. Geochimica et Cosmochimica Acta, 8, pp. 22-48; 137-170; 198-212.
- CIFE (Canadian Institute of Formation Evaluation), 1989. *DST pressure listings*. CIFE, Calgary.
- Collins, A.G., 1975. *Geochemistry of oilfield waters*. Elsevier Scientific Publishing, Amsterdam.
- Corbet, T.F. and C.M. Bethke, 1992. *Disequilibrium fluid pressures and groundwater flow in the western Canada sedimentary basin*. Journal of Geophysical Research, 97 (B5), p. 7203-7217.
- Creaney, S. and J. Allan, 1990. *Hydrocarbon generation and migration in the western Canada sedimentary basin*. In: Classic Petroleum Provinces. J.Brooks (ed.). Geological Society, London, Special Publication 50, p. 189-202.
- Dahlberg, E.C., 1982. *Applied hydrodynamics in petroleum exploration*. Springer-Verlag, New York, 191 p.

Dake, L.P., 1978. *Fundamentals of reservoir engineering*. Elsevier, Amsterdam, *Developments in petroleum science* 8, 443 p.

Darcy, H., 1856. *Determination of the laws of the flow of water through sand*. Translation in *Physical Hydrogeology*. R.A. Freeze and W. Back (eds.). Hutchinson Ross, New York. *Benchmark Papers in Geology* 72, p. 14-19.

Davies, P.B., 1987. *Modeling areal, variable-density groundwater flow using equivalent freshwater head - analysis of potentially significant errors*. In: *Proceedings of Solving Groundwater Problems with Models Conference*, NWWA/IGWMC, Feb., 10-12, 1987, Denver, Colorado. National Water Well Association, Dublin, Ohio, p. 888-903.

Davis, J.C., 1973. *Statistics and data analysis in geology*. 2nd. Edition. John Wiley & Sons, New York, 646 p.

De Marsily, 1986. *Quantitative hydrogeology*. Academic Press, San Diego, 440 p.

Deroo, G., T.G. Powell, B. Tissot and R.G. McGrossan (eds.), 1977. *The origin and migration of petroleum in the western Canadian sedimentary basin, Alberta*. Geological Survey of Canada, Ottawa, GSC Bulletin 262, 136 p.

Dix, G.R., 1990. *Stages of platform development in the Upper Devonian (Frasnian), Leduc Formation, Peace River Arch, Alberta*. *Bulletin of Canadian Petroleum Geology*, 38A, p. 66-92.

Domenico, P.A. and V.V. Palciauskas, 1973. *Theoretical analysis of forced convective heat transfer in regional groundwater flow*. *Geological Society of America Bulletin*, 84 (12), p. 3803-3814.

Domenico, P.A. and F.W. Schwartz, 1990. *Physical and chemical hydrogeology*. Wiley, New York, 824 p.



Dowdle, W.L. and W.M. Cobb, 1975. *Static formation temperature from well logs - an empirical method*. Journal of Petroleum Technology, Nov. 1975, p.1326-1330.

Ehrmann, L., undated. *Drill stem testing and chart interpretation manual*. LYNES United Services, Technical Manual.

ERCB (Energy Resources Conservation Board), 1986. *Gulf Canada Corporation, Trout Keg River A Pool conventional reservoir study, (submitted to ERCB, Dec., 1986)*. In: ERCB Ultimate Reserve Estimate Submissions, ERCB, Calgary.

ERCB (Energy Resources Conservation Board), 1990 a. *Datum depth and initial pressure listing for Alberta oil pools, (updated 31 Dec., 1990)*. ERCB, Calgary.

ERCB (Energy Resources Conservation Board), 1990 b. *Geophysical well log file*. ERCB, Calgary.

ERCB (Energy Resources Conservation Board), 1991 a. *Alberta's reserves of crude oil, gas, natural gas liquids and sulphur*. ERCB ST-18, ERCB, Calgary.

ERCB (Energy Resources Conservation Board), 1991 b. *Fluid analyses: oil, gas, water*. ERCB ST-6, ERCB, Calgary.

ERCB (Energy Resources Conservation Board), 1991 c. *Core analyses*. ERCB ST-98, ERCB, Calgary.

ERCB (Energy Resources Conservation Board), 1991 d. *Drill stem tests*. ERCB ST-62, ERCB, Calgary.

Ershaghi, I., and J.J. Woodbury, 1985. *Examples of pitfalls in well test analysis*. Journal of Petroleum Technology, Feb., 1985, p. 335-341.

Fertl, W.H. and P.A. Wichman, 1977. *How to determine static BHT from well-log data*. World Oil, 184, p. 105-106.

Frape, S.K. and P. Fritz, 1982. *Saline groundwater in the Canadian Shield - a first overview*. Chemical Geology, 36, p. 179-190.

Fritz, P. and S.K. Frape (eds.), 1987. *Saline water and gases in crystalline rock*. Geological Association of Canada, Special Paper 33.

Freeze, R.A. and P. Witherspoon, 1966. *Theoretical analysis of regional groundwater flow, 1. analytical and numerical solutions to the mathematical model*. Water Resources Research, 2 (4), p. 641-656.

Freeze, R.A. and P. Witherspoon, 1967. *Theoretical analysis of regional groundwater flow, 2. effect of water-table configuration and subsurface permeability variation*. Water Resources Research, 3 (2), p. 623-634.

Freeze, R.A. and J.A. Cherry, 1979. *Groundwater*. Prentice-Hall, Englewood Cliffs, N.J., 604 p.

Fulton, R.J, 1989. *Foreword to the Quaternary geology of Canada and Greenland*. In: Geology of Canada and Greenland. R.J. Fulton (ed.). Geological Survey of Canada, Geology of Canada, No. 1, also Geological Survey of America, The Geology of North America, v.K-1.

Galloway, W.E. and D.K. Hobday, 1983. *Terrigenous clastic depositional systems: applications to petroleum, coal and uranium exploration*. Springer-Verlag, New York, 423 p.

Gascoyne, M., C.C. Davison, J.D. Ross and R. Pearson, 1987. *Saline groundwaters and brines in plutons in the Canadian Shield*. In: Saline water and gases in crystalline rocks. P. Fritz and S.K. Frape (eds.). Geological Association of Canada, Special Paper 33, p. 53-68.

Garven, G., and R.A. Freeze, 1984. *Theoretical analysis of the role of groundwater flow in the genesis of stratabound ore deposits: 1. mathematical and numerical model*. American Journal of Science, 284, (10), p. 1085-1124.

Garven, G., 1989. *A hydrogeologic model for the formation of the giant oil sands deposits of the western Canada sedimentary basin*. American Journal of Science, 289 (2), p. 105-166.

Glass, D.J., (ed.), 1990. *Lexicon of Canadian stratigraphy, volume 4*. Canadian Society of Petroleum Geologists, Calgary, 772 p.

Green, R, 1972, *Geological map of Alberta*. Alberta Geological Survey, Research Council of Alberta, Edmonton.

Gretener, P.E., 1981. *Geothermics: using temperature in hydrocarbon exploration*. American Association of Petroleum Geologists, Tulsa, Oklahoma, AAPG Education Course Note Series 17, 170 p.

Hacquebard, P.A., 1977. *Rank of coal as an index of organic metamorphism for oil and gas in Alberta*. In: The origin and migration of petroleum in the western Canadian sedimentary basin. G. Deroo, T.G. Powell, B. Tissot and R.G. McGrossan (eds.). Geological Survey of Canada, GSC Bulletin 262, p. 11-22.

Hall, H.N., 1953. *Compressibility of reservoir rocks*. Transactions of AIME, 198, p.309.

Hanor, J.S., 1987. *Origin and migration of subsurface sedimentary brines*. Society of Economic Paleontologists and Mineralogists, SEPM Short Course 21, 247 p.

Harrison, R.S., 1982. *Geology, and production history of the Grosmont carbonate pilot project, Alberta, Canada*. Proceedings of the Second International Conference on Heavy Crude and Tar Sands (Feb., 7-17, 1982), Vol. 1, Caracas, Venezuela.

Hedberg, H.D., 1974. *Relation of methane generation to undercompacted shales, shale diapirs and mud volcanoes*. American Association of Petroleum Geologists, Bulletin, 58, p. 661-673.

Hedberg, H.D., 1980. *Methane generation and petroleum migration*. In: Problems of Petroleum Migration. W.H. Roberts III and R.J. Cordell (eds.). American Association of Petroleum Geologists, AAPG Studies in Geology No. 10, p. 179-206.

Helander, D.P., 1983. *Formation evaluation*. Oil and Gas Consultants International Inc., Oklahoma.

Hem, J.D., 1989. *Study and interpretation of the chemical characteristics of natural water*. 3rd. edition, United States Geological Survey.

Hermanrud, C., 1986. *On the importance to petroleum generation of heating effects from compaction-derived water: an example from the northern North Sea*. In: Thermal Modeling of Sedimentary Basins. J. Burrus (ed.). Éditions Technip, Paris, Vol. 44, p. 247-269.

Hitchon, B., 1969. *Fluid flow in the western Canada sedimentary basin: 2. effect of geology*. Water Resources Research, 5, p. 460-469.

Hitchon, B., 1984. *Geothermal gradients, hydrodynamics and hydrocarbon occurrences, Alberta, Canada*. American Association of Petroleum Geologists, Bulletin, 68 (6), p. 713-743.

Hitchon, B., S. Bachu and J.R. Underschultz, 1990. *Regional subsurface hydrogeology, Peace River Arch area, Alberta and British Columbia*. Bulletin of Canadian Petroleum Geology, Special Volume 38A, p. 196-217.

Hitchon, B. and Friedman, I., 1969. *Geochemistry and origin of formation waters in the western Canada sedimentary basin, I. stable isotopes of hydrogen and oxygen*. *Geochimica & Cosmochimica Acta*, 33, p. 1321-1349.

Hitchon, B. and M.K. Horn, 1974. *Petroleum indicators in formation waters from Alberta, Canada*. *American Association of Petroleum Geologists, Bulletin*, 58 (3), p. 464-473.

Holland, J.G. and R.S.J. Lambert, 1972. *Major element chemical composition of shields and the continental crust*. *Geochimica et Cosmochimica Acta*, 36, p. 673-683.

Holysh, S., 1989. *Petroleum related geochemical signatures and regional groundwater flow, Chauvin area, east-central Alberta*. M.Sc. Thesis (unpublished), University of Alberta, Edmonton, Alberta.

Horner, D.R., 1951. *Pressure build-up in wells*. Third World Petrol. Congress, Proc., Sect.II. Leiden, Holland, p. 503-521.

Horvitz, L., 1980. *Near-surface evidence of hydrocarbon movement from depth*. In: Problems of Petroleum Migration. W.H. Roberts III and R.J. Cordell (eds.). American Association of Petroleum Geologists, AAPG Studies in Geology No. 10, p. 241-269.

Howell, J.V., 1934. *Historical development of the structural theory of accumulation of oil and gas*. In: Problems of petroleum geology, American Association of Petroleum Geologists, p. 1-23.

Hubbert, M.King, 1940. *The theory of groundwater motion*. *Journal of Geology*, 48 (8), p. 785-944.

Hubbert, M.King, 1953. *Entrapment of petroleum under hydrodynamic conditions*. *American Association of Petroleum Geologists, Bulletin*, 37 (8), p. 1954-2026.

- Hubbert, M.King, 1965. *History of petroleum geology and its bearing upon present and future exploration*. U.S. Geological Survey, pre-print, Oct., 1965.
- Hunt, T.S. 1861. *Bitumens and mineral oils*. Montreal Gazette, March 1, 1861.
- Hunt, T.S., 1862. *Notes on the history of petroleum or rock oil*. Smithsonian Institution, Annual Report for 1861.
- Illich, H.A., F.R. Haney and M. Mendoza, 1981. *Geochemistry of oil from Santa Cruz Basin, Bolivia: case study of migration-fractionation*. American Association of Petroleum Geologists, Bulletin, 65, p. 2388-2402.
- Illing, V.C., 1933. *The migration of oil and natural gas*. Petroleum Technologists Journal, 19, p. 229-274.
- Istok, J.D., 1989. *Groundwater modeling by the finite element method*. Water Resources Monographs. American Geophysical Union, Washington D.C.
- Jessop, A.M., 1992. *Thermal input from the basement of the western Canada sedimentary basin*. Bulletin of Canadian Petroleum Geology, 40, p.198-206.
- Johnson, R.H.J., 1988. *Belly River water study*. Water Chemistry Study of Belly River Formation, Alberta, Canada. Opus Petroleum Engineering Ltd.
- Jones, F.W., H.L. Lam and J.A. Majorowicz, 1985. *Temperature distributions at the Paleozoic and Pre-Cambrian surfaces and their implications for geothermal energy recovery in Alberta*. Canadian Journal of Earth Sciences, 22, p. 1774-1780.

Jones, R., 1980. *Some mass balance and geological constraints on migration mechanisms*. In: Problems of Petroleum Migration. W.H. Roberts III and R.J. Cordell (eds.). American Association of Petroleum Geologists, AAPG Studies in Geology No. 10, p. 47-68.

Judge, A.S., Washington D.C., 1973. *Deep temperature observations in the Canadian north*. National Academy of Sciences. The North American contribution to the Second International Conference, Session 1: Thermal aspects of permafrost formation and evolution, p. 35-40.

Keith, J.W., 1990. *The influence of the Peace River Arch on Beaverhill Lake sedimentation*. Bulletin of Canadian Petroleum Geology, Special Volume 38A, p. 55-65.

King, F.H., 1899. *Principles and conditions of the movements of groundwater*. U.S. Geological Survey, 19th. Annual Report.

Klassen, R.W, 1989. *Quaternary geology of the southern Canadian Interior Plains*. In: Chapter 2 of Geology of Canada and Greenland. R.J. Fulton (ed.). Geological Survey of Canada, Geology of Canada, No. 1, also Geological Survey of America, The Geology of North America, v.K-1.

Leblanc, Y., H.L. Lam, L.J. Pascoe and F.W. Jones. 1982. *A comparison of two methods of estimating static formation temperature from well logs*. Geophysical Prospecting, 30, p. 348-357.

Levorsen, A.I., 1936. *Stratigraphic versus structural accumulation*. American Association of Petroleum Geologists, Bulletin, 20 (5), p. 521-530.

Levorsen, A.I., 1967. *Geology of petroleum*. 2nd. edition, W.H. Freeman and Co., San Francisco.

Luszczynski, N., 1961. *Head and flow of groundwater of variable density*. Journal of Geophysical Research, 66 (12), p. 4247-4256.

Maccagno, M., 1991. *The common use of pressure-depth and pressure-elevation plots to analyze groundwater flow*. MSc. Thesis (unpublished), University of Alberta, Edmonton, Alberta.

MacElvain, R.C., 1963. *What do near-surface signs really mean in oil finding?* Oil and Gas Journal, 18, p. 132-136.

Majorowicz, J.A. and A.M. Jessop, 1981. *Regional heat flow patterns in the western Canada sedimentary basin*. Tectonophysics, 74, p. 209-238.

Majorowicz, J.A. and A.M. Jessop, 1992. *Relation between basement heat flow and thermal state of the sedimentary succession, Alberta basin*. Bulletin of Canadian Petroleum Geology, (submitted Sept 92).

Majorowicz, J.A., F.W. Jones and H.L. Lam, 1984. *Heat flow and geothermal gradient studies in the Alberta basin. An essential part of geothermal potential evaluation*. In: F. Curtis (ed.), Energex 84, Pergamon Press, p. 279-284.

Majorowicz, J.A., M. Rahman, F.W. Jones and N.J. McMillan, 1985. *The Paleogeothermal and present thermal regimes of the Alberta basin and their significance for petroleum occurrences*. Bulletin of Canadian Petroleum Geology, 33 (1), p. 12-21.

Maxey, G.B., 1964. *Hydrostratigraphic units*. Journal of Hydrology, 2, p.124-129.

McAuliffe, C.D., 1980. *Oil and gas migration: chemical and physical constraints*. In: Problems of Petroleum Migration. W.H. Roberts III and R.J. Cordell (eds.). American Association of Petroleum Geologists, AAPG Studies in Geology No. 10, p. 89-109.

Meijer-Drees, N.C., 1986. *Evaporitic deposits of western Canada*. Geological Survey of Canada, Ottawa, GSC Paper 85-20, 118 p.



Monger, J.W.H., 1989. *Overview of cordilleran geology*. In: B.D. Ricketts (ed.), *Western Canada sedimentary basin - a case history*. Canadian Society of Petroleum Geologists, Calgary, Alberta, p. 9-32.

Munn, M.J., 1909. *The anticlinal and hydraulic theories of oil and gas accumulation*. *Economic Geology*, 4 (6), p. 509-529.

Muskat, M., 1937. *Flow of homogeneous fluids through porous media*. I.H.R.D.C. Publications, Boston, Massachusetts.

Neuzil, C.E., 1985. *Comment on "Possible effects of erosional changes of the topographic relief on pore pressures at depth" by J. Tóth and R.F. Millar*. *Water Resources Research*, 21 (6), p. 895-898.

North, F.K., 1985. *Petroleum geology*. Allen & Unwin, Boston, Massachusetts.

Nurkowski, J.R., 1984. *Coal quality, rank and its relation to reconstructing overburden. Upper Cretaceous and Tertiary plains coal, Alberta, Canada*. *American Association of Petroleum Geologists, Bulletin*, 68 (3), p. 285-295.

O'Connell, S.C., G.R. Dix and J.E. Barclay, 1990. *The origin, history and regional structural development of the Peace River Arch, western Canada*. *Bulletin of Canadian Petroleum Geology*, Special Volume 38A (Dec 1990), p. 4-24.

Osadetz, K.G., 1989. *Basin analysis applied to petroleum geology in western Canada*. In: B.D. Ricketts (ed.), *Western Canada Sedimentary Basin. A Case History*. Canadian Society of Petroleum Geologists, Calgary, p. 287-306.

Ozoray, G., unpublished. *Hydrogeology of the Wadlin Lake-Vermillion Chutes area, Alberta*. Alberta Research Council, Edmonton, Alberta.

Parks, K., 1989. *Groundwater flow, pore pressure anomalies and petroleum entrapment, Belly River Formation, west-central Alberta*. M.Sc. Thesis (unpublished), University of Alberta, Edmonton, Alberta.

Piggot, N. and M.D. Lines, 1991. *A case study of migration from the west Canada basin*. In: Petroleum Migration, W.A. England and A.J. Fleet (eds.). Geological Society, Special Publication 59, p. 207-225.

Podruski, J.A., J.E. Barclay and A.P. Hamblin, 1987. *Conventional oil resources of western Canada*. Geological Survey of Canada. GSC Paper 87-26, 149 p.

Porter, J.W., R.A. Price and R.G. McGrossan, 1982. *The western Canada sedimentary basin*. Philosophical Transactions of the Royal Society of London, 305, p. 169-192.

PUBCO, 1990 a. *Geobase well database*.

PUBCO, 1990 b. *Geobase oil and gas production database*.

Pugh, D.C., 1973. *Subsurface lower Paleozoic stratigraphy in northern and central Alberta*. Geological Survey of Canada, GSC Paper 72-12.

Ramey, H.J. Jr., 1976. *Practical use of modern well test analysis*. Society of Petroleum Engineers of AIME (American Institute of Mining, Metallurgical and Petroleum Engineers) Paper No. SPE 5878.

Ramey, H.J. Jr., 1982. *Pressure transient testing*. Journal of Petroleum Technology, July 1982, p. 1407-1413.

Rich, J.L., 1921. *Moving underground water as a primary cause of the migration and accumulation of oil and gas*. Economic Geology, 16 (6), p. 347-371.

Roberts III, W.H. and R.J. Cordell (eds.) 1980. *Problems of petroleum migration*. American Association of Petroleum Geologists, Tulsa, Oklahoma. AAPG Studies in Geology No. 10, 273 p.

Rostron, B.J. and J. Tóth, 1992. *Numerical simulation of oil migration and entrapment in a lenticular reservoir*. Applied Hydrogeology, 1, (2), p. 15-33.

Rutter, N.W., 1980. *Late Pleistocene history of the western Canadian ice-free corridor*. Canadian Journal of Anthropology, 1, p. 1-8.

Sampson, R.J., 1975. *Surface II graphics system*. Kansas Geological Survey, Lawrence, Kansas. 240 p.

Schowalter, T., 1979. *Mechanics of secondary hydrocarbon migration and entrapment*. American Association of Petroleum Geologists, Bulletin, 63 (5), pp.723.

Seaber, P.R., 1988. *Hydrostratigraphic units*. In: W. Back, J.S. Rosenshein and P.R. Seaber (eds.). Hydrogeology. Geological Society of America, Boulder, Colorado. The Geology of North America, Q-2, p. 9-14.

Silverman, S.R., 1965. *Migration and segregation of oil and gas*. In: A. Young and J.E. Galley (eds.). Fluids in subsurface environments. American Association of Petroleum Geologists, Tulsa. AAPG Memoir 4, p. 53-65.

Spencer, C.W., 1987. *Hydrocarbon generation as a mechanism for overpressuring in Rocky Mountain region*. American Association of Petroleum Geologists, Bulletin, 71 (4), p. 368-388.

Stiff, H.A., Jr., 1951. *The interpretation of chemical water analysis by means of patterns*. Journal of Petroleum Technology, 3 (10), p. 15-16.

Taylor, R.S., W.H. Mathews and W.O. Kupsch, 1964. *Tertiary*. In: Geological history of western Canada. R.G. McGrossan and R.P. Glaister (eds.). Alberta Society of Petroleum Geologists, Calgary, Alberta, p. 190-194.

Theis, C.V., 1935. *The relation between the lowering of the piezometric surface and the rate and duration of discharge of a well using groundwater storage*. Transactions of the American Geophysical Union, 2, p. 519-524.

Tissot, B. and D. Welte, 1978. *Petroleum formation and occurrence*. Springer Verlag, New York.

Tóth, J., 1962. *A theory of groundwater motion in small drainage basins in central Alberta, Canada*. Journal of Geophysical Research, 67 (11), p. 4375-4387.

Tóth, J., 1963. *A theoretical analysis of groundwater flow in small drainage basins*. Journal Geophysical Research, 68 (16), p. 4795-4812.

Tóth, J., 1972. *Properties and manifestations of regional groundwater movement*. Proceedings of the 24th International Geological Congress, Section 2, p. 153-163, also, Contribution No. 548, Research Council of Alberta.

Tóth, J., 1978. *Gravity-induced cross-formational flow of formation fluids, Red Earth region, Alberta, Canada: Analysis, patterns, evolution*. Water Resources Research, 14 (5), p. 805-843.

Tóth, J., 1979. *Patterns of dynamic pressure increment of formation fluid flow in large drainage basins, exemplified by the Red Earth region, Alberta, Canada*. Bulletin of Canadian Petroleum Geology, 27 (1), p. 63-83.

Tóth, J., 1980. *Cross-formational gravity-flow of groundwater: a mechanism of the transport and accumulation of petroleum (the Generalized Hydraulic Theory of Petroleum Migration)*. In: Problems of Petroleum Migration. W.H. Roberts III and R.J. Cordell (eds.). American Association of Petroleum Geologists, AAPG Studies in Geology No. 10, p. 121-169.

Tóth, J., 1984. *The role of regional gravity flow in the chemical and thermal evolution of groundwater*. In: B. Hitchon and E.I. Wallick (eds.), Proceedings of the First Canadian/American Conference on Hydrogeology, Practical applications of groundwater geochemistry. National Water Well Association, Worthington, Ohio, p. 3-29.

Tóth, J., 1988. *Ground water and hydrocarbon migration*. In: W. Back, J.S. Rosenshein and P.R. Seaber (eds.). Hydrogeology. Geological Society of America, Boulder, Colorado. The Geology of North America, Q-2, p. 485-502.

Tóth, J. and T. Corbet, 1986. *Post-Paleocene evolution of regional groundwater flow-systems and their relation to petroleum accumulations, Taber area, southern Alberta, Canada*. Bulletin of Canadian Petroleum Geology, 34 (3), p. 339-363.

Tóth, J. and R. Millar, 1983. *Possible effects of erosional changes of the topographic relief on pore pressures at depth*. Water Resources Research, 19 (6), p. 587.

Williams, G.K., 1983. *Some musings on the Devonian Elk Point basin, western Canada*. Bulletin of Canadian Petroleum Geology, 32 (2), p. 216-232.

Wright, G.N., (ed.), 1984. *The western Canada sedimentary basin - a series of geological sections illustrating basin stratigraphy and structure*. Canadian Society of Petroleum Geologists and Geological Society of Canada, Calgary.

## **Appendices**

### **Appendix 1 Laboratory Procedure for Core Analysis**

The procedure described here is taken from a core analysis report of Robertson Research. Additional information is from the Geotech manual "Applications of Core Analysis" prepared for Dome Petroleum.

#### **A1.1 Core Retrieval**

Conventional core retrieval involves tripping to fit a special core bit and hollow core barrel to the drill string. Drilling then proceeds and a column of rock (the core) is obtained in the inner barrel. When the desired amount of core has been cut, it is snapped off at the base as the drill string is lifted off bottom. The barrel is then returned to the surface, the core is removed, quickly sealed in numbered containers and dispatched immediately to the laboratory for analysis.

#### **A1.2 Core Preparation**

When received in the lab the core is laid out on tables, checked for proper order and drilling fluid residuum is cleaned off, care being taken not to contaminate the formation fluids within the core. A brief lithological description is made to facilitate sample selection.

#### **Spectral Gamma Ray Log**

The spectral gamma ray log measures the natural gamma radioactivity of the core in API units: % potassium; ppm uranium and ppm thorium. This log is used to correlate the top and base of the core with downhole geophysical logs.

#### **Sample Selection and Cutting**

Samples are selected according to the clients instruction or at the discretion of the core company geologist. Samples are horizontally drilled plugs (2" diameter) or full diameter slabs, cut or drilled with fluid appropriate to the lithology. For highly fractured core, small rock chips can be analyzed.

### **Sample Cleaning and Drying**

Samples used for permeability and porosity determination are cleaned usually with toluene, in a CO<sub>2</sub> - toluene extractor or with a vapour phase extractor. Samples are dried in a steam heated oven at a temperature of approximately 100 °C. Humidity controlled ovens are used to prevent shrinkage in sensitive clays. Samples destined for fluid summation and residual saturation determination are preserved in their original condition.

### **A1.3 Residual Saturations - Fluid Summations**

A retort oven is used to distill fluids from fresh core samples from which residual oil and water saturations can be obtained quickly. A slower extraction-distillation process (the Dean Stark method) gives more accurate determinations.

### **A1.4 Porosity**

Porosity is defined as the ratio of pore volume to the total rock (bulk) volume and is usually expressed as a percentage i.e.

$$\text{Porosity (\%)} = \frac{\text{pore volume}}{\text{bulk volume}} * 100,$$

Porosities of common petroleum reservoir rocks range from 10% to 20% for sandstones and 5% to 25% for carbonates.

### **Laboratory Determination of Porosity**

Since the bulk volume of a rock comprises the grain volume plus the pore volume, porosity can be determined by measuring any two of these three quantities. A variety of methods are used to determine porosity. The grain and bulk volume are determined directly by gravimetric or volumetric methods and the void volume by extraction of gas or air content, by saturation with a liquid or by calculation from Boyle's Law upon compression or expansion of gas in the sample. All methods require the prior extraction of fluids and drying of samples.

### Accuracy of Porosity Determinations

Core porosities may exceed the in situ reservoir porosity if the sample has expanded appreciably since the release of the subsurface confining pressure, or has been damaged during coring or subsequent handling. Geotech indicate that their Boyle's Law porosimeter gives grain volume determinations with an error of +/- 2%.

### **A1.5 Permeability**

Permeability is an empirically determined measure of the force exerted against fluid flow due to the size, shape, surface area and geometry of the grains and pores or other channels of a rock. It is measured in units of darcies. One darcy permits one millilitre of fluid with a dynamic viscosity of one centipoise (e.g. water at 20 °C) to flow at a rate of one centimetre per second through a one centimetre cube of porous material under a pressure gradient of 101 kPa (one atmosphere). One darcy is approximately equal to  $10^{-8}$  cm<sup>2</sup>. Intrinsic permeability (k) is the permeability of a porous medium to any liquid at 100% saturation and is an invariant property of the medium. Different lithological materials exhibit intrinsic permeabilities which range over some 13 orders of magnitude, an enormous range compared to that for porosity. Most reservoir rocks exhibit permeabilities in the 1-1000 millidarcy range.

The presence of multiple immiscible fluids (e.g. oil, gas and water) generally reduces the effective permeability ( $k_e$ ) of the rock to each individual fluid. In such a case the relative permeability of the medium to each individual fluid must be determined by experiment with the particular rock-fluid system. Relative permeability ( $k_r$ ) is defined as:

$$k_r = \frac{k_e}{k},$$

where  $k_e$  = effective permeability to a given fluid at partial saturation

$k$  = the intrinsic or absolute permeability to a fluid at 100% saturation

Irreducible or residual saturation occurs when the saturation level of one fluid in a multi-fluid system is sufficiently low that the relative



permeability of the medium to that fluid is zero. A fluid at residual saturation is effectively immobile regardless of the intrinsic permeability of the medium. Permeability determinations from standard core analyses are made with respect to a single fluid and are therefore intrinsic permeabilities.

Finally permeability is a tensor property whose magnitude usually varies with the direction of measurement. In most sedimentary materials the maximum permeability is parallel to bedding.

### **Laboratory Determination of Permeability**

Permeability is determined by simply measuring the rate of flow of a fluid of known viscosity (usually air or nitrogen gas) through a sample under a known pressure gradient. Permeability can then be calculated from Darcy's Law (Equation 2.8). To prevent turbulent flow which would invalidate Darcy's Law, relatively low pressures are used. For horizontally drilled plugs permeability is measured parallel to the plug axis. For full diameter slabs three measurements are made: the maximum horizontal permeability the horizontal permeability at  $90^\circ$  and one vertical.

### **Accuracy of Permeability Determinations**

As mentioned for porosity determinations, core permeabilities will exceed the in situ reservoir value if the sample has expanded appreciably under the pressure release associated with removal from the subsurface, or has been damaged during coring or subsequent handling.

Secondly core permeabilities are measured with respect to air or nitrogen gas. Because gas molecules at low pressure are less subject to frictional drag on pore walls than liquids, gas flow rates may be twice as high as liquid rates. This so-called "Klinkenberg effect" can thus result in calculated permeabilities which are twice as high as they should be. Gas permeabilities are easily converted to liquid permeability (the permeability to gas is proportional to the mean pressure used during the measurement of flow), by applying a correction factor proportional to the pressure used in the determination.

## Appendix 2 Quantitative DST Interpretation

### A2.1 Drill Stem Test Procedure

A drillstem test (DST) is a short term production test conducted on a temporarily completed well. A DST tool, attached to the drill string, is lowered into the well bore and positioned opposite the geologic interval of interest. This interval is then sealed off from the mud column in the well bore by one or more inflatable packers. Oil industry DSTs are of a few hours duration, and usually comprise two periods of production during which formation fluids flow into the drill string (reducing the pressure in the formation) followed by shut-in periods during which the pressure buildup is monitored by pressure recorders mounted in the DST tool. The rate and nature of pressure recovery are determined by the hydraulic character of the geologic media in the isolated interval. From proper interpretation of the test data we can infer:

- i) The stable pore fluid pressure ( $p_i$ ) of the geologic interval tested
- ii) The permeability of the interval
- iii) The radius of investigation of the test.

### A2.2 Pressure versus Time Buildup Plots

#### 1 Horner Plots

A Horner (semi-log) plot, graphs the pressures recorded during the shut-in periods ( $p_{ws}$ ) on a linear vertical scale against a dimensionless time variable ( $t + \Delta t / \Delta t$ ) on a logarithmic horizontal scale. Here  $t$  is the cumulative flow time and  $\Delta t$  is the time elapsed since shut-in.

A number of simplifying assumptions are implicit in Horner analysis including:

- i) single phase fluid flow in the reservoir
- ii) radial flow to the well bore
- iii) horizontal reservoir of infinite extent
- iv) wells fully penetrate the reservoir

Ramey's idealized figure (Figure A2.1) shows a number of characteristic pressure buildup curves that may be generated during a DST

as they would appear on a Horner plot, and indicates their probable origin. Note that one shut-in period of a DST produces a single curve - the multiple curves on the figure represent numerous possibilities superimposed. The patterns of pressure buildup fall into three distinct phases.

1) **EARLY PHASE:** The early pressure buildup is dominated by flow within and immediately adjacent to the wellbore (collectively termed wellbore storage effects), and is independent of the geologic-hydraulic character of the tested interval. This phase of pressure buildup may reveal formation damage (permeability reduction around the wellbore caused by drilling), or stimulation (permeability enhancement due to induced fracturing or acid treatment). See curves A and B on Figure A2.1.

2) **MIDDLE PHASE:** A later phase of the shut-in response is controlled by flow within the formation. Pressure buildup during this phase is determined by the geologic-hydraulic character of the porous media within the tested interval. If flow through the formation to the well is radial, the buildup curve on a Horner plot will be a straight line whose slope is inversely proportional to the transmissivity of the medium (see curve C on Figure A2.1). This is the "correct" straight line for the determination of the formation permeability. If flow is non-radial (e.g., linear, bi-linear and spherical flow are all possible), then no meaningful straight line will appear on a Horner plot and the data must be analyzed on a different type of plot. I describe some of these alternative plots below.

3) **LATE PHASE:** The radius of investigation during a DST increases with time. Reservoir boundary effects may be evident in the final phase of the pressure buildup. Pressure depletion due to drawdown within a small finite reservoir, or due to pumping in an adjacent well may also be apparent during this phase. See curves D and E on Figure A2.1. Note that abrupt discontinuities (e.g., 'impermeable' faults, reef margins etc.) will be easier to detect and interpret than gradual changes in permeability or formation thickness which may give the appearance of some kind of non-radial flow. Since petroleum industry DST's are usually short term tests

with a radius of investigation limited to a few tens of metres, boundary effects are rarely seen in practice.

Two differences between Figure A2.1 and a typical oil industry DST should be noted. First the duration of a typical DST is rather short so two log cycles are usually sufficient to display the entire pressure buildup (Ramey's figure shows five log cycles). Second, since most DSTs involve two periods of flow and shut-in, two distinct curves are generated. Because the second flow and shut-in periods are longer than the first, the correct straight line usually develops during the second shut-in period.

## **2 Plots Relevant to Non-Radial Flow**

Different fluid flow geometries (radial, linear and spherical flow etc.) are governed by different flow equations. A graphical solution to a given equation will, in the absence of wellbore effects plot as a straight line on a graph of pressure versus some function of time, with appropriate axes (Ershaghi and Woodbury, 1985, p. 335). It is theoretically possible therefore, to diagnose the type of flow by graphing a single data set on numerous type plots and simply searching for a straight line. The type of plot on which a straight line appears will diagnose the relevant flow geometry.

### ***The Log-Log Plot***

#### **Well-Bore Storage Effects**

Since radial flow is dominant in many porous media, a Horner plot is the best bet for a "first look" at the data. A useful adjunct to the Horner plot, is a log-log graph of the pressure rise  $p_{ws} - p_{wf}$ , where  $p_{wf}$  is the pressure recorded at the end of the flow period prior to shut-in, versus  $\Delta t$  the time elapsed since shut-in. On such a plot, well bore storage effects will produce a straight line with unit slope. Having identified the time at which wellbore storage effects end on a log-log plot, one can return to the Horner plot and identify the start of the correct semi-log straight line by simply eliminating storage effects.

### Linear Flow in Vertical Fractures

The log-log plot is also useful for identifying linear flow in vertical fractures which is manifest as a distinctive straight line with a half slope.

#### **Linear, Spherical and Bi-linear Flow Plots**

Other plots of pressure versus some function of time which theoretically yield straight lines for specific types of flow include:  $p_{ws}$  versus  $\sqrt{\Delta t}$  for linear flow,  $p_{ws}$  versus  $1/\sqrt{\Delta t}$  for spherical flow, and  $p_{ws}$  versus  $\sqrt[4]{\Delta t}$ , for bi-linear flow. Characteristic curves for the first three flow types are shown in Figure A2.2.

The use of these plots in transient pressure analysis over the last few decades is described in an excellent review paper by Ramey (1982). Ershaghi and Woodbury (1985), are less enthusiastic about the diagnostic properties of such plots, and present field evidence that pressure versus time data for one particular known style of flow will often produce “pseudosraight” lines on two or more characteristic plots

### **A2.3 Formulas used in DST interpretation**

The stable formation pressure  $p_i$  (known as the “initial” pressure but which actually means the stable and possibly disturbed formation pressure at the time of the test) can be derived from:

$$p_{ws} = p_i - m * \log \frac{t + Dt}{Dt},$$

where

- $p_{ws}$  = shut-in pressure (kPa)
- $p_i$  = “initial” (stable) formation pressure (kPa)
- $m$  = slope of the build up curve
- $t$  = cumulative flow time (min)
- $Dt$  = time elapsed since shut-in (min).

which is an equation for a straight line of the form  $y = a + m * x$ . Thus a plot of  $p_{ws}$  versus  $\log (t + \Delta t / \Delta t)$ , produces a straight line of slope  $m$  whose intercept on the vertical axis at  $\log (t + \Delta t / \Delta t) = 1$  is equal to  $p_i$ , the stable formation pressure. In practice a semi-log plot is used with  $(t + \Delta t / \Delta t)$  plotted on the log axis. The slope ( $m$ ) of the Horner plot

“correct straight line” for liquid analysis (kPa/log cycle) determined from the final buildup is

$$m = \frac{2121 B q_a \mu}{k b},$$

where  $B$  = OFVF, the oil formation volume factor (m<sup>3</sup>/m<sup>3</sup>)  
 $q_a$  = average liquid production rate during test (m<sup>3</sup>/day)  
 $\mu$  = dynamic viscosity of liquid in cP (mPa.s)  
 $k$  = permeability (millidarcy)  
 $b$  = net pay thickness (m)

An increase in slope of a buildup curve with time elapsed may indicate a decrease in the permeability or thickness or an increase in fluid viscosity e.g., a fluid interface in a petroleum pool. It is assumed that the production rate remains constant throughout the test.

The permeability of the formation to reservoir fluids and the approximate radius of investigation of the test are determined as follows:

$$\text{Transmissibility} = \frac{k b}{m} = \frac{2121 B q_a}{m},$$

$$\text{Permeability} = k = \frac{2121 B q_a}{m} * \frac{m}{b},$$

$$\text{Approx radius of investigation} = 0.00049 * \sqrt{\frac{k t}{f m c}}$$

where  $k$  = permeability (millidarcy)  
 $t$  = cumulative flow time (min)  
 $f$  = effective porosity (fraction)  
 $m$  = dynamic viscosity of liquid in cP (mPa.s)  
 $c$  = liquid compressibility (per kPa)

I constructed Horner and log-log plots for 24 wells in the present study area, and used the formulas given above to calculate the stable formation pressure, formation permeability and radius of investigation of the test.

A sample of these plots and my DST analysis charts are presented below.

**A2.4 DST Analysis Charts, Horner and Log-Log Plots for Selected DSTs.**

<b>DLS Location</b>	<b>DST#</b>	<b>Calculated Head (m)</b>	<b>My Evaluation of Test Quality</b>
10-34-91-24W4	1	616	Reliable
11-33-94-22W4	1	1030*	Supercharged
6-31-98-22W4	1	1039*	Faulty Device
3-31-100-22W4	2	1062*	Supercharged

\* Used by Tóth (1978, Figure 16) for Keg River Aquifer potentiometric surface.



BRITISH Units		RESERVOIR Parameters		FLUID Parameters	
DLS Well ID	10-34-91-24-W4	Thickness (m)	10	Density @STP	
KB (ft)	1785	Porosity Frac	5.3%	Viscosity cP	0.65
DST#	1	Temp (C) !!	40	beta (per kPa)	4.80E-07
Depth from	3610	alpha (per kPa)	4.77E-08		
Depth to	3680				
Elev from	-1825	Date of Test	26 Mar 1968		
Elev to	-1895				
Formation	KEG RIVER				
BUILDUP data		Time min	Pressure psi	HORNER Plot	
Initial Hydrostatic			2006	extrapolation	slope psi
Pre-Flow	3		90	psi	per log cycle
2nd Flow	60		400		
Initial Shut In	30		1648	1672	593
Final Shut In	90		1632	1679	206
Final Hydrostatic			2006		
Initial minus Final (psi)		Hydrostatic	0	Horner Extrap	-7
% Depletion (>3% is serious)			0.00%		-0.4%
Horner Slope Ratio (1st:2nd)					2.88
RECORDER		CORE DATA		none	
Type	MECH	Metric Equivalents	Depth from		
Depth ft	3633	1107	Depth to		
Elevation ft	-1848	-363	Perm a.m. (mD)		
Range psi	4000	27579	Porosity		
Mech error (+/-)	10	69			
PIPE SIZES		capacity m3/m	volume m3	flow rate m3/d	
DC ID (inch)	2.875	.004	.179	26.6	
DC length (ft)	140.35				
hole radius (mm) !!	100			total volume m3	
Pipe ID (inch) est.	3.826	.007	.983	1.162	
FLUID RECOVERY (ft)		density (lb/gal)	RESULTS (metric units)		
water	575	10.100	Transmissibility (mD*m/cP)	40	
mud			Capacity (mD m)	26	
oil			Permeability (mD)	2.6	
gas			Approx Investigation Radius (m)	49	
TOTAL	575		Skin Factor (+ve = damage)	2	
COMMENTS			Dynamic Pressure Increment (kPa)	702	
Final SI extrapolation used to calculate head			FW Equip Hydraulic Head (m)	616	
Well "cleaned up" on final SI			+/- mech error (m)	7	
Pressure is representative			FW head elevation above KB (m)	72	
ABBREVIATIONS					
alpha	aquifer compressibility				
beta	water compressibility				
mech	mechanical				
DC	drill collar				
SI	shut in				

Table A2.1 DST Analysis Table for 10-34-91-24W4, DST#1

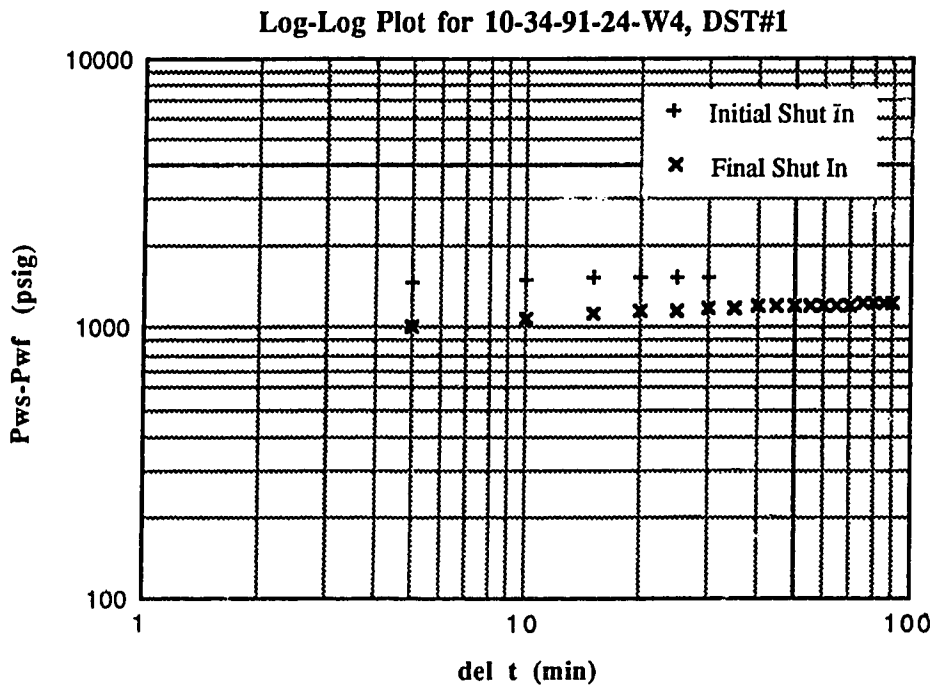
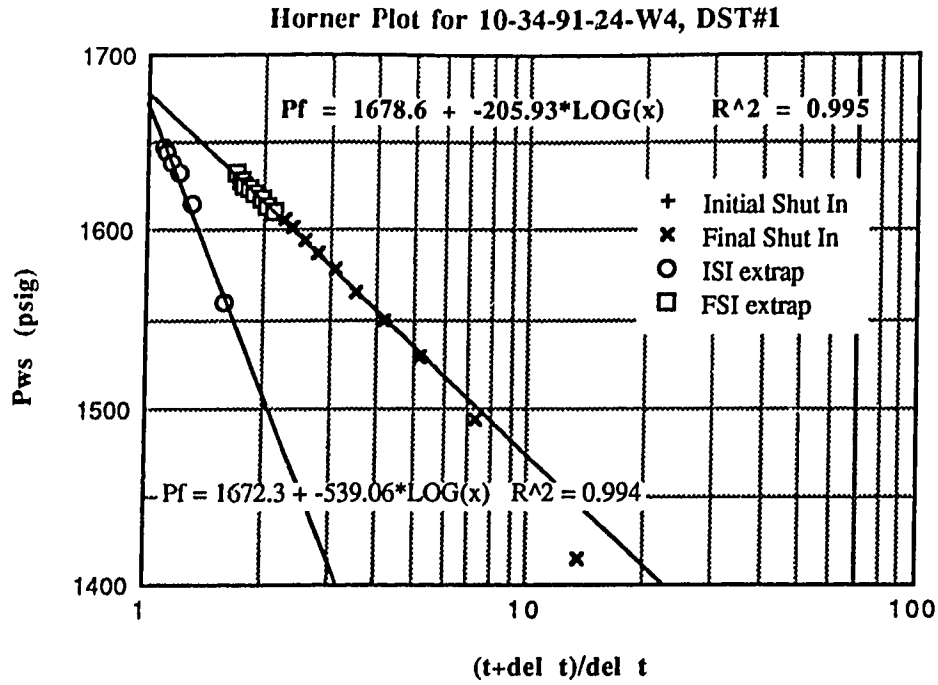


Figure A2.3 Horner and Log-Log Plots for 10-34-91-24W4, DST#1

BRITISH Units		RESERVOIR Parameters		FLUID Parameters	
DLS Well ID	11-33-94-22-W4	Net Pay (m) est.	10	Density @STP	1.27
KB (ft)	2564	Porosity Frac	5.3%	Viscosity cP	0.65
DST#	1	Temp (C) !!	40	beta (per kPa)	4.80E-07
Depth from	4143	alpha (per kPa)	4.77E-08		
Depth to	4227				
Elev from	-1579	Date of Test	19 Feb , 1973		
Elev to	-1663				
Formation	KEG RIVER				
BUILDUP data		Time min	Pressure psi	extrapolation	slope psi
Initial Hydrostatic			2371	psi	per log cycle
Pre-Flow	5		79		
Final Flow	60		92		
Initial Shut In	60		2100	2157	1626
Final Shut In	90		1883	2086	847
Final Hydrostatic			2362		
		Hydrostatic	Horner Extrap		
Initial minus Final (psi)		9	71		
% Depletion (>3% is serious)		0.38%	3.3%		
Horner Slope Ratio (initial:final)			1.9		
RECORDER		CORE DATA		none in Kegr	
Type	MECH	Metric Equivalents	Depth from		
Depth (ft)	4154	1266	Depth to		
Elevation (ft)	-1590	-485	Perm a.m. (mD)		
Range (psi)	4000	27579	Porosity		
Mech error (+/-)	10	69			
PIPE SIZES		capacity m3/m	volume m3	flow rate m3/d	
DC ID (inch)	2.875	.004	.443	9.825	
DC length (ft)	347.39				
hole radius (mm) !!	100			total volume m3	
Pipe ID (inch)	3.826	.007	.000	.443	
FLUID RECOVERY (ft)		density or concn	RESULTS (metric units)		
water			Transmissibility (mD*m/cP)	4	
mud	90	10.700	Capacity (mD m)	2	
oil			Permeability (mD)	0.2	
gas			Approx Investigation Radius (m)	15	
TOTAL	90		Skin Factor (+ve = damage)	-2	
COMMENTS	Lost circ at 4159' depth, 15 Feb, 1973.		FW Equiv Hydraulic Head (m)	1030	
	Hydraulic head 248 m above ground		+/- mech error (m)	7	
	Serious depletion - reservoir SUPERCHARGED		Dynamic Pressure Increment (kPa)	2439	
	Keg River = 32 m thick (no pinnacle reef)		FW head elevation above KB (m)	248	
ABBREVIATIONS					
alpha	aquifer compressibility				
beta	water compressibility				
mech	mechanical				
DC	drill collar				
SI	shut in				

Table A2.2 DST Analysis Table for 11-33-94-22W4, DST#1

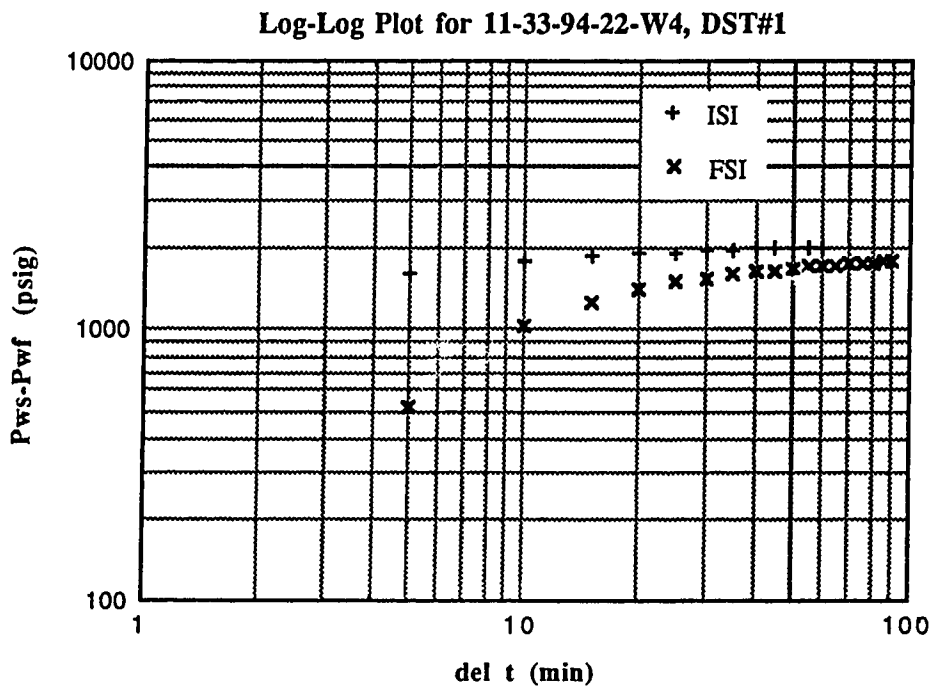
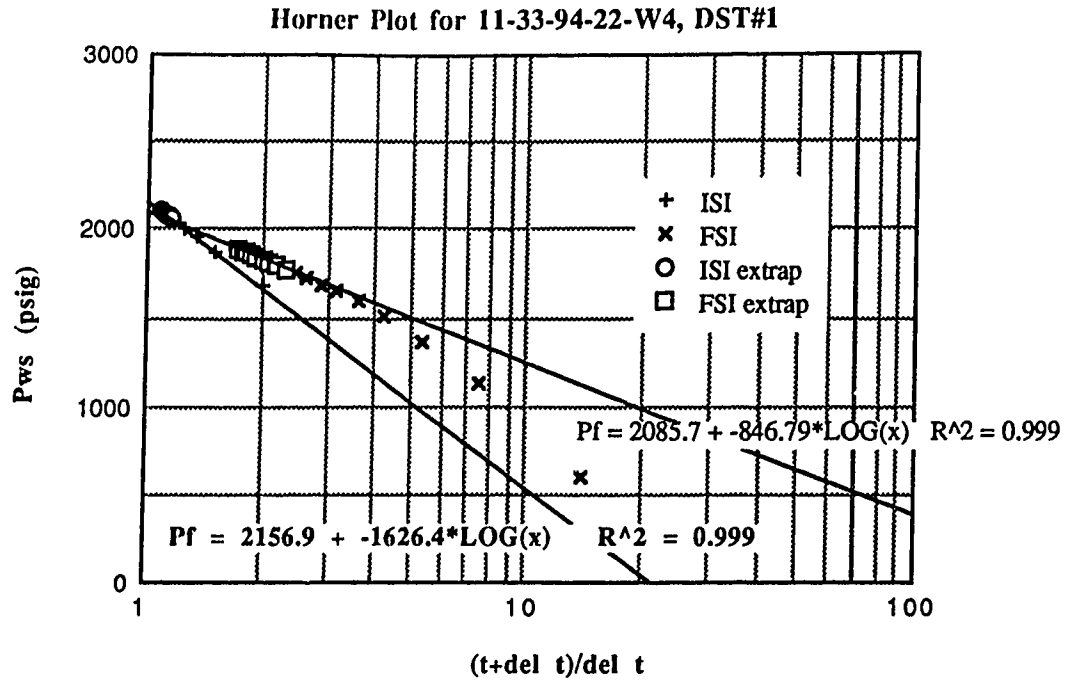


Figure A2.4 Horner and Log-Log Plots for 11-33-94-22W4, DST#1

BRITISH Units		RESERVOIR Parameters		FLUID Parameters	
DLS Well ID	6-31-98-22-W4	Net Pay (m) est.	10	Density @STP	
KB (ft)	2189	Porosity Frac	5.7%	Viscosity cP	0.69
DST#	1	Temp (C) DST	36.63	beta (per kPa)	4.80E-07
Depth from	3484	alpha (per kPa)	4.98E-08		
Depth to	3750				
Elev from	-1295	Date of Test	28 Feb, 1968		
Elev to	-1561				
Formation	MUSKEG-KEG RIVER			<b>HORNER Plot</b>	
<b>BUILDUP data</b>	<b>Time min</b>	<b>Pressure psi</b>	<b>extrapolation</b>	<b>slope psi</b>	
1st Hydrostatic		1992	psi	per log cycle	
Pre-Flow	5	98			
2nd Flow	240	960			
1st Shut In	60	1989	2034	1393	
2nd Shut In	120	1860	2016	323	
2nd Hydrostatic		1968			

	Hydrostatic	Horner Extrap
Initial minus Final (psi)	24	18
% Depletion (>3% is serious)	1.20%	0.9%
Horner Slope Ratio (1st:2nd)		4.3

RECORDER		Metric Equivalents	CORE DATA	
Type	MECH		Depth from (m)	1080.2
Depth (ft)	3464	Depth to (m)	1111.0	
Elevation (ft)	-1275	Perm a.m. (mD)	0.35	
Range (psi)	3300	Perm g.m. (est.)	0.012	
Mech error (+/-)	8.25	Porosity	5.73%	
<b>PIPE SIZES</b>		<i>capacity m3/m</i>	<i>volume m3</i>	<i>flow rate m3/d</i>
DC ID (inch)	2.875	4.19E-03	2.30E-01	1.25E+01
DC length (ft)	180			
hole radius (mm) !!	111.125			total volume m3
Pipe ID (inch)	2.9	4.26E-03	1.90E+00	2.13E+00

FLUID RECOVERY (ft)		density or concn	RESULTS (metric units)	
water	1640	1.234=0.533psi/ft	Transmissibility (mD*m/cP)	12
mud		10=0.519psi/ft	Capacity (mD m)	8
oil			Permeability (mD)	0.824
gas			Approx Investigation Radius (m)	50
TOTAL	1640		Skin Factor (+ve = damage)	-2
<b>COMMENTS</b>		Keg River Fm 73m thick (pinnacle reef?)	FW Equiv Hydraulic Head (m)	1039
Final flow pressure=960psi/0.533=1801 ft recovery?			+/- mech error (m)	6
Fw head 372 m above ground!			Dynamic Pressure Increment (kPa)	3656
Extrapolated pressure > hydrostatic, recorder reading high?			FW head elevation above KB (m)	372
<b>ABBREVIATIONS</b>				
alpha	aquifer compressibility			
beta	water compressibility			
mech	mechanical			
DC	drill collar			
SI	shut in			

Table A2.3 DST Analysis Table for 6-31-98-22W4, DST#1

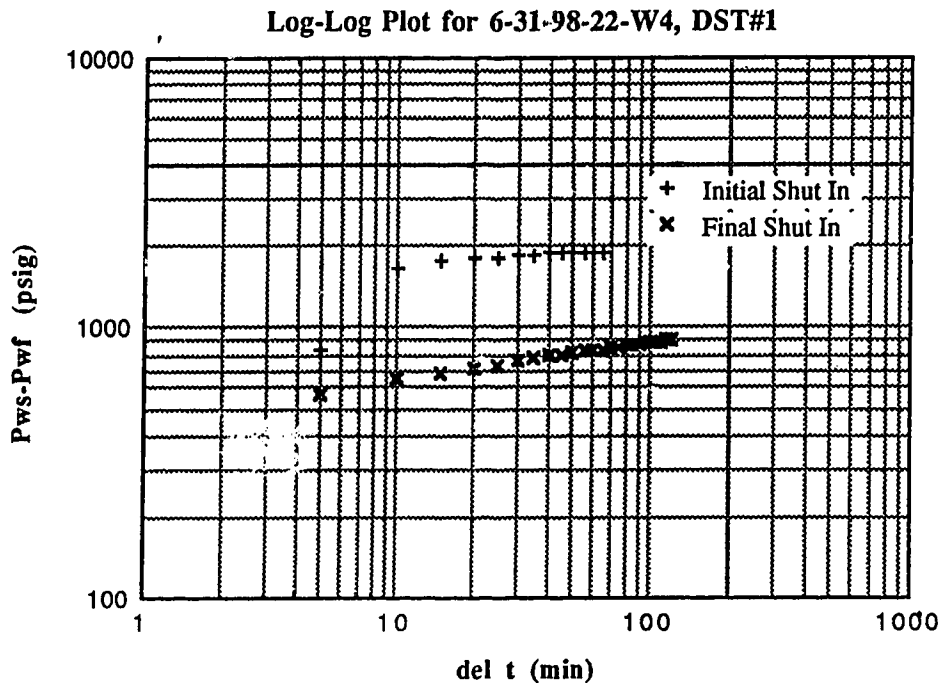
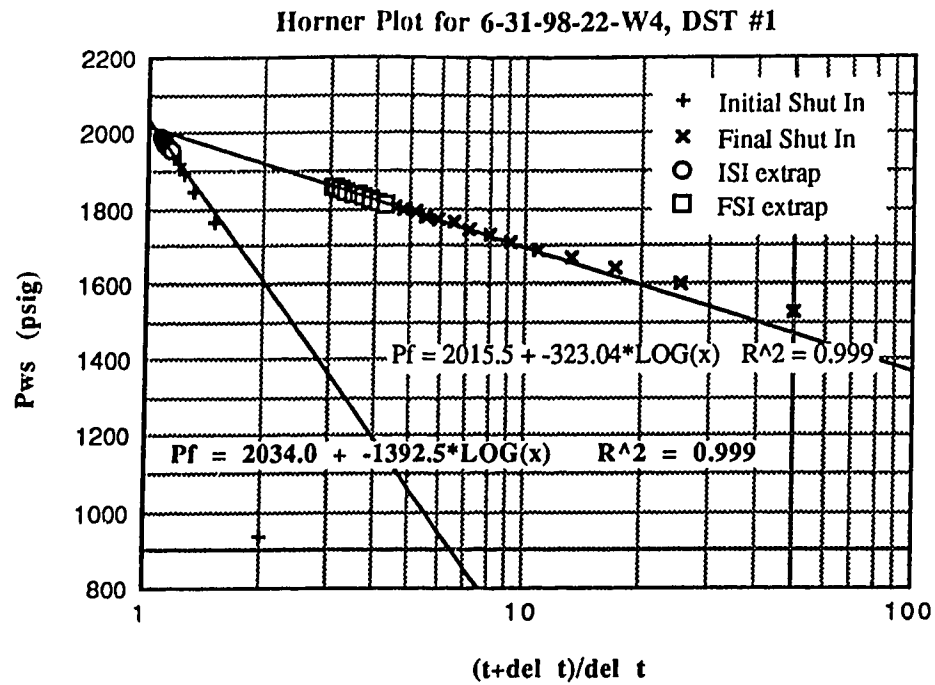


Figure A2.5 Horner and Log-Log Plots for 6-31-98-22W4, DST#1

BRITISH Units		RESERVOIR Parameters		FLUID Parameters	
DLS Well ID	3-31-100-22-W4	Net Pay (m) est.	10	Density @STP	
KB (ft)	2351	Porosity Frac	2.5%	Viscosity cP	0.65
DST#	2	Temp (C) !!	40	beta (per kPa)	4.80E-07
Depth from	3650	alpha (per kPa)	3.35E-08		
Depth to	3710				
Elev from	-1299	Date of Test	1 March, 1970		
Elev to	-1359				
Formation	KEG RIVER				
				<b>HORNER Plot</b>	
<b>BUILDUP data</b>	<b>Time min</b>	<b>Pressure psi</b>	<b>extrapolation</b>	<b>slope psi</b>	
1st Hydrostatic		2117	psi	per log cycle	
Pre-Flow	10	143			
2nd Flow	150	236			
1st Shut In	60	2074	2086	184	
2nd Shut In	150	1921	1972	162	
2nd Hydrostatic		2098			

	Hydrostatic	Horner Extrap
Initial minus Final (psi)	19	114
% Depletion (>3% is serious)	0.90%	5.5%
Horner Slope Ratio (1st:2nd)		1.1

RECORDER		CORE DATA		
Type	MECH	Metric Equivalents	Depth from	
Depth (ft)	3672	1119	1069.848	
Elevation (ft)	-1321	-403	Depth to	
Rang : (psi)	4000	27579	1106.424	
Mech error (+/-)	10	69	Perm a.m. (mD)	
			0.1	
			Perm g.m. est.	
			0.002	
			Porosity	
			2.5%	
<b>PIPE SIZES</b>		<i>capacity m3/m</i>	<i>volume m3</i>	<i>flow rate m3/d</i>
DC ID (inch)	2.875	.004	.443	6.249
DC length (ft)	347.39			
hole radius (mm) !!	111.125			
Pipe ID (inch) est.	3.64	.007	.251	total volume m3
				.694

FLUID RECOVERY (ft)		density or concn	RESULTS (metric units)	
water	235		Transmissibility (mD*m/cP)	12
mud	235		Capacity (mD m)	8
oil			Permeability (mD)	0.8
gas			Approx Investigation Radius (m)	62
TOTAL	470		Skin Factor (+ve = damage)	10
<b>COMMENTS</b>			FW Equiv Hydraulic Head (m)	1062
Head 345m above ground!			+/- mech error (m)	7
SUPERCHARGE and depletion of small reservoir			Dynamic Pressure Increment (kPa)	3392
Keg River = 105m (pinnacle)			FW head elevation above KB (m)	345
<b>ABBREVIATIONS</b>				
alpha	aquifer compressibility			
beta	water compressibility			
mech	mechanical			
DC	drill collar			
SI	shut in			

Table A2.4 DST Analysis Table for 3-31-100-22W4, DST#2

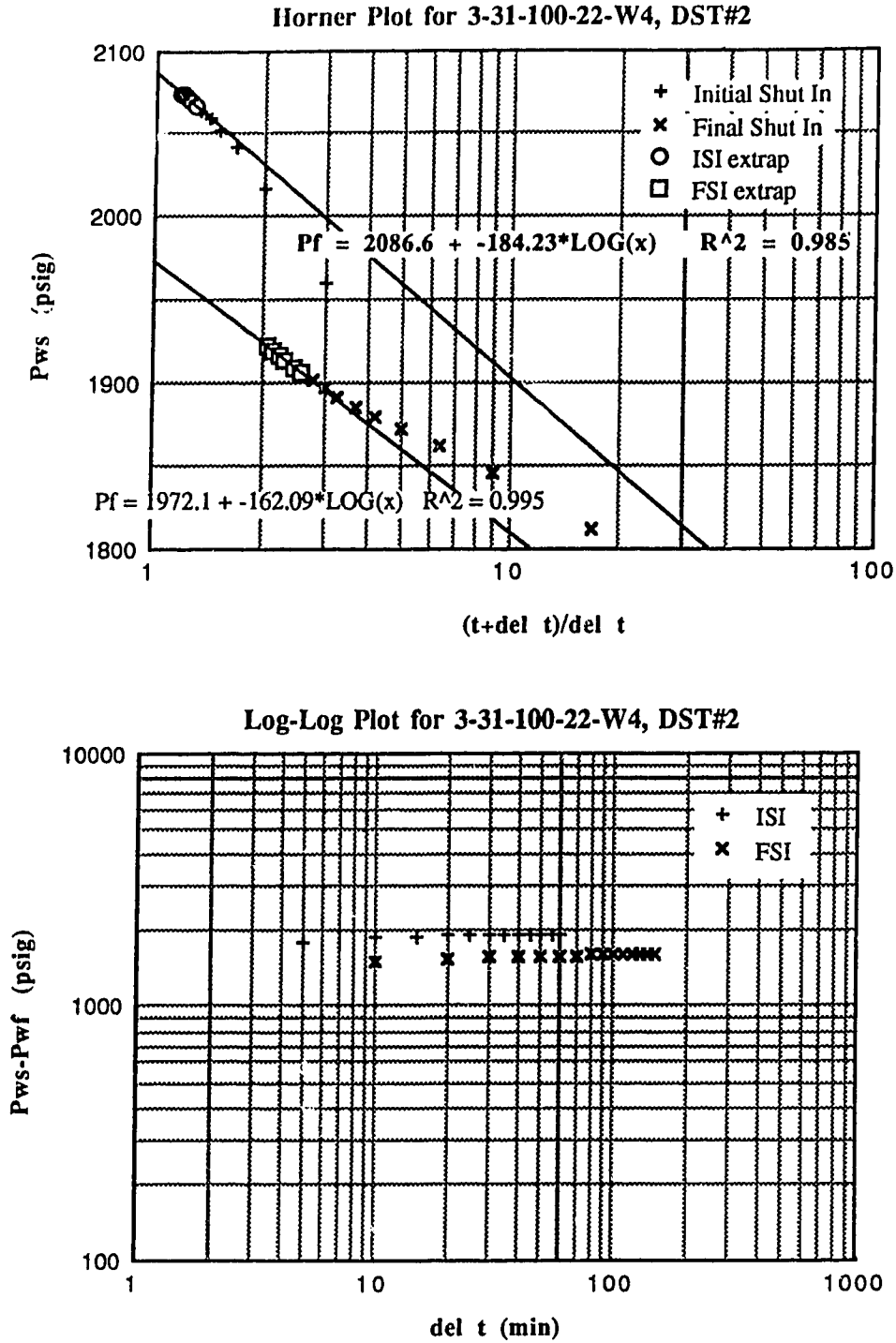


Figure A2.6 Horner and Log-Log Plots for 3-31-100-22W4, DST#2



## Appendix 3 Instrument Error

### A3.1 Pressure

#### DST pressure recorders

According to the DST Manual produced by Lynes United Services (Ehrmann, undated), pressure recorder instrument errors can be calculated as:

Mechanical recorder error = +/- 0.25% of full range

Electronic recorder error = +/- 0.05% of full range

Both types of recorder are most efficient when operating in the middle of full range. In the present study area, the Keg River - Granite Wash aquifer lies at a depth of around 1500 m. Nominal hydrostatic pressure is therefore about 15 000 kPa g, (10 kPa/m \* 1500 m) so the recorder range is usually set at about 30 000 kPa (4354 psi). The average instrument errors in the present study area are thus:

+/- 75 kPa, for a mechanical recorder set at 30 000 kPa full range

+/- 15 kPa, for an electronic recorder set at 30 000 kPa full range

These pressures are equivalent to between 1 and 8 m of fresh water hydraulic head respectively.

### A3.2 Temperature

#### BHT temperature recorders

Most deep subsurface temperature data are obtained during the routine logging of oil wells. A temperature sensitive device (max temperature mercury thermometer in old wells or an electrical temperature sensor in more recent ones) is lowered into the borehole as part of a geophysical tool, and the temperature recorded. Theoretically, the degree to which this recorded temperature represents the true formation temperature is affected by three factors:

- 1) The reading accuracy of the temperature measuring device
- 2) The thermal instability of the bore hole fluid
- 3) The thermal disequilibrium around the well due to drilling

### **Instrument Accuracy**

Mercury maximum thermometers measure a single temperature per run which is assigned to the maximum depth reached by the tool. According to Gretener (p.35) temperatures are at best accurate to +/- 0.1 C or F.

Electrical devices are more accurate, modern thermistors for example have a resolution of +/- 0.01 C (0.02 F).

### **Thermal Instability**

Hales (1931) investigated the thermal stability of a fluid filled tube subjected to a temperature gradient. His calculations indicate that most oil wells will be thermally unstable, the drilling fluid flowing by convective overturn within the borehole. Gretener (1981, p.27,31) presents field evidence which confirms Hales' calculations and concludes that in oilwells, thermal instabilities of +/- 0.02 C (+/- 0.04 F) are common, which places a limit on the resolution of temperature logging tools.

### **Thermal Disequilibrium**

The action of drilling and the circulation of drilling fluid in the borehole disturb formation temperatures. In general the deep portion of the borehole is cooled and the shallow part is warmed (see Figure 2.12). Bottom hole temperatures are recorded before thermal equilibrium is reestablished and are therefore lower than the true formation temperature. The method I used to correct BHTs is given in Section 3.3.2.

### **Reporting Errors**

Historically BHTs have been collected as a low priority task under uncontrolled conditions so recording and reporting errors are both possible. No systematic correction can be made for such errors other than to cull wildly erroneous values. Leblanc et al (1982) assume an absolute error of  $\pm 5^{\circ}\text{C}$  in reported BHTs.

### **A3.3 Water Chemistry**

According to a recent USGS publication (Hem, 1989, p.163) major ions can be determined under optimum conditions with an accuracy of  $\pm 2\%$  for solutes present at concentrations exceeding 100 mg/L, and with an accuracy of  $\pm 10\%$  for solutes at less than 1 mg/L.

**Appendix 4 Culled Data Files**

**A4.1 Culled Pressure Data**

LE	L	S	T	R	M	ESQ	DST#	Formation†	Depth (m)	Pressure (kPa)	Elevation (m)	FW Head (m)	P/d Ratio (kPa/m)	Fluid Recovery	Extrap By
0	15	10	89	2	5	0	1	mshg-kegr	1436	13419	-645	722	9.3	w	CIFE
0	15	10	89	2	5	0	2	kegr	1449	13591	-658	726	9.4	w	CIFE
0	5	12	89	2	5	0	1	kegr	1475	13618	-667	719	9.2	w	CIFE
0	13	28	89	2	5	0	3	kegr	1416	13390	-663	701	9.5	w	CIFE
0	13	28	89	2	5	0	4	mshg-kegr	1422	13445	-668	701	9.5	m	CIFE
0	5	22	89	3	5	0	1	mshg-kegr	1472	13955	-687	734	9.5	o	CIFE
0	5	22	89	3	5	0	2	kegr	1491	14121	-705	733	9.5	w	CIFE
0	3	27	89	3	5	0	3	kegr	1489	14238	-719	731	9.6	w	CIFE
0	3	34	89	3	5	0	1	mshg-kegr	1463	13811	-688	719	9.4	o	CIFE
0	11	29	89	4	5	0	2	kegr	1477	14314	-729	729	9.7	w	CIFE
0	11	29	89	4	5	0	1	kegr-cncg	1492	14632	-744	746	9.8	w	CIFE
0	9	7	89	7	5	0	3	wbmn	453	2517	131	387	5.6	w	CIFE
0	8	19	89	7	5	0	1	gtng	414	1875	155	346	4.5	w	CIFE
0	8	19	89	7	5	0	3	gtng - wbmn	420	2034	148	355	4.8	m	CIFE
0	16	19	89	7	5	0	1	cncg-gmw	1455	15783	-891	717	10.9	w	CIFE
0	1	10	89	8	5	0	1	gtng	22	1948	150	349	4.8	g	CIFE
0	1	10	89	8	5	0	2	gmw-pcmb	39	15266	-936	618	10.3	o	CIFE
0	9	10	89	8	5	0	1	mnvl	386	1885	164	355	4.9	g	CIFE
0	11	18	89	8	5	0	1	kegr	1405	15762	-899	706	11.2	w	CIFE
0	6	22	89	8	5	0	2	gtng	389	1855	141	330	4.8	w	CIFE
0	3	24	89	8	5	0	2	mnvl	165	1255	386	514	7.6	w	CIFE
0	3	24	89	8	5	0	5	kegr-gmw-pcmb	1446	15459	-895	679	10.7	w	CIFE
0	16	26	89	9	5	0	2	gmw	1411	15693	-912	686	11.1	w	CIFE
0	7	29	89	9	5	0	2	kegr-gmw-pcmb	1403	15534	-899	683	11.1	o	CIFE
0	4	31	89	9	5	0	1	kegr-gmw	1436	15838	-925	688	11	w	CIFE
0	7	35	89	9	5	0	3	kegr-gmw	1410	15824	-911	701	11.2	w	CIFE
0	7	35	89	9	5	0	2	gmw	1413	15872	-913	703	11.2	w	CIFE
0	7	35	89	9	5	0	1	gmw-pcmb	1417	16024	-918	714	11.3	w	CIFE

LE	L	S	T	R	M	ESQ	DST#	Formation†	Depth (m)	Pressure (kPa)	Elevation (m)	FW Head (m)	P/d Ratio (kPa/m)	Fluid Recovery	Extrap By
0	12	11	89	10	5	0	2	kegr-grnw	1461	15700	-923	676	10.7	w	CIFE
0	4	25	89	10	5	0	1	gnw	1449	15769	-922	684	10.9	w	CIFE
0	6	28	89	10	5	0	3	gnw	1497	16093	-944	695	10.7	w	CIFE
0	6	29	89	10	5	0	2	kegr-grnw	1497	15872	-927	689	10.6	w	CIFE
0	10	32	89	10	5	0	2	gnw	1486	15990	-926	702	10.8	o	CIFE
0	10	32	89	10	5	0	3	gnw	1506	16252	-946	709	10.8	o	CIFE
0	1	5	89	11	5	0	2	gnw-pcmb	1602	16127	-962	681	10.1	o	CIFE
0	1	11	89	11	5	0	1	kegr-grnw	1548	15921	-942	679	10.3	w	CIFE
0	1	33	90	1	5	0	1	kegr	1176	12087	-608	623	10.3	m	CIFE
0	9	7	90	3	5	0	3	mshg-kegr-cncg-pcmb	1458	13824	-690	718	9.5	w	CIFE
0	10	9	90	3	5	0	1	kegr	1478	13838	-689	720	9.4	o	CIFE
0	7	13	90	3	5	0	1	mshg-kegr	1370	13597	-653	731	9.9	o	CIFE
0	8	14	90	3	5	0	1	mshg-kegr	1401	13631	-667	721	9.7	w	CIFE
0	14	16	90	3	5	0	1	kegr	1445	13997	-702	723	9.7	m	CIFE
0	8	18	90	3	5	0	2	mshg-kegr	1430	13500	-686	688	9.4	o	CIFE
0	8	18	90	3	5	0	1	mshg-kegr	1439	13790	-695	709	9.6	m	CIFE
0	10	21	90	3	5	0	1	mshg-kegr	1343	13811	-692	714	10.3	w	CIFE
0	10	21	90	3	5	0	2	mshg-kegr	1345	13783	-694	709	10.2	w	CIFE
0	4	25	90	3	5	0	1	mshg-kegr	1290	13452	-661	709	10.4	o	CIFE
0	16	30	90	3	5	0	1	mshg-kegr	1323	13756	-701	700	10.4	m	CIFE
0	2	36	90	3	5	0	1	kegr	1321	13542	-683	696	10.3	w	CIFE
0	10	32	90	5	5	0	2	kegr	1481	14169	-748	695	9.6	o	CIFE
0	10	32	90	5	5	0	1	kegr	1486	14259	-753	699	9.6	w	CIFE
0	10	35	90	5	5	0	3	slvp	1201	12935	-529	789	10.8	m	CIFE
0	10	35	90	5	5	0	2	mshg-kegr	1432	14321	-760	698	10	w	CIFE
0	3	5	90	7	5	0	2	slvp	1185	11515	-643	530	9.7	w	CIFE
0	10	1	90	8	5	0	1	gng	369	1931	155	352	5.2	o	CIFE
0	4	3	90	8	5	0	4	kegr-grnw	1404	15645	-895	699	11.1	w	CIFE

LE	L	S	T	R	M	ESQ	DST#	Formation†	Depth (m)	Pressure (kPa)	Elevation (m)	FW Head (m)	P/d Ratio (kPa/m)	Fluid Recovery	Extrap By
0	5	25	90	8	5	0	2	slvp - grnw	1197	11659	-693	494	9.7	m	CIFE
0	5	25	90	8	5	0	3	kegr-grnw	1390	15734	-886	716	11.3	w	CIFE
0	3	31	90	8	5	0	2	mshg	1374	15334	-878	684	11.2	w	CIFE
0	3	12	90	9	5	0	4	kegr-grnw	1400	15748	-901	702	11.3	w	CIFE
0	7	6	90	10	5	0	2	kegr-grnw	1511	16121	-941	701	10.7	o	CIFE
0	7	6	90	10	5	0	4	grnw-pcmb	1516	16231	-946	706	10.7	w	CIFE
0	3	11	90	10	5	0	1	kegr-grnw-pcmb	1458	15927	-931	691	10.9	w	CIFE
0	7	15	90	10	5	0	3	kegr	1447	15796	-920	689	10.9	w	CIFE
0	11	27	90	10	5	0	3	wbinn	631	4337	-93	349	6.9	w	CIFE
0	11	27	90	10	5	0	2	wibr	675	4771	-137	349	7.1	w	CIFE
0	14	19	90	12	5	0	3	bnff	628	3572	140	503	5.7	w	CIFE
0	10	23	90	12	5	0	2	slvp	1529	13473	-816	556	8.8	m	CIFE
0	10	23	90	12	5	0	1	mshg-grnw-pcmb	1683	16451	-970	706	9.8	w	CIFE
0	6	35	90	12	5	0	1	gting	600	2599	138	402	4.3	w	CIFE
0	10	2	90	13	5	0	1	bnff	577	4123	147	566	7.1	w	CIFE
0	6	23	90	13	5	0	6	slvp	1614	13928	-839	579	8.6	o	CIFE
0	5	24	90	13	5	0	2	slvp	1643	14142	-858	582	8.6	w	CIFE
0	2	32	90	13	5	0	1	slvp	1641	14059	-831	600	8.6	m	CIFE
0	8	28	91	2	5	0	1	kegr	1197	12383	-643	618	10.3	w	CIFE
0	2	21	91	3	5	0	2	mshg-kegr	1314	13776	-692	710	10.5	w	CIFE
0	13	1	91	5	5	0	7	grsm	707	3861	-49	344	5.5	o	CIFE
0	9	4	91	5	5	0	1	mshg-kegr	1425	14066	-725	707	9.9	o	CIFE
0	9	4	91	5	5	0	3	mshg-kegr	1425	13997	-725	706	9.8	o	CIFE
0	9	4	91	5	5	0	2	kegr	1441	14149	-741	699	9.8	o	CIFE
0	7	5	91	5	5	0	1	kegr-pcmb	1477	14217	-745	703	9.6	o	CIFE
0	8	7	91	5	5	0	1	mshg-kegr	1409	14245	-752	698	10.1	g	CIFE
0	1	11	91	5	5	0	2	kegr	1333	14055	-716	715	10.5	o	CIFE
0	1	11	91	5	5	0	1	kegr	1342	14073	-725	708	10.5	o	CIFE

LE	L	S	T	T	R	M	ESQ	DST#	Formation†	Depth (m)	Pressure (kPa)	Elevation (m)	FW Head (m)	P/d Ratio (kPa/m)	Fluid Recovery	Extrap By
0	10	15	91	5	5	5	0	6	kegr	1359	14135	-747	692	10.4	w	CIFE
0	7	20	91	5	5	5	0	1	kegr	1372	14086	-737	697	10.3	o	CIFE
0	7	20	91	5	5	5	0	2	kegr	1388	14238	-754	696	10.3	w	CIFE
0	4	22	91	5	5	5	0	2	kegr	1333	14004	-728	698	10.5	o	CIFE
0	4	22	91	5	5	5	0	1	kegr	1345	14169	-740	702	10.5	w	CIFE
0	15	23	91	5	5	5	0	1	mshg-kegr	1306	13852	-710	701	10.6	o	CIFE
0	6	29	91	5	5	5	0	1	mshg-kegr	1314	13893	-694	721	10.6	o	CIFE
0	6	29	91	5	5	5	0	1	pcmb	1333	13976	-713	710	10.5	o	CIFE
0	16	30	91	5	5	5	0	2	mshg-kegr	1342	13797	-726	679	10.3	o	CIFE
0	8	4	91	6	5	5	0	1	kegr	1441	14514	-789	689	10.1	o	CIFE
0	12	4	91	6	5	5	0	1	mshg-kegr	1401	14535	-776	704	10.4	o	CIFE
0	13	10	91	6	5	5	0	3	kegr	1436	14452	-782	689	10.1	w	CIFE
0	13	10	91	6	5	5	0	2	kegr	1451	14748	-798	704	10.2	w	CIFE
0	9	35	91	6	5	5	0	1	kegr	1378	14576	-774	710	10.6	w	CIFE
0	7	23	91	7	5	5	0	1	cncg-gmw-pcmb	1363	15493	-853	725	11.4	o	CIFE
0	12	18	91	8	5	5	0	1	cncg-gmw	1393	15486	-896	681	11.1	w	CIFE
0	2	13	91	9	5	5	0	1	cncg-gmw-pcmb	1382	15569	-884	701	11.3	w	CIFE
0	2	25	91	9	5	5	0	2	cncg-gmw	1384	15390	-885	683	11.1	w	CIFE
0	7	26	91	9	5	5	0	1	grnw-pcmb	1387	15652	-883	711	11.3	w	self
0	5	3	91	10	5	5	0	1	kegr-pcmb	1481	15893	-931	688	10.7	w	CIFE
0	11	4	91	10	5	5	0	1	grnw-pcmb	1481	15659	-920	674	10.6	o	CIFE
0	2	5	91	10	5	5	0	1	kegr-gmw	1494	15810	-928	682	10.6	w	CIFE
0	12	25	91	10	5	5	0	1	kegr-gmw-pcmb	1436	15790	-908	700	11	w	CIFE
0	11	11	91	11	5	5	0	1	kegr-gmw	1633	16258	-951	705	10	w	self
0	8	16	91	11	5	5	0	1	mshg-kegr-gmw-pcmb	1715	15838	-940	673	9.2	w	CIFE
0	4	11	91	12	5	5	0	4	nlkn - gting	674	2289	138	371	3.4	w	CIFE
0	15	21	91	12	5	5	0	1	blsk	642	2344	150	389	3.7	w	CIFE
0	4	31	91	12	5	5	0	1	slvp - fvlim	1587	13645	-785	605	8.6	o	CIFE



LE	L	S	T	R	M	ESQ	DST#	Formation†	Depth (m)	Pressure (kPa)	Elevation (m)	FW Head (m)	P/d Ratio (kPa/m)	Fluid Recovery	Extrap By
0	8	32	91	12	5	0	1	slvp	1594	13597	-788	596	8.5	0	CIFE
0	11	8	92	3	5	0	1	kegr	1250	13142	-682	656	10.5	0	CIFE
0	6	19	92	3	5	0	2	mshg-kegr	1290	13211	-664	681	10.2	0	CIFE
0	8	1	92	4	5	0	1	mshg-kegr	1257	13266	-687	664	10.6	w	self
0	11	23	92	4	5	0	1	mshg-kegr	1253	13411	-670	695	10.7	0	CIFE
0	8	26	92	4	5	0	1	kegr	1244	13294	-655	698	10.7	0	CIFE
0	7	27	92	4	5	0	1	u.kegr	1248	13425	-674	693	10.8	0	self
0	7	27	92	4	5	0	2	m.kegr	1267	13611	-693	693	10.7	w	self
0	11	31	92	4	5	0	1	kegr	1266	13507	-696	680	10.7	0	CIFE
0	7	33	92	4	5	0	1	mshg-u.kegr	1226	14169	-676	767	11.6	0	self
0	7	33	92	4	5	0	2	m.kegr	1241	13631	-692	696	11	w	self
0	6	36	92	4	5	0	1	u.kegr	1294	13314	-669	687	10.3	w	self
2	5	3	92	5	5	0	2	kegr	1310	13831	-720	689	10.6	0	CIFE
0	4	10	92	5	5	0	1	mshg-kegr	1273	13921	-698	719	10.9	0	CIFE
0	13	30	92	6	5	0	2	mshg-kegr	1278	13542	-708	671	10.6	0	CIFE
0	11	23	92	7	5	0	1	kegr	1273	13583	-776	607	10.7	0	CIFE
0	10	16	92	9	5	0	2	mshg-kegr-gmw-pcmb	1283	14073	-783	650	11	m	CIFE
0	16	21	92	11	5	0	1	kegr-gmw-pcmb	1403	15576	-891	695	11.1	w	CIFE
0	16	30	92	11	5	0	1	kegr-gmw-pcmb	1642	16134	-953	690	9.8	w	CIFE
0	15	33	92	11	5	0	2	ntkn - gting	1713	16293	-962	698	5.5	w	CIFE
0	15	35	92	11	5	0	1	gting	548	2186	138	361	4	g	CIFE
0	6	11	92	13	5	0	1	ntkn - gting	468	2108	151	365	4.5	m	CIFE
0	10	30	92	13	5	0	1	gting	682	2275	137	368	3.3	m	CIFE
0	10	30	92	13	5	0	1	gting	612	2779	98	381	4.5	w	CIFE
0	10	30	92	13	5	0	1	gting	612	2786	98	382	4.6	w	CIFE
0	10	30	92	13	5	0	2	wbrmn	689	3468	21	375	5	m	CIFE
0	16	23	93	2	5	0	3	kegr	1251	11590	-596	585	9.3	w	CIFE
0	10	5	93	3	5	0	4	grsm	511	2399	99	343	4.7	w	CIFE

LE	L	S	T	R	M	ESQ	DST#	Formation†	Depth (m)	Pressure (kPa)	Elevation (m)	FW Head (m)	P/d Ratio (kPa/m)	Fluid Recovery	Extrap By
0	1	10	93	4	5	0	2	mshg-kegr	1250	13404	-675	690	10.7	m	CIFE
0	7	31	93	4	5	0	1	mshg-kegr	1252	13273	-687	665	10.6	m	CIFE
0	11	18	93	5	5	0	1	mshg-kegr	1267	13728	-703	695	10.8	o	CIFE
0	15	19	93	5	5	0	1	kegr	1288	13666	-713	678	10.6	o	CIFE
0	11	30	93	5	5	0	1	kegr	1288	13742	-709	690	10.7	o	CIFE
0	8	36	93	7	5	0	2	kegr?	1268	13156	-761	579	10.4	o	CIFE
0	10	10	93	8	5	0	1	kegr	1361	14328	-800	659	11.2	w	CIFE
0	11	29	93	10	5	0	1	mshg-kegr-grnw-pranh	1451	15265	-873	681	10.5	m	CIFE
0	10	22	93	13	5	0	1	kegr-grnw	1447	16445	-992	683	9.6	w	CIFE
0	2	28	94	1	5	0	2	mshg	1337	14180	-564	880	10.6	m	CIFE
0	2	28	94	1	5	0	1	mshg-kegr	1358	11518	-585	588	8.5	w	CIFE
0	15	3	94	2	5	0	1	mshg-kegr	1281	11811	-599	604	9.2	m	CIFE
0	3	7	94	3	5	0	3	slvp	1021	11065	-400	727	10.8	m	self
0	3	7	94	3	5	0	2	mshg-kegr	1267	12342	-646	611	9.7	w	CIFE
0	3	4	94	4	5	0	1	mshg-kegr	1245	12411	-674	590	10	w	CIFE
0	3	4	94	4	5	0	2	mshg-kegr	1247	12508	-676	598	10	w	CIFE
2	6	17	94	4	5	0	1	kegr	1246	12542	-663	614	10.1	w	CIFE
0	5	30	94	4	5	0	2	mshg-kegr	1261	12439	-673	594	9.9	m	CIFE
0	10	2	94	5	5	0	2	grsm	676	4151	-115	307	6.1	w	CIFE
0	10	2	94	5	5	0	1	mshg-kegr	1254	13273	-693	658	10.6	m	CIFE
0	6	20	94	5	5	0	1	kegr	1234	13438	-679	689	10.9	w	CIFE
0	10	7	94	6	5	0	1	kegr	1253	13204	-734	611	10.5	o	CIFE
0	2	18	94	6	5	0	2	kegr	1276	13259	-758	592	10.4	o	CIFE
0	3	22	94	6	5	0	1	mshg-kegr	1267	13618	-736	651	10.7	m	CIFE
0	3	22	94	6	5	0	5	mshg-kegr	1267	13645	-735	654	10.8	w	CIFE
0	14	1	94	7	5	0	1	kegr	1257	13328	-765	593	10.6	o	CIFE
0	9	12	94	7	5	0	4	kegr	1268	12976	-765	556	10.2	w	CIFE
0	9	12	94	7	5	0	2	kegr	1276	13273	-773	579	10.4	w	CIFE

LE	L	S	T	R	M	ESQ	DST#	Formation†	Depth (m)	Pressure (kPa)	Elevation (m)	FW Head (m)	P/d Ratio (kPa/m)	Fluid Recovery	Extrap By
0	6	6	94	10	5	0	5	gmw-pcmb	1557	16003	-947	682	10.3	w	CIFE
0	2	23	94	10	5	0	2	kegr	1408	14879	-865	650	10.6	w	CIFE
0	7	17	94	13	5	0	2	kegr-gmw-pcmb	1706	16851	-1020	696	9.9	w	CIFE
0	9	36	95	2	5	0	1	kegr	1300	11473	-595	574	8.8	w	CIFE
0	9	6	95	4	5	0	2	slvp	986	10649	-422	663	10.8	w	self
0	9	6	95	4	5	0	1	u.kegr	1229	12580	-665	617	10.2	w	self
0	3	20	95	6	5	0	1	mshg-kegr-cncg-pcmb	1227	13018	-691	635	10.6	o	CIFE
0	14	20	95	6	5	0	1	blsk	345	1393	193	335	4	w	CIFE
0	10	32	95	6	5	0	1	mshg-kegr	1216	12611	-698	586	10.4	w	CIFE
0	7	34	95	6	5	0	1	mshg-kegr	1228	12618	-670	615	10.3	o	CIFE
0	7	34	95	6	5	0	2	kegr-cncg-gmw-pcmb	1251	12818	-693	612	10.2	w	CIFE
0	10	18	95	7	5	0	1	mshg-kegr	1241	13721	-773	625	11.1	w	CIFE
0	5	16	95	10	5	0	2	grsm	738	4668	-107	368	6.3	w	CIFE
0	10	23	95	12	5	0	2	gtng	612	2200	98	322	3.6	w	CIFE
0	10	28	95	12	5	0	1	gtng	562	2289	133	366	4.1	g	CIFE
0	10	28	95	12	5	0	2	kegr	1628	15755	-933	671	9.7	w	CIFE
0	10	28	95	12	5	0	3	kegr-grm.v	1663	16245	-968	686	9.8	w	CIFE
0	6	29	95	12	5	0	1	gtng	518	2165	144	365	4.2	g	CIFE
0	6	29	95	12	5	0	2	gtng - wbm	550	2324	112	349	4.2	w	CIFE
0	16	2	96	2	5	0	1	mshg-u.kegr	1275	11378	-593	566	8.9	w	self
0	4	5	96	6	5	0	1	mshg-kegr	1199	12914	-691	624	10.8	w	CIFE
2	3	11	96	6	5	0	1	mshg-kegr-cncg-pcmb	1201	12452	-648	620	10.4	o	CIFE
0	7	16	96	6	5	0	3	kegr	1205	12521	-682	593	10.4	w	CIFE
0	15	16	96	6	5	0	1	mshg-kegr-cncg-pcmb	1165	12156	-641	597	10.4	o	CIFE
0	5	26	96	6	5	0	1	mshg-kegr	1202	12335	-658	598	10.3	m	CIFE
0	3	36	96	11	5	0	1	mshg-kegr	1642	14362	-848	615	8.7	g	CIFE
0	6	8	96	12	5	0	1	gtng	492	2337	268	506	4.7	w	CIFE
0	9	13	96	12	5	0	1	mshg-kegr-pcmb	1688	15031	-879	651	8.9	w	CIFE

LE	L	S	T	R	M	ESQ	DST#	Formation†	Depth (m)	Pressure (kPa)	Elevation (m)	FW Head (m)	P/d Ratio (kPa/m)	Fluid Recovery	Extrap By
0	6	15	96	13	5	0	2	blsk	528	2565	133	394	4.9	m	CIFE
0	4	8	97	2	5	0	1	mshg-kegr	1178	11328	-586	567	9.6	w	CIFE
0	11	30	97	5	5	0	1	mshg-kegr	1195	12321	-675	580	10.3	w	CIFE
0	10	13	97	6	5	0	1	grsm	595	3999	-63	344	6.7	g	CIFE
0	4	16	97	7	5	0	1	mshg-kegr	1207	12852	-733	576	10.7	w	CIFE
0	11	3	97	11	5	0	1	ccpd-grnw-pcmb	1738	15872	-934	682	9.1	w	CIFE
0	7	27	97	12	5	0	1	gting	622	2379	125	368	3.8	w	CIFE
0	10	35	97	13	5	0	3	grnw-pcmb	1642	16252	-985	670	9.9	w	CIFE
0	6	6	98	1	5	0	3	mshg-kegr	1088	10639	-517	566	9.8	w	CIFE
0	7	11	98	3	5	0	1	kegr	1141	11763	-611	587	10.3	w	self
0	14	8	98	6	5	0	1	mshg-kegr	1170	12452	-677	592	10.6	w	CIFE
0	12	26	98	7	5	0	1	gting?	257	1544	188	345	6	w	CIFE
0	10	19	98	8	5	0	1	mshg-kegr	1191	13169	-757	584	11.1	w	CIFE
0	6	31	98	10	5	0	2	gting	407	1917	151	346	4.7	w	CIFE
0	8	17	98	11	5	0	1	gting	664	2080	140	352	3.1	m	CIFE
0	6	11	98	12	5	0	1	gting	660	2399	130	374	3.6	w	CIFE
0	14	36	99	6	5	0	2	wibr	282	1455	151	299	5.2	g	CIFE
0	3	8	99	7	5	0	1	mshg-kegr	1152	12625	-726	560	11	w	CIFE
0	6	28	99	8	5	0	1	wibr	310	2013	95	300	6.5	w	CIFE
0	4	31	99	9	5	0	2	blsk	1448	13101	-790	544	9	w	self
0	10	21	99	12	5	0	1	gting	501	2213	146	371	4.4	m	CIFE
2	10	8	99	13	5	0	3	kegr	1630	13487	-943	431	8.3	w	CIFE
2	10	8	99	13	5	0	4	bdbd-grnw	1706	16727	-1018	685	9.8	w	CIFE
0	6	10	100	5	5	0	1	mshg-kegr-cncg	1068	11597	-635	546	10.9	w	CIFE
0	4	3	100	7	5	0	4	l.mshg	1091	12383	-685	576	11.4	w	self
0	4	3	100	7	5	0	2	mshg-kegr	1106	12597	-701	582	11.4	w	CIFE
0	3	7	101	5	5	0	2	mshg-kegr	1020	11487	-625	545	11.3	w	CIFE
0	10	6	101	6	5	0	1	gting - wbrmn	187	834	189	274	4.5	w	CIFE

LE	L	S	T	R	M	ESQ	DST#	Formation†	Depth (m)	Pressure (kPa)	Elevation (m)	FW Head (m)	P/d Ratio (kPa/m)	Fluid Recovery	Extrap By
0	10	6	101	6	5	0	5	mstg-kegr	1053	12080	-677	553	11.5	w	CIFE
0	11	7	01	10	5	0	1	wbr	594	1648	142	310	2.8	m	CIFE
0	7	24	101	12	5	0	1	kegr	1667	12710	-836	458	7.6	w	CIFE
0	6	16	102	5	5	0	1	kegr	994	11611	-635	548	11.7	m	CIFE
0	6	16	102	5	5	0	2	kegr	1008	11625	-649	535	11.5	w	CIFE
0	6	36	102	5	5	0	2	mstg-kegr	914	10798	-572	527	11.8	m	CIFE
0	5	22	102	7	5	0	3	mstg-kegr	1033	12039	-679	547	11.7	w	CIFE
0	7	14	89	25	4	0	1	gdpd	178	841	423	509	4.7	w	CIFE
0	7	14	89	25	4	0	4	irtn	472	2089	129	342	4.4	w	CIFE
0	10	34	91	24	4	0	1	kegr	110	1177	-563	616	10.5	w	self
0	15	34	93	24	4	0	1	kegr	128	1170	-558	579	8.7	w	CIFE
0	7	34	97	23	4	0	2	bfish-vkng	325	696	437	508	2.1	w	CIFE
0	7	34	97	23	4	0	1	blsk	507	1689	255	427	3.3	w	CIFE
0	7	34	98	24	4	0	2	gdpp-grsm	350	869	274	362	2.5	w	CIFE

†from PUBCO (1990 a)

## Abbreviations (cont. overpage)

## In Titles

LE: Location exception code

L: Legal Sub-Division

S: Section

T: Township

R: Range

M: Meridian

ESQ: Event sequence code

DST: Drill Stem Test

FW Head: Freshwater Equivalent Head

P/d Ratio: Pressure-Depth Ratio

Extrap: Extrapolation

CIFE: Canadian Institute of Formation Evaluation

Note: Additional Slave Point pressure data used (CIFE c and d quality) to generate Slave Point head map.

Abbreviations (cont.)

- Formation Names**  
 bfish Base of Fish Scales  
 bnff Banff  
 ccpd Contact Rapids  
 cncg Chinchaga  
 gpdp Grand Rapids  
 gmw Granite Wash  
 grsm Grosmont  
 gtng Gething  
 kegr Kegon  
 mnvl Mannville  
 mskg Muskeg  
 mssp Mississippian  
 ntkn Notekwin  
 pcmb Pre-Cambrian  
 slvp Slave Point  
 udev Upper Devonian  
 vkng Viking  
 wbmw Wabamun  
 wrbr Winterburn

**Recovery Fluids**

- g: gas  
 w: water  
 o: oil  
 m: mud

**Summary**

Hstrat Unit	#	Fluid Recovery	#
kegr	176	g	9
mshg	3	w	143
slvp	11	o	55
irtn	1	m	31
udev-mssp	14		
mnvl	32		
vkng	1		
<b>TOTAL</b>	<b>238</b>	<b>TOTAL</b>	<b>238</b>

**A4.2 Culled Temperature Data**

LE	L	S	T	R	M	ESQ	Elevation (m)	Depth (m)	Formation†	Tf (deg C)	BHT Quality (1-4)	Grad T* (deg C/km)
0	6	21	89	1	5	0	-745	1487	Pre-Cambrian	36.2	3	23
0	15	10	89	2	5	0	-689	1480	Pre-Cambrian	49.5	1	32
0	5	12	89	2	5	0	-724	1532	Pre-Cambrian	57.2	2	36
0	15	17	89	2	5	0	-780	1564	Pre-Cambrian	45.6	3	28
0	14	18	89	2	5	0	187	599	Grand Rapids	26.2	2	40
0	14	18	89	2	5	0	-742	1528	Chinchaga	45.4	2	28
0	14	18	89	2	5	0	-742	1528	Chinchaga	45.7	2	29
0	13	28	89	2	5	0	-751	1505	Pre-Cambrian	39.9	1	25
0	2	10	89	3	5	0	-691	1452	Keg River?	62.0	1	41
0	3	15	89	3	5	0	-713	1510	Pre-Cambrian	45.2	1	29
0	11	15	89	3	5	0	-753	1539	Pre-Cambrian	47.1	1	29
0	5	22	89	3	5	0	-733	1518	Pre-Cambrian	41.9	1	26
0	3	27	89	3	5	0	-746	1516	Pre-Cambrian	39.9	1	25
0	1	30	89	3	5	0	-785	1531	Pre-Cambrian	47.8	1	30
0	3	34	89	3	5	0	-738	1514	Pre-Cambrian	42.2	1	27
0	16	19	89	5	5	0	-849	1575	Pre-Cambrian	38.8	1	23
0	16	19	89	5	5	0	-849	1575	Pre-Cambrian	39.1	2	24
0	16	19	89	5	5	0	-849	1575	Pre-Cambrian	41.2	2	25
0	12	21	89	6	5	0	-844	1507	Pre-Cambrian	38.2	3	24
0	4	4	89	7	5	0	-917	1532	Pre-Cambrian	42.7	1	27
0	16	5	89	7	5	0	-864	1472	Pre-Cambrian	43.3	1	28
0	10	6	89	7	5	0	-922	1515	Pre-Cambrian	49.5	1	31
0	11	9	89	7	5	0	-886	1472	Pre-Cambrian	47.8	3	31
2	2	17	89	7	5	0	-872	1455	Pre-Cambrian	59.6	2	40
0	8	19	89	7	5	0	93	475	Wabamun	27.8	2	54
0	16	19	89	7	5	0	-914	1478	Pre-Cambrian	39.6	2	25
0	10	23	89	7	5	0	-883	1480	Pre-Cambrian	40.3	3	26
0	10	23	89	7	5	0	-883	1480	Pre-Cambrian	46.0	3	30
0	15	4	89	8	5	0	-935	1466	Pre-Cambrian	44.0	1	29
0	2	6	89	8	5	0	-786	1300	Muskeg	43.0	1	32
0	4	6	89	8	5	0	-893	1405	Pre-Cambrian	46.4	2	32
0	12	6	89	8	5	0	-957	1466	Pre-Cambrian	45.4	3	30
0	12	7	89	8	5	0	-952	1460	Pre-Cambrian?	40.2	3	26
0	1	10	89	8	5	0	-527	1079	Beaverhill Lk.?	24.6	4	21
0	1	10	89	8	5	0	-909	1461	Pre-Cambrian	47.1	1	31
0	9	10	89	8	5	0	-918	1467	Pre-Cambrian?	45.3	1	29
0	5	11	89	8	5	0	-920	1474	Pre-Cambrian?	49.8	1	32
0	3	12	89	8	5	0	-927	1498	Pre-Cambrian	58.2	1	38
0	3	15	89	8	5	0	-880	1412	Pre-Cambrian	42.1	3	28
0	12	15	89	8	5	0	-892	1430	Pre-Cambrian	45.2	1	30
0	13	16	89	8	5	0	-904	1422	Pre-Cambrian	39.4	1	26
0	11	18	89	8	5	0	-932	1438	Pre-Cambrian	38.7	3	26
0	15	19	89	8	5	0	-932	1435	Pre-Cambrian	36.9	1	24
0	6	21	89	8	5	0	-906	1425	Pre-Cambrian	39.8	3	27
0	4	22	89	8	5	0	-918	1450	Pre-Cambrian	44.1	3	29
0	7	22	89	8	5	0	-900	1436	Pre-Cambrian	53.5	1	36
0	15	22	89	8	5	0	-823	1355	Muskeg	40.5	1	28



1	E	L	S	T	R	M	ESQ	Elevation (m)	Depth (m)	Formation†	Tf (deg C)	BHT Quality (1-4)	Grad T* (deg C/km)
0	16	22	89	8	5	0		-905	1437	Pre-Cambrian	40.7	1	27
0	3	24	89	8	5	0		-917	1467	Pre-Cambrian	49.4	3	32
0	15	25	89	8	5	0		-644	1180	Beaverhill Lk.	27.8	3	22
0	15	25	89	8	5	0		-887	1423	Pre-Cambrian?	46.8	1	31
0	5	26	89	8	5	0		-897	1428	Pre-Cambrian	43.7	3	29
0	15	26	89	8	5	0		-899	1428	Pre-Cambrian	41.8	1	28
0	13	27	89	8	5	0		-902	1420	Pre-Cambrian	39.1	3	26
0	8	28	89	8	5	0		-889	1407	Pre-Cambrian	41.9	3	28
0	11	28	89	8	5	0		111	400	Wabamun	21.5	3	49
0	10	32	89	8	5	0		-910	1411	Pre-Cambrian	52.5	1	36
0	4	1	89	9	5	0		-966	1466	Pre-Cambrian	44.9	3	29
0	1	9	89	9	5	0		-942	1450	Pre-Cambrian	44.5	1	29
0	3	12	89	9	5	0		-951	1451	Pre-Cambrian	46.5	1	31
0	4	16	89	9	5	0		-950	1456	Pre-Cambrian	49.9	2	33
0	4	16	89	9	5	0		-950	1456	Pre-Cambrian	62.5	2	42
0	16	21	89	9	5	0		-933	1440	Pre-Cambrian	41.3	3	27
0	14	22	89	9	5	0		-928	1434	Pre-Cambrian	39.9	3	26
0	4	23	89	9	5	0		-967	1470	Pre-Cambrian	33.9	3	22
0	16	26	89	9	5	0		-935	1434	Pre-Cambrian	43.1	1	29
0	6	28	89	9	5	0		118	386	Wabamun	21.2	3	50
0	7	29	89	9	5	0		-929	1433	Pre-Cambrian	39.5	1	26
0	9	30	89	9	5	0		-946	1455	Pre-Cambrian	32.6	1	21
0	9	31	89	9	5	0		-930	1436	Pre-Cambrian	36.7	1	24
0	10	34	89	9	5	0		-892	1393	Keg River	25.7	2	17
0	7	35	89	9	5	0		-942	1442	Pre-Cambrian	34.0	3	22
0	1	1	89	10	5	0		-949	1471	Pre-Cambrian	47.4	1	31
0	11	1	89	10	5	0		78	451	Wabamun	17.2	3	34
0	1	10	89	10	5	0		-930	1473	Pre-Cambrian	51.9	3	34
0	3	11	89	10	5	0		-938	1475	Pre-Cambrian	36.5	1	23
0	12	11	89	10	5	0		-971	1510	Pre-Cambrian	44.6	1	28
0	7	13	89	10	5	0		-968	1487	Pre-Cambrian	53.0	1	34
0	10	15	89	10	5	0		-966	1509	Pre-Cambrian	59.0	1	38
0	10	16	89	10	5	0		-964	1518	Pre-Cambrian	54.9	3	35
0	10	17	89	10	5	0		-980	1546	Pre-Cambrian	42.5	1	26
0	10	18	89	10	5	0		-969	1549	Pre-Cambrian	48.3	3	30
0	14	18	89	10	5	0		-964	1546	Pre-Cambrian	49.3	1	31
0	11	20	89	10	5	0		-980	1548	Pre-Cambrian	44.0	1	27
0	4	25	89	10	5	0		-938	1465	Pre-Cambrian	53.6	1	35
0	1	26	89	10	5	0		109	421	Wabamun	24.4	2	53
0	6	28	89	10	5	0		-967	1521	Pre-Cambrian	42.2	2	26
0	14	28	89	10	5	0		-967	1519	Pre-Cambrian	44.8	1	28
0	6	29	89	10	5	0		-968	1538	Pre-Cambrian	55.6	3	35
0	6	32	89	10	5	0		-946	1512	Pre-Cambrian	49.2	2	31
0	6	32	89	10	5	0		-974	1541	Pre-Cambrian	55.7	2	35
0	10	32	89	10	5	0		-952	1512	Pre-Cambrian?	52.9	2	34
0	14	32	89	10	5	0		-962	1530	Pre-Cambrian	48.1	2	30
0	3	3	89	11	5	0		-994	1621	Pre-Cambrian	39.7	3	23

LE	L	S	T	R	M	ESQ	Elevation (m)	Depth (m)	Formation†	Tf (deg C)	BHT Quality (1-4)	Grad T* (deg C/km)
0	5	4	89	11	5	0	-993	1631	Pre-Cambrian	45.8	1	27
0	1	5	89	11	5	0	-990	1630	Pre-Cambrian	40.6	3	24
0	16	5	89	11	5	0	-990	1640	Pre-Cambrian	37.8	1	22
0	5	8	89	11	5	0	-1009	1660	Pre-Cambrian	47.7	1	28
0	1	9	89	11	5	0	-1006	1641	Pre-Cambrian	47.1	3	27
0	1	11	89	11	5	0	-995	1600	Pre-Cambrian	47.2	1	28
0	9	16	89	11	5	0	-964	1606	Pre-Cambrian	44.5	1	26
0	2	19	89	11	5	0	-999	1683	Pre-Cambrian	46.0	1	26
0	7	21	89	11	5	0	-981	1628	Pre-Cambrian	38.4	3	22
0	12	33	89	11	5	0	-994	1650	Pre-Cambrian	45.0	3	26
0	4	35	89	11	5	0	-988	1607	Pre-Cambrian	49.9	3	30
0	9	13	89	12	5	0	-957	1651	Pre-Cambrian	50.3	1	29
0	4	23	89	12	5	0	-1023	1772	Pre-Cambrian	37.3	3	20
0	1	24	89	12	5	0	-987	1690	Pre-Cambrian	42.1	3	24
0	5	32	89	12	5	0	-1019	1752	Pre-Cambrian	45.1	1	25
0	1	33	89	12	5	0	-1004	1778	Pre-Cambrian	45.2	2	24
0	1	33	89	12	5	0	-1004	1778	Pre-Cambrian	54.1	1	29
0	3	34	89	12	5	0	-1009	1780	Pre-Cambrian	50.7	3	27
0	1	36	89	12	5	0	-1010	1720	Pre-Cambrian	47.2	1	26
0	10	11	89	13	5	0	-1041	1777	Pre-Cambrian	39.9	1	21
0	10	20	89	13	5	0	-1009	1703	Pre-Cambrian	42.9	2	24
0	10	35	89	13	5	0	-995	1711	Pre-Cambrian	50.3	1	28
0	14	5	89	14	5	0	-1039	1748	Pre-Cambrian	48.0	1	26
0	4	7	89	14	5	0	-1037	1748	Pre-Cambrian	45.7	3	25
0	8	15	89	14	5	0	-1003	1702	Muskeg?	43.7	1	25
0	10	18	89	14	5	0	-1026	1707	Pre-Cambrian	39.7	1	22
0	3	30	89	14	5	0	-1055	1745	Pre-Cambrian	55.2	1	31
0	1	33	90	1	5	0	-656	1224	Pre-Cambrian	37.8	1	29
0	5	1	90	2	5	0	-718	1384	Pre-Cambrian	40.4	3	28
0	12	7	90	2	5	0	-723	1439	Pre-Cambrian	41.1	3	27
0	2	18	90	2	5	0	-717	1352	Pre-Cambrian	43.0	3	30
0	11	18	90	2	5	0	-763	1406	Pre-Cambrian	48.6	1	33
0	11	23	90	2	5	0	-685	1359	Pre-Cambrian	42.7	1	30
0	8	1	90	3	5	0	-747	1510	Pre-Cambrian	41.5	1	26
0	15	2	90	3	5	0	-761	1535	Pre-Cambrian	54.2	3	34
0	6	3	90	3	5	0	-752	1530	Pre-Cambrian	43.4	1	27
0	9	7	90	3	5	0	-752	1520	Pre-Cambrian	32.1	1	20
0	8	8	90	3	5	0	-748	1536	Pre-Cambrian	57.4	3	36
0	10	9	90	3	5	0	-754	1542	Pre-Cambrian	42.2	1	26
0	14	11	90	3	5	0	-730	1507	Pre-Cambrian	39.6	1	25
0	6	12	90	3	5	0	-724	1487	Pre-Cambrian	43.4	3	28
0	8	12	90	3	5	0	-736	1480	Pre-Cambrian	41.6	3	27
0	15	12	90	3	5	0	-728	1466	Pre-Cambrian	40.9	1	27
0	4	13	90	3	5	0	-741	1473	Pre-Cambrian	40.0	1	26
0	14	13	90	3	5	0	-704	1405	Pre-Cambrian	46.0	1	31
0	8	14	90	3	5	0	-730	1464	Pre-Cambrian	38.7	1	25
0	9	14	90	3	5	0	-729	1440	Pre-Cambrian	40.0	1	26

LE	L	S	T	R	M	ESQ	Elevation (m)	Depth (m)	Formation†	Tf (deg C)	BHT Quality (1-4)	Grad T* (deg C/km)
0	11	14	90	3	5	0	-732	1435	Pre-Cambrian	46.1	1	31
0	14	16	90	3	5	0	-758	1501	Pre-Cambrian	42.8	1	27
0	8	18	90	3	5	0	-756	1500	Pre-Cambrian	45.0	1	29
0	10	21	90	3	5	0	-771	1422	Pre-Cambrian	43.5	3	29
0	1	24	90	3	5	0	-733	1390	Pre-Cambrian	43.6	3	30
0	3	24	90	3	5	0	-726	1410	Pre-Cambrian	40.8	1	28
0	12	24	90	3	5	0	-735	1370	Pre-Cambrian	39.3	1	27
0	4	25	90	3	5	0	-728	1357	Pre-Cambrian	36.1	1	25
0	8	25	90	3	5	0	-727	1355	Pre-Cambrian	42.4	1	30
0	6	26	90	3	5	0	-758	1386	Pre-Cambrian	37.8	2	26
0	6	26	90	3	5	0	-756	1384	Pre-Cambrian	40.0	2	27
0	16	30	90	3	5	0	-784	1407	Pre-Cambrian	42.1	3	29
0	2	36	90	3	5	0	178	460	Wabamun	22.1	3	44
0	2	36	90	3	5	0	-767	1405	Pre-Cambrian	38.4	1	26
0	14	8	90	4	5	0	-831	1560	Pre-Cambrian	48.6	3	30
0	10	32	90	4	5	0	-758	1413	Pre-Cambrian	38.4	3	26
0	12	21	90	5	5	0	-791	1525	Pre-Cambrian	39.7	3	25
0	12	23	90	5	5	0	-824	1548	Pre-Cambrian	57.7	4	36
0	1	32	90	5	5	0	-787	1520	Pre-Cambrian	43.2	3	27
0	10	32	90	5	5	0	-778	1511	Pre-Cambrian	41.4	2	26
0	10	32	90	5	5	0	-778	1511	Pre-Cambrian	44.7	1	28
0	14	32	90	5	5	0	-769	1505	Pre-Cambrian	44.9	3	29
0	16	8	90	6	5	0	-833	1482	Pre-Cambrian	38.1	3	24
0	10	9	90	6	5	0	-822	1487	Pre-Cambrian	39.3	1	25
0	14	13	90	6	5	0	-786	1515	Pre-Cambrian	43.3	1	27
0	3	5	90	7	5	0	-877	1419	Pre-Cambrian	45.3	2	31
0	7	12	90	7	5	0	-855	1446	Pre-Cambrian	49.6	1	33
0	8	27	90	7	5	0	-874	1433	Pre-Cambrian	44.5	4	30
0	8	27	90	7	5	0	-874	1433	Pre-Cambrian	54.2	3	36
0	4	3	90	8	5	0	-947	1456	Pre-Cambrian	62.0	2	41
0	11	5	90	8	5	0	-926	1422	Pre-Cambrian	40.8	3	27
0	15	11	90	8	5	0	-348	860	Ireton?	26.4	2	28
0	15	11	90	8	5	0	-895	1407	Pre-Cambrian	41.8	1	28
0	5	25	90	8	5	0	-435	939	Ireton	23.9	2	23
0	5	25	90	8	5	0	-444	948	Ireton	25.7	2	25
0	6	26	90	8	5	0	-875	1382	Pre-Cambrian	35.7	1	24
0	3	31	90	8	5	0	-895	1391	Pre-Cambrian	62.1	3	43
0	1	4	90	9	5	0	110	390	Wabamun	22.2	4	52
0	9	6	90	9	5	0	-940	1445	Pre-Cambrian	39.4	3	26
0	3	12	90	9	5	0	-925	1423	Pre-Cambrian	31.7	4	21
0	6	27	90	9	5	0	115	385	Wabamun	20.3	1	47
0	10	31	90	9	5	0	-949	1455	Pre-Cambrian	32.0	1	21
0	10	35	90	9	5	0	137	362	Wabamun	20.2	4	50
0	4	4	90	10	5	0	-983	1538	Pre-Cambrian	51.7	2	32
0	4	4	90	10	5	2	-986	1541	Pre-Cambrian	52.6	1	33
0	1	5	90	10	5	0	-956	1517	Pre-Cambrian	52.9	2	34
0	3	5	90	10	5	0	-682	1243	Beaverhill Lk.	47.2	2	36

LE	L	S	T	R	M	ESQ	Elevation (m)	Depth (m)	Formation†	Tf (deg C)	BIT Quality (1-4)	Grad T* (deg C/km)
0	3	5	90	10	5	0	-993	1555	Pre-Cambrian	36.2	1	22
0	3	5	90	10	5	0	-989	1551	Pre-Cambrian	51.5	4	32
0	3	5	90	10	5	0	-989	1551	Pre-Cambrian	53.7	2	33
0	10	5	90	10	5	0	-985	1544	Pre-Cambrian	56.8	2	35
0	7	6	90	10	5	0	-972	1542	Pre-Cambrian	48.7	1	30
0	3	11	90	10	5	0	-937	1464	Pre-Cambrian	45.5	2	30
0	3	11	90	10	5	0	-937	1464	Pre-Cambrian	50.5	4	33
0	10	14	90	10	5	0	-579	1100	Ireton	35.7	1	31
0	10	14	90	10	5	0	-948	1469	Pre-Cambrian	34.0	1	22
0	7	15	90	10	5	0	-959	1487	Pre-Cambrian	50.4	1	33
0	9	22	90	10	5	0	-937	1465	Pre-Cambrian	39.0	1	25
0	10	25	90	10	5	0	-959	1474	Pre-Cambrian	42.0	1	27
0	11	27	90	10	5	0	-945	1483	Pre-Cambrian	51.7	1	34
0	4	1	90	11	5	0	-993	1587	Pre-Cambrian	38.9	3	23
0	10	1	90	11	5	0	-989	1572	Pre-Cambrian	37.2	1	22
0	7	3	90	11	5	0	-972	1582	Pre-Cambrian	39.7	1	24
0	7	12	90	11	5	0	-979	1550	Pre-Cambrian	37.3	3	23
0	7	12	90	11	5	0	-1011	1582	Pre-Cambrian	41.2	3	25
0	6	16	90	11	5	0	-975	1608	Pre-Cambrian	60.5	1	36
0	5	25	90	11	5	0	-1004	1587	Pre-Cambrian	43.0	3	26
0	7	26	90	11	5	0	-997	1605	Pre-Cambrian	36.5	1	21
0	4	35	90	11	5	0	-980	1600	Pre-Cambrian	47.8	1	29
0	11	6	90	12	5	0	-1016	1734	Pre-Cambrian	43.2	1	24
0	15	10	90	12	5	0	-990	1744	Pre-Cambrian	42.9	1	23
0	6	12	90	12	5	0	-991	1705	Pre-Cambrian	65.7	1	37
0	14	19	90	12	5	0	-967	1735	Pre-Cambrian	58.7	1	33
0	15	22	90	12	5	0	-998	1708	Pre-Cambrian	55.7	1	31
0	10	23	90	12	5	0	-990	1703	Pre-Cambrian	45.2	1	25
0	7	29	90	12	5	0	-877	1609	Muskeg?	52.7	4	32
0	6	30	90	12	5	0	-992	1773	Pre-Cambrian	36.9	1	20
0	15	33	90	12	5	0	-998	1735	Pre-Cambrian	40.9	1	22
0	6	35	90	12	5	0	-992	1730	Pre-Cambrian	38.9	1	21
0	12	1	90	13	5	0	-886	1612	Muskeg?	46.8	1	28
0	2	2	90	13	5	0	-996	1715	Pre-Cambrian	41.8	2	23
0	2	2	90	13	5	0	-996	1715	Pre-Cambrian	42.3	1	23
0	10	2	90	13	5	0	-988	1712	Pre-Cambrian	64.3	4	36
0	3	6	90	13	5	0	-1028	1728	Pre-Cambrian	50.0	1	28
0	6	23	90	13	5	0	-1011	1786	Pre-Cambrian	37.0	1	20
0	5	24	90	13	5	0	-1069	1854	Pre-Cambrian	57.0	1	30
0	7	26	90	13	5	0	-1014	1812	Pre-Cambrian	55.3	1	29
0	15	28	90	13	5	0	-997	1783	Pre-Cambrian	63.3	1	34
0	2	32	90	13	5	0	-1008	1818	Pre-Cambrian	39.9	1	21
0	14	36	90	13	5	0	-1012	1812	Pre-Cambrian	47.7	1	25
0	10	2	90	14	5	0	-1024	1730	Pre-Cambrian	57.0	1	32
0	6	8	90	14	5	0	-1023	1730	Pre-Cambrian	47.2	3	26
0	15	27	90	14	5	0	-1038	1827	Pre-Cambrian	55.0	1	29
0	6	35	90	14	5	0	-1023	1832	Pre-Cambrian	49.8	1	26

LE	L	S	T	R	M	ESQ	Elevation (m)	Depth (m)	Formation†	Tf (deg C)	BHT Quality (1-4)	Grad T* (deg C/km)
0	10	6	91	1	5	0	-728	1320	Pre-Cambrian	54.8	3	40
0	6	9	91	2	5	0	-726	1355	Pre-Cambrian?	34.4	1	24
0	6	14	91	2	5	0	-677	1255	Pre-Cambrian?	32.5	4	24
0	8	28	91	2	5	0	-733	1287	Pre-Cambrian	38.0	1	28
0	5	29	91	2	5	0	-716	1290	Pre-Cambrian	36.2	1	27
0	6	2	91	3	5	0	-778	1397	Pre-Cambrian	46.4	1	32
0	16	10	91	3	5	0	-760	1408	Pre-Cambrian	48.2	3	33
0	2	21	91	3	5	0	-773	1395	Pre-Cambrian	32.2	1	22
0	11	21	91	3	5	0	-776	1381	Pre-Cambrian	52.4	3	36
0	7	28	91	3	5	0	-760	1351	Pre-Cambrian?	33.1	1	23
0	9	30	91	3	5	0	-747	1337	Pre-Cambrian?	39.6	1	28
0	16	30	91	3	5	0	-781	1370	Pre-Cambrian	43.3	3	30
0	9	5	91	4	5	0	-748	1364	Pre-Cambrian	40.7	1	28
0	7	10	91	4	5	0	-766	1400	Pre-Cambrian	41.0	1	28
0	15	21	91	4	5	0	-780	1339	Pre-Cambrian	40.0	3	28
0	13	1	91	5	5	0	140	518	Wabamun	20.6	4	36
2	13	1	91	5	5	0	-750	1410	Pre-Cambrian	44.3	1	30
0	5	3	91	5	5	0	-814	1495	Pre-Cambrian?	38.7	1	25
0	8	4	91	5	5	0	-772	1476	Pre-Cambrian	43.9	3	28
0	8	7	91	5	5	0	-799	1456	Pre-Cambrian	41.9	2	27
0	8	7	91	5	5	0	-799	1456	Pre-Cambrian	42.1	1	28
0	9	8	91	5	5	2	-811	1516	Pre-Cambrian	50.2	1	32
0	2	9	91	5	5	0	-752	1452	Pre-Cambrian	42.2	3	28
0	15	9	91	5	5	0	-771	1460	Pre-Cambrian	35.9	3	23
0	1	11	91	5	5	0	-756	1373	Pre-Cambrian	36.5	1	25
0	1	11	91	5	5	0	-756	1373	Pre-Cambrian	37.9	1	26
0	9	11	91	5	5	0	167	445	Bluesky	27.2	1	57
0	9	11	91	5	5	0	-735	1347	Pre-Cambrian	38.1	2	27
0	2	14	91	5	5	0	-797	1403	Pre-Cambrian	39.9	1	27
0	2	14	91	5	5	0	-797	1403	Pre-Cambrian	44.9	2	31
0	10	15	91	5	5	0	-815	1427	Pre-Cambrian?	35.9	3	24
0	4	19	91	5	5	0	-835	1505	Pre-Cambrian	40.0	2	25
0	7	20	91	5	5	0	-795	1430	Pre-Cambrian	39.6	1	26
0	15	23	91	5	5	0	-757	1353	Pre-Cambrian	34.7	1	24
0	15	25	91	5	5	0	-761	1330	Chinchaga	40.7	1	29
0	15	25	91	5	5	2	-792	1361	Pre-Cambrian	61.6	3	44
0	2	29	91	5	5	0	-743	1358	Pre-Cambrian	38.3	1	27
0	6	29	91	5	5	0	-736	1356	Pre-Cambrian	41.0	3	29
0	1	30	91	5	5	0	-745	1383	Pre-Cambrian	42.1	1	29
0	12	34	91	5	5	0	-810	1403	Pre-Cambrian	36.4	1	24
0	8	4	91	6	5	0	-833	1485	Pre-Cambrian	49.4	3	32
0	12	4	91	6	5	0	-818	1444	Pre-Cambrian	40.3	1	27
0	13	10	91	6	5	0	-899	1552	Pre-Cambrian	51.1	1	32
0	12	14	91	6	5	0	-808	1439	Pre-Cambrian	48.1	1	32
0	2	17	91	6	5	0	-869	1440	Pre-Cambrian	44.2	2	29
0	15	23	91	6	5	0	-797	1418	Pre-Cambrian	36.6	1	24
0	14	26	91	6	5	0	-763	1368	Pre-Cambrian	45.7	1	32

LE	L	S	T	R	M	ESQ	Elevation (m)	Depth (m)	Formation†	Tf (deg C)	BHT Quality (1-4)	Grad T* (deg C/km)
0	11	29	91	6	5	0		1404	Pre-Cambrian	62.7	3	43
0	3	34	91	6	5	0		1370	Pre-Cambrian	32.9	1	23
0	9	35	91	6	5	0		1159	Slave Point	48.8	1	40
0	9	35	91	6	5	0		1434	Pre-Cambrian	46.2	4	31
0	12	35	91	6	5	0	-784	1370	Pre-Cambrian	41.2	3	29
0	2	17	91	7	5	0	-615	1427	Slave Point	28.5	4	24
0	2	17	91	7	5	0	-905	1417	Pre-Cambrian	42.5	2	29
0	2	17	91	7	5	0	-90	1417	Pre-Cambrian	43.9	4	30
0	7	23	91	7	5	0	-85	1365	Pre-Cambrian	34.0	1	23
0	2	26	91	7	5	0	-85	1352	Pre-Cambrian	38.6	3	27
0	14	27	91	7	5	0	-856	136	Pre-Cambrian	44.6	1	31
0	10	28	91	7	5	0	-897	1407	Pre-Cambrian	46.2	3	31
0	4	34	91	7	5	0	-885	1368	Pre-Cambrian	45.7	1	34
0	15	34	91	7	5	0	-867	1369	Pre-Cambrian	33.1	3	23
0	6	35	91	7	5	0	-848	1353	Pre-Cambrian	35.7	2	28
0	8	6	91	8	5	0	-890	1388	Pre-Cambrian	32.4	2	22
0	8	6	91	8	5	0	-890	1388	Pre-Cambrian	35.4	4	24
0	4	8	91	8	5	0	-881	1380	Pre-Cambrian	36.6	4	25
0	4	8	91	8	5	0	-881	1380	Pre-Cambrian	38.2	2	26
0	12	18	91	8	5	0	-909	1407	Pre-Cambrian	45.7	4	31
0	13	18	91	8	5	0	-929	1428	Pre-Cambrian	39.8	2	26
0	9	20	91	8	5	0	-938	1431	Pre-Cambrian	42.7	1	28
0	7	4	91	9	5	0	150	354	Wabamun	20.2	4	51
0	15	6	91	9	5	0	-956	1470	Pre-Cambrian	39.0	1	25
0	2	13	91	9	5	0	-185	683	Grosmont?	32.7	4	45
0	2	13	91	9	5	0	-391	889	Ireton	33.9	4	36
0	2	13	91	9	5	0	-911	1409	Pre-Cambrian	39.6	4	27
0	10	21	91	9	5	0	114	394	Wabamun	19.5	1	44
0	2	25	91	9	5	0	-903	1403	Pre-Cambrian	39.8	1	27
0	7	26	91	9	5	0	-907	1411	Pre-Cambrian	49.7	2	34
0	7	26	91	9	5	0	-907	1411	Pre-Cambrian	63.0	2	43
0	5	3	91	10	5	0	-705	1255	Beaverhill Lk.	44.4	3	34
0	5	3	91	10	5	0	-946	1496	Pre-Cambrian	37.1	1	23
0	12	3	91	10	5	0	-951	1504	Pre-Cambrian	36.1	4	23
0	12	3	91	10	5	0	-951	1504	Pre-Cambrian	39.0	1	25
0	2	4	91	10	5	0	-917	1474	Pre-Cambrian	42.9	3	28
0	10	4	91	10	5	0	-927	1483	Pre-Cambrian	54.4	3	35
0	11	4	91	10	5	0	-941	1502	Pre-Cambrian	42.2	1	27
0	2	5	91	10	5	0	-956	1521	Pre-Cambrian	52.6	3	33
0	1	9	91	10	5	0	-573	1126	Ireton?	24.1	2	20
0	3	9	91	10	5	0	-957	1521	Pre-Cambrian	36.0	1	22
0	12	22	91	10	5	0	-969	1528	Pre-Cambrian	49.3	3	31
0	12	25	91	10	5	0	-921	1449	Pre-Cambrian	51.8	3	34
0	12	3	91	11	5	0	-970	1712	Pre-Cambrian	37.0	1	20
0	11	11	91	11	5	0	-969	1651	Pre-Cambrian	38.9	3	22
0	8	16	91	11	5	0	-972	1747	Pre-Cambrian	40.9	3	22
0	10	25	91	11	5	0	-955	1550	Slave Point?	37.5	1	23

LI	L	S	T	R	M	ESQ	Elevation (m)	Depth (m)	Formation†	Tf (deg C)	BHT Quality (1-4)	Grad T* (deg C/km)
0	3	30	91	11	5	0	-967	1752	Pre-Cambrian?	43.3	1	24
0	14	6	91	12	5	0	-983	1810	Pre-Cambrian	47.8	3	25
0	8	7	91	12	5	0	-994	1814	Pre-Cambrian	39.4	3	21
0	9	7	91	12	5	0	-996	1801	Pre-Cambrian	43.4	3	23
0	11	7	91	12	5	0	-984	1787	Pre-Cambrian	42.5	3	23
0	12	8	91	12	5	0	-985	1781	Pre-Cambrian	42.7	3	23
0	15	9	91	12	5	0	-988	1786	Pre-Cambrian	48.5	3	26
0	4	11	91	12	5	0	-958	1770	Pre-Cambrian?	40.1	1	22
0	8	14	91	12	5	0	-983	1794	Pre-Cambrian	41.6	1	22
0	4	17	91	12	5	0	-995	1770	Pre-Cambrian	42.3	1	23
0	2	18	91	12	5	0	-993	1770	Pre-Cambrian	41.3	3	22
0	4	18	91	12	5	0	-989	1785	Pre-Cambrian?	44.0	3	24
0	10	18	91	12	5	0	-1002	1762	Pre-Cambrian	44.8	3	24
0	12	18	91	12	5	0	-998	1768	Pre-Cambrian?	45.9	1	25
0	2	19	91	12	5	0	-985	1780	Pre-Cambrian	46.3	1	25
0	6	19	91	12	5	0	-994	1771	Pre-Cambrian	48.8	1	26
0	10	19	91	12	5	0	-974	1765	Pre-Cambrian	43.9	1	24
0	12	19	91	12	5	0	-988	1763	Pre-Cambrian	44.5	1	24
0	7	20	91	12	5	0	-960	1776	Pre-Cambrian	41.2	1	22
0	14	20	91	12	5	0	-972	1780	Pre-Cambrian	62.8	1	34
0	15	21	91	12	5	0	-998	1790	Pre-Cambrian	39.8	1	21
0	13	26	91	12	5	0	-997	1779	Pre-Cambrian	62.7	2	34
0	4	28	91	12	5	0	-980	1772	Pre-Cambrian	39.8	1	21
0	4	28	91	12	5	0	-980	1772	Pre-Cambrian	42.9	2	23
0	13	28	91	12	5	0	-950	1752	Pre-Cambrian	52.8	1	29
0	2	29	91	12	5	0	-972	1781	Pre-Cambrian	57.2	1	31
0	14	29	91	12	5	0	-983	1795	Pre-Cambrian	54.5	1	29
0	16	29	91	12	5	0	-143	949	Wabamun	25.0	1	24
0	16	29	91	12	5	0	-694	1500	Beaverhill Lk.	48.5	4	31
0	16	29	91	12	5	0	-989	1796	Pre-Cambrian	39.4	1	21
0	6	30	91	12	5	0	-1001	1770	Pre-Cambrian	48.6	1	26
0	13	30	91	12	5	0	-991	1770	Pre-Cambrian	49.8	3	27
0	4	31	91	12	5	0	-698	1500	Beaverhill Lk.	41.8	1	27
0	4	31	91	12	5	0	-981	1784	Pre-Cambrian	47.3	1	25
0	8	32	91	12	5	0	-995	1800	Pre-Cambrian	45.6	1	24
0	10	32	91	12	5	0	-149	938	Wabamun	48.8	3	50
0	10	32	91	12	5	0	-1003	1792	Pre-Cambrian	47.0	1	25
0	4	33	91	12	5	0	-145	950	Wabamun	30.4	1	30
0	4	33	91	12	5	0	-975	1780	Pre-Cambrian	50.1	1	27
0	10	2	91	13	5	0	-767	1575	Beaverhill Lk.	36.3	1	22
0	10	2	91	13	5	0	-1042	1850	Pre-Cambrian	49.4	1	26
0	16	5	91	13	5	0	-1050	1824	Pre-Cambrian	43.1	1	23
0	11	10	91	13	5	0	-1024	1790	Pre-Cambrian	65.7	1	36
0	8	12	91	13	5	0	-990	1800	Pre-Cambrian	41.5	3	22
0	9	12	91	13	5	0	-984	1790	Pre-Cambrian	45.2	1	24
0	11	12	91	13	5	0	-1009	1812	Pre-Cambrian	52.8	1	28
0	2	13	91	13	5	0	-863	1650	Muskeg?	40.9	3	24

LE	L	S	T	R	M	ESQ	Elevation (m)	Depth (m)	Formation†	Tt (deg C)	BHT Quality (1-4)	Grad T* (deg C/km)
0	4	13	91	13	5	0	-1003	1797	Pre-Cambrian	58.7	1	32
0	4	20	91	13	5	0	-1023	1771	Pre-Cambrian	40.5	3	22
0	2	24	91	13	5	0	-1009	1767	Pre-Cambrian	57.0	1	31
0	15	24	91	13	5	0	-860	1620	Muskeg?	57.8	3	34
0	2	25	91	13	5	0	-857	1618	Muskeg?	50.9	1	30
0	16	25	91	13	5	0	-1002	1790	Pre-Cambrian	43.0	1	23
0	10	27	91	13	5	0	-1001	1775	Pre-Cambrian	42.3	1	23
0	10	27	91	13	5	0	-1001	1775	Pre-Cambrian	43.8	4	24
0	6	32	91	13	5	0	-905	1668	Muskeg?	46.8	1	27
0	15	35	91	13	5	0	-1020	1830	Pre-Cambrian	50.6	1	27
0	1	36	91	13	5	0	-859	1667	Muskeg?	38.5	1	22
0	5	2	91	14	5	0	-1022	1828	Pre-Cambrian	43.6	1	23
0	15	4	91	14	5	0	-645	1430	Ireton	37.3	2	25
0	15	4	91	14	5	0	-1020	1805	Pre-Cambrian	46.5	1	25
0	7	19	91	14	5	0	-1049	1797	Pre-Cambrian	43.0	3	23
0	14	20	91	14	5	0	-1030	1760	Pre-Cambrian	48.2	1	26
0	13	25	91	14	5	0	-1063	1816	Pre-Cambrian	47.4	1	25
0	12	31	91	14	5	0	-1082	1808	Pre-Cambrian	46.3	4	25
0	16	31	92	1	5	0	-684	1284	Pre-Cambrian	37.6	1	28
0	11	8	92	3	5	0	-754	1322	Pre-Cambrian	33.6	3	24
0	6	18	92	3	5	0	-715	1326	Pre-Cambrian?	44.5	1	32
0	6	19	92	3	5	0	-725	1351	Pre-Cambrian?	33.5	3	23
0	8	1	92	4	5	0	-731	1301	Pre-Cambrian?	37.9	1	28
0	15	4	92	4	5	0	-185	735	Ireton	22.8	3	28
0	15	4	92	4	5	0	-739	1289	Pre-Cambrian	36.2	3	27
0	13	7	92	4	5	0	-762	1323	Pre-Cambrian?	37.5	1	27
0	7	9	92	4	5	0	-743	1300	Pre-Cambrian	40.0	1	29
0	16	20	92	4	5	0	-743	1274	Pre-Cambrian	40.3	2	30
0	16	22	92	4	5	0	-746	1322	Pre-Cambrian	38.8	3	28
0	11	23	92	4	5	0	-711	1294	Pre-Cambrian	28.6	1	21
0	11	24	92	4	5	0	-703	1320	Pre-Cambrian	39.1	1	28
0	8	26	92	4	5	0	-701	1289	Pre-Cambrian	40.1	1	30
0	11	26	92	4	5	0	-715	1298	Pre-Cambrian?	52.1	3	39
0	7	27	92	4	5	0	-726	1300	Pre-Cambrian?	36.3	1	26
0	7	31	92	4	5	0	-754	1321	Pre-Cambrian	39.8	3	29
0	11	31	92	4	5	0	-757	1327	Pre-Cambrian	41.8	2	30
0	7	33	92	4	5	0	-729	1279	Chinchaga	34.9	2	26
0	7	34	92	4	5	0	-693	1269	Keg River?	32.4	1	24
0	15	34	92	4	5	0	-714	1286	Keg River?	52.6	1	39
0	6	35	92	4	5	0	176	408	Bluesky	24.5	1	55
0	6	35	92	4	5	0	-663	1247	Muskeg	34.5	2	26
0	14	35	92	4	5	0	-700	1283	Pre-Cambrian?	34.2	4	25
0	6	36	92	4	5	0	-737	1362	Pre-Cambrian	32.3	3	22
0	5	3	92	5	5	0	-753	1343	Pre-Cambrian	37.4	2	26
2	5	3	92	5	5	0	-753	1343	Pre-Cambrian	51.7	2	37
0	13	3	92	5	5	0	-746	1327	Pre-Cambrian	39.1	3	28
0	6	5	92	5	5	0	-769	1378	Pre-Cambrian	43.2	1	30



LE	L	S	T	R	M	ESQ	Elevation (m)	Depth (m)	Formatio..†	Tf (deg C)	BHT Quality (1-4)	Grad T* (deg C/km)
0	4	10	92	5	5	0	-748	1323	Pre-Cambrian	41.1	1	30
0	14	10	92	5	5	0	-755	1324	Pre-Cambrian	40.0	1	29
0	11	15	92	5	5	0	-750	1320	Pre-Cambrian	39.5	1	28
0	11	16	92	5	5	0	-760	1351	Pre-Cambrian	36.9	2	26
0	9	18	92	5	5	0	-795	1378	Pre-Cambrian	40.6	3	28
0	11	27	92	5	5	0	-802	1393	Pre-Cambrian	27.5	3	18
0	11	28	92	5	5	0	-777	1370	Pre-Cambrian	36.9	3	25
0	7	32	92	5	5	0	-823	1396	Pre-Cambrian	40.3	3	27
0	9	32	92	5	5	0	-765	1338	Pre-Cambrian	40.6	3	29
0	6	33	92	5	5	0	-800	1372	Pre-Cambrian	46.3	3	32
2	3	36	92	5	5	0	-778	1347	Pre-Cambrian	39.1	3	28
2	3	36	92	5	5	0	-841	1410	Pre-Cambrian	47.0	1	33
0	4	2	92	6	5	0	-784	1366	Pre-Cambrian	48.2	1	34
0	14	3	92	6	5	0	-821	1383	Pre-Cambrian	45.5	3	31
0	10	30	92	6	5	0	-844	1347	Pre-Cambrian	37.3	3	26
0	13	30	92	6	5	0	-863	1360	Pre-Cambrian	38.8	3	27
0	4	13	92	7	5	0	-849	1351	Pre-Cambrian	32.9	3	23
0	2	16	92	7	5	0	-363	860	Ireton	15.9	1	16
0	2	16	92	7	5	0	-864	1360	Pre-Cambrian	36.6	1	25
0	11	23	92	7	5	0	-838	1338	Pre-Cambrian	37.1	1	26
0	7	25	92	7	5	0	-811	1307	Keg River?	39.8	3	29
0	10	5	92	8	5	0	-917	1409	Pre-Cambrian	34.1	4	23
0	12	22	92	8	5	0	-880	1362	Pre-Cambrian	39.6	3	28
0	6	27	92	8	5	0	-883	1365	Pre-Cambrian	51.2	3	36
0	10	16	92	9	5	0	-891	1403	Pre-Cambrian	36.7	1	25
0	4	29	92	10	5	0	-984	1554	Pre-Cambrian	46.6	1	29
0	6	7	92	11	5	0	89	704	Wabamun	28.6	3	38
0	13	13	92	11	5	0	-945	1554	Pre-Cambrian?	45.8	2	28
0	2	17	92	11	5	0	-983	1748	Pre-Cambrian	54.0	1	30
0	16	21	92	11	5	0	-975	1663	Pre-Cambrian	50.3	4	29
0	16	30	92	11	5	0	-991	1743	Pre-Cambrian	59.0	1	33
0	16	33	92	11	5	0	-974	1660	Pre-Cambrian	38.9	1	22
0	15	35	92	11	5	0	-945	1563	Pre-Cambrian	54.3	3	33
0	9	3	92	12	5	0	-1003	1775	Pre-Cambrian	45.9	1	25
0	4	6	92	12	5	0	-1024	1845	Pre-Cambrian	39.2	1	20
0	7	12	92	12	5	0	-977	1770	Pre-Cambrian	47.2	1	26
0	6	29	92	12	5	0	85	693	Wabamun	23.2	1	31
0	13	1	92	13	5	0	-994	1773	Pre-Cambrian	44.2	2	24
0	2	2	92	13	5	0	-869	1688	Muskeg?	35.3	1	20
0	7	2	92	13	5	0	-860	1675	Muskeg?	48.8	1	28
0	10	7	92	13	5	0	-1019	1765	Pre-Cambrian	39.8	1	21
0	6	11	92	13	5	0	87	732	Banff	30.9	1	39
0	14	14	92	13	5	0	-1014	1778	Pre-Cambrian	58.8	1	32
0	8	27	92	13	5	0	-990	1755	Pre-Cambrian	40.1	1	22
0	10	30	92	13	5	0	-1027	1737	Pre-Cambrian	35.2	4	19
0	14	34	92	13	5	0	-1008	1770	Pre-Cambrian	39.7	3	21
0	5	5	92	14	5	0	-1087	1841	Pre-Cambrian	56.7	2	30

LE	L	S	T	R	M	ESQ	Elevation (m)	Depth (m)	Formation†	T† (deg C)	BHT Quality (1-4)	Grad T* (deg C/km)
0	5	5	92	14	5	0	-1087	1841	Pre-Cambrian	57.0	1	30
0	5	14	92	14	5	0	-917	1665	Muskeg?	39.7	1	23
0	7	24	92	14	5	0	-1053	1745	Pre-Cambrian	55.1	1	30
0	5	30	92	14	5	0	-1071	1819	Pre-Cambrian	60.6	1	32
0	7	8	93	1	5	0	-725	1387	Pre-Cambrian	39.0	1	27
0	10	10	93	1	5	0	-682	1335	Pre-Cambrian	47.4	3	34
2	10	10	93	1	5	0	-681	1334	Pre-Cambrian	48.5	3	35
0	16	23	93	2	5	0	-700	1355	Pre-Cambrian	39.9	1	28
0	14	3	93	3	5	0	-688	1318	Pre-Cambrian	35.1	3	25
0	10	5	93	3	5	0	-700	1310	Pre-Cambrian	38.6	1	28
0	11	10	93	4	5	0	-742	1317	Pre-Cambrian	33.8	2	24
0	7	31	93	4	5	0	-776	1341	Pre-Cambrian	43.6	1	31
0	4	4	93	5	5	0	-773	1346	Pre-Cambrian	46.3	2	33
0	1	5	93	5	5	0	-756	1330	Pre-Cambrian	44.1	3	32
0	9	5	93	5	5	0	-744	1323	Pre-Cambrian	35.3	3	25
0	10	7	93	5	5	0	-788	1364	Pre-Cambrian	45.4	1	32
0	1	8	93	5	5	0	-735	1320	Pre-Cambrian	41.0	3	30
0	5	8	93	5	5	0	-728	1317	Pre-Cambrian	43.8	1	32
0	6	8	93	5	5	0	-504	1093	Ft. Vermillion?	42.4	2	37
0	6	8	93	5	5	0	-781	1371	Pre-Cambrian	54.3	4	38
0	5	17	93	5	5	0	-768	1346	Pre-Cambrian	38.8	2	27
0	10	17	93	5	5	0	-793	1367	Pre-Cambrian	38.0	1	26
0	12	17	93	5	5	0	-741	1313	Pre-Cambrian	41.8	1	30
0	1	18	93	5	5	0	-780	1354	Granite Wash?	43.3	3	30
0	15	19	93	5	5	0	-773	1347	Pre-Cambrian	40.2	3	28
0	11	20	93	5	5	0	-746	1313	Pre-Cambrian	38.7	3	28
0	4	30	93	5	5	0	-764	1333	Pre-Cambrian	40.0	3	29
0	7	30	93	5	5	0	-753	1330	Pre-Cambrian	51.9	1	38
0	11	30	93	5	5	0	-761	1333	Pre-Cambrian	39.2	3	28
0	6	5	93	6	5	0	-817	1321	Chinchaga	32.8	1	23
0	11	13	93	6	5	0	-785	1343	Pre-Cambrian	38.0	1	27
0	9	2	93	7	5	0	-870	1360	Pre-Cambrian	35.9	1	25
0	8	36	93	7	5	0	-818	1325	Pre-Cambrian?	38.6	1	28
0	10	10	93	8	5	0	-879	1360	Pre-Cambrian?	59.0	1	42
0	10	15	93	8	5	0	-298	781	Ireton	22.2	2	26
0	10	15	93	8	5	0	-873	1355	Pre-Cambrian	41.6	4	29
0	2	26	93	9	5	0	-968	1468	Pre-Cambrian	42.3	1	27
0	11	29	93	10	5	0	-917	1495	Pre-Cambrian	39.8	3	25
0	15	27	93	11	5	0	-941	1644	Pre-Cambrian	56.8	3	33
0	6	5	93	13	5	0	74	629	Wabamun	27.8	2	41
0	10	22	93	13	5	0	-1038	1763	Pre-Cambrian	38.6	1	21
0	6	23	93	14	5	0	96	564	Wabamun?	26.2	2	43
0	9	23	93	14	5	0	-1047	1725	Pre-Cambrian	46.9	3	26
0	2	28	94	1	5	0	-691	1464	Pre-Cambrian	56.5	2	37
0	15	3	94	2	5	0	-333	1015	Muskeg	42.6	4	40
0	3	7	94	3	5	0	-692	1313	Pre-Cambrian	39.1	3	28
0	3	4	94	4	5	0	-741	1312	Pre-Cambrian?	40.8	1	30

LI:	L	S	T	R	M	ESQ	Elevation (m)	Depth (m)	Formation†	Tf (deg C)	BHT Quality (1-4)	Grad T* (deg C/km)
0	5	8	94	4	5	0	-708	1275	Pre-Cambrian	44.9	1	34
2	6	17	94	4	5	0	-744	1327	Pre-Cambrian	44.8	1	32
0	5	30	94	4	5	0	-779	1367	Pre-Cambrian	35.2	3	24
0	11	1	94	5	5	0	-735	1305	Pre-Cambrian	37.5	1	27
0	10	2	94	5	5	0	-779	1340	Pre-Cambrian	37.1	3	26
0	5	17	94	5	5	0	-765	1324	Pre-Cambrian	39.6	3	28
0	6	20	94	5	5	0	-707	1261	Pre-Cambrian	35.9	1	27
0	12	28	94	5	5	0	-765	1295	Pre-Cambrian	35.6	2	26
0	10	7	94	6	5	0	-791	1310	Pre-Cambrian	36.6	1	26
0	11	7	94	6	5	0	-830	1340	Pre-Cambrian	47.6	1	34
0	1	19	94	6	5	0	-756	1278	Pre-Cambrian	36.0	1	27
0	3	22	94	6	5	0	-830	1361	Pre-Cambrian	37.6	1	26
0	3	22	94	6	5	0	-830	1361	Pre-Cambrian	39.4	1	27
0	14	1	94	7	5	0	-802	1295	Chinchaga	37.5	4	27
0	14	1	94	7	5	0	-822	1315	Pre-Cambrian	37.5	3	27
0	9	12	94	7	5	0	-837	1340	Pre-Cambrian	51.3	1	37
0	6	18	94	7	5	0	-876	1341	Pre-Cambrian	29.5	1	20
0	15	30	94	8	5	0	-870	1355	Pre-Cambrian	42.1	1	30
0	6	6	94	10	5	0	-948	1557	Pre-Cambrian	50.3	4	31
0	2	23	94	10	5	0	-928	1471	Pre-Cambrian	41.1	3	27
0	9	11	94	11	5	0	-975	1689	Pre-Cambrian	47.4	3	27
0	7	17	94	13	5	0	-1039	1725	Pre-Cambrian	52.6	3	29
0	7	15	94	14	5	0	-1067	1632	Pre-Cambrian	41.8	3	24
0	10	30	94	14	5	0	-891	1459	Muskeg?	44.8	3	29
0	6	7	95	2	5	0	-678	1325	Pre-Cambrian?	43.1	1	31
0	9	36	95	2	5	0	-674	1379	Pre-Cambrian	39.7	1	27
0	9	6	95	4	5	0	-687	1251	Keg River	35.1	2	26
0	9	6	95	4	5	0	-714	1278	Pre-Cambrian	36.0	1	27
0	4	19	95	4	5	0	-731	1270	Pre-Cambrian?	37.4	3	28
0	1	31	95	4	5	0	-677	1207	Pre-Cambrian?	49.0	1	39
0	1	31	95	4	5	0	-677	1207	Pre-Cambrian?	49.6	2	39
0	10	1	95	5	5	0	-774	1317	Pre-Cambrian	40.7	3	29
0	1	23	95	5	5	0	-733	1240	Pre-Cambrian	42.4	1	33
0	10	25	95	5	5	0	-667	1182	Pre-Cambrian	48.6	3	39
0	9	26	95	5	5	0	-709	1221	Pre-Cambrian	42.2	3	33
0	16	34	95	5	5	0	-188	709	Ireton	26.6	1	35
0	16	34	95	5	5	0	-723	1244	Pre-Cambrian	41.2	1	32
0	15	3	95	6	5	0	-804	1368	Pre-Cambrian	38.8	1	27
0	10	8	95	6	5	0	-749	1281	Pre-Cambrian	37.0	1	27
0	2	10	95	6	5	0	-732	1299	Pre-Cambrian	42.3	2	31
0	3	20	95	6	5	0	-729	1265	Pre-Cambrian	40.3	3	30
0	14	20	95	6	5	0	-714	1252	Pre-Cambrian	40.8	3	31
0	16	22	95	6	5	0	-286	854	Beaverhill Lk.	17.1	2	18
0	16	22	95	6	5	0	-726	1294	Pre-Cambrian	41.7	1	31
0	15	27	95	6	5	0	-767	1325	Chinchaga	41.9	3	30
0	10	32	95	6	5	0	-759	1277	Pre-Cambrian	41.0	3	31
0	7	34	95	6	5	0	-122	680	Ireton	20.4	1	27

LE	L	S	T	R	M	ESQ	Elevation (m)	Depth (m)	Formation†	T† (deg C)	BHT Quality (1-4)	Grad T* (deg C/km)
0	7	34	95	6	5	0	-722	1280	Pre-Cambrian	35.0	1	26
0	10	18	95	7	5	0	-822	1291	Pre-Cambrian?	36.1	3	26
0	4	22	95	8	5	0	-903	1363	Pre-Cambrian	37.3	4	26
0	12	4	95	9	5	0	-932	1456	Pre-Cambrian	39.5	4	26
0	15	12	95	9	5	0	-853	1332	Pre-Cambrian	47.8	1	34
0	13	10	95	10	5	0	-900	1462	Keg River?	46.1	1	30
0	5	16	95	10	5	0	-891	1522	Pre-Cambrian	46.4	2	29
0	10	15	95	11	5	0	-933	1738	Pre-Cambrian	42.8	1	23
0	9	16	95	11	5	0	-875	1706	Pre-Cambrian	46.5	3	26
0	10	23	95	12	5	0	73	637	Wabamun	36.3	1	54
0	10	28	95	12	5	0	100	594	Wabamun	24.6	2	38
0	10	28	95	12	5	0	-993	1687	Pre-Cambrian	42.2	1	24
0	6	29	95	12	5	0	122	541	Bluesky	33.5	2	58
0	6	23	95	13	5	0	78	558	Wabamun?	33.8	1	57
0	10	32	95	13	5	0	75	499	Wabamun?	29.6	1	55
0	6	31	95	14	5	0	44	535	Wabamun?	33.5	1	59
0	6	11	96	1	5	0	-666	1445	Pre-Cambrian	40.8	1	27
0	16	2	96	2	5	0	-21	703	Ireton	27.2	4	36
0	16	2	96	2	5	0	-691	1373	Pre-Cambrian?	42.4	3	29
0	4	33	96	4	5	0	-692	1211	Pre-Cambrian	45.5	1	36
0	7	1	96	5	5	0	-631	1146	Pre-Cambrian	39.9	1	33
0	1	25	96	5	5	0	-740	1274	Pre-Cambrian	39.2	1	29
0	11	2	96	6	5	0	-705	1275	Pre-Cambrian	55.2	3	42
0	15	2	96	6	5	0	-693	1251	Pre-Cambrian	39.2	1	30
0	1	3	96	6	5	0	-720	1278	Pre-Cambrian	41.5	3	31
0	3	5	96	6	5	0	-682	1192	Pre-Cambrian	38.6	3	31
0	4	5	96	6	5	0	-142	650	Ireton	24.2	2	34
0	4	5	96	6	5	0	-766	1274	Pre-Cambrian	47.2	1	36
0	13	9	96	6	5	0	-701	1223	Pre-Cambrian	33.0	3	25
0	9	10	96	6	5	0	-124	667	Winterburn?	38.1	3	54
0	9	10	96	6	5	0	-739	1282	Pre-Cambrian	38.0	2	28
0	3	11	96	6	5	0	-685	1240	Pre-Cambrian	41.8	2	32
0	3	16	96	6	5	0	-665	1185	Pre-Cambrian	40.1	3	32
0	7	16	96	6	5	0	-115	638	Beaverhill Lk.?	36.5	1	54
0	7	16	96	6	5	0	-731	1254	Pre-Cambrian	48.4	3	37
0	15	16	96	6	5	0	-688	1212	Pre-Cambrian	43.3	1	34
0	1	21	96	6	5	0	-721	1244	Pre-Cambrian	42.9	3	33
0	14	22	96	6	5	0	-662	1187	Pre-Cambrian	36.3	1	29
0	5	26	96	6	5	0	-709	1253	Pre-Cambrian	37.2	3	28
0	7	27	96	6	5	0	-690	1220	Pre-Cambrian	39.9	3	31
0	16	27	96	6	5	0	-126	655	Ireton	24.9	2	35
0	16	27	96	6	5	0	-664	1193	Pre-Cambrian	39.5	3	31
0	16	16	96	7	5	0	-836	1309	Pre-Cambrian	39.1	1	28
0	15	17	96	9	5	0	-889	1388	Pre-Cambrian	35.9	1	24
0	3	36	96	11	5	0	-927	1721	Pre-Cambrian?	49.0	1	27
0	6	8	96	12	5	0	106	654	Grand Rapids	28.2	2	40
0	9	13	96	12	5	0	-920	1729	Pre-Cambrian	48.0	1	27

LE	L	S	T	R	M	ESQ	Elevation (m)	Depth (m)	Formation†	Tf (deg C)	BHT Quality (1-4)	Grad T* (deg C/km)
0	6	3	96	14	5	0	96	486	Cretaceous	29.5	3	51
0	4	8	97	2	5	0	-681	1273	Pre-Cambrian	37.4	1	28
0	10	13	97	6	5	0	-747	1279	Chinchaga	42.8	1	32
0	7	28	97	8	5	0	-855	1319	Keg River?	47.9	1	35
0	4	6	97	9	5	0	-910	1418	Pre-Cambrian	55.5	4	38
0	11	7	97	10	5	0	-956	1695	Pre-Cambrian	47.6	1	27
0	13	20	97	10	5	0	-994	1654	Pre-Cambrian?	43.1	1	25
0	13	20	97	10	5	0	-972	1632	Pre-Cambrian?	43.5	2	25
0	11	3	97	11	5	0	-951	1755	Pre-Cambrian	53.1	2	29
0	7	8	97	12	5	0	43	761	Wabamun	37.2	3	46
0	7	27	97	12	5	0	59	689	Wabamun	35.3	3	48
0	10	!	97	14	5	0	-1057	1665	Pre-Cambrian	42.4	1	24
0	10	6	97	14	5	0	-490	1049	Banff?	36.9	2	33
0	10	6	97	14	5	0	-1081	1640	Pre-Cambrian	41.5	3	24
0	6	6	98	1	5	0	-632	1202	Pre-Cambrian	31.7	1	25
0	5	20	98	1	5	0	-589	1132	Chinchaga	53.6	3	46
0	6	22	98	1	5	0	-600	1195	Pre-Cambrian?	33.8	3	27
0	13	3	98	2	5	0	-670	1205	Pre-Cambrian	40.8	2	32
0	7	11	98	3	5	0	-691	1221	Pre-Cambrian?	54.5	1	43
0	14	8	98	6	5	0	-807	1300	Pre-Cambrian	42.5	1	31
0	12	26	98	7	5	0	-817	1261	Pre-Cambrian	42.6	1	32
0	10	19	98	8	5	0	-855	1289	Pre-Cambrian	42.5	3	31
0	10	28	98	9	5	0	-891	1359	Pre-Cambrian	49.5	4	35
0	6	5	98	10	5	0	-420	1027	Beaverhill Lk.?	31.7	4	29
0	6	31	98	10	5	0	-922	1480	Pre-Cambrian	51.9	2	34
0	6	15	98	11	5	0	-923	1699	Pre-Cambrian?	48.2	2	27
0	8	17	98	11	5	0	-920	1724	Pre-Cambrian	53.4	3	30
0	6	11	98	12	5	0	-948	1738	Pre-Cambrian?	54.7	4	30
0	11	2	98	14	5	0	-1056	1692	Pre-Cambrian	44.7	1	25
0	5	12	99	4	5	0	-723	1237	Pre-Cambrian?	41.8	3	32
0	8	10	99	5	5	0	-761	1235	Pre-Cambrian	40.8	3	31
0	14	36	99	6	5	0	-766	1199	Pre-Cambrian	55.5	4	45
0	3	8	99	7	5	0	-862	1288	Pre-Cambrian	40.7	1	30
0	6	33	99	7	5	0	-39	446	Winterburn	23.5	4	48
0	6	33	99	7	5	0	-814	1221	Pre-Cambrian	49.6	3	39
0	6	28	99	8	5	0	-529	934	Muskeg	50.7	4	52
0	4	31	99	9	5	0	-874	1532	Pre-Cambrian	58.5	3	37
0	11	34	99	9	5	0	-877	1326	Pre-Cambrian	66.9	1	49
0	10	21	99	12	5	0	112	536	Ireton?	22.1	1	38
2	10	8	99	13	5	0	-1030	1718	Pre-Cambrian	43.6	2	24
0	7	34	99	13	5	0	-234	893	Banff?	30.1	2	31
0	16	3	100	2	5	0	-676	1160	Pre-Cambrian	30.0	1	24
0	7	2	100	4	5	0	-307	763	Slave Point	23.9	4	29
0	7	2	100	4	5	0	-690	1146	Pre-Cambrian	36.5	4	30
0	16	11	100	4	5	0	-719	1159	Pre-Cambrian	41.9	1	34
0	7	36	100	4	5	0	-653	1063	Pre-Cambrian	40.3	1	36
0	6	10	100	5	5	0	-712	1145	Pre-Cambrian	49.7	3	42

LE	L	S	T	R	M	ESQ	Elevation (m)	Depth (m)	Formation†	TT (deg C)	BHT Quality (1-4)	Grad T* (deg C/km)
0	4	3	100	7	5	0	-817	1223	Pre-Cambrian	45.0	4	35
0	10	7	100	9	5	0	-860	1469	Pre-Cambrian	59.5	1	39
2	10	17	100	12	5	0	-957	1597	Pre-Cambrian	49.1	1	29
0	6	14	101	1	5	0	-632	1082	Pre-Cambrian	36.7	1	32
0	7	29	101	1	5	0	-555	976	Chinchaga	40.0	3	39
0	1	11	101	2	5	0	-662	1084	Pre-Cambrian	42.8	1	38
0	3	7	101	5	5	0	-752	1147	Pre-Cambrian	41.3	1	34
0	4	12	101	5	5	0	-721	1120	Pre-Cambrian	43.1	1	37
0	6	31	101	5	5	0	-747	1119	Pre-Cambrian	39.6	1	34
0	10	6	101	6	5	0	-779	1156	Pre-Cambrian	59.0	3	49
0	11	4	101	9	5	0	-853	1355	Pre-Cambrian?	47.8	3	34
0	11	7	101	10	5	0	-906	1642	Pre-Cambrian	49.8	3	29
0	4	15	101	11	5	0	-606	1430	Muskeg	49.4	1	33
0	7	24	101	12	5	0	-935	1766	Pre-Cambrian	55.0	1	30
0	1	31	101	13	5	0	-996	1822	Pre-Cambrian	56.0	1	30
AA	10	17	89	23	4	0	-14	525	Wabamun?	20.6	2	35
0	10	29	89	23	4	0	-650	1162	Pre-Cambrian	43.6	1	36
0	14	36	89	23	4	0	314	187	Clearwater	12.5	4	56.1
0	14	36	89	23	4	0	-294	795	Woodbend?	30.2	4	35
0	14	36	89	23	4	0	-602	1103	Granite Wash?	30.4	4	26
0	14	36	89	23	4	0	-627	1127	Pre-Cambrian	32.2	4	27
0	12	7	89	25	4	0	-680	1383	Keg River?	39.8	1	27
0	6	11	89	25	4	0	209	413	Winterburn	21.0	1	46
0	7	14	89	25	4	0	106	495	Grosmont	27.7	2	52
0	11	28	89	25	4	0	-706	1313	Pre-Cambrian	37.9	4	27
0	7	19	90	23	4	0	18	497	Wabamun?	22.8	3	42
0	11	21	90	23	4	0	49	474	Wabamun?	26.8	2	52
0	10	36	91	23	4	0	276	295	Bluesky?	19.5	3	59
0	11	12	91	24	4	0	26	492	Ireton	18.7	1	34
0	10	34	91	24	4	0	-679	1223	Pre-Cambrian?	37.7	1	29
0	5	12	92	24	4	0	-676	1241	Pre-Cambrian	39.9	1	31
0	10	21	92	24	4	0	48	545	Ireton	24.1	3	41
0	7	1	93	23	4	0	273	373	Grosmont	10.2	2	22.1
0	4	25	93	24	4	0	-609	1283	Pre-Cambrian?	34.9	1	26
0	15	34	93	24	4	0	-626	1350	Pre-Cambrian	36.9	1	26
0	10	35	93	24	4	0	243	487	Grosmont	27.9	2	53
0	10	15	93	25	4	0	151	527	Grosmont	24.8	2	43
0	10	15	93	25	4	0	22	656	Beaverhill Lk.?	29.6	2	42
0	11	24	93	25	4	0	-680	1314	Pre-Cambrian	40.6	1	29
0	10	33	93	25	4	0	-673	1425	Pre-Cambrian	35.9	3	24
0	10	33	93	25	4	0	-673	1425	Pre-Cambrian	48.7	3	33
0	11	33	93	25	4	0	-676	1419	Pre-Cambrian	39.5	3	26
0	11	2	94	23	4	0	278	492	Grosmont	25.3	3	47
0	12	7	94	23	4	0	-565	1362	Pre-Cambrian?	39.0	1	27
0	4	19	94	23	4	0	251	543	Grosmont	32.2	3	56
0	6	27	94	23	4	0	210	572	Wabamun?	20.5	3	32
0	7	1	94	24	4	0	520	230	Base Fish Sc.	12.6	4	46.0

LE	L	S	T	R	M	ESQ	Elevation (m)	Depth (m)	Formation†	Tf (deg C)	BHT Quality (1-4)	Grad T* (deg C/km)
0	7	1	94	24	4	0	300	450	Bluesky?	26.0	4	53
0	6	12	94	24	4	0	249	541	Grosmont	28.1	3	48
0	10	18	94	24	4	0	429	276	Viking	18.2	4	59
0	10	18	94	24	4	0	423	282	Joli Fou	18.2	4	57
0	10	23	95	23	4	0	309	472	Bluesky?	23.9	2	46
0	10	19	95	24	4	0	-13	807	Ireton	30.9	2	36
0	10	19	95	24	4	0	-257	1051	Slave Point	35.2	2	32
0	10	19	95	24	4	0	-646	1440	Pre-Cambrian	41.2	2	27
0	10	28	95	24	4	0	-649	1434	Pre-Cambrian	50.9	1	34
0	6	11	96	23	4	0	165	582	Wabamun?	29.5	2	47
0	7	24	96	23	4	0	210	577	Wabamun?	33.1	2	54
0	11	27	96	23	4	0	254	536	Grosmont	28.3	1	49
0	11	15	96	24	4	0	252	591	Grosmont	31.1	1	49
0	6	24	96	24	4	0	251	593	Grosmont	31.6	3	50
0	16	23	96	25	4	0	-660	1461	Pre-Cambrian	34.2	1	22
0	7	2	97	23	4	0	186	639	Wabamun?	27.2	3	39
0	6	7	97	23	4	0	-418	1258	Muskeg	41.2	1	31
0	6	7	97	23	4	0	-599	1439	Pre-Cambrian?	47.9	1	32
0	7	34	97	23	4	0	192	571	Wabamun?	33.6	1	55
0	11	3	97	24	4	0	263	561	Grosmont	35.0	3	59
0	6	5	97	24	4	0	259	519	Grosmont	29.7	1	53
0	10	15	97	24	4	0	232	548	Grosmont	34.4	2	59
0	11	19	97	24	4	0	250	473	Grosmont	28.9	1	57
0	6	24	97	24	4	0	-553	1344	Pre-Cambrian	45.7	3	33
0	6	1	97	25	4	0	271	436	Winterburn	23.4	4	49
0	4	11	98	23	4	0	-517	1186	Pre-Cambrian?	44.5	3	36
0	7	30	98	23	4	0	183	452	Wabamun?	26.2	1	54
0	6	5	98	24	4	0	152	563	Ireton	26.9	2	44
0	6	15	98	24	4	0	263	481	Winterburn	28.2	3	54
0	7	3	98	25	4	0	-591	1274	Pre-Cambrian	39.4	3	29
0	6	6	99	24	4	0	262	321	Bluesky?	18.0	3	50
0	6	6	99	24	4	0	179	404	Grosmont	22.7	2	51
0	7	18	99	24	4	0	244	350	Grosmont	21.1	3	55
0	10	14	100	23	4	0	-560	1249	Pre-Cambrian	45.5	1	35
0	7	10	100	24	4	0	240	376	Grosmont	18.2	3	43
0	7	10	100	24	4	0	171	445	Ireton	20.9	3	42
0	1	29	101	24	4	0	-600	1070	Pre-Cambrian	46.4	1	42
0	2	10	102	23	4	0	-560	1075	Pre-Cambrian	41.2	1	37
0	16	27	102	24	4	0	-580	992	Pre-Cambrian	30.8	1	29

**Abbreviations (cont. overpage)**

LE: Location exception code

L: Legal Sub-Division

S: Section

T: Township

R: Range

M: Meridian

ESQ: Event sequence code

†from PUBCO (1990 a)

\* Average vertical  
temperature gradient  
calculated as:  
(Tf-Ts)/depth

**Abbreviations cont.**

**BHT:** Bottom Hole temperature

**Tf:** corrected formation temperature

**Ts:** average annual ground surface temperature (4 deg C)

**d:** thermometer depth

**BHT Quality Codes**

**1:** multiple temperature measurements (Horner corrected)

**2:** one temperature measurement with time elapsed since circulation stopped known

**3:** first temperature measurement with time elapsed since circulation stopped known

**4:** one temperature measurement, with time elapsed since circulation stopped unknown



**A4.3 Culled Major Ion Water Chemistry Data**

Formation	L	S	T	R	M	DST#	depth (m)	Cl (mg/l)	CO3 (mg/l)	HCO3 (mg/l)	SO4 (mg/l)	Na (mg/l)	K (mg/l)	Ca (mg/l)	Mg (mg/l)	TDS from fiche	Relative Density	pH	Na:Cl (moles)
Bluesky	3	12	89	8	5	DST 1	416	279	0	1745	1113	1162	38	92	43	4472	1.00	8.3	6.4
Bluesky	12	11	89	10	5	DST	10458	10458	0	110	91	6253	51	80	81	17125		6.4	0.9
Bluesky	3	12	90	9	5	DST 1	8237	8237	0	1903	4620	7572	0	383	137	22852	1.01	7.5	1.4
Bluesky	6	35	90	12	5	DST 1	4700	4700	0	1950	113	3590	47	80	44	10514	1.01	8.2	1.2
Bluesky	15	21	91	12	5	DST 1	3875	3875	0	1220	716	3110	66	22	19	7650	1.01	8.3	1.2
Bluesky	6	32	91	13	5	DST 1	8881	8881	0	3676	65	7115	0	39	10	19785	1.01	7.8	1.2
Bluesky	7	14	91	18	4	DST 1	586	586	0	2712	25	1329	17	26	24	4719	1.00	8.0	3.5
Bluesky	10	14	91	20	4	DST 8	1505	1505	0	738	10	1123	0	54	39	3469	1.00	7.8	1.2
Bluesky	10	24	91	24	5	DST 11	9752	9752	0	2030	11	6951	0	106	12	18862	1.01	7.5	1.1
Bluesky	16	33	92	11	5	DST 1	3690	3690	0	1980	137	2880	69	106	58	8920	1.01	7.9	1.2
Bluesky	16	33	92	11	5	DST 2	11600	11600	0	1640	55	7750	113	146	200	21500	1.01	7.8	1.0
Bluesky	15	35	92	11	5	DST 1	4410	4410	0	766	573	2920	61	67	46	8840	1.01	7.9	1.0
Bluesky	10	5	92	18	4	DST 1	675	675	0	3977	49	1868	30	30	21	6650	1.00	7.9	4.3
Bluesky	6	5	93	13	5	DST 2	15625	15625	0	337	48	1324	14375	220	134	32063	1.02	8.1	0.1
Bluesky	6	12	93	23	4	flareline	3100	3100	90	2928	13	3033	47	16	34	9261	1.00	9.0	1.5
Bluesky	10	23	95	12	5	DST 1,4	16050	16050	0	1879	133	10038	0	432	340	28872	1.02	7.9	1.0
Bluesky	11	1	96	12	5	DST 1	16540	16540	0	1655	39	9998	0	602	358	29192	1.02	7.0	0.9
Bluesky	6	8	96	12	5	DST 1	11090	11090	0	2005	218	7335	75	232	214	21169	1.01	7.9	1.0
Bluesky	7	27	97	12	5	DST 1	15450	15450	120	1025	51	9848	0	220	221	26935	1.02	8.5	1.0
Bluesky	7	34	97	23	4	DST 1	6080	6080	0	2180	49	4506	0	125	73	13015	1.01	7.7	1.1
Bluesky	6	31	98	10	5	DST 2	5672	5672	0	1296	0	4400	75	27	40	10874	1.01	8.0	1.2
Bluesky	8	17	98	11	5	DST 1	14400	14400	0	503	38	7910	74	304	247	23500	1.01	7.3	0.8
Bluesky	6	1	99	16	5	DST 2	14060	14060	0	1196	226	8800	0	376	234	24892	1.02	7.7	1.0
Grosmont	14	21	89	21	4	DST 2	530	530	0	3340	59	1591	0	20	9	5549	1.01	8.0	4.6
Grosmont	14	21	89	21	4	DST 1	564	564	0	3670	44	1726	0	19	12	6035	1.01	7.7	4.7
Grosmont	14	21	89	21	4	DST 3	508	508	0	3150	36	1489	0	25	9	5217	1.01	8.1	4.5
Grosmont	7	14	89	25	4	DST 2	7100	7100	0	1684	78	4849	0	193	108	14012	1.01	6.8	1.1
Grosmont	13	31	90	4	5	swab	8425	8425	0	769	107	5494	66	110	121	15092	1.01	8.2	1.0
Grosmont	1	16	92	21	4	open hole	275	275	0	580	198	321	31	56	29	1490	1.00	7.9	1.8
Grosmont	13	28	93	2	5	DST 6	7000	7000	0	2360	51	4940	0	230	138	14718	1.01	7.1	1.1
Grosmont	13	28	93	2	5	DST 5	6580	6580	0	2270	135	4730	0	217	119	14051	1.01	7.4	1.1
Grosmont	10	5	93	3	5	DST 4	103000	103000	0	610	5940	64793	0	3604	485	178432	1.12	6.8	1.0
Grosmont	14	31	93	23	4	?	4000	4000	0	610	82	2440	8	76	63	7279	1.01	8.8	0.9
Grosmont	10	1	95	5	5	flowing	18215	18215	0	1410	12	11042		566	349	31594	1.02	8.3	0.9

Formation	L	S	T	R	M	DST#	depth (m)	Cl (mg/l)	CO3 (mg/l)	HCO3 (mg/l)	SO4 (mg/l)	Na (mg/l)	K (mg/l)	Ca (mg/l)	Mg (mg/l)	TDS from fiche	Relative Density	pH	Na:Cl (moles)
Grosmont	5	16	95	10	5	DST2	757	26800	0	355	2860	15000	183	1440	395	47100	1.03	6.9	0.9
Grosmont	7	2	95	22	4	?	599	9260	0	627	29	5831	0	66	183	15996	1.01	8.3	1.0
Grosmont	10	15	95	22	4	?	535	9230	0	1037	4	5504	0	335	259	16369	1.01	7.7	0.9
Grosmont	10	13	97	6	5	DST1	586	8800	0	740	123	5741	0	96	101	15601	1.01	8.2	1.0
Grosmont	6	6	98	1	5	DST1	365	5421	0	1810	103	4233	0	44	62	11875	1.01	8.6	1.2
Wabamun	9	7	89	7	5	DST3	451	1820	10	508	120	1260	27	40	24	3809	1.00	8.4	1.1
Wabamun	8	19	89	7	5	DST3	425	3048	0	1690	152	2619	20	21	16	7566	1.00	8.1	1.3
Wabamun	6	22	89	8	5	DST2	389	12900	0	1484	330	7100	270	610	290	22986	1.02	8.1	0.8
Wabamun	10	35	90	5	5	swab 16	517	15062	0	696	816	9647	0	283	238	26742	1.11	7.5	1.0
Wabamun	4	35	90	11	5	DST2	769	6703	0	505	1899	4689	0	414	148	14358	1.01	8.3	1.1
Wabamun	10	2	90	13	5	DST1	585	4574	108	2767	118	4048	0	42	23	11680	1.01	8.5	1.4
Wabamun	10	2	90	13	5	DST1	585	5344	102	3196	46	4692	0	35	31	13446	1.01	8.6	1.4
Wabamun	10	26	92	8	5	flowline	327	4349	312	1181	9	3399	0	11	52	9313	1.01	9.7	1.2
Wabamun	6	5	93	6	5	DST1	384	6232	0	1366	308	4384	0	125	94	12509	1.01	7.7	1.1
Wabamun	10	6	101	6	5	DST1	187	5610	360	1020	150	4319	0	22	13	11494	1.02	9.4	1.2
Winterburn	11	27	90	10	5	DST2	677	19250	0	386	27	6266	9092	531	218	35770	1.02	8.1	0.5
Winterburn	11	27	92	5	5	DST1	475	179520	0	162	126	74021	0	29058	4860	287752	1.20	6.9	0.6
Winterburn	13	28	93	2	5	DST8	452	10100	0	973	1018	3570	0	2960	232	18853	1.01	6.5	0.5
Winterburn	6	8	93	5	5	DST1	453	135102	12	25	350	84321	0	2250	454	222514	1.15	7.9	1.0
Winterburn	14	36	99	6	5	DST2	276	89000	0	355	6897	58550	0	1874	227	156903	1.11	7.5	1.0
Ireton	10	4	93	23	4	?	427	340	0	268	5	230	4	30	13	890	1.00	7.8	1.0
Ireton	1	21	93	23	4	?	482	3750	0	1781	7	2830	43	24	63	8498	1.01	8.1	1.2
Ireton	10	27	93	23	4	?	515	1963	0	1800	66	1790	35	56	39	5749	1.00	8.3	1.4
Ireton	10	27	93	23	4	rev circ	535	5600	0	1739	37	4065	85	40	78	11644	1.00	8.3	1.1
Ireton	6	1	94	23	4	core sleeve	548	2263	0	1970	16	2025	31	48	34	6387	1.00	7.9	1.4
Ireton	6	1	94	23	4	core barrel	519	2150	0	1940	18	1980	20	16	32	6156	1.00	8.3	1.4
Ireton	6	1	94	23	4	core sleeve	535	438	0	732	8	555	16	28	19	1796	1.00	8.4	2.0
Ireton	7	28	97	8	5	DST1	673	90100	0	595	16230	57660	187	2583	1166	168521	1.12	7.3	1.0
Ireton	7	28	97	8	5	RFT 10	?	136000	0	327	17070	86870	278	2923	1725	245193	1.16	7.3	1.0
Slave Point	11	29	89	4	5	DST3	1278	191000	27	802	94500	905	15060	4253	306547	1.21	6.3	0.8	
Slave Point	12	6	89	8	5	flow	1238	80000	230	1350	35256	10911	2552	130299	1.10	6.1	0.7		
Slave Point	1	10	89	8	5	?	1256	83600	98	1170	37000	480	11400	2780	137000	1.11	6.0	0.7	
Slave Point	11	18	89	8	5	flow	1240	77700	300	1426	34357	9914	2877	126574	1.09	6.3	0.7		
Slave Point	16	22	89	8	5	swab#5	1219	78750	378	1428	31440	345	10550	3052	125943	1.09	6.3	0.6	

Formation	L	S	T	R	M	DST#	depth (m)	Cl (mg/l)	CO3 (mg/l)	HCO3 (mg/l)	SO4 (mg/l)	Na (mg/l)	K (mg/l)	Ca (mg/l)	Mg (mg/l)	TDS from fiche	Relative Density	pH	Na:Cl (moles)
Slave Point	5	26	89	8	5	swab #3	1209	89300		776	2060	35800	368	17600	3900	149600	1.12	7.0	0.6
Slave Point	4	1	89	9	5	treater	1251	74500		270	1633	33449		9109	2795	121756	1.09	6.6	0.7
Slave Point	3	12	89	9	5	treater	1247	78000		480	1639	34307		10010	3038	127474	1.09	6.7	0.7
Slave Point	14	5	89	14	5	DST 5	1636	70800		63	2909	35950	216	5574	1677	118189	1.08	6.9	0.8
Slave Point	4	7	89	14	5	DST 1	1657	80000		193	2250	43320	235	8016	2431	136300	1.11	6.9	0.8
Slave Point	3	5	90	7	5	DST 2	1197	67800		120	2010	33469		6519	2124	112042	1.08	5.8	0.8
Slave Point	11	5	90	8	5	pump	1215	76000		571	1280	32185		11351	2588	123975	1.09	7.0	0.7
Slave Point	6	8	90	14	5	DST 3	1625	56700		166	3185	29580	182	2899	1555	94267	1.07	7.1	0.8
Slave Point	16	30	91	3	5	DST 3	1038	180200		71	379	72920	894	28310	4204	286978	1.19	6.2	0.6
Slave Point	9	35	91	6	5	DST 1	1369	180350		244	4461	68241		29469	9058	291823	1.20	6.3	0.6
Slave Point	11	27	92	5	5	DST 3	1097	172480		122	136	68524		30060	5346	276670	1.20	6.6	0.6
Slave Point	10	31	92	6	5	DST 2	1034	148000		146	2012	81869	1075	11210	728	245039	1.16	7.7	0.9
Slave Point	11	23	92	7	5	swab	1057	85000		456	1062	20820	2322	22640	3123	135423	1.10	6.2	0.4
Slave Point	10	5	93	3	5	DST 3	1020	174500		220	4300	111634		2403	461	293518	1.19	7.2	1.0
Slave Point	7	18	93	6	5	DST 4	1030	178000		76	583	99900	894	12600	83	292000	1.20	6.9	0.9
Slave Point	3	7	94	3	5	DST 2	1256	129000	8	55	965	65900	712	10500	466	208000	1.15	8.1	0.8
Slave Point	12	28	94	5	5	DST 1	1162	151000		137	464	91600	250	2010	4	245000	1.17	8.1	0.9
Slave Point	11	7	94	6	5	DST 2	1023	185000		162	2450	107000	800	5120	2	301000	1.20	7.0	0.9
Slave Point	9	6	95	4	5	DST 2	975	142000	165		1170	75100	528	11100	1	230000	1.15	10.7	0.8
Slave Point	3	16	96	6	5	DST 2	957	128000		110	1901	67360	455	9009	352	207187	1.13	8.0	0.8
Slave Point	4	31	99	9	5	WLT 2	1235	90000		210	4510	53646		5205	510	154081	1.10	6.6	0.9
Muskeg	4	3	100	7	5	DST 4	1090	166200		210	2805	104193		3051	778	277237	1.17	6.8	1.0
Muskeg	7	11	98	3	5	DST 1	1154	188125		391	463	96721		17197	3123	306020	1.22	7.4	0.8
Muskeg	7	24	101	12	5	DST 1	1672	103100		212	3127	55020	700	9850	2017	174026	1.11	8	0.8
Muskeg	5	22	102	7	5	DST 2	984	113360		137	5456	73715		2124	19	194809	1.14	7.7	1.0
Keg River	5	12	89	2	5	DST 1	1474	190000		61	31	81300	1260	24400	4260	301000	1.21	6.15	0.7
Keg River	13	28	89	2	5	rig tank	1425	156400		117	346	62050	705	24300	5176	249094	1.19	5.5	0.6
Keg River	5	2	89	3	5	DST 2	1455	175000		24	163	77700	1480	21600	3000	279000	1.21	5.09	0.7
Keg River	1	3	89	3	5	DST 1	1429	185000		29	160	73400	1350	25900	3720	290000	1.21	5.43	0.6
Keg River	2	4	89	3	5	DST 1	1464	198000		56	200	74700	1700	30900	4710	310000	1.21	6.06	0.6
Keg River	9	10	89	3	5	DST 2	1491	189000		153	298	80000	1420	25000	4040	300000	1.21	7.21	0.7
Keg River	2	11	89	3	5	DST 1	1434	155000		60	584	75000	912	16000	2480	250000	1.19	6.53	0.7
Keg River	4	11	89	3	5	DST 1	1463	178000		185	775	81400	1530	24900	3230	290000	1.21	7.85	0.7
Keg River	2	15	89	3	5	DST 2	1490	164000		14	828	81500	998	15800	2540	266000	1.19	5	0.8

Formation	L	S	T	R	M	DST#	depth (m)	Cl (mg/l)	CO3 (mg/l)	HCO3 (mg/l)	SO4 (mg/l)	Na (mg/l)	K (mg/l)	Ca (mg/l)	Mg (mg/l)	TDS from fiche	Relative Density	pH	Na:Cl (moles)
Keg River	15	15	89	3	5	DST 2	1478	169000	76	380	81600	1020	20100	3439	276000	1.20	5.87	0.7	
Keg River	15	15	89	3	5	DST 1	1482	176000	56	270	81400	1180	25700	4120	289000	1.20	5.74	0.7	
Keg River	9	18	89	3	5	DST 2	1497	197000	38	255	74300	1380	35200	4780	313000	1.20	5.54	0.6	
Keg River	6	21	89	3	5	DST 2	1477	190000	49	383	73790	1144	29590	5881	300837	1.21	5.8	0.6	
Keg River	12	30	89	3	5	DST 3	1473	188000	88	310	79000	1080	27000	4060	300000	1.21	6.39	0.6	
Keg River	12	30	89	3	5	DST 2	1477	199000	37	335	85600	1250	25200	3260	315000	1.20	5.58	0.7	
Keg River	2	32	89	3	5	DST 1	1445	181000	31	683	102000	1170	8850	865	295000	1.21	6.26	0.9	
Keg River	12	10	89	4	5	DST 1	1470	169542	76	396	65300	1064	32342	3993	272712	1.20	5	0.6	
Keg River	13	12	89	4	5	DST 1	1522	183000	46	401	93200	1290	24900	3080	306000	1.20	6.41	0.8	
Keg River	11	29	89	4	5	DST 2	1480	199000	61	687	94940	981	19900	4253	319822	1.23	6	0.7	
Keg River	11	29	89	4	5	DST 1	1511	191800	29	551	74880	1014	30390	6512	305176	1.22	5.7	0.6	
Keg River	16	1	89	5	5	DST 1	1469	187000	122	354	70740	1155	30910	5176	295457	1.21	5.6	0.6	
Keg River	3	16	89	5	5	DST 1	1475	179471	131	374	63000	1250	14089	16899	275213	1.20	5.9	0.5	
Keg River	16	19	89	5	5	DST 1	1521	173000	171	346	69200	1600	29700	4810	277227	1.20	6.9	0.6	
Keg River	3	27	89	5	5	DST 1	1487	196000	149	437	90200	1600	23300	3830	316000	1.21	7.11	0.7	
Keg River	1	33	89	5	5	DST 2	1458	193000	168	352	104600	1420	20200	2390	323000	1.21	7.06	0.8	
Keg River	4	33	89	5	5	DST 2	1486	189000	148	765	105000	1500	21400	2280	320000	1.21	7.32	0.9	
Keg River	2	35	89	6	5	DST 1	1525	189000	183	796	78146	1026	26030	3278	298459	1.21	7.6	0.6	
Keg River	3	12	89	8	5	DST 2	1464	127500	224	848	55434	960	19460	2552	206978	1.14	6	0.7	
Keg River	11	10	89	9	5	DST 1	1435	119000	54	1121	52100	635	15020	2551	190481	1.13	5.3	0.7	
Keg River	16	21	89	9	5	DST 3	1414	109798	11	1563	49000	455	16795	2536	180160	1.13	6.5	0.7	
Keg River	4	23	89	9	5	DST 2	1442	119700	39	903	52650	577	15620	3353	192842	1.12	6.8	0.7	
Keg River	4	31	89	9	5	DST 1	1436	116300	303	1016	50380	635	15260	2479	186373	1.13	5.9	0.7	
Keg River	7	35	89	9	5	DST 3	1410	108022	117	1166	46715	15621	15621	3185	174826	1.12	6.35	0.7	
Keg River	11	20	89	10	5	DST 1	1509	110400	68	2642	53119	13365	2333	181927	1.12	6.9	0.7		
Keg River	4	25	89	10	5	DST 1	1452	115931	73	640	52528	16313	2262	187747	1.13	7	0.7		
Keg River	14	28	89	10	5	DST 1	1491	108348	63	844	50015	14376	2215	175861	1.12	6.5	0.7		
Keg River	5	8	89	11	5	DST 2	1621	105678	43	2087	49500	569	13894	2032	173803	1.12	6.2	0.7	
Keg River	12	33	89	11	5	RFT	1619	79700	63	7045	39890	502	9842	1808	138850	1.09	7.4	0.8	
Keg River	4	35	89	11	5	DST 1	1564	109400	27	1187	47850	452	13550	2952	175418	1.12	5.7	0.7	
Keg River	11	18	90	2	5	DST 1	1326	171814	339	611	86308	1166	17262	3013	279347	1.19	7.6	0.8	
Keg River	6	3	90	3	5	DST 1	1467	178900	81	533	79030	1166	26430	4933	291073	1.18	6.5	0.7	
Keg River	9	7	90	3	5	DST 3	1486	184300	72	412	76492	28541	5540	295357	1.20	5.5	0.6		
Keg River	8	8	90	3	5	DST 1	1488	183000	92	243	76700	1160	26100	4370	292000	1.20	6.42	0.6	

Formation	L	S	T	R	M	DST#	depth (m)	Cl (mg/l)	CO <sub>3</sub> (mg/l)	HCO <sub>3</sub> (mg/l)	SO <sub>4</sub> (mg/l)	Na (mg/l)	K (mg/l)	Ca (mg/l)	Mg (mg/l)	TDS from fiche	Relative Density	pH	Na:Cl (moles)
Keg River	10	9	90	3	5	DST 1	1482	186200		122	712	89740	929	21660	4350	303713	1.20	5.6	0.7
Keg River	6	12	90	3	5	DST 1	1430	198000	45	136	63500	1550	1550	46200	4500	313923	1.28	5.6	0.5
Keg River	8	12	90	3	5	rig tank#2	1416	188800	320	401	74990	1166	1166	31670	5492	302839	1.20	6.1	0.6
Keg River	8	12	90	3	5	?	1428	188400	261	296	76630	1166	1166	29750	5565	302068	1.20	6.2	0.6
Keg River	8	14	90	3	5	DST 1	1405	180600	138	463	76779	1040	1040	27230	4617	290867	1.20	5.3	0.7
Keg River	9	14	90	3	5	DST 1	1379	184800	78	922	102700	556	8673	2377	300106	1.19	6.8	0.9	
Keg River	11	14	90	3	5	DST 1	1386	182500	146	385	82300	1199	24420	5127	296161	1.19	8.8	0.7	
Keg River	14	16	90	3	5	DST 2	1426	180200	100	395	75430	1134	26070	5443	288772	1.19	6.5	0.6	
Keg River	15	24	90	3	5	DST 1	1327	175000	47	268	73600	1170	20300	3430	274000	1.19	5.53	0.6	
Keg River	1	24	90	3	5	DST 1	1311	145000	178	400	70800	1270	16600	3470	238000	1.19	7.13	0.8	
Keg River	8	25	90	3	5	DST 1	1295	171000	31	442	73900	1120	19900	3590	270000	1.18	5.47	0.7	
Keg River	16	30	90	3	5	DST 2	1322	196000	256	293	79200	1140	28200	5650	311000	1.20	8.04	0.6	
Keg River	2	36	90	3	5	DST 1	1318	171000	217	930	88510	604	14850	2612	278723	1.17	7.6	0.8	
Keg River	6	2	90	5	5	DST 2	1480	180200	98	488	70090	960	27270	6998	284979	1.20	6.6	0.6	
Keg River	6	2	90	5	5	DST 3	1482	180800	61	461	66380	960	27270	6998	282930	1.20	5.8	0.6	
Keg River	10	5	90	5	5	DST 2	1499	171000	107	391	68000	1180	29100	4140	276000	1.19	6.97	0.6	
Keg River	10	5	90	5	5	DST 1	1502	170000	70	362	70600	1170	26500	4070	275000	1.19	6.86	0.6	
Keg River	4	12	90	5	5	DST 1	1483	173000	105	441	73600	1080	25000	4192	277000	1.19	6.88	0.7	
Keg River	16	15	90	5	5	DST 2	1480	185500	336	527	98125	495	15820	2355	303158	1.21	7.4	0.8	
Keg River	16	15	90	5	5	DST 3	1488	157600	427	556	79790	770	18420	1942	259505	1.19	7.6	0.8	
Keg River	12	21	90	5	5	DST 1	1478	155521	86	693	73500	760	19355	2415	252329	1.16	6.6	0.7	
Keg River	2	27	90	5	5	DST 1	1474	171000	63	496	96900	744	12000	2090	283000	1.20	7.1	0.9	
Keg River	3	28	90	5	5	DST 2	1488	139000	49	485	63200	933	20700	3510	228000	1.17	5.96	0.7	
Keg River	3	28	90	5	5	DST 3	1508	150000	31	450	60900	992	24800	3840	241000	1.17	5.57	0.6	
Keg River	2	31	90	5	5	DST 1	1498	150000	85	625	58395	880	19220	8498	237703	1.18	5.7	0.6	
Keg River	10	32	90	5	5	DST 2	1480	144000	76	1040	64500	988	19600	3110	233000	1.16	6.54	0.7	
Keg River	11	33	90	5	5	DST 1	1470	167700	172	977	69200	1180	28200	3240	271187	?	7.68	0.6	
Keg River	3	24	90	6	5	DST 1	1506	173000	75	330	79000	1330	24600	3480	282000	1.21	6.52	0.7	
Keg River	8	24	90	6	5	DST 2	1514	190000	85	382	80800	1060	26300	3180	303000	1.22	5.84	0.7	
Keg River	8	24	90	6	5	DST 1	1517	197000	251	632	80770	992	25310	4204	311033	1.21	7.7	0.6	
Keg River	9	29	90	6	5	DST 1	1407	173000	174	317	70000	1090	26000	3890	276000	1.19	7.63	0.6	
Keg River	9	29	90	6	5	DST 2	1414	186000	139	251	80300	1060	28200	3380	301000	1.20	6.94	0.7	
Keg River	1	36	90	6	5	DST 2	1506	152000	244	3325	89940	391	5205	292	251397	1.16	8.2	0.9	
Keg River	3	7	90	9	5	DST 2	1439	110300	51	1584	49520	538	14410	2187	178590	1.13	5.8	0.7	

Formation	L	S	T	R	M	DST#	depth (m)	Cl (mg/l)	CO3 (mg/l)	HCO3 (mg/l)	SO4 (mg/l)	Na (mg/l)	K (mg/l)	Ca (mg/l)	Mg (mg/l)	TDS from ficine	Relative Density	pH	Na:Cl (moles)
Keg River	4	4	90	10	5	DST 2	1494	111000		29	1035	52000		14440	2064	180568	1.12	6.1	0.7
Keg River	4	4	90	10	5	DST 7	1494	112500		159	1037	52083		15160	2124	183063	1.13	6.2	0.7
Keg River	4	12	90	10	5	DST 2	1458	111000		61	1300	46660	1075	13910	2794	176800	1.13	5.5	0.6
Keg River	10	14	90	10	5	DST 2	1444	111000		107	1212	52320	534	13790	3414	182377	1.12	6.3	0.7
Keg River	6	18	90	10	5	DST 1	1505	108900		55	1053	49679	776	14890	2066	177419	1.12	6.1	0.7
Keg River	7	3	90	11	5	DST 1	1557	96400		115	1802	46260	579	10570	2272	157998	1.11	6.3	0.7
Keg River	6	16	90	11	5	DST 1	1534	110300		51	1029	49090	509	14130	2175	177284	1.12	6.3	0.7
Keg River	10	23	90	12	5	DST 1	1689	115600		7	1078	47670		18819	3281	186455	1.12	5.8	0.6
Keg River	6	14	91	2	5	DST 1	1206	155200		170	635	73883		18098	3353	251339	1.17	6.6	0.7
Keg River	5	29	91	2	5	DST 1	1215	133700		103	1728	65400	486	11970	3426	216812	1.14	7.7	0.8
Keg River	6	2	91	3	5	DST 1	1303	174000	18	85	1690	99200	666	7210	1070	284000	1.18	8.53	0.9
Keg River	2	21	91	3	5	DST 1	1304	178700		246	1333	94500	585	10850	3912	290126	1.19	6.9	0.8
Keg River	11	21	91	3	5	DST 1	1293	184000		15	268	82000	1130	22500	3900	294000	1.20	5.15	0.7
Keg River	7	28	91	3	5	flow	1266	186800		110	339	87222		22783	4204	301458	1.20	6	0.7
Keg River	9	5	91	4	5	DST 1	1313	183100		320	1128	103000	850	12770	1118	302286	1.21	7.6	0.9
Keg River	5	3	91	5	5	DST 3	1438	165000		61	535	68670	1025	24700	5419	265410	1.17	6.1	0.6
Keg River	9	4	91	5	5	DST 2	1445	161659		15	1401	77500	714	18875	2770	262936	1.19	6.2	0.7
Keg River	8	7	91	5	5	DST 1	1411	165500		198	550	68800	1110	25600	4230	266592	?	7.69	0.6
Keg River	16	8	91	5	5	DST 4	1460	163931		562	910	69000	930	24362	5318	265013	1.18	8	0.6
Keg River	2	9	91	5	5	DST 1	1432	140000		69	1490	77600	634	10100	725	231000	1.16	5.84	0.9
Keg River	15	9	91	5	5	DST 2	1432	160900		32	1148	63980	912	22420	4423	253815	1.16	6.2	0.6
Keg River	1	11	91	5	5	DST 1	1348	179300		39	613	68990	978	30150	5638	28538	1.20	4.7	0.6
Keg River	4	19	91	5	5	DST 2	1440	165491		80	398	71000	1135	25607	3285	266996	1.18	6.6	0.7
Keg River	7	20	91	5	5	DST 2	1389	170700		92	652	69430	860	29030	3645	274409	1.19	6.3	0.6
Keg River	15	20	91	5	5	DST 1	1375	173000		154	1149	66700	978	31230	4496	277706	1.20	6.6	0.6
Keg River	4	22	91	5	5	DST 1	1352	161000		24	436	60100	924	27300	3530	253000	1.18	5.21	0.6
Keg River	12	22	91	5	5	DST 1	1341	178200		24	350	62680	970	31350	5395	278969	1.20	5.6	0.5
Keg River	15	25	91	5	5	DST 1	1298	187000		6	266	72400	1170	30900	3510	295000	1.20	5.1	0.6
Keg River	12	34	91	5	5	DST 2	1328	123000		146	4041	68410	293	8008	583	204481	1.14	7.5	0.9
Keg River	12	34	91	5	5	DST 3	1332	142000		244	921	63900		21200	2370	230635	1.17	7.9	0.7
Keg River	10	4	91	6	5	DST 2	1433	154651		137	427	66500	850	22576	3985	249126	1.17	7	0.7
Keg River	1	5	91	6	5	DST 1	1431	170534		171	327	63400	944	33077	4746	273202	1.18	7.1	0.6
Keg River	13	10	91	6	5	DST 2	1448	151298		77	613	65000	828	23278	3040	244134	1.17	6	0.7
Keg River	13	18	91	8	5	DST 2	1380	119500		171	790	54010	547	20020	2309	197347	1.14	5.4	0.7

Formation	L	S	T	R	M	DST#	depth (m)	Cl (mg/l)	CO3 (mg/l)	HCO3 (mg/l)	SO4 (mg/l)	Na (mg/l)	K (mg/l)	Ca (mg/l)	Mg (mg/l)	TDS from fiche	Relative Density	pH	Na:Cl (moles)
Keg River	2	25	91	9	5	DST 2	1385	138200		24	747	59186		21582	3183	222922	1.15	6.7	0.7
Keg River	12	3	91	10	5	DST 1	1482	113800	78	1214	46110	521		15620	2673	180016	1.12	6.4	0.6
Keg River	2	5	91	10	5	DST 1	1497	112800	32	1082	52528			14815	2187	183440	1.13	5.9	0.7
Keg River	12	25	91	10	5	DST 1	1439	117000	33	1010	51541			15536	3694	188814	1.12	6.4	0.7
Keg River	11	11	91	11	5	DST 1	1632	109258	151	1144	50483			14678	2191	177905	1.12	6.3	0.7
Keg River	11	8	92	3	5	MFE tool	1247	171614	134	495	79046			22175	3755	277219	1.19	6.29	0.7
Keg River	8	1	92	4	5	DST 1	1265	169800	88	665	80299			20220	3669	274741	1.19	6.6	0.7
Keg River	15	4	92	4	5	DST 1	1243	180000	198	323	74500	1200		28100	4630	289000	1.20	7.89	0.6
Keg River	5	7	92	4	5	DST 2	1269	172000	88	353	72100	1150		25400	4680	276000	1.20	6.7	0.6
Keg River	16	7	92	4	5	DST 2	1262	181000	169	324	74700	1150		22800	4780	285000	1.21	7.97	0.6
Keg River	16	7	92	4	5	DST 1	1270	184000	146	360	75600	1210		26600	4500	292000	1.20	7.52	0.6
Keg River	14	9	92	4	5	DST 1	1270	185200	51	163	1020	76600	1140	30400	5180	301367	?	8.31	0.6
Keg River	15	9	92	4	5	DST 1	1253	163213	167	236	63600	1074		33051	1155	262496	1.20	8.1	0.6
Keg River	11	15	92	4	5	DST 2	1247	194900	76	864	94721	1232		21260	2671	315724	1.21	7.1	0.7
Keg River	11	15	92	4	5	DST 1	1258	192000	127	749	79897	1079		25310	5269	304431	1.21	7.1	0.6
Keg River	1	17	92	4	5	flow	1236	175735	63	350	74000	1020		26781	4609	282558	1.19	5.6	0.6
Keg River	16	20	92	4	5	DST 2	1213	168000	120	462	71800	1030		18800	3620	264000	1.18	7.06	0.7
Keg River	16	20	92	4	5	DST 1	1225	182000	166	332	76100	1150		22900	4090	287000	1.20	7.91	0.6
Keg River	7	27	92	4	5	flowing	1249	172388	137	1705	78425			27344	1517	281516	1.19	5.7	0.7
Keg River	7	27	92	4	5	DST 2	1266	170924	102	370	72204			26670	4372	274642	1.19	6.08	0.7
Keg River	7	31	92	4	5	DST 1	1266	187000	175	360	82800	1250		22200	4170	298000	1.19	8.49	0.7
Keg River	7	33	92	4	5	DST 2	1229	184200	205	597	84778			23383	4325	297488	1.20	7	0.7
Keg River	7	33	92	4	5	DST 2	1244	185351	78	352	83681			25737	3807	299006	1.20	5.55	0.7
Keg River	7	34	92	4	5	swab	1250	176327	176	235	71194			29341	5118	282391	1.19	5.8	0.6
Keg River	5	3	92	5	5	separator	1296	175258	10	277	65000	879		35371	3748	280543	1.19	4.6	0.6
Keg River	10	13	92	5	5	DST 1	1274	184000	104	206	75400	1240		25500	4160	291000	1.20	6.92	0.6
Keg River	5	25	92	5	5	DST 1	1283	181700	140	933	76800	800		24200	4500	289842	?	6.61	0.7
Keg River	11	27	92	5	5	DST 5	1318	170370	171	320	70668			26630	5020	273179	?	7.3	0.6
Keg River	7	32	92	5	5	DST 2	1310	160000	166	389	68100	855		22100	3580	255000	1.19	8.17	0.7
Keg River	3	33	92	5	5	DST 1	1306	157000	159	399	66000	938		23900	3950	252000	1.19	7.49	0.6
Keg River	6	33	92	5	5	DST 1	1288	176500	25	156	1210	72400	1300	27800	6470	283808	?	8.18	0.6
Keg River	6	33	92	5	5	DST 2	1294	166900	166	1060	72000	1150		25900	5770	273837	?	6.72	0.7
Keg River	8	36	92	5	5	swab#20	1267	173642	96	424	78000	1050		24794	4970	282976	1.20	5.5	0.7
Keg River	10	30	92	6	5	DST 1	1275	131000	134	922	59870	610		16220	3523	212279	1.15	6.7	0.7



Formation	L	S	T	R	M	DST#	depth (m)	Cl (mg/l)	CO3 (mg/l)	HCO3 (mg/l)	SO4 (mg/l)	Na (mg/l)	K (mg/l)	Ca (mg/l)	Mg (mg/l)	TDS from fiche	Relative Density	pH	Na:Cl (moles)
Keg River	13	30	92	6	5	DST 2	1279	115000		256	1410	50500		16600	3020	186786	1.15	7.9	0.7
Keg River	16	23	92	7	5	DST 1	1279	135500		122	1010	56105	782	16620	3642	213781	1.15	6.3	0.6
Keg River	11	35	92	7	5	DST 2	1268	124178		73	1547	58500	580	15733	2642	203252	1.14	5.9	0.7
Keg River	6	27	92	8	5	swab#36	1309	141000		224	550	60700	641	19753	4690	227566	1.20	6	0.7
Keg River	7	8	93	1	5	DST 1	1265	162000		76	549	71300	1380	17400	2970	256000	1.18	6.13	0.7
Keg River	10	10	93	1	5	DST 1	1245	158200		145	697	76233		17377	3587	256239	1.17	6.6	0.7
Keg River	16	23	93	2	5	DST 3	1262	142000		79	564	65700	1350	16100	2990	229000	1.17	6.17	0.7
Keg River	4	5	93	4	5	DST 1	1253	180000		47	481	79700	1420	21700	3960	287000	1.20	6.05	0.7
Keg River	1	7	93	4	5	DST 2	1256	184000		92	356	82700	1270	22200	3960	295000	1.20	5.58	0.7
Keg River	4	7	93	4	5	DST 1	1269	179000		183	273	84900	1320	19500	3610	289000	1.20	7.46	0.7
Keg River	15	7	93	4	5	swab line	1262	185000	42	244	336	82180	845	22460	5002	296067	1.20	6.2	0.7
Keg River	15	7	93	4	5	DST 1	1267	187000		88	906	89600	915	23500	4240	306999	?	8.99	0.7
Keg River	3	8	93	4	5	DST 1	1255	176000	15	201	400	81100	1170	20000	3340	282000	1.19	8.27	0.7
Keg River	11	10	93	4	5	storage tank	1252	183232		239	473	87064		21467	3944	296419	1.20	6.1	0.7
Keg River	12	17	93	4	5	swab#19	1262	175360	42	390	76200	76200	1010	26207	3649	282858	1.20	5.2	0.7
Keg River	12	17	93	4	5	DST 1	1269	179800		172	815	85000	1060	21000	3920	292916	?	8.31	0.7
Keg River	8	29	93	4	5	?	1241	61000		537	224	17440	13800	6478	2379	101858	1.07	6.2	0.4
Keg River	4	4	93	5	5	DST 3	1289	171000	139	376	64500	1030	28400	3850	269000	1.19	7.18	0.6	
Keg River	4	4	93	5	5	DST 2	1309	168000	130	525	65300	1120	28200	3870	267000	1.19	7.05	0.6	
Keg River	10	7	93	5	5	DST 1	1300	163000	26	381	67200	990	23500	3700	259000	1.19	5.18	0.6	
Keg River	2	17	93	5	5	DST 1	1301	170000	43	452	72100	1220	22500	3980	270000	1.19	6.2	0.7	
Keg River	10	17	93	5	5	DST 1	1295	168000	136	378	70300	1210	18400	3660	262000	1.16	7.31	0.6	
Keg River	12	17	93	5	5	separator	1251	162000	43	450	75200	978	20100	4290	263047	1.23	6.1	0.7	
Keg River	1	18	93	5	5	DST 2	1296	165000	98 <sup>1</sup>	246	67800	1030	18400	3670	261000	1.18	6.42	0.6	
Keg River	1	18	93	5	5	DST 1	1337	173000	126	341	71800	1090	24100	3790	274000	1.18	7.98	0.6	
Keg River	4	19	93	5	5	DST 1	1291	161700	151	930	70200	956	21100	3700	259377	?	7.94	0.7	
Keg River	15	19	93	5	5	separator	1283	160000	45	470	72200	938	17700	3640	254974	1.23	6.1	0.7	
Keg River	11	30	93	5	5	stock tank	1281	169000	59	560	76630	937	19260	6269	272715	1.18	6.9	0.7	
Keg River	11	13	93	6	5	DST 1	1278	152544	93	912	76500	678	17146	1522	249395	1.17	7.9	0.8	
Keg River	7	18	93	6	5	?	1259	123000	81	216	66800	782	12400	2350	206000	1.17	6.57	0.8	
Keg River	7	18	93	6	5	DST 3	1261	147000	63	689	73400	580	17300	2960	242000	1.17	5.23	0.8	
Keg River	9	2	93	7	5	DST 2	1278	136100	107	1165	59840	654	16380	3961	218207	1.14	6.8	0.7	
Keg River	8	36	93	7	5	DST 2	1272	146800	73	1240	76000	480	14600	2520	242130	?	7.49	0.8	
Keg River	8	36	93	7	5	DST 1	1290	165700	51	4130	102400	200	4190	557	277380	?	7.69	1.0	

Formation	L	S	T	R	M	DST#	depth (m)	Cl (mg/l)	CO <sub>3</sub> (mg/l)	HCO <sub>3</sub> (mg/l)	SO <sub>4</sub> (mg/l)	Na (mg/l)	K (mg/l)	Ca (mg/l)	Mg (mg/l)	TDS from fiche	Relative Density	pH	Na:Cl (moles)
Keg River	10	10	93	8	5	DST 1	1293	138000		88	659	58200	796	19300	3320	220000	1.16	7.3	0.7
Keg River	12	26	93	9	5	DST 1	1347	132000		32	757	54830	752	16460	4666	209497	1.15	7.2	0.6
Keg River	2	28	94	1	5	DST 1	1358	168400		43	755	76400	1670	19800	3700	271474	?	6.06	0.7
Keg River	14	1	94	2	5	swab#20	1295	163935		126	491	75000	1500	20680	3334	265066	1.18	6.5	0.7
Keg River	3	7	94	3	5	DST 2	1241	129000	8	55	965	67900	712	10500	466	208000	1.15	8.12	0.8
Keg River	3	4	94	4	5	DST 1	1248	185000		90	209	100177		13774	2163	301413	1.21	6.6	0.8
Keg River	5	8	94	4	5	DST 1	1226	188000	8	217	1040	102000	993	11400	81	304000	1.20	7.84	0.8
Keg River	5	30	94	4	5	DST 1	1269	160100		734	5020	99720	288	4404	850	271116	1.18	7.1	1.0
Keg River	11	1	94	5	5	DST 1	1247	183000		137	928	102000	1140	12700	42	300000	1.20	6.62	0.9
Keg River	6	20	94	5	5	DST 1	1233	157800		112	621	68230	1025	19060	4714	251562	1.17	7.3	0.7
Keg River	12	28	94	5	5	DST 1	1162	151000		137	464	91600	250	2010	4	245000	1.17	8.09	0.9
Keg River	11	7	94	6	5	DST 1	1269	141000		119	56	60500	837	15500	2660	221000	1.16	7.11	0.7
Keg River	2	18	94	6	5	wellhead	1273	167000		107	530	61000	920	40200	3200	272904	1.25	6.4	0.6
Keg River	14	1	94	7	5	DST 1	1258	136370		142	815	64000	711	16622	3114	221774	1.15	6.8	0.7
Keg River	14	1	94	7	5	?	1259	134000		55	560	59200	887	17400	3120	215000	1.15	6.29	0.7
Keg River	9	12	94	7	5	DST 3	1264	187777		304	1678	106800	802	9279	44	306686	1.21	7.1	0.9
Keg River	9	12	94	7	5	DST 4	1269	135487		116	873	59500	780	18087	2450	217295	1.16	6.7	0.7
Keg River	9	12	94	7	5	DST 2	1277	130853		120	739	57900	803	18255	3164	211836	1.15	6.8	0.7
Keg River	6	6	94	10	5	DST 4	1517	116702		170	1251	54787		14079	2847	189836	1.13	7.7	0.7
Keg River	2	23	94	10	5	DST 2	1425	129100		44	975	58514		16064	3606	208303	1.14	6.5	0.7
Keg River	9	36	95	2	5	DST 1	1311	165648		234	561	79005		18632	3919	267999	1.18	6.25	0.7
Keg River	4	8	95	4	5	DST 3	1217	190700	17	165	882	106200	835	9670	1110	309868		8.02	0.9
Keg River	9	10	95	4	5	swab #1	1214	153182		104	283	67900	1122	20993	3176	246760	1.17	5.7	0.7
Keg River	9	10	95	4	5	last swab	1223	158480		157	304	73200	1150	21557	169	255017	1.17	6.1	0.7
Keg River	9	10	95	4	5	last swab	1227	154062		112	348	70400	1083	20556	1014	247575	1.17	6.3	0.7
Keg River	10	1	95	5	5	DST 1	1230	168558		210	1672	103063		4591	990	279084	1.18	6.92	0.9
Keg River	15	27	95	6	5	DST 1	1244	150100		27	1055	91890	484	11490	121	255167	1.16	7.5	0.9
Keg River	7	34	95	6	5	DST 2	1264	135800		73	872	53740	621	20100	3329	214335	1.15	7	0.6
Keg River	10	18	95	7	5	DST 1	1243	136600		228	1671	63950		16577	3426	222452	1.15	8	0.7
Keg River	10	28	95	12	5	DST 2	1632	95303		166	3300	49878	608	9455	1440	159542	1.10	7.9	0.8
Keg River	16	2	96	2	5	DST 1	1261	171000		224	4296	102762		6486	1288	286664	1.18	7.5	0.9
Keg River	6	36	96	2	5	DST 1	1206	164000		220	703	85300		14500	2580	267303	1.20	7.5	0.8
Keg River	4	5	96	6	5	DST 1	1212	141500		205	961	61370	992	20420	4739	230187	1.14	8.2	0.7
Keg River	3	16	96	6	5	DST 1	1178	138500		173	1800	74340	501	9149	389	224852	1.14	7.6	0.8

Formation	L	S	T	R	M	DST#	depth (m)	Cl (mg/l)	CO <sub>3</sub> (mg/l)	HCO <sub>3</sub> (mg/l)	SO <sub>4</sub> (mg/l)	Na (mg/l)	K (mg/l)	Ca (mg/l)	Mg (mg/l)	TDS from fiche	Relative Density	pH	NaCl (moles)
Keg River	9	13	96	12	5	DST 1	1707	116900	127	1144	54280	708	14190	3025	190374	1.13	6.8	0.7	
Keg River	4	8	97	2	5	DST 1	1224	202923	128	519	102757		18974	3899	329757	1.22	6.1	0.8	
Keg River	4	16	97	7	5	DST 1	1217	140000	168	782	62900	909	16365	2730	224000	1.16	7.51	0.7	
Keg River	10	35	97	13	5	DST 1	1578	120200	154	1710	58138		13657	2643	196502	1.14	6.9	0.7	
Keg River	6	6	98	1	5	DST 3	1092	192000	225	584	103842		14294	2430	313370	1.21	7.2	0.8	
Keg River	10	19	98	8	5	DST 1	1189	143000	267	627	63600	1780	16600	3000	229000	1.16	7.88	0.7	
Keg River	6	11	98	12	5	DST 4	1689	126592	150	1099	61117		14801	2409	206168	1.14	7.1	0.7	
Keg River	3	8	99	7	5	DST 1	1163	103500	81	1718	52470	735	9469	1774	169747	1.12	6.9	0.8	
Keg River	6	33	99	7	5	DST 1	1119	157000	150	853	77134		17472	2681	255290	1.18	6.5	0.8	
Keg River	4	31	99	9	5	DST 2	1446	112800	110	1494	57163		11652	1774	184993	1.12	6	0.8	
Keg River	6	10	100	5	5	DST 1	1085	167500	171	553	77913		21221	3524	270882	1.19	6.2	0.7	
Keg River	4	3	100	7	5	DST 2	1110	152400	120	764	75049		15335	3475	247143	1.16	6.3	0.8	
Keg River	10	17	100	12	5	DST 3	1513	135516	170	1091	65460		15582	2700	220519	1.15	7.1	0.7	
Keg River	3	7	101	5	5	DST 2	1033	165463	312	2200	98829		6294	1290	274388	1.19	5.95	0.9	
Keg River	10	6	101	6	5	DST 5	1058	182400	220	466	86736		19905	4753	294480	1.19	6.6	0.7	
Keg River	5	22	102	7	5	DST 3	1042	159594	156	587	81139		14317	3324	259117	1.18	6.4	0.8	
Keg River	1	16	102	10	5	DST 1	1275	127000	464	2712	58970	1075	13290	2533	205844	1.14	7.5	0.7	
Keg River	10	34	91	24	4	DST 1	1111	172400	145	940	95825		10410	2381	282101	1.19	6.6	0.9	
Keg River	11	33	93	25	4	DST 1	1319	169132	345	426	79000	1301	20364	3625	274193	1.19	8.1	0.7	
Granite Wash	4	4	89	7	5	DST 1	1505	140000	85	566	57920		21280	4620	224471	1.15	6.3	0.6	
Granite Wash	10	23	89	7	5	DST 1	1467	166800	139	1115	85662		16737	2041	272494	1.18	7.3	0.8	
Granite Wash	12	7	89	8	5	DST 2	1441	130000	105	902	56501		19019	3402	209929	1.14	6.4	0.7	
Granite Wash	1	10	89	8	5	DST 2	1453	70600	58	2199	37645	645	5489	1334	117970	1.09	7.4	0.8	
Granite Wash	5	11	89	8	5	DST 1	1458	134800	37	798	57548	727	20940	3062	217912	1.15	5.7	0.7	
Granite Wash	11	18	89	8	5	DST 1	1408	126000	73	782	56134		17818	2916	203723	1.14	6.9	0.7	
Granite Wash	15	19	89	8	5	DST 2	1401	127000	20	864	54600	755	16700	2730	203000	1.14	5.52	0.7	
Granite Wash	3	24	89	8	5	DST 5	1451	124000	68	1360	62997	1300	14000	2300	206051	1.17	7.1	0.8	
Granite Wash	1	9	89	9	5	DST 1	1436	116800	22	893	50700	350	19900	2440	191493	?	6.2	0.7	
Granite Wash	16	21	89	9	5	DST 3	1414	109798	11	1563	49000	455	16795	2536	180160	1.13	6.5	0.7	
Granite Wash	16	26	89	9	5	DST 1	1410	107537	112	1287	48857		14912	2345	175050	1.12	6.8	0.7	
Granite Wash	9	30	89	9	5	DST 1	1431	115300	56	1362	54500	896	14810	3426	190350	1.12	7	0.7	
Granite Wash	10	34	89	9	5	DST 2	1419	119804	85	1035	53968		16324	2925	194178	1.13	8.3	0.7	
Granite Wash	7	35	89	9	5	DST 2	1413	110029	127	660	49600		15554	2263	178233	1.13	6.5	0.7	
Granite Wash	7	35	89	9	5	DST 1	1431	112617	132	935	49195		17840	2048	182767	1.13	6.35	0.7	

Formation	L	S	T	R	M	DST#	depth (m)	Cl (mg/l)	CO3 (mg/l)	HCO3 (mg/l)	SO4 (mg/l)	Na (mg/l)	K (mg/l)	Ca (mg/l)	Mg (mg/l)	TDS from fiche	Relative Density	pH	Na:Cl (moles)
Granite Wash	1	1	89	10	5	DST 1	1461	123987	73	913	54993	17856	2848	200670	1.14	6.6	0.7		
Granite Wash	12	11	89	10	5	DST 2	1459	107000	6	348	1130	44700	700	15600	2630	172000	1.11	8.42	0.6
Granite Wash	10	16	89	10	5	DST 2	1495	105547	88	1146	48146	14468	2266	171661	1.12	7.1	0.7		
Granite Wash	10	17	89	10	5	DST 2	1505	112200	56	1292	51449	627	14810	2418	182852	1.12	6.7	0.7	
Granite Wash	10	32	89	10	5	DST 3	1505	100000	49	1729	46335	13614	1967	163693	1.12	6.9	0.7		
Granite Wash	3	3	89	11	5	DST 1	1595	111000	51	1307	47960	642	14610	3742	179312	1.11	5.1	0.7	
Granite Wash	1	5	89	11	5	DST 2	1603	74200	73	2913	35320	430	9810	1823	124569	1.08	7.3	0.7	
Granite Wash	16	5	89	11	5	DST 1	1610	109000	46	1352	49160	559	13450	2430	175997	1.12	6.7	0.7	
Granite Wash	10	14	89	11	5	DST 1	1552	106500	51	1142	49810	594	13920	2343	174360	1.12	6.9	0.7	
Granite Wash	15	15	89	11	5	DST 2	1582	109000	49	1331	49350	645	14010	2187	176572	1.12	5.3	0.7	
Granite Wash	15	15	89	11	5	DST 1	1589	111000	24	1414	54620	723	14410	2916	185107	1.12	5.2	0.8	
Granite Wash	5	32	89	12	5	DST 1	1733	106500	49	1837	44998	16640	3097	173121	1.12	7.1	0.7		
Granite Wash	14	5	89	14	5	DST 3	1726	99200	41	1998	41200	510	16960	2564	162473	1.11	6.1	0.6	
Granite Wash	3	24	90	3	5	DST 1	1348	182000	98	3860	115000	566	4484	170	306178	1.18	6.8	1.0	
Granite Wash	7	13	90	6	5	DST 2	1533	180000	70	806	101000	1250	13200	1090	297000	1.20	6.55	0.9	
Granite Wash	14	13	90	6	5	DST 4	1508	197000	29	502	69800	970	39300	3400	311013	1.27	5.6	0.5	
Granite Wash	15	11	90	8	5	DST 1	1393	149500	195	914	60500	651	23300	3353	238413	1.16	7.2	0.6	
Granite Wash	3	7	90	9	5	?	1425	110000	73	934	46100	744	15200	2190	175000	1.12	6.62	0.6	
Granite Wash	10	31	90	9	5	DST 2	1415	113912	75	2496	52091	16324	2250	187148	1.12	6.9	0.7		
Granite Wash	3	5	90	10	5	DST 2	1504	109900	81	1169	52280	13640	2068	179138	1.12	5.7	0.7		
Granite Wash	3	5	90	10	5	DST 1	1508	113400	12	1243	54688	13600	2024	184967	1.12	6.3	0.7		
Granite Wash	7	6	90	10	5	DST 3	1513	105151	117	1094	48797	14162	1967	171287	1.12	6.95	0.7		
Granite Wash	7	6	90	10	5	DST 4	1527	103259	39	1122	47570	14133	1975	168099	1.12	6.3	0.7		
Granite Wash	3	11	90	10	5	DST 1	1456	108322	405	1172	49876	14464	2377	176616	1.12	6.9	0.7		
Granite Wash	10	14	90	10	5	DST 3	1439	110800	29	1549	47960	457	13610	2564	176969	1.12	6.6	0.7	
Granite Wash	11	27	90	10	5	DST 1	1465	105000	17	1658	50450	12910	1910	171945	1.12	6.7	0.7		
Granite Wash	4	1	90	11	5	DST 4	1543	110400	49	224	53680	657	15580	2187	182777	1.12	6.9	0.7	
Granite Wash	6	35	90	12	5	DST 3	1710	108316	12	1285	48700	80	14178	2953	175526	1.13	5.8	0.7	
Granite Wash	9	35	91	6	5	DST 2	1413	108224	344	1222	54602	11295	1769	177456	1.12	7.39	0.8		
Granite Wash	2	17	91	7	5	DST 1	1393	160400	85	459	67079	27147	3183	258353	1.17	5.8	0.6		
Granite Wash	4	34	91	7	5	DST 1	1381	163000	61	441	67275	26667	4253	261697	1.17	6	0.6		
Granite Wash	12	18	91	8	5	DST 1	1391	123000	49	922	54247	17538	3086	198842	1.13	6.3	0.7		
Granite Wash	2	13	91	9	5	DST 3	1389	117600	85	823	53881	14535	3232	190156	1.13	6.8	0.7		
Granite Wash	7	26	91	9	5	DST 1	1402	119300	98	816	54319	15816	2807	193156	1.14	5.9	0.7		

Formation	L	S	T	R	M	DST#	depth (m)	Cl (mg/l)	CO3 (mg/l)	HCO3 (mg/l)	SO4 (mg/l)	Na (mg/l)	K (mg/l)	Ca (mg/l)	Mg (mg/l)	TDS from fiche	Relative Density	pH	Na:Cl (moles)
Granite Wash	5	3	91	10	5	DST 1	1479	113300	73	1125	52319	450	15220	2102	184589	1.13	6.8	0.7	
Granite Wash	3	30	91	11	5	DST 1	1739	110000	61	1500	54800	768	12700	2190	182000	1.12	6.08	0.8	
Granite Wash	4	20	91	13	5	DST 4	1759	125400	220	1007	45988		24705	3985	201305	1.14	8.1	0.6	
Granite Wash	10	16	92	9	5	DST 2	1402	125800	120	904	57320		16136	3281	203561	1.13	7.2	0.7	
Granite Wash	16	21	92	11	5	DST 1	1652	112600	37	1075	50100		15215	3159	182186	1.12	6.6	0.7	
Granite Wash	16	30	92	11	5	DST 1	1728	118000	18	991	49200	609	15100	1900	186000	1.12	5.84	0.6	
Granite Wash	13	28	93	2	5	DST 4	1269	147000	215	1280	74800		10500	4950	238745	1.15	7.1	0.8	
Granite Wash	6	6	94	10	5	DST 7	1336	117691	120	1320	55442		14079	2847	191499	1.13	7.3	0.7	
Granite Wash	6	6	94	10	5	DST 5	1553	116702	120	965	53802		15523	2409	189521	1.13	7	0.7	
Granite Wash	2	23	94	10	5	DST 1	1461	130100	270	811	57585		18034	3470	210270	1.14	6.9	0.7	
Granite Wash	7	17	94	13	5	DST 2	1714	122138	81	1361	54982		16449	3195	198206	1.13	7.05	0.7	
Granite Wash	10	28	95	12	5	DST 3	1667	111187	39	1071	49142		16070	2675	180184	1.11	6.19	0.7	
Granite Wash	16	16	96	7	5	DST 1	1302	128000	59	562	55700	1800	16200	5000	207295	1.18	6.3	0.7	
Granite Wash	11	3	97	11	5	DST 1	1745	118129	59	754	54899		15316	2393	191550	1.13	6	0.7	
Granite Wash	10	35	97	13	5	DST 3	1643	119100	150	1090	55802		14818	2640	193600	1.14	7.08	0.7	
Granite Wash	6	11	98	12	5	DST 2	1733	118680	90	825	52523		16245	3285	191648	1.13	7.8	0.7	
Pre-Cambrian	3	15	89	3	5	DST 1	1504	179000	46	509	90100	925	16000	1540	288000	1.19	6.48	0.8	
Pre-Cambrian	4	3	90	8	5	DST 4	1408	130800	51	1498	53710	537	21660	3523	211779	1.14	6.5	0.6	
Pre-Cambrian	4	3	90	8	5	DST 3	1430	148100	146	667	59466	603	28190	2236	239408	1.16	5.6	0.6	
Pre-Cambrian	5	25	90	8	5	DST 3	1391	166500	44	823	69220	822	20980	4884	263273	1.18	5.6	0.6	
Pre-Cambrian	9	6	90	9	5	DST 3	1427	112500	305	1481	52440	655	15420	2066	184867	1.13	7.8	0.7	
Pre-Cambrian	9	6	90	9	5	DST 3	1427	113200	146	1325	51040	665	15620	1677	183673	1.13	6.7	0.7	
Pre-Cambrian	9	22	91	5	5	DST 2	1380	189572	107	339	86400	1160	27856	2180	307615	1.21	6.7	0.7	
Pre-Cambrian	10	28	91	7	5	DST 3	1381	132800	87	337	58300	225	18000	835	210500	1.18	6.7	0.7	
Pre-Cambrian	15	35	92	11	5	DST 2	1545	109000	28	1160	47100	698	12200	2030	172000	1.13	6.26	0.7	
Pre-Cambrian	1	5	90	10	5	DST 1	1508	110473	20	431	49500	960	15775	1470	178630	1.12	5.8	0.7	
Pre-Cambrian	13	10	91	6	5	DST 2	1508	152876		545	67000	871	22045	3309	246646	1.17	4.1	0.7	
Pre-Cambrian	3	9	91	10	5	DST 1	1491	64100	193	3457	32370	400	8649	467	109636	1.07	7.1	0.8	
Pre-Cambrian	7	32	92	5	5	DST 1	1385	145000	38	70	849	62400	924	24200	3030	237000	1.12	8.79	0.7

Abbreviations

L: Legal Sub-Division

S: Section

T: Township

R: Range

M: Meridian

depth: sample depth or depth of mid-point of sample interval